

REPORT DOCUMENTATION PAGE		READ INSTRUCTIONS BEFORE COMPLETING FORM
1. REPORT NUMBER TR-279	2. GOVT ACCESSION NO.	3. RECIPIENT'S CATALOG NUMBER TR 279
4. TITLE (and Subtitle) Description, Analysis, and Prediction of Sea Floor Roughness Using Spectral Models		5. TYPE OF REPORT & PERIOD COVERED
		6. PERFORMING ORG. REPORT NUMBER
7. AUTHOR(s) Christopher G. Fox		8. CONTRACT OR GRANT NUMBER(s)
9. PERFORMING ORGANIZATION NAME AND ADDRESS Advanced Technology Staff Naval Oceanographic Office NSTL, MS 39522-5001		10. PROGRAM ELEMENT, PROJECT, TASK AREA & WORK UNIT NUMBERS
11. CONTROLLING OFFICE NAME AND ADDRESS Naval Oceanographic Office Bay St. Louis NSTL, MS 39522-5001		12. REPORT DATE
		13. NUMBER OF PAGES
14. MONITORING AGENCY NAME & ADDRESS (if different from Controlling Office)		15. SECURITY CLASS. (of this report) Unclassified
		15a. DECLASSIFICATION/DOWNGRADING SCHEDULE
16. DISTRIBUTION STATEMENT (of this Report) Approved for public release; distribution unlimited		
17. DISTRIBUTION STATEMENT (of the abstract entered in Block 20, if different from Report)		
18. SUPPLEMENTARY NOTES		
19. KEY WORDS (Continue on reverse side if necessary and identify by block number) Roughness, frequency spectrum, marine geology and geophysics, acoustic bottom interaction, multi-beam sonar, bathymetry, numerical modelling.		
20. ABSTRACT (Continue on reverse side if necessary and identify by block number) A method has been developed which allows a valid statistical model of the variability of oceanic depths to be derived from existing digital bathymetric soundings. The bathymetry of the world ocean has been mapped using a variety of acoustic sounding instruments and traditional contouring methods. The bathymetric contours represent a low-frequency, deterministic model of the seafloor. To describe the higher frequency (continue on reverse)		

variability, or roughness, of the seafloor requires the development of an appropriate statistical method for generating a valid stochastic model. The smooth contoured surface (often preserved as a geographic grid of depths), when supplemented by such a roughness model, provides a complete description of the relief. The statistical model of seafloor roughness is also a valuable tool for predicting acoustic scattering and bottom loss, and in addition contains a wealth of geological information for interpreting deep-sea processes.

To allow the variability of depths to be described as a function of scale (spatial frequency), the amplitude spectrum is employed as the fundamental statistic underlying the model. Since the validity of the amplitude spectrum depends upon the assumption of a statistically stationary sample space, a computer algorithm operating in the spatial domain was developed which delineates geographic provinces of limited statistical heterogeneity. Within these provinces, the spectral model is derived by fitting the amplitude estimates within the province with one or several two-parameter power law functions, using standard regression techniques.

The distribution of the model parameters is examined for a test area adjacent to the coast of Oregon (42°N - 45°N , 130°W - 124°W), which includes a variety of geologic environments. The distribution of roughness corresponds generally with the various physiographic provinces observed in the region. Within some provinces, additional complexities are apparent in the roughness model which cannot be inferred by simply studying the bathymetry. These patterns are related to a variety of geological processes operating in the region, such as the convergence of the continental margin and the presence of a propagating rift on the northern Gorda Rise.

In many cases, the roughness statistics are not constant when observed in different directions, due to the anisotropic nature of the seafloor relief. A simple model is developed which describes the roughness statistics as a function of azimuth. The parameters of this model quantify the anisotropy of the seafloor, allowing insight into the directionality of the corresponding relief-forming processes. Finally, the model is used to successfully predict the roughness of a surface at scales smaller than those resolvable by surface sonar systems. The model regression line (derived from a hull-mounted sonar) is compared to data from deep-towed sonars and bottom photographs. The amplitude of roughness is predicted to within half an order of magnitude over five decades of spatial frequency.

Naval Oceanographic Office .

Bay St. Louis,
NSTL,
Mississippi 39522-5001

Technical Report
TR 279
April 1985

LIBRARY
RESEARCH REPORTS DIVISION
NAVAL POSTGRADUATE SCHOOL
MONTEREY, CALIFORNIA 93940



TR 279

Description, Analysis, and Prediction of Sea-Floor Roughness Using Spectral Models

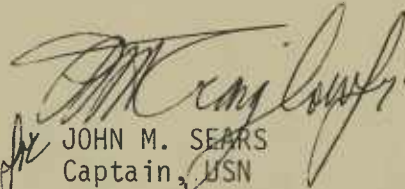
CHRISTOPHER G. FOX
Advanced Technology Staff

Approved for public release; distribution unlimited.

Prepared under the authority of
Commander,
Naval Oceanography Command

FOREWORD

Knowledge of sea-floor characteristics is required to interpret deep-sea processes correctly. This technical report discusses the use of spectral models in describing, analyzing and predicting sea-floor roughness.



JOHN M. SEARS
Captain, USN
Commanding Officer

**DESCRIPTION, ANALYSIS AND PREDICTIONS OF SEA-FLOOR ROUGHNESS
USING SPECTRAL MODELS**

Christopher Gene Fox

**Submitted in partial fulfillment of the
requirements for the degree of
Doctor of Philosophy
in the Graduate School of Arts and Sciences**

COLUMBIA UNIVERSITY

1985

ABSTRACT

Description, Analysis and Prediction of Sea-Floor Roughness Using Spectral Models

CHRISTOPHER GENE FOX

A method has been developed which allows a valid statistical model of the variability of oceanic depths to be derived from digital bathymetric soundings. Existing bathymetric contour charts represent low-frequency, deterministic models of the sea floor. To describe the higher frequency variability, or roughness, of the sea floor requires the development of a valid stochastic model. The statistical model of sea-floor roughness is also a valuable tool for predicting acoustic scattering and in addition contains a wealth of geological information for interpreting deep-sea processes.

To allow the variability of depths to be described as a function of scale (spatial frequency), the amplitude spectrum is employed as the fundamental statistic underlying the model. Since the validity of the amplitude spectrum depends upon the assumption of a statistically stationary sample space, a computer algorithm operating in the spatial domain was developed which delineates geographic provinces of limited statistical heterogeneity. Within these provinces, the spectral model

is derived by fitting the amplitude estimates with one or two power law functions.

The distribution of the model parameters is examined for a test area adjacent to the coast of Oregon. The distribution of roughness corresponds generally with the various physiographic provinces observed in the region. Additional complexities are apparent in the roughness model which can not be inferred by simply studying the bathymetry. These patterns are related to geological processes operating in the region.

In many cases, the roughness statistics are not constant when observed in different directions, due to the anisotropic nature of the sea-floor relief. A simple model is developed which describes the roughness statistics as a function of azimuth. The parameters of this model quantify the anisotropy of the sea floor, allowing insight into the directionality of the corresponding relief-forming processes. Finally, the model is used to successfully predict the roughness of a surface at scales smaller than those resolvable by surface sonar systems. The model regression line (derived from a hull-mounted sonar) is compared to data from deep-towed sonars and bottom photographs. The amplitude of roughness is predicted to within half an order of magnitude over five decades of spatial frequency.

Table of Contents

ACKNOWLEDGEMENTS.....	ix
LIST OF SYMBOLS.....	x
LIST OF ILLUSTRATIONS.....	xiii
1. INTRODUCTION.....	1
2. APPLICATIONS.....	4
3. PREVIOUS WORK.....	7
4. STATISTICAL CONSIDERATIONS.....	11
A. Statistical Measures of Roughness.....	11
B. Validity of Measurement Over Large Areas.....	16
C. Functional Representation of Spectra.....	19
D. Extension of Model into High Frequencies.....	28
E. Effect of Linear Features.....	32
F. Summary.....	42

5.	DELINEATION OF STATISTICALLY HOMOGENEOUS PROVINCES.....	45
A.	General Philosophy.....	45
B.	Generation of Amplitude Spectra.....	48
C.	Physical Interpretation of the Amplitude Spectrum...	50
D.	The Phase Spectrum.....	56
E.	Creation of the Model and Interpretation.....	63
6.	ANISOTROPY OF SURFACES.....	79
A.	Theoretical Model.....	79
B.	Comparison of Theoretical Functional Forms with Multibeam Sonar Data.....	87
C.	Estimation of Two-Dimensional Spectra from Randomly Oriented Ship Track.....	103
7.	PREDICTION OF HIGH FREQUENCY ROUGHNESS.....	107
A.	Source of Error in Spectral Estimates.....	107
B.	Propagation of Error to High Frequency Estimates....	111
C.	Comparison of Surface-Ship Sonar Results to Deep-Towed Sonar Results and Results from Bottom Photography.....	112

8. SUMMARY AND CONCLUSIONS.....	117
9. REFERENCES.....	120
APPENDIX A.1 Algorithms for Performing Power Law Regression Analysis.....	124
A.2 FORTRAN Software for Weighted log-log Fit.....	131
A.3 FORTRAN Software for Iterative linear- linear Fit.....	132
APPENDIX B.1 Algorithm and Performance Tests for Amplitude Spectrum Province Picker.....	135
B.2 FORTRAN Software for Province Picker.....	149
APPENDIX C.1 Linear Combination of Sinusoids of Identical Wavelength.....	178
C.2 FORTRAN Software for Iterative Sinusoid Fit.....	181
APPENDIX D. FORTRAN Software for Computing Pre- Whitened Spectra.....	185
APPENDIX E. Azimuthally Dependent Variations of Spectra Derived from Artificially Generated Anisotropic Surfaces.....	202
DESCRIPTION OF TERMS.....	215

Acknowledgments

This study was conducted while the author was simultaneously a graduate student at Lamont-Doherty Geological Observatory (L-DGO) and an employee of the U.S. Naval Oceanographic Office (NAVOCEANO). Original funding was provided through the long-term training program of NAVOCEANO and I thank all who are involved with the program for providing such a fine opportunity. Additional funding for the effort at L-DGO was provided through the Office of Naval Research, and special thanks are due to Murray MacDonald and Gerald Morris. The remainder of the project was performed with the support of NAVOCEANO and, in particular, Tom Davis and my colleagues on the Advanced Technology Staff.

The original concept of the study, many of the approaches used, and the recognition of the value of the study to underwater acoustics are all from the fertile mind of Tom Davis, NAVOCEANO. Special thanks to my major professor, Dennis Hayes, L-DGO, for recognizing and pursuing the geological aspects of the study, and guiding me through the graduate school maze under such unusual circumstances. Also thank you to the staff of L-DGO (especially Mia Leo and Mary Ann Garland), my friends and fellow graduate students at L-DGO, and my friends and colleagues at NAVOCEANO, in particular Terry Blanchard for computer assistance.

Data were provided from several sources and many thanks are due to all of the following:

John Farre	Columbia University	SEAMARC-1
Jeff Fox	Univ. of Rhode Island	SEABEAM
Geology Branch	NAVOCEANO	Bathymetry
Geomagnetics Division	NAVOCEANO	Magnetics
Richard Gregory	NAVOCEANO	SASS
Mary Linzer	Scripps Inst. of Ocean.	Deep-Tow
Arthur Nowell	Univ. of Washington	Bottom Photo
Mark Wimbush	Univ. of Rhode Island	Bottom Photo

In addition, to Drs. Davis and Hayes, many ideas were provided by Jim Cloutier of NAVOCEANO, David Berman of the Naval Research Laboratory, and Benoit Mandelbrot of IBM Watson Research Center.

Word processing chores were most graciously performed at L-DGO by Carol Elevitch and Erika Free.

Illustrations were laboriously constructed by Donna Waters (NAVOCEANO) and David Johnson (L-DGO).

List of Symbols

a	coefficient of spatial frequency
a_0, b_0	initial estimates of a, b for iterative regression
$\hat{a}, \hat{b}, \hat{x}$	estimated values based on regression estimate
$\Delta a, \Delta b$	correction increments for a, b
$a(\theta), b(\theta)$	azimuthally dependent function of a, b
A	amplitude
b	exponent of spatial frequency (spectral slope)
C_k	cross product at lag k
D	Fractal dimension
E	expected value
$f_a(\theta), f_b(\theta)$	azimuthally dependent function of a, b
$f(x)$	general function
$F(s)$	Fourier transform of $f(x)$
FFT	Fast Fourier Transform algorithm
k	lag
n	number of observations

N	number of values in ensemble average
$P()$	conditional probability distribution function
P	power
r	final residuals in least squares technique
RMS	root mean square
s	spatial frequency
u	mean level of $a(\theta)$
v	amplitude of cosine component of $a(\theta)$
Var	variance of random distribution
x	general independent variable
X	random variable
X_1	observation 1
\bar{X}	statistical mean of random variable X
y	general dependent variable
α	scaling factor
ϵ	residual error
$Y(k)$	autocovariance as a function of lag
λ	spatial wavelength

λ'	apparent wavelength
v	minimized residuals
$p(k)$	autocorrelation as a function of lag
θ	azimuth
θ_0	azimuth perpendicular to trend (strike) of surface
\supset	has the Fourier transform

List of Illustrations

4-1	Scale dependence of stationarity of the mean.....	18
4-2	Method of Davis (1974) for defining homogeneous provinces in a designated wave band	20
4-3	Typical amplitude spectrum of sea-floor topography.....	23
4-4	Spectral estimates derived by T.H. Bell (1975b).....	27
4-5	White-noise level of an amplitude spectrum.....	31
4-6	Effect of directional sampling of corrugated surface.....	33
4-7	Bathymetric chart of the Mendocino Fracture Zone.....	36
4-8	North-south profile of Mendocino Fracture Zone and amplitude spectrum.....	37
4-9	East-west profile of Mendocino Fracture Zone and amplitude spectrum.....	38
4-10	Comparison of Figures 4-8 and 4-9.....	39
5-1	Importance of prewhitening of amplitude spectra.....	51
5-2	Relationship of spectral slope parameter to the aspect ratio of sinusoids at different frequencies.....	54
5-3	Microrelief map of sea floor collected August 16, 1981.....	57
5-4	Microrelief map of sea floor collected July 20, 1981.....	58
5-5	Composite spectra from sea-floor microrelief.....	59
5-6	Typical phase spectrum and statistical distribution of phase angles from sea-floor relief.....	61
5-7	Distribution of roughness in the vicinity of the Gorda Rise, Northwest Pacific Ocean.....	63a

5-8	Schematic illustration (from Hey, 1977) of the magnetic anomaly pattern resulting from a propagating rift.....	69
5-9	Magnetic anomaly chart of the Gorda Rise.....	70
5-10	Amplitude spectrum of a long bathymetric profile spanning non-homogeneous reliefs.....	73
5-11	Typical amplitude spectrum of relief from the Tufts Abyssal Plain, Northwest Pacific Ocean.....	74
5-12	Typical amplitude spectrum of relief from the Continental Rise, east coast U.S.....	76
5-13	Location of bathymetric profiles showing similar amplitude spectra.....	78
6-1	Graphic representation of an elementary theoretical model for anisotropic surfaces.....	82
6-2	Radial sampling pattern used in anisotropy studies.....	83
6-3	Distribution of spectral parameters versus azimuth for theoretical anisotropic surface.....	85
6-4	Location of two-dimensional SASS bathymetry from the Gorda Rise.....	89
6-5	Graphic representation of bathymetry from the Gorda Rise.....	91
6-6	Distribution of spectral parameters versus azimuth for Gorda Rise bathymetry.....	92
6-7	Comparison of model spectrum to measured spectrum for "worst case" profile.....	94
6-8	Location of two-dimensional SASS bathymetry from the upper continental rise.....	95
6-9	Graphic representation of bathymetry from the upper continental rise.....	97
6-10	Distribution of spectral parameters versus azimuth for upper continental rise bathymetry.....	98
6-11	Location of SEAMARC - 1 derived bathymetry from the Carteret Canyon.....	100

6-12	Distribution of spectral parameters versus azimuth for Carteret Canyon bathymetry.....	101
6-13	Two-dimensional amplitude spectrum from the Gorda Rise with model spectrum.....	104
7-1	Results of ensembling spectral estimates from sixteen parallel profiles from a multi-beam sonar system.....	110
7-2	Composite amplitude spectrum of bathymetry profiles of various scales.....	115
B-1	Frequency response of band-pass filters used to estimate the amplitude spectrum discretely in the spatial domain.....	137
B-2	Uniformly distributed random noise with corresponding amplitude spectrum.....	140
B-3	Normally distributed random noise with corresponding amplitude spectrum.....	141
B-4	Inverse FFT generated white noise with corresponding amplitude spectrum.....	142
B-5	Province picker output with white-noise input.....	144
B-6	Province picker output with mixed input of known signals.....	146
B-7	Province output with input of digital bathymetry.....	148
E-1	Graphic representation and spectral parameters versus azimuth for artificial surface composed of two identical orthogonal trends.....	204
E-2	Graphic representation and spectral parameters versus azimuth for artificial surface composed of two orthogonal trends of different spectral levels.....	206
E-3	Graphic representation and spectral parameters versus azimuth for artificial surface	

	composed of two orthogonal trends of different spectral slope.....	208
E-4	Graphic representation and spectral parameters versus azimuth for artificial surface composed of two orthogonal trends of different spectral slope and intercept.....	210
E-5	Location of two-dimensional SASS bathymetry from the Mendocino Fracture Zone.....	211
E-6	Graphic representation and spectral parameters versus azimuth for Mendocino Fracture Zone.....	213

1. Introduction

The contour map of oceanic depths, or bathymetric chart, has provided a fundamental tool for inferring deep-sea processes, both sedimentological and tectonic. The identification of the major features of the sea floor led to more elaborate geophysical studies and such unifying theories as sea-floor spreading. The efforts of numerous institutions world-wide have produced comprehensive contour charts of global bathymetry, which have formed the basis of further geophysical survey efforts.

The method of contouring has the mathematical equivalent of fitting a continuous surface to discrete three-dimensional data. In the case of bathymetric contours, the discrete data are usually in the form of variably spaced and randomly oriented ship tracks along which are discrete soundings at some interval. Modern soundings are normally estimated from surface ships using acoustic sounders in which the two-way travel time of a pulse of sound is interpreted as a depth at a discrete point. Geometric spreading of the sound with depth causes a large area of the sea floor to be insonified (often called the "footprint"), and the measure of the first significant return of sound to the ship is interpreted as a sample of the shallowest depth from this large insonified area. The uncertainties in the precise location of the measured depth, the sound velocity structure of the water column and the positioning of the ship at sea, combine to introduce a noise component into the output signal. The random noise of measurement, in addition to the uncertainty of interpolation between often widely spaced samples and ship tracks,

imposes a physical limit on both the vertical (depth) accuracy and the spatial resolution possible in utilizing bathymetric contouring methods.

Despite its inherent uncertainties, a bathymetric contour chart does provide an absolute estimate of depth at all points in space. In the terminology of numerical modelling, a contour chart can be considered a "deterministic model" of sea-floor topography. Because such a model is analogous to fitting a least-squares surface through randomly spaced, noisy data, it is by nature a smoothed representation of the actual submarine topography. The degree of smoothing required (or equivalently the cutoff frequency for low-pass filtering of spatial frequency) depends upon the accuracy, resolution, and density of data used in the contouring. Van Wyckhouse (1973) demonstrated the deterministic aspect of bathymetric charts with the creation of SYNBAAPS (Synthetic Bathymetric Profiling System), a data base containing depths on an evenly spaced grid. The grid cell spacing of 5' of latitude and longitude used for SYNBAAPS, seems to represent a workable estimate of a suitable interpolation interval for deterministic modelling. Recent work at the U.S. Naval Oceanographic Office has extended this 5' grid world-wide.

There are also some practical considerations, in addition to the physical limitations, in determining submarine topography to high spatial frequencies. Survey instruments such as deep-towed sleds incorporating stereo photography, narrow-beam sounders and side-scan sonar, are able to map small areas of the sea floor with high resolution. However, it is practically impossible to extend these surveys globally, due to the operational difficulties and the great expense of these methods. Another practical difficulty of extending deterministic, gridded models

to a smaller grid cell spacing is the storage requirements of the data. For example, the 5' gridded data set extended from 70°S to 70°N being developed by the Naval Oceanographic Office will require approximately five million storage locations. To extend this grid to the order of 100 meters spacing (assuming this was determinable globally) would require approximately 5×10^{10} storage locations.

In light of the physical and practical limits of describing high spatial frequency sea-floor topography deterministically, the apparent alternative is some probabilistic (stochastic) model describing the distribution of features in a statistical sense rather than determining the exact locations of depths. To be useful, this stochastic model must describe, with a reasonable number of parameters, most of the true variability of a region of sea floor. Using a stochastic representation of high frequency feature distribution in combination with the lower frequency deterministic models being developed, an essentially complete description of the sea floor is possible. The development of such a stochastic model of sea-floor topography is the intent of this dissertation.

2. Applications

In addition to the intellectual satisfaction of completing the description of sea-floor depths, a stochastic model of high spatial frequency submarine topography, or surface roughness, has many practical scientific and engineering applications. Many of the most direct applications are in the field of underwater acoustics. Clay and Medwin (1977) provide one of the best physical descriptions of the interaction of an acoustic signal with a rough surface. Matthews (1980) reviews the importance of relative scale in acoustic bottom interaction. Briefly, the relative spatial frequencies of the incident acoustic signal and the bottom roughness determine whether the surface acts as a reflector or as a scatterer of energy. This relationship illustrates the necessity of describing bottom roughness in terms of spatial frequency.

The importance of acoustics to marine geophysical surveying systems cannot be overstated. Sea-floor bottom loss of sonar and seismic systems, ranging of side-scan sonars, and signal strength of outer beams on multibeam sounders all depend heavily on bottom roughness. In navigation applications, the roughness of the sea floor has an impact on the backscattering of Doppler sonar, as well as determining the background noise for navigation by bottom features. A major application for the U.S. Navy of bottom roughness information is as environmental input into long-range acoustic propagation models, used in submarine and surface ship tracking. For engineering applications, the a priori knowledge of the spatial frequency composition of the bottom could be used in

computer-aided design of future sensing systems, as well as aid in maintaining coherent signals for underwater communication systems.

Another field with significant applications for sea-floor roughness information is physical oceanography. This requirement led to the extensive work of T. H. Bell. Planetary Rossby waves are strongly affected by bottom roughness in long wavelengths (Rhines and Bretherton, 1973). The propagation of long surface waves such as tides and tsunamis are also affected (Rhines, 1977). Bell (1973, 1975a) showed that the interaction of deep ocean currents and bottom topography may lead to the generation of internal gravity waves in the oceans, a major influence in ocean dynamics as well as submarine operations.

Another geophysical application is in the general field of survey design. Davis (1974) has formulated a method which, with a knowledge of the spectral content of the field being measured, allows a predetermined survey accuracy to be attained. Briefly, the two-dimensional (or in some applications, three-dimensional) spectral content estimates are used in algorithms which prescribe preferred track spacing, sampling intervals and track orientation. The method has been successfully applied to gravity, magnetic and physical oceanographic surveys. The availability of an adequate spectral content model for submarine topography would make this technology available for bathymetric survey design.

In the detection of anomalous features in a field, the "normal" background variability must be removed by filtering to aid detection. This method has been applied successfully in magnetic anomaly detection and theoretically could be applied to bathymetric anomaly detection. McDonald, Katz and Faas (1966) applied this concept to submarine detection, specifically in the search for the nuclear submarine Thresher.

There are many applications of sea-floor topography modelling to the geologic interpretation of seafloor processes. Deterministic models illustrate that sea-floor relief is often decidedly anisotropic. This investigation will provide insight into the systematic nature of such spatial patterns and at several scales. Hayes and Conolly (1972) demonstrated the value of spectral techniques in studying the complex topography of the Australian-Antarctic Discordance. Since many geological processes result in linear features of characteristic wavelengths, an accurate, frequency-dependent, stochastic model could provide the capability of decomposing such features and delineating their geographic distributions. It is anticipated that many important but totally unforeseen relationships will be discovered in exploiting this higher frequency model in the same manner that numerous fundamental relationships were discovered through the generation of global bathymetric charts.

3. Previous Work

Although a great deal of quantitative geomorphology has been done on terrestrial landscape, as well as on lunar and planetary landscapes, relatively little quantitative study has been done on sea-floor morphology. Only since the late 1950's, when acoustic sonar systems became commercially available, has it been possible to attempt such statistical studies of bathymetry. The continuing refinement of sonar and navigational systems has given recent investigators even greater opportunities for success. Equally important has been the development of large digital computers and efficient statistical algorithms such as the fast Fourier transform, which allow sophisticated statistical analyses on large volumes of data, which were impractical until recently.

The work of previous investigators is somewhat sparse and inconsistent, and is reviewed only briefly here. More information is given in later sections as it becomes pertinent to various aspects of the study. Some of the earliest studies were done by Agapova (1965), who generated mean, variance, skewness, and kurtosis statistics from measurements of slopes of a transect of the mid-Atlantic ridge. Heezen and Holcombe (1965) were able to describe physiographic provinces over a large portion of the North Atlantic Ocean. After rejecting spectral and filtering techniques, these authors developed a method of comparing the spacing of adjacent peaks and troughs. In effect, the method calculates the average distribution of slopes without regard to spatial frequency.

Krause and Menard (1965) studied depth distributions from 15 profiles in the east Pacific Ocean and found them to be normally distrib-

uted. In studying normalized autocorrelation functions derived from the same profiles, the authors found no regularity with respect to lag. The profiles were used for delineating provinces on the basis of height versus width ratio of the abyssal hills. Smith et al. (1965) continued the work of Krause and Menard (1965) and concluded that the distribution of depths is Gaussian when observed in distinct wavebands of 2 to 16 nautical miles. Larson and Spiess (1970) later used a deep-towed instrument package to study the distribution of slopes in a small area of the eastern North Pacific. Krause, Grim and Menard (1973) generated simple cumulative frequency plots of slopes in two areas of the East Pacific Rise. They found a very consistent power law form to describe these distributions and concluded that marine geomorphology could be described using only a few parameters.

Neidell (1966) generated spectral estimates of bathymetric, magnetic and gravity profiles from the Atlantic and Indian Oceans. All spectra showed a "red-noise" character, that is, a decrease of power with increasing spatial frequency. The comparison of the various spectra was shown to be a valuable tool in investigation of complex geophysical problems. McDonald and Katz (1969) in their study of the directional dependence of roughness developed a polar autocorrelation function. Hayes and Conolly (1972) used spectral analysis as an interpretive tool in an area south of Australia. Distinct linear trends were interpreted by projecting randomly oriented tracks into north-south and east-west profiles and investigating the consistency of the resulting spectra.

Clay and Leong (1974) rigorously described the relationship between surface roughness and the coherence of acoustic reflections. The dura-

tions of returned pulses from hull-mounted sonars were used to estimate RMS roughness of microtopography (<0.2 km). Histograms of spectral estimates (periodograms) were generated by hand and shown to map consistently in an area southwest of Spain.

Bell (1975b), also analyzing data from the eastern North Pacific Ocean, used power spectral techniques to generate composite estimates from several sources. He discovered a functional relationship for power versus spatial frequency of the form ax^b (power law form) to be consistent over a large range of observation scales. In a later paper (Bell, 1978), this relationship was shown to hold for an enlarged data base, which is also confined to the same geographic area. The importance of anisotropy was recognized, and an initial look at the aspect ratios of submarine features was presented.

Berkson (1975) generated spectra from a variety of bottom types and attempted to fit these with a power law form. Although a wide variety of coefficients were calculated, the power law form seemed to be consistent over many types of topography. Akal and Hovem (1978) generated two-dimensional spectra of sea-floor roughness from two sets of stereo-pair bottom photographs and a contoured bathymetric chart. They noted a remarkable consistency of form in all three spectra. Matthews (1980) developed a deterministic approach to describe bottom roughness. The North Atlantic and North Pacific Oceans were divided into 30×30 nautical mile squares and the maximum relief calculated. These cells were then grouped by range of relief (0-1100 m, 1100-1900 m, >1900 m) and the results mapped. Recently, Naudin and Prud'homme (1980) quantitatively described bottom morphologies from several areas based on multibeam

sonar data collected by the SEABEAM system. Most recently, Berkson and Matthews (1983) have extended the work of Berkson (1975) and included estimates of sediment-basaltic interface roughness.

4. Statistical Considerations

In order to develop a useful model of sea-floor roughness, one must select, from a seemingly infinite variety of available methods, an approach which is both suitable and tractable. In addition to considering the nature of the sea floor itself, one must also consider such aspects as data resolution, computer storage capacity, statistical validity, and compatibility with various applications. Often, the choice of a particular method involves trade-offs between several of these considerations. In the following sections, many of these fundamental considerations are addressed, and an initial approach to developing this particular model is presented.

Statistical Measures of Roughness

If one considers surface roughness to be the variability of heights (or depths), the realm of statistics offers a multitude of measures to describe the roughness of a surface. Perhaps the most fundamental statistic available to describe roughness would be one of the standard measures of data dispersion, such as the root mean square, standard deviation, or variance. These measures have the advantage of producing a simple parameter to describe the variability of depths in a given sample. The major disadvantage of such simple measures is that they do not provide information for roughness in terms of wavelength, and the statistic derived depends upon the sample spacing and length of sampling as well as the actual roughness of the surface.

To illustrate the importance of having control over frequency dependence, consider two examples. If a generally flat surface which contains a high frequency roughness component of wavelength λ , were sampled at spacing λ or any integer multiple thereof, each sample would fall at precisely the same depth and yield a variance of zero. Mathematically, all values of X would be identical, therefore the mean

$$\bar{X} = \frac{1}{n} \sum_{i=1}^n X_i \text{ would be equal to all } X\text{'s and therefore}$$

$$\text{Var } (X_i) = \frac{\sum_{i=1}^n (X_i - \bar{X})^2}{n - 1} = 0$$

Although this example presents an extreme case, it is obvious that to assure an accurate measure of the variance at a given frequency, the sample spacing must be less than that corresponding wavelength, and the sample length long enough to sample all portions of the cycle.

A more important shortcoming of these standard dispersion measures occurs at the longer wavelengths. Consider a generally smooth but broadly sloping surface. Examples from the deep sea might be a continental rise or an abyssal fan. Since these dispersion measures record the average variation of individual samples from the sample mean, it is obvious that a relatively long sample would span a greater range of depths and produce a larger dispersion statistic than a smaller sample located in the same data. In this case, the measure of roughness would depend largely on the sample length.

Many acoustic models of bottom interaction use the more general dispersion measure of the root mean square (RMS) roughness. In these acoustic models, this value represents the RMS variation of depth about some predicted value, normally the smoothed bathymetry.

$$\text{RMS roughness} = \left[\frac{\sum_{i=1}^n (X_i - \hat{X}_i)^2}{n - 1} \right]^{1/2}$$

where \hat{X}_i represents a predicted value of depth at point i . By measuring the roughness relative to a predicted depth, rather than a simple mean as in the case of the standard deviation, the effect of long wavelength slopes on sampling is reduced. This improved measure does not, however, provide control over the distribution of roughness with frequency. Since the reflection or scattering of an incident acoustic signal on a surface is dependent upon spatial frequency, this often used parameter appears inadequate.

Another possible measure of roughness is termed the "roughness coefficient" by Bloomfield (1976), and has the form

$$\frac{\sum_{i=1}^{n-1} (X_i - X_{i-1})^2}{\sum_{i=1}^{n-1} (X_i - \bar{X})^2}$$

Because this measure (also referred to as the von Neumann ratio and the Durbin-Watson statistic) is normalized by the total sum of squares of the residuals, the dependence on sample length is minimized. However, because this measure also depends on the squared differences of adjacent points, it measures only the variability of the signal at a wavelength corresponding to the sampling interval. This roughness coefficient then is essentially a ratio of the high frequency variability of a signal to its long-term trend, an interesting statistic, but not adequate for a complete stochastic model.

Several statistical functions exist which describe the sample variability as a function of discrete data spacings or lags (see Chatfield,

1980). Perhaps the simplest function of this type is the mean cross-product of terms at given lags k

$$C_k = \frac{1}{n-k} \sum_{i=k}^{n-1} X_i \cdot X_{i-k} \approx E[(X_i)(X_{i-k})]$$

This function (called simply the autocorrelation function in electrical engineering literature; see Bracewell, 1978) is both unnormalized and uncentered (the mean is not removed). Because it depends on absolute magnitude values (in this case, the total water depth), this simple measure can be improved for the purposes of roughness modelling by removing the sample mean, which yields the autocovariance function

$$\gamma(k) = E[(X_i - \bar{X})(X_{i-k} - \bar{X})]$$

It is obvious that at a lag of $k=0$, $(\gamma(0))$ is simply the sample variance. By normalizing the autocovariance by the sample variance $\gamma(0)$, one derives the normalized autocorrelation function

$$\rho(k) = \gamma(k)/\gamma(0)$$

Notice the equivalence between the normalized autocorrelation function at lag $k=1$, $(\rho(1))$ and the roughness coefficient described previously. In comparing the roughness of two different samples, it is undesirable to normalize by the sample variance, therefore, the autocovariance function provides the best measure of variability with frequency (centered, but unnormalized).

Fully describing the variability of a process with its autocovariance function requires values at all n lags. By taking the Fourier transform of either the autocovariance or the unnormalized autocorrelation function, the process can be expressed more concisely as a function of frequency. This measure is the well known power spectral density function and can be estimated directly from the data with Fourier transforms. Besides providing a concise expression for the roughness as a function of frequency, the power spectrum also has many useful properties which are described in Chapter 6 of Bracewell (1978). One theorem of particular interest is the derivative theorem which states that if a function $f(x)$ has the transform $F(s)$, then its derivative $f'(x)$ has the transform $i2\pi sF(s)$. In this application, given the power spectrum of depths as a measure of roughness, the distribution of slopes (first derivative of depth) can be directly calculated.

An additional measure of bottom roughness, which is particularly favored by those interested in acoustic modelling of bottom interaction, is the two-point conditional probability distribution function $P(h_1, h_2 | \underline{r}_1, \underline{r}_2)$. This function defines the probability of measuring two heights (h_1 and h_2) given two distance vectors (\underline{r}_1 and \underline{r}_2). Two considerations make this approach intractable. First, the description of the function requires a large number of parameters to be retained. Secondly, complete two-dimensional data are required to adequately generate the function. This type of survey data is rarely available and only in areas which have been surveyed using multibeam sonar.

The power spectral density function appears to be the best choice of statistical measure for bottom roughness, and it will underlie the stochastic model generated in this study. For convenience, the ampli-

tude spectrum (square root of power spectrum) will be used. When properly normalized, the amplitude spectrum allows the amplitude of component sinusoids to be expressed in simple length units, which can be interpreted more easily than units of length-squared. The method of calculation will follow Davis (1974) with proper windowing, prewhitening, etc. As will be discussed in later sections, the simple and consistent functional form of spectra of topography allows relatively easy description and manipulation of the model. Also, recent work by Brown (1982, 1983) has shown the value of working in the frequency domain in modelling scattering from rough surfaces.

Validity of Measurement Over Large Areas

In generating the variance, autocovariance, or power spectrum from a discrete sample, only one realization of an infinite number of possible realizations within the population is observed. The degree to which this realization is valid over the entire population depends upon the degree of homogeneity of the process. The condition of spatial homogeneity is generally known as "stationarity" and the population being described referred to as a "stationary process". The term "process" is used in the statistical sense of the variation of data with either time or space. In the case of sea-floor topography, the depths vary as a function of space.

Stationarity is normally defined in two ways (see Chatfield, 1980; Papoulis, 1962). A spatial series is said to be "strictly" (or "first-order") stationary if the joint distribution of the process does not depend upon position. This implies that the mean and variance do not

depend on position. The less restrictive definition of "weakly" (or "second-order") stationary processes requires the mean to be constant and the autocovariance function to depend only on lag, not on position. This second definition has somewhat greater application, however, it is still too restrictive for general use with a spatial process as varied as submarine topography.

Consider a broadly sloping surface, such as an abyssal fan. The mean depth in this province would by definition vary with position, and therefore would not satisfy the first requirement for stationarity. Yet if the process is homogeneous in higher spatial frequencies, one might prefer to treat this province as a homogeneous area for modelling. In practice the existing deterministic model could be used to describe the low-frequency trend. The sample data could be high-pass filtered to remove the non-stationary trend before generation of a spectrum.

The presence of a low-frequency trend in samples of geophysical data is quite typical. In almost any length sample of a natural process, there are frequency components present with wavelengths greater than the sample length. In most natural systems, there is a finite limit on the rate of change of the process, causing the longer wavelength components to be also of greater amplitude. This typical spectrum of natural processes was termed a "red-noise" spectrum by Shapiro and Ward (1960), an analogy to the red color of low frequency visible light.

Although the red-noise spectrum is the usual form in natural systems, Figure 4-1 illustrates schematically that the presence of non-stationary components (in this case the statistical mean) can occur at any frequency and is dependent upon the horizontal extent of the sample.

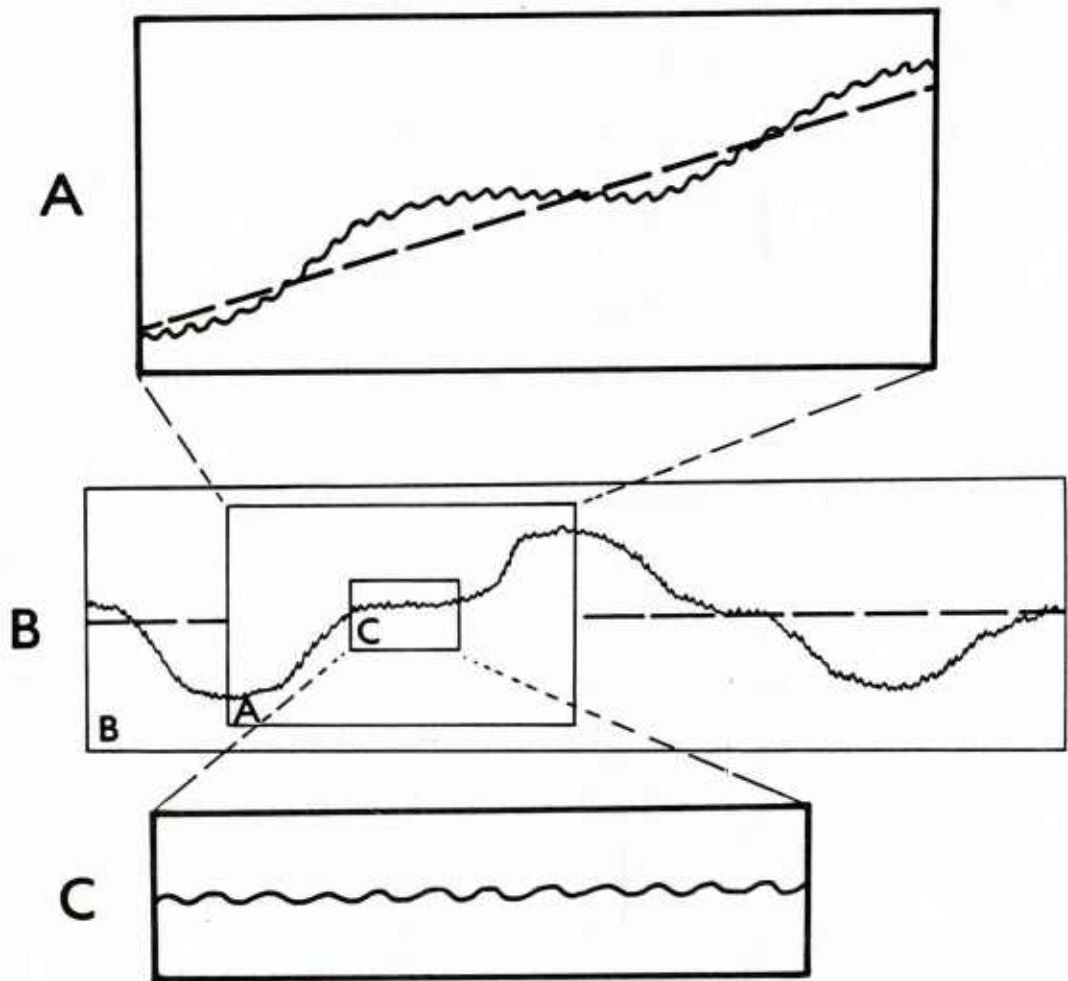


Figure 4-1 Schematic illustration of the scale dependence of stationarity. All traces are derived from the same function (B), however the inferred stationarity of the mean would be different depending upon the scale of observation. Observed at the scale of frame A, the mean is obviously non-stationary. However, the mean appears stationary at the larger scale of B or the smaller scale of C. In most natural systems, the non-stationary components occur in the partially resolved low spatial frequencies. This difficulty can be handled analytically by defining homogeneous provinces on the basis of stationarity and prewhitening of the spectra.

In order to generate a stochastic model of sea-floor topography, we must ensure that the process is stationary within some limit and over some defined area, with respect to the statistical parameters being calculated. Ideally, this is accomplished by identifying homogeneous provinces based upon these criteria. Davis (1974) developed such a "province picker" for use in geophysical survey design, and his method is illustrated in Figure 4-2.

By actively defining provinces which are weakly stationary in the frequency band of interest, one improves the validity of the statistical measures generated within each province. In addition, by delineating province boundaries, one can also alleviate the problems associated with the least-squares or averaging nature of Fourier transforms. In generating a power spectrum from a data set, the operator must select the length and location of the sample series to be transformed. The resulting spectrum will reflect the average frequency composition over the sample. If the sample spanned two distinct statistical processes, the result would provide the average composition of the two provinces, and would accurately represent neither. By confining one's samples within the boundaries of a homogeneous province, one insures a valid and representative statistic. These concepts will be discussed in detail in Chapter 5.

Functional Representation of Spectra

One property which makes the Fourier transform, both continuous and discrete, such a powerful analytical tool is its ability to express a spatial process in the spatial frequency domain both exactly and com-

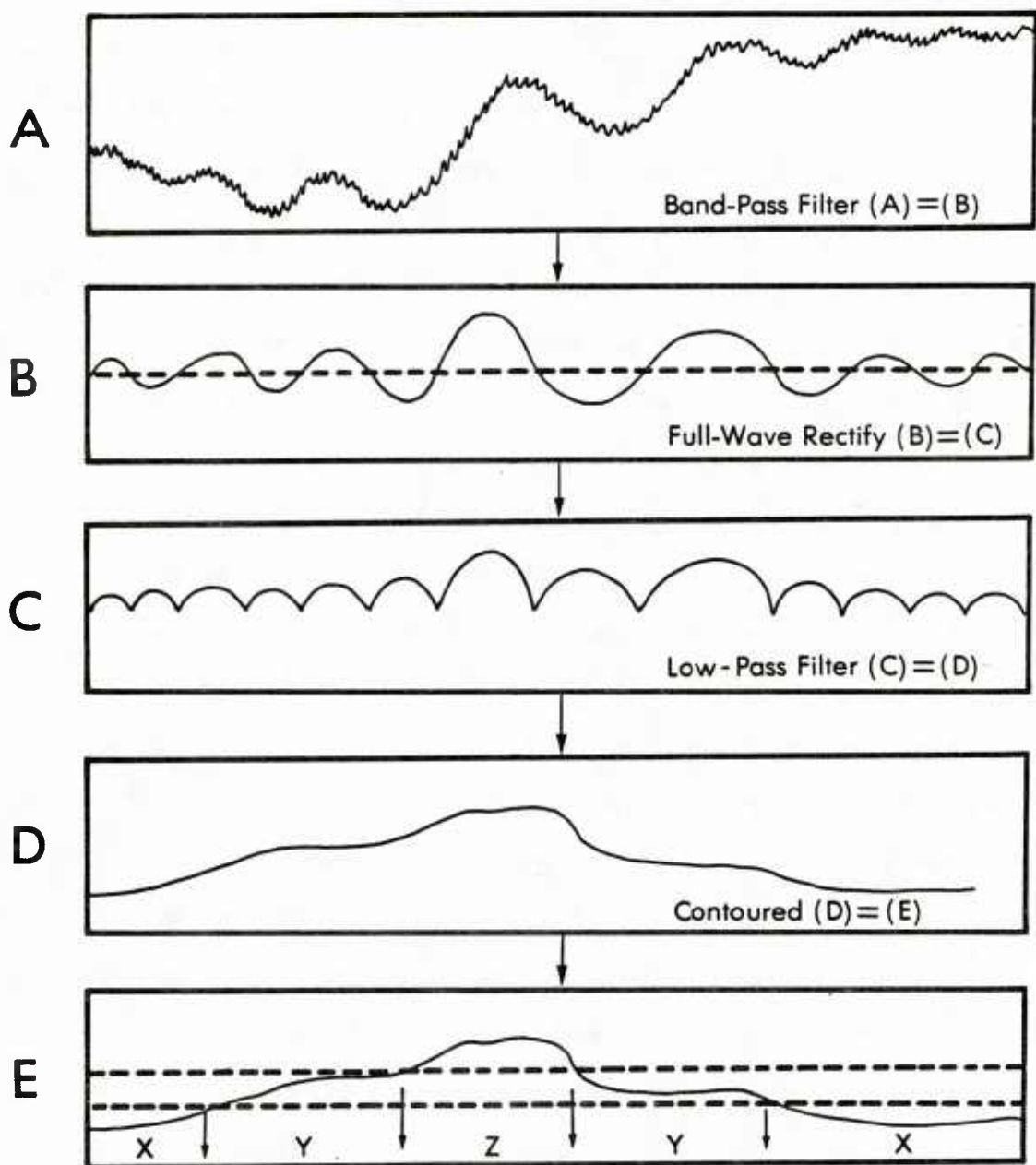


Figure 4-2 Schematic illustration of the method developed by Davis (1974) for delineating homogeneous roughness provinces within a given spatial waveband. The original signal (A) is band-pass filtered at a pre-selected wave band of interest to produce B. The now centered data of B is full-wave rectified by taking the absolute value of all terms to produce C. This output is low-pass filtered (smoothed) to yield the continuous function of D. Finally, this function is contoured at some selected interval (not necessarily linear) to delineate the boundaries of provinces X, Y, and Z in frame E.

pletely. This complete correspondence between domains allows detailed analyses to be made on the spectra with the assurance that there is an exact analog in the spatial domain. In order to maintain this correspondence, it is necessary to retain the complete transform, (both amplitude and phase components) in the spatial frequency domain. In the case of discrete data and transforms, it would be necessary to retain all of the degrees of freedom present in the original data set.

In the creation of a probabilistic model, it makes little sense to retain as much information in the model as was present in the original data. Presumably, one would prefer to use the original data as a deterministic model. Also, the purpose of the model is to describe the general high frequency structure of the sea floor, rather than to analyze in detail the individual frequency components. Finally, the restrictions of computer storage space require a limited number of parameters in the model.

All of the above considerations argue strongly for a severe paring of information in the frequency domain model. The phase spectrum, which requires fully half of the information in the spatial frequency domain, defines the origin in space of all component sinusoids of the amplitude spectrum and adds very little insight into the general structure of the sea-floor. An analysis of bathymetric phase spectra presented in Chapter 5 will show that the phase is in fact randomly distributed. For the purpose of this model, no phase spectra will be retained, as none of the previously stated applications require phase information.

All measured data contain a component of random noise. Remotely sensed data are especially susceptible to measurement noise, the particular noise problems in measuring oceanic depths having been mentioned in

the introduction. The presence of noise in the spatial data manifests itself in two ways in spatial frequency spectra. Inaccuracies of vertical measurements in the spatial domain result in the presence of a horizontal "white-noise level" in all amplitude or power spectra. This problem will be treated in detail in the following section. Uncertainty in the location of features in the spatial domain results in the scattering of amplitude estimates about the true frequency spectrum. These distinctions in the sources of error are somewhat artificial since the vertical and horizontal uncertainties are interdependent.

Figure 4-3 reproduces a typical amplitude spectrum of depths. The red-noise character of the distribution as well as the scattering of amplitude values is apparent. The spectrum was derived from data collected by the U.S. Naval Oceanographic Office using SASS (Sonar Array Subsystem), and represents the highest resolution bathymetric information currently available from a surface ship (see Glenn, 1970). Control over relative horizontal location (navigational accuracy) of soundings is especially good due to the use of large, stable surveying platforms (in this case, USNS Dutton) and SINS (Ship's Inertial Navigation System). The degree of scattering of amplitude estimates would presumably be greater in less sophisticated systems.

Several methods come to mind to smooth this somewhat noisy spectrum. A simple moving average taken over the amplitude estimates in the frequency spectrum would smooth the data. However, information would be lost from the high and low frequency extremes of the spectrum, while the density of data in the intermediate frequencies would not be reduced. The use of spectral windows or lag windows could be used both to smooth the spectrum and decrease the data density. The use of data windows in

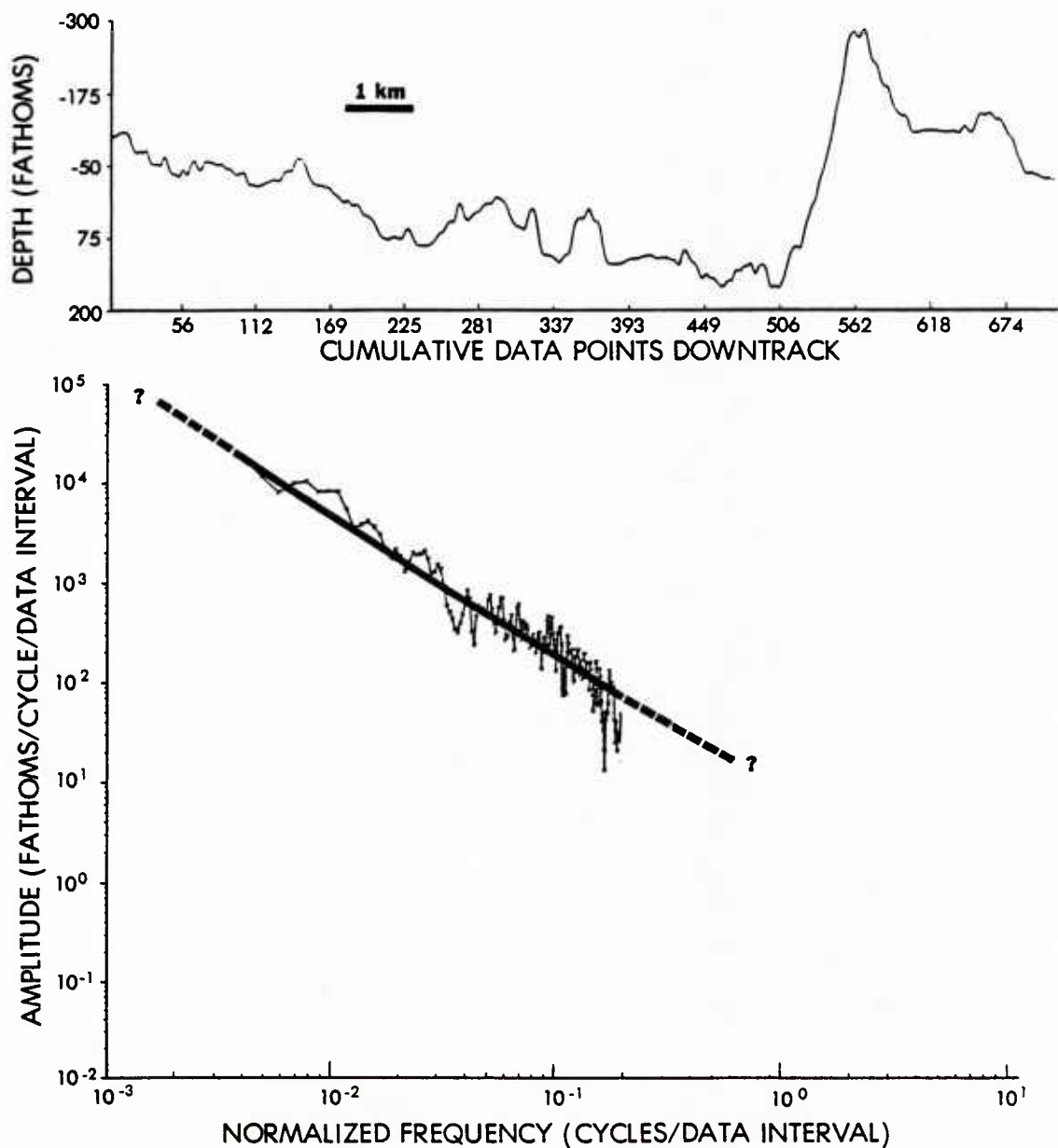


Figure 4-3 Illustration of a typical amplitude spectrum of sea floor topography. A profile of the data, collected by SASS on the Gorda Rise, is presented above. The spectrum shows clearly the power law form as a linear fit on log-log plot. Possible extrapolations of the trend are shown as dashed lines beyond the fundamental and Nyquist frequencies.

the smoothing of spectra is discussed in many texts (see for example Bloomfield, 1976) and will not be discussed in detail here. The spectrum presented in Figure 4-3 was in fact generated using the method of Davis (1974) which utilizes prewhitening as well as low-pass filtering of the spectral estimates.

Another method of smoothing this rough spectrum is through the use of regression techniques. Calculating a continuous mathematical function to describe the distribution of amplitudes would produce a smooth representation of the spectrum while, depending upon the complexity of the function used to fit the data, greatly reducing the number of parameters retained in the model. This least-squares representation will be used in this study.

By describing the spectrum with a simple, continuous mathematical function, one can more easily take advantage of the many symmetry properties of the Fourier transform described by Bracewell (1978). For example, Rayleigh's Theorem (or Parseval's Formula for discrete series) states that the integral of the power spectrum equals the integral of the squared modulus of the function, or

$$\int_{-\infty}^{\infty} |f(x)|^2 dx = \int_{-\infty}^{\infty} |F(s)|^2 ds$$

This is equivalent to stating that the total energy in one domain is exactly equal to the total energy in the other. If one were interested in the total energy in a particular band of frequency (in order to study the bottom interaction of sound of a particular wavelength, for example), the high and low frequencies of the band pass would become the limits of integration of the power spectrum. With the spectrum repre-

sented as a simple function, this definite integral could be evaluated analytically to derive the RMS variability for a discrete waveband.

Having decided to use functional representations as the basis of a stochastic model of sea-floor roughness, the selection of a suitable functional form for the spectra becomes crucial. In order to minimize the size of the model, the simplest functional form which is justified by the data should be the best. An examination of Figure 4-3 as well as many other spectra presented later, would suggest the use of a simple straight line fit to the data. In light of the scatter in this already smoothed data, no higher order functional form is justified.

The normal form for fitting a straight line to data is the estimation of the coefficients \hat{a} and \hat{b} in the equation

$$y = \hat{b} x + \hat{a}$$

Notice in Figure 4-3, however that the data are plotted versus logarithmic scales. The regression equation would therefore be written,

$$\log A = \hat{b} \log s + \log \hat{a}$$

where A = amplitude and s = frequency. This equation can be rewritten in terms of A as,

$$A = \hat{a} \cdot s^{\hat{b}}$$

This inferred relationship between amplitude and frequency is often termed a "power law" or "power function" relationship. Appropriate

regression techniques must be selected in order to assure a proper regression fit to the power law form. Of prime concern is whether the residuals are minimized in log-log space or linear-linear space. The methods used in this study with accompanying theory and computer software are presented as Appendix A.

The power law form seems to represent the best model for describing sea-floor topography in the spatial frequency domain. Its simplicity permits the frequency structure of a sample profile to be described using only two parameters, a considerable reduction of the original, deterministic data. Extensive work by Benoit Mandelbrot (1982) has produced a theoretical basis for this consistent relationship, formulated in terms of fractal dimension, a parameter functionally related to coefficient \hat{b} above (see Berry and Lewis, 1980). Bell (1975b) discovered the same power law relationship in data from the Pacific Ocean that including lower spatial frequencies than those of interest in this study (see Fig. 4-4). Notice that Figure 4-4 plots power spectral density, rather than amplitude as in Figure 4-3 and other example spectra. Because the vertical axis in both plots is logarithmic, this exponentiation appears graphically as a linear transformation. Mathematically, the squaring of amplitude represents a simple doubling of the slope, i.e., multiplication of the \hat{b} term by a factor of two.

Bell (1975b) finds a fairly consistent relationship at many size scales, with the slope of the log transformed power spectrum of $\hat{b} = -2$. Although this value probably represents a good mean estimate, the examination of many spectra in this study will show an accountable variation in this value. Berkson (1975) also discovered a significant variation of regression coefficients for spectra generated from differ-

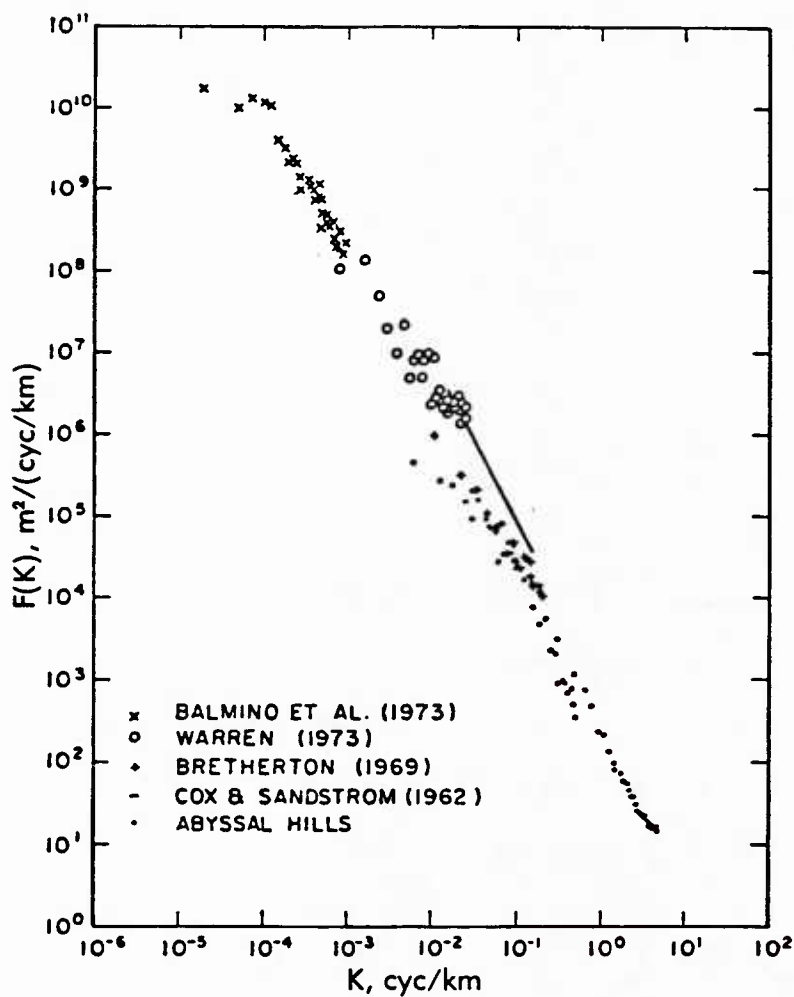


Figure 4-4 Spectral estimates collected by T. H. Bell (1975b) from various sources. The linear distribution of the data illustrates the power law form of submarine topography spectra for a wide range of scales. Notice that this spectrum is plotted versus power (amplitude squared) which results in a doubling of the ordinate and the slope of an amplitude spectrum. Refer to Bell (1975b) for data sources.

ent bottom types. Analyses presented in Chapter 5 will link this "universal" relationship

$$A = a \cdot s^{-1}$$

to the absence of stationary provincing techniques.

Extension of Spectra into High Frequencies

The component of random noise present in all empirical data, includes uncertainties from many possible sources in the total measurement system. There are uncertainties associated with the measuring device itself, for example, the errors in the timing of the arrival of a sonar pulse. The interference of external sources, such as radio waves, may also affect the measuring instruments. The nature of the environment between the detection device and the process being sampled may introduce error, such as the variability of sea water sound velocity in bathymetric surveying. The truncation of significant digits in the storage of digital data introduces a finite level of noise, often called "round-off error." All of these sources combine to form a total noise level for a measured data set.

With the exception of round-off error, which is calculable, the source of these random errors can not be decomposed. However, using spectral techniques the level of the total noise can be estimated. It is a well-known property (see Bracewell, 1978, Chapter 16, for a complete discussion) that the spectrum of a randomly generated signal varies

about a constant value. This makes intuitive sense, since one would not expect any particular frequencies to dominate a random series. Again in analogy to the spectrum of visible light, this random component of a signal is often called "white noise", reflecting the equal contribution of all frequencies.

In the same way that Rayleigh's or Parseval's theorems can be used to relate energy in one domain to energy in the other, the level of noise in a spatial signal can be estimated from the amplitude of the noise level of an amplitude spectrum. The noise level in the spatial domain is normally expressed as a simple dispersion measure of the variability of the data, in this case, the oceanic depths. The following formula relates the white-noise level of the power spectrum to the root mean square.

$$\text{RMS} = \sqrt{P/n}$$

where n = number of data points in series; and P = the mean power level of the white noise. In the case of sonar systems, knowledge of this RMS level defines the resolving capability of the system for a given signal level. Using these simple spectral techniques, the resolving power of the various sounding systems in use today can be calculated and compared.

The red-noise structure of natural systems has been mentioned and illustrated previously (see Fig. 4-3). The interaction of natural signals with instrument noise takes the form of a decreasing red-noise spectrum of the signal "intersecting" the horizontal white-noise level. In the spatial domain perspective, lower frequency features tend to have

higher amplitude and therefore the signal in these frequencies is "visible" above the RMS noise. The frequency at which the spectrum of the signal intersects the noise level represents the highest frequency that is being resolved in the system.

Figure 4-5 illustrates these concepts on a spectrum of SASS data. Notice that Figure 4-5 shows an obvious noise level while the spectrum shown in Figure 4-3 does not. Both sets of data were collected using the same sounding system within days of each other, and it is expected that the instrument noise in each is approximately equal. The difference is therefore that the data in Figure 4-3 represent a rougher area in which the signal energy in the highest frequencies is sufficient to maintain the resolution of the signal above the noise. The noise level is present in both sample spectra, however, it was never intersected in the sample from higher energy sea floor. The ability of a sonar to resolve horizontal features depends not only on the horizontal resolving power limitations of the instrument (normally limited by the size of the "footprint"), but also by the amplitude of features present in the sea floor.

In light of the limitations of noise in all measurement systems, a fundamental question in the development of a stochastic model of sea-floor roughness from widely available surface sonar, is how far into the high frequencies the model can be extended. One could argue that due to the persistent exponential form of the spectra noted in this study, as well as the work of Bell (1975b), that this functional form can simply be mathematically extrapolated into higher frequencies. Further justification might be provided by the generation of spectra from deep-towed instrument packages, bottom photographs, and direct observations, to

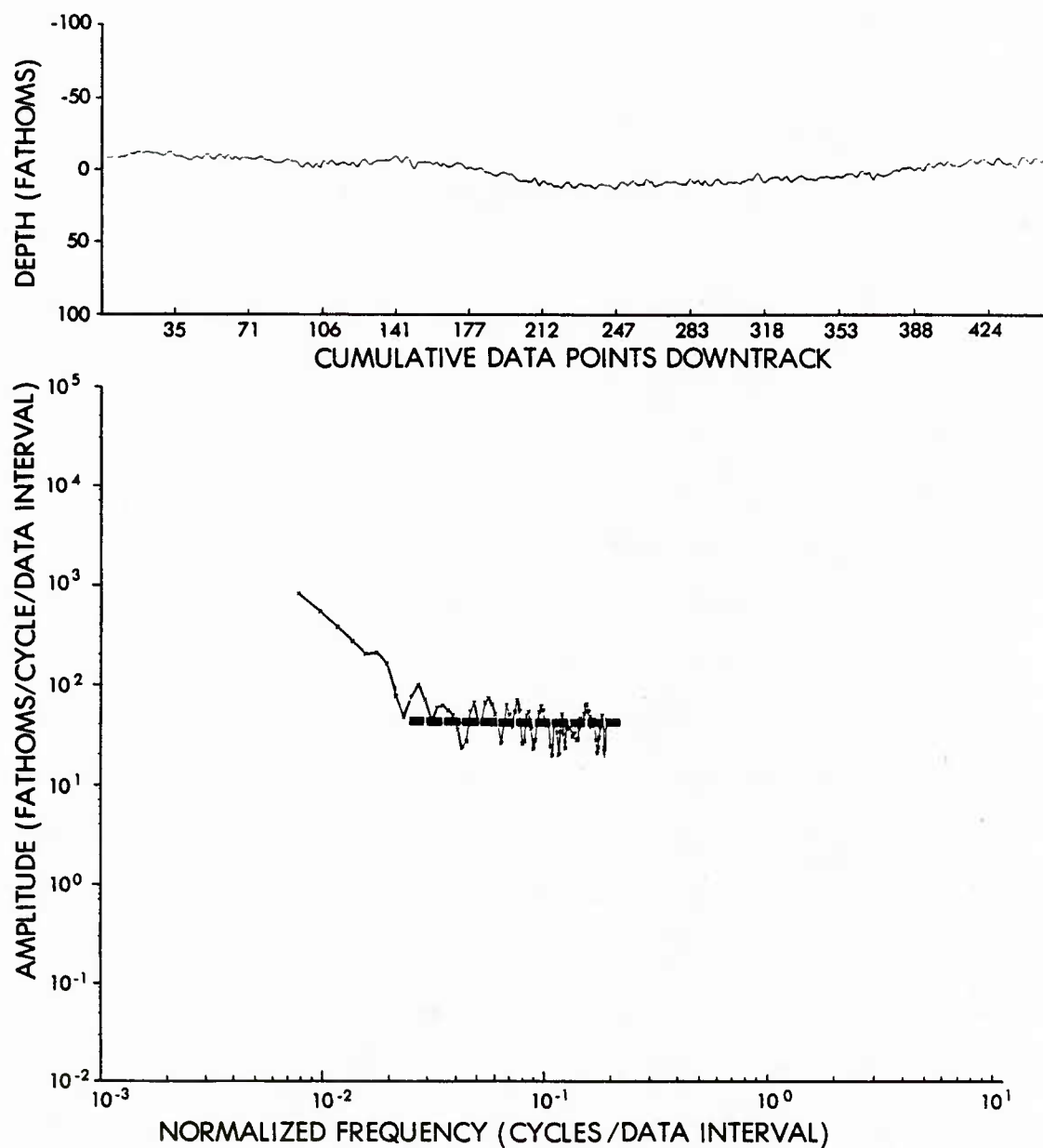


Figure 4-5 Illustration of an amplitude spectrum of sea floor topography which has encountered the "white-noise" level in the data. The spectrum of random noise has the form of a horizontal line. This noise level, which was derived from data collected by SASS, corresponds to a random component in the spatial data with root mean square dispersion of 1.9 fathoms.

provide spot checks of the high frequency structure. This approach will be pursued in Chapter 7.

Effect of Linear Features

In generating a Fourier transform of topography within a stationary province, a one-dimensional statistic is generated from a two-dimensional surface. Provided the surface is isotropic, that is that there is no significant directional dependence, statistics derived from a one-dimensional sample would be equally valid for any orientation. Even a cursory examination of a deep-sea bathymetric chart reveals clearly that the sea floor, at least in the lower spatial frequencies presented in a contour chart, is quite anisotropic. There is extensive evidence that bathymetric lineations also exist to some extent in the higher spatial frequency roughness of interest to this study. To completely model sea-floor roughness, it is essential to account for any major directional dependence of the topographic features.

Figure 4-6 illustrates the effect of sampling a simple two-dimensional periodic function in differing directions. Notice that the true wavelength (λ) of the feature is sampled only when the sampling is exactly perpendicular to strike ($\theta = 0^\circ$). Any oblique angle produces an apparent wavelength (λ') which is greater than λ . At $\theta = 90^\circ$ (a sample taken parallel to strike), the feature is not expressed at all ($\lambda' = \infty$). The apparent wavelength is related to the true wavelength by

$$\lambda' = |\cos^{-1}\theta| \cdot \lambda$$

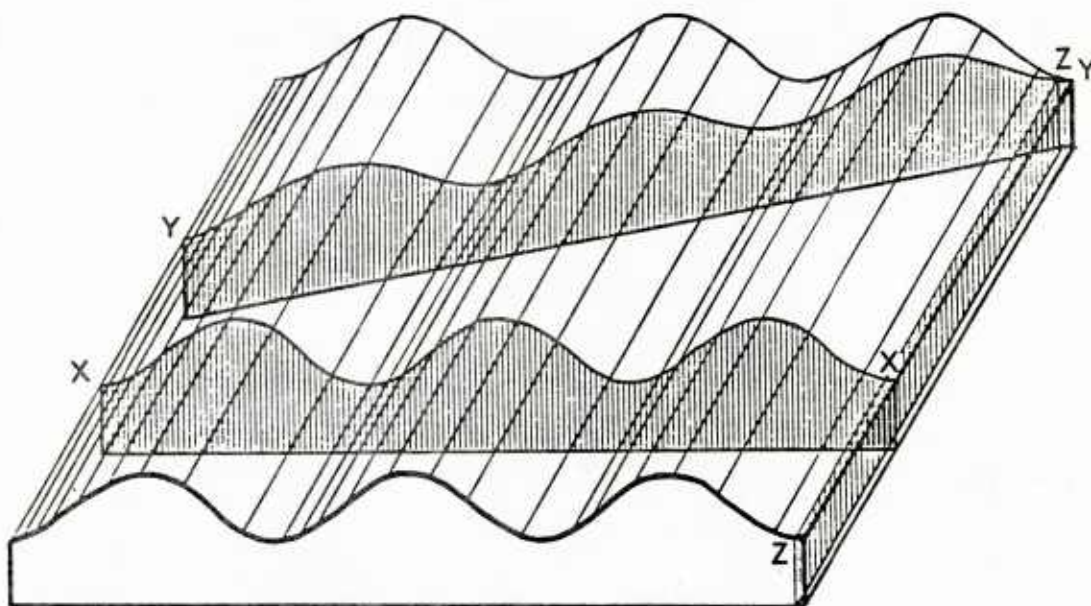


Figure 4-6 Schematic illustration of the effect of directional sampling on spatial frequency estimation. The figure illustrates the increase of apparent wavelength of a simple periodic waveform when sampled at any angle other than exactly perpendicular to strike.

Notice that the amplitude of the feature is not affected, provided a full wave form is sampled.

The effect of directional sampling in the spatial frequency domain can be calculated using the previous relationship in combination with the similarity theorem of Fourier transforms (see Bracewell, 1978, p. 101). The similarity theorem states that given the transform pair $f(x) \supset F(s)$, then

$$f(ax) \supset |a|^{-1} F(s/a)$$

Applying the geometry for directional sampling of linear features, i.e., $a = |\cos \theta|$

$$f(|\cos \theta| \cdot x) \supset |\cos \theta|^{-1} \cdot F(s/\cos \theta)$$

Because $|\cos \theta|$ must always be less than one, the effect of oblique sampling in the frequency domain is to shift the amplitude peak to lower frequencies, narrow its width, and increase its amplitude. This is a result of the fact that a signal of equal height but lower frequency has greater power than its higher frequency counterpart. It is important to note that these theorems assume an infinite continuous signal. In analyzing finite length signals, it is necessary to normalize the spectrum by the sample length, that is, divide each amplitude estimate by the number of values in the time series. This normalization preserves the true amplitude of the individual waveforms, and allows comparisons between samples of different length. The effect of anisotropy on sampling a surface with continuous spectra is developed in a later section.

Several authors have recognized the importance of anisotropy of the sea floor to power spectral studies. Hayes and Conolly (1972) recognized distinct peaks in their spectral analysis of the bathymetry of the Australian-Antarctic Discordance. These groups were normalized to two linear trends by projecting the data to simulate north-south and east-west samples. Distinct trends were successfully identified, however, in longer wavelengths than the high spatial frequency band of interest in this study. Bell (1978) also recognized the importance of anisotropic features in his study of abyssal hills in the north Pacific Ocean. One result reported in his study of the aspect ratios of features in this province is that the degree of anisotropy tends to decrease in the higher spatial frequencies. Whether or not this is a true relationship or the result of resolving limitations will be discussed further in Chapter 6.

Figure 4-7 shows the sample locations for two spectra from the linear Mendocino Fracture Zone in the northeastern Pacific Ocean. Figure 4-8 presents the profile and amplitude spectrum for line A-A', which was sampled perpendicular to strike, reflecting the long wavelength fracture zone. Figure 4-9 is the corresponding plots for line B-B', which parallels strike and is located in the zone of disturbance. The exponential form of both spectra is evident, however Figure 4-10, which shows a composite of the trend of both spectra, illustrates the differences in slope (exponent) of the two spectra. Segment A-A' contains more power in the low spatial frequencies, while segment B-B' contains more power in the high spatial frequencies.

Both spectra are valid representations of the spatial frequency distribution in this physiographic province, but neither spectrum indi-

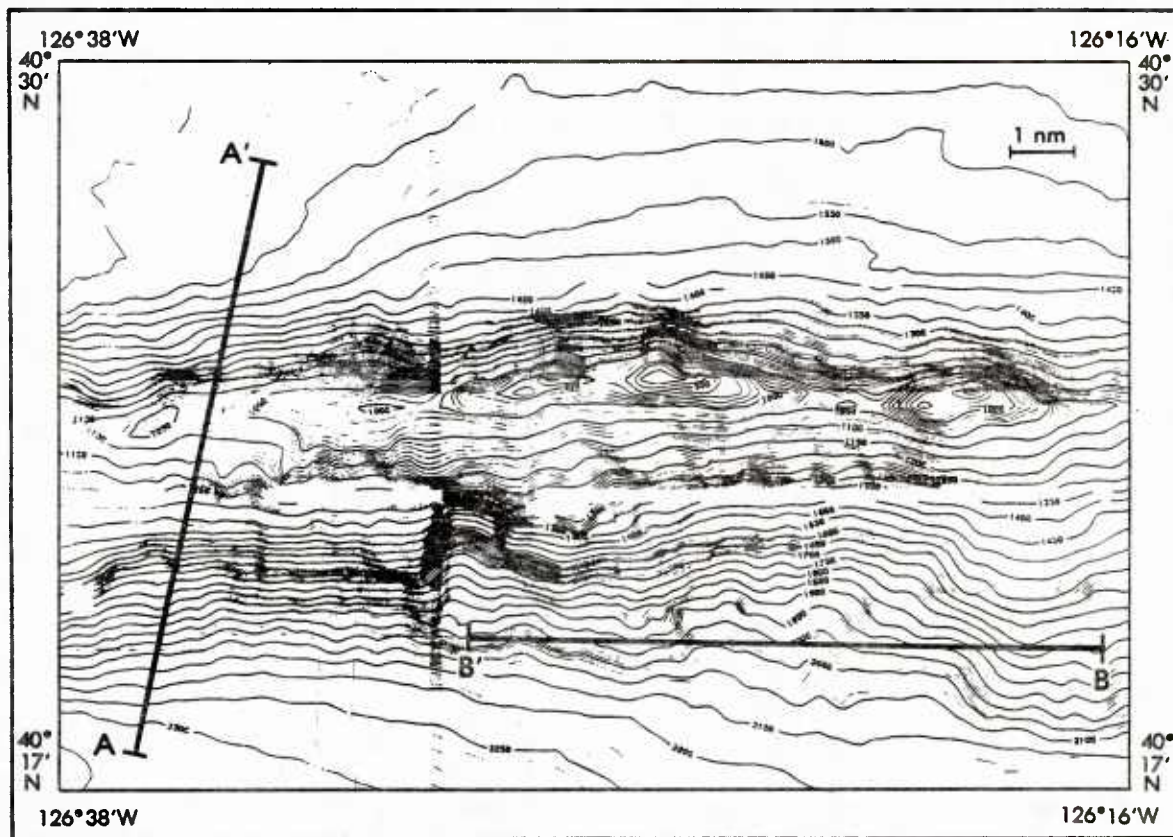


Figure 4-7 Bathymetric chart from the Mendocino Fracture Zone of the eastern Pacific Ocean showing the location of the data used in Figures 4-8 and 4-9. Notice that both samples lie within the same bottom environment, but that A-A' is sampled across the long axis of the fracture while B-B' is sampled along the axis.

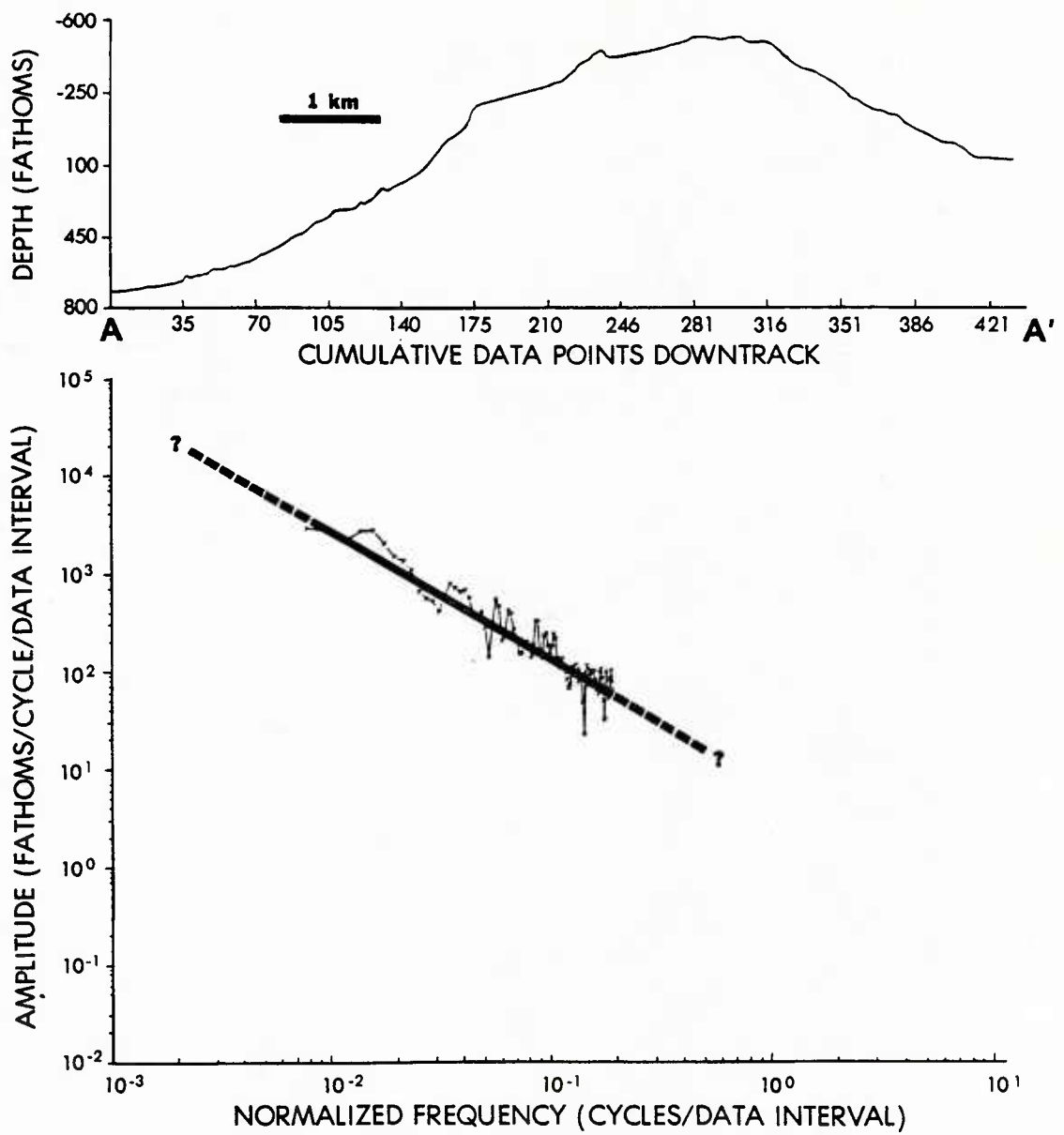


Figure 4-8 Profile and amplitude spectrum of SASS data collected along line A-A' in Figure 4-7.

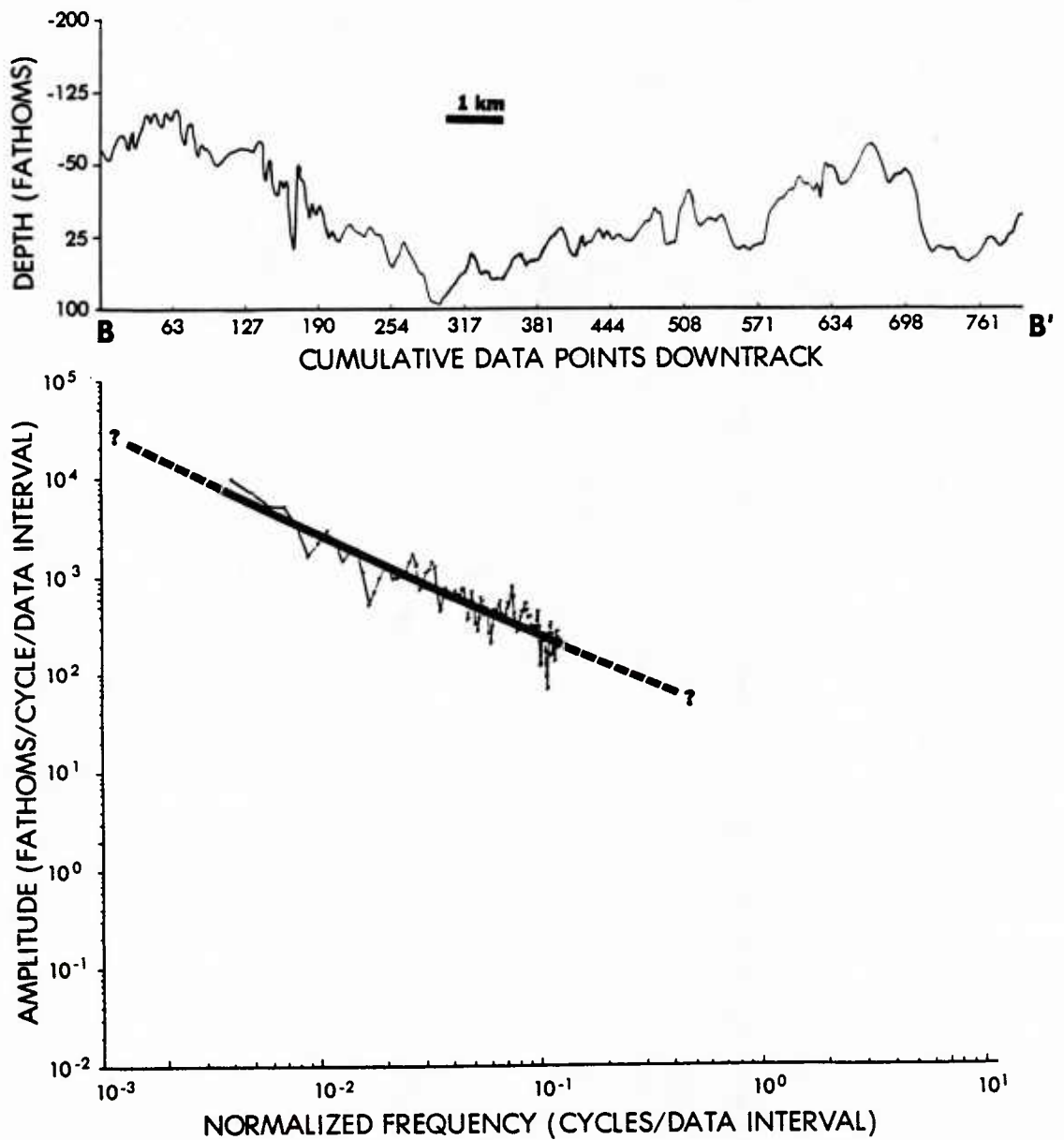


Figure 4-9 Profile and amplitude spectrum of SASS data collected along line B-B' in Figure 4-7.

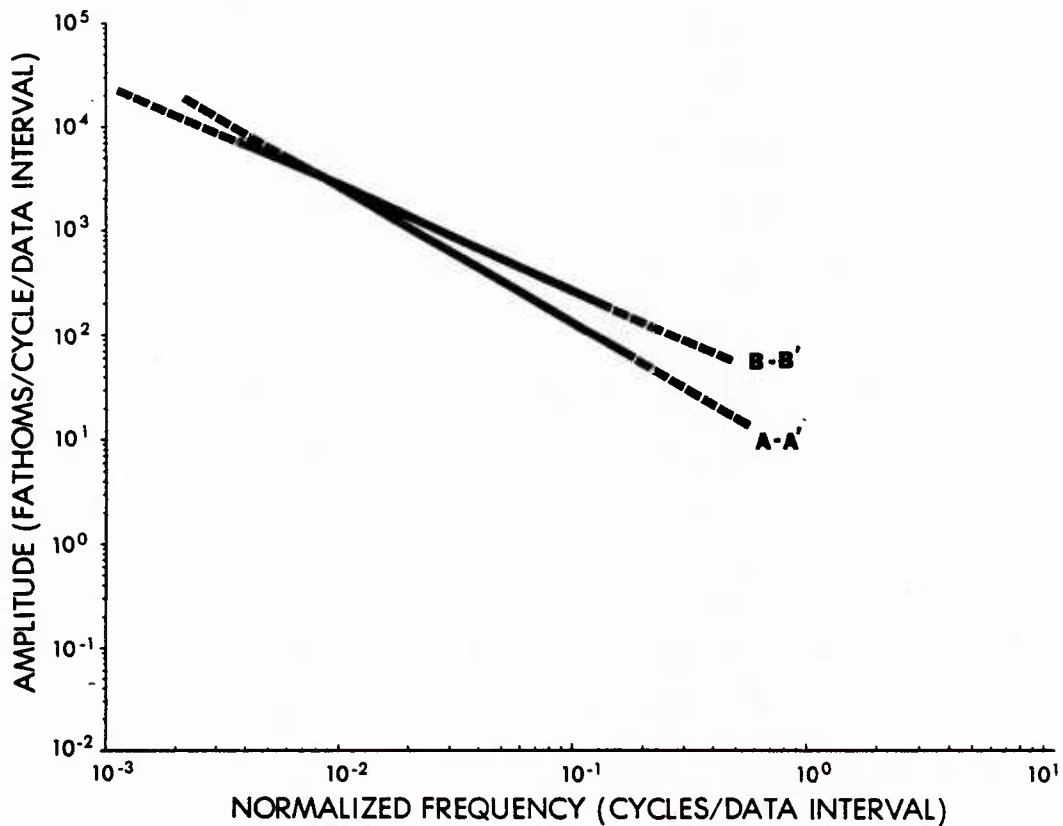


Figure 4-10 Composite of Figures 4-8 and 4-9 illustrating the anisotropy of the sea floor in the Mendocino Fracture zone. Although both spectra retain their power law form, there is an obvious difference in slope and intercept. Profile B-B' appears to contain more high spatial frequency energy, while profile A-A' contains more energy in lower spatial frequencies.

vidually describes the roughness in all directions. The need for a directionally dependent function is obvious. The two-dimensional Fourier transform might appear to be appropriate, since it describes the two-dimensional roughness of a surface. However, its calculation requires a complete two-dimensional grid of data values which is generally unavailable. The double Fourier transform, well described in Davis (1973), is calculated from two orthogonal one-dimensional spectra. This method, especially without the retention of the phase spectra, can not unambiguously identify the orientation of trend. Both the two-dimensional and double Fourier transforms require a large two-dimensional matrix to be retained in the model.

McDonald and Katz (1969) describe a method for estimating autocorrelation functions as a function of azimuth θ . A similar approach will be attempted here for use with amplitude spectra. By studying the azimuthally dependent distribution of the coefficients derived from the power law regression, \hat{a} and \hat{b} , it is anticipated that some functional form or forms will be revealed to allow modelling of the entire process as a function of both spatial frequency (s) and true azimuth (θ). If $\hat{a}=f_a(\theta)$ and $\hat{b}=f_b(\theta)$ then

$$F(\theta,s) = f_a(\theta) \cdot s^{f_b(\theta)}$$

With this functional form, input into the model of simple compass direction for a given location would return the unique spatial-frequency-dependent function coefficients for the amplitude spectrum in that particular direction. Evaluation of these θ dependent functions should provide a simple measure of the degree and direction of bottom anisotropy.

The derivation of the functional form of this θ dependence would best be investigated and verified in areas where complete two-dimensional measures of depth are available. Areas surveyed with multi-beam sonar systems such as SASS and SEABEAM are ideal for this purpose. If a functional form is determined to be consistent, discrete samples from randomly oriented tracklines could be fitted with this functional model and $F(\theta, s)$ estimated. Such studies will be presented in Chapter 6 and Appendix E.

One complication that could arise due to anisotropic roughness is in the use of the province picker for the delineation of stationary provinces. In a highly lineated area, the power level of particular narrow frequency bands would be directionally dependent. The province picker, however, measures total energy (integrated power) rather than discrete power, and as mentioned previously, the peak shift due to oblique sampling of a linear feature does not affect the total energy measured. Unless a major spectral peak is shifted beyond the low cut-off frequency of the band pass used in the province picker, the results should not be adversely affected by directional sampling problems. Even this problem seems unlikely to arise as thus far in all spectra sampled, none have shown unusual low spatial frequency peaks such as are seen by Hayes and Conolly (1972), and which are probably unique to a few tectonic provinces such as the Antarctic-Australian Discordance.

Summary

In summarizing the preceding sections, a tentative strategy can be formulated for approaching the stochastic modelling of sea-floor roughness.

- (1) Delineations of homogeneous provinces, using a province picker, such as that developed by Davis (1974), would insure some degree of stationarity, and therefore validity, for the statistics describing the area. As will be discussed in the following chapter, this province-picking algorithm must be based on the same statistical measure that underlies the model, that is, the frequency spectrum.
- (2) Generation of amplitude spectra from available data within the delineated provinces would follow. Sample lengths for spectra generation would be confined to within the province boundaries defined in stage 1. One-dimensional spectra would describe the roughness in several orientations to provide input for later modelling of topographic anisotropy.
- (3) Regression analyses would be performed on these amplitude spectra to generate the coefficients of the functional form chosen to represent the spectra. Preliminary indications are that this form will be one or several power law relationships, each of which require only two coefficients to describe.
- (4) Anisotropy of the bottom would be modelled by studying the variation of the coefficients \hat{a} and \hat{b} of the power law model as a function of direction θ . In areas where complete infor-

mation is available in two dimensions, such as a SASS or SEABEAM survey area, it might be possible to verify through regression analysis a simple θ dependent function to describe \hat{a} and \hat{b} . These functional forms, $f_a(\theta)=\hat{a}$ and $f_b(\theta)=\hat{b}$, could then define the best model for estimating model coefficients in areas where only randomly oriented track data is available.

- (5) Extension of the functional representations beyond the spatial frequency at which the surface sonar encountered its white-noise level, would be attempted by studying the spectra of deep-towed sonar and bottom photographs. It is anticipated that a general functional form, perhaps a simple extrapolation of the power law form, will be discovered. In the many areas where high resolution bathymetry is not available, this extrapolated function should provide the best available estimate of spatial frequency structure at very short wavelengths.
- (6) Incorporation of the model into existing data sets would be the final development stage. This roughness model would be calculated for 5' grid cells and merged with the existing gridded data sets being developed at the Naval Oceanographic Office. All grid cells within a homogeneous province would be represented by coefficients generated from data located anywhere within that province. By integrating this stochastic model with the existing deterministic models of oceanic depths, an essentially complete description of the sea floor will be contained in a single data base. This data base, when combined with similar gridded models of sea water sound velocity, sediment column sound velocity, sediment thickness, and

other geophysical data, would provide a comprehensive environmental data base for further acoustical, oceanographic, geological, and geophysical modelling and interpretation.

The following chapters generally follow the approach presented above, beginning with a more rigorous look at the delineation of stationary provinces. The method used for generating valid amplitude spectra are fully described in Davis (1974), and are reviewed only briefly. The regression techniques used in the study are described in detail in Appendix A. The problems of anisotropy and extension of the model into high spatial frequencies are discussed in detail in later chapters. Throughout, interpretation of the results in terms of geological processes are presented.

5. Delineation of Statistically Homogeneous Provinces

General Philosophy

The importance of defining statistically homogeneous provinces was described in the previous chapter. The validity of frequency spectra, and indeed nearly all statistical measures, requires a stationary sample space. Unfortunately, truly stationary phenomena are usually only available to theoreticians and experimentalists. The statistics of most natural phenomena vary in either time, space, or both. It is therefore essential in attempting to describe statistically non-stationary phenomena, to delineate areas in which the statistic being generated varies minimally and only within defined limits. In order to accomplish this preliminary procedure of "province picking," it is necessary to design a detection algorithm which takes account of the phenomenon being described and the statistic being used.

To illustrate this principle of matching the province detector to the statistic being generated, we begin with an elementary statistic. As an example, assume that it is necessary to describe the areal distribution of height of the people of Africa. Assume for this discussion that the desired significance of the mean requires samples of at least 10,000 individuals. One approach might be simply to divide the continent into regular square areas and randomly select 10,000 heights from each area to generate a mean. The means so generated should indeed represent the populations of these arbitrary squares.

To illustrate the effect of non-stationarity on the validity of the measured statistic, assume that in a particular sample square, the southern region is inhabited exclusively by Pygmies, averaging only 4 feet tall, while the northern region is inhabited by Watusis, averaging 7 feet tall. The method just described would predict a single population, averaging 5'6" height, inhabiting the area. In fact, very few of the individuals in the population are near this height and our statistic has failed to perform its intended function; to describe the areal distribution of heights of the population.

In order to confine our sampling to relatively homogeneous sample spaces, it is necessary to detect the boundary between independent populations prior to final sampling. The best method for accomplishing this "province picking" is to measure the mean crudely with much smaller samples, say ten individuals or even one individual over smaller areas. Even these crude measures could be sufficient to define the large gradient in population mean across the boundary. Notice that the same statistical measure (the mean) is used to describe the population and to define the province boundary. After the provinces are delineated, sampling within homogeneous provinces ensures statistical validity, at least to the degree that stationarity was confined in the province picking procedure. An additional operational advantage of the province picking procedure is that very large areas of stationary means might be detected which would require only one random sample of 10,000 individuals to describe a large area, rather than conducting several repetitive samplings using the arbitrary grid technique.

When one uses more advanced statistical measures to describe the earth, it becomes necessary to design more complex procedures for homo-

geneous province detection. The method used by Davis (1974) was described in Figure 4-2. In this application, the design of optimum survey spacing for marine gravity data collection, the statistic used was the total RMS energy in a particular spatial frequency band. The location of this band in frequency was dictated by later applications of the marine gravity data. Construction of a digital model of oceanographic sound speed requires delineating provinces in space and time based on statistics describing the shape of oceanographic profiles (T.M. Davis, personal communication, 1983).

In order to delineate stationary provinces for the description of sea-floor roughness using frequency spectra, it becomes necessary to make a crude estimate of the amplitude spectrum discretely in the spatial domain. Recall that in transforming to the frequency domain, stationarity has already been assumed, and therefore Fourier transform techniques are not appropriate. The method used in this study takes advantage of the relationship between band-limited energy in the spatial and frequency domains (Parseval's Formula), and the inferred power law form of amplitude spectra of topographic surfaces. Just as amplitude spectra represent the amplitude of component sinusoids at discrete frequencies, an equivalent estimate can be made in the spatial domain by band-pass filtering the frequency of interest and evaluating its amplitude. While the frequency domain estimate represents the least squares average amplitude over the entire length of sample, the amplitude can be estimated discretely in the spatial domain using the Hilbert Transform. This is very similar to the method developed by Davis (1974) for a single frequency band.

In order to estimate the full spectrum, it is necessary to evaluate the amplitude at several frequencies, spanning the range of the desired spectrum. This is accomplished by convolving a bank of band pass filters, centered at different frequencies, with the data and evaluating the amplitude of the band-limited signals discretely. Knowing the "power law" functional form of the spectrum in advance, one can fit the several amplitude versus frequency estimates at discrete points in space, using the iterative regression technique described in Appendix A. The regression coefficients \hat{a} and \hat{b} , now available at every point along the profile, are often highly variable and must be smoothed. Also, because the two parameters are statistically correlated, it is preferable to use the exponent of frequency (\hat{b}) and total band-limited RMS as detection parameters. Just as the presence of white noise at high frequencies must not be included in the regression analysis of the amplitude spectrum, amplitude estimates at the noise level in the spatial domain are also ignored. The method is described in detail in Appendix B, along with the results of various performance tests on signals of known properties used to calibrate the sensitivity of the detector.

Generation of Amplitude Spectra

Having delineated statistically homogeneous segments of data on the basis of their estimated frequency spectra, the next step is to generate amplitude spectra from these segments. Were the spatial domain estimates adequate, it would not be necessary to generate the spectra at all. However, due largely to instabilities in the slope (\hat{b}) parameter, those estimates are not adequate and true FFT's must be run to estimate

the model parameters. Also, the Fourier transform method has the additional advantage of estimating the amplitude at many more frequencies than the ten bands arbitrarily selected for the spatial domain algorithm.

Since the proper generation of spectra is the basis for the entire model, great care has been taken to ensure that the best estimate of the true amplitude spectrum are obtained. The techniques used are described in detail by Davis (1974) and will only be reviewed here. The computer software used in this study was modified from programs provided by T.M. Davis and is presented as Appendix D.

In using a finite length sample to represent an infinite series, the observer has in effect multiplied the infinite series by another infinite series consisting of zeros beyond the sample and ones at all sample locations. The multiplication of this so-called "boxcar" function in the spatial domain, causes the true transform of the signal to be convolved with the boxcar's transform, a sinc function, in the frequency domain (see Bracewell, 1965). The presence in the frequency domain of side lobes on the sinc function, causes energy to be "leaked" into adjacent frequencies during convolution. Because of the red-noise character of spectra of sea-floor topography, this "leakage" tends to transfer energy artificially from lower to higher frequency.

Although the use of tapered windows rather than boxcar sampling tends to reduce leakage, the preferred technique uses the method of prewhitening. Tapered windows have a sinc function transform with reduced sidelobes and a broadened mainlobe, which reduce spectral leakage at the expense of spectral resolution. In prewhitening, a specially designed high-pass filter is convolved with the signal, modifying it such that

its spectrum appears flat, or white, rather than red. When this prewhitened signal is then passed through the Fourier transform, there is no preferential transfer of energy in either frequency direction. To obtain the "corrected" spectrum which approximates that of the true (infinite) signal, the prewhitened spectrum is divided by the impulse response of the prewhitening filter. This operation is equivalent to deconvolving the filter in the spatial domain.

The importance of proper prewhitening can not be overstated. Leakage of energy into high frequencies would cause a consistent underestimation of the magnitude of \hat{b} (spectral slope), and degrade the ability of the model to estimate high frequency roughness (i.e., overestimation of amplitude at high frequencies). Figure 5-1 illustrates prewhitening by showing a raw spectrum, prewhitened spectrum, and corrected spectrum on one plot. Further examples can be found in Davis (1974).

Physical Interpretation of Spectral Model Parameters

Before examining the distribution of the spectral roughness model in selected study areas, it is worthwhile to discuss the physical meaning of the model parameters \hat{a} and \hat{b} . The proportionality constant \hat{a} in the expression

$$A = \hat{a} \cdot s^{\hat{b}}$$

where A = amplitude

s = spatial frequency

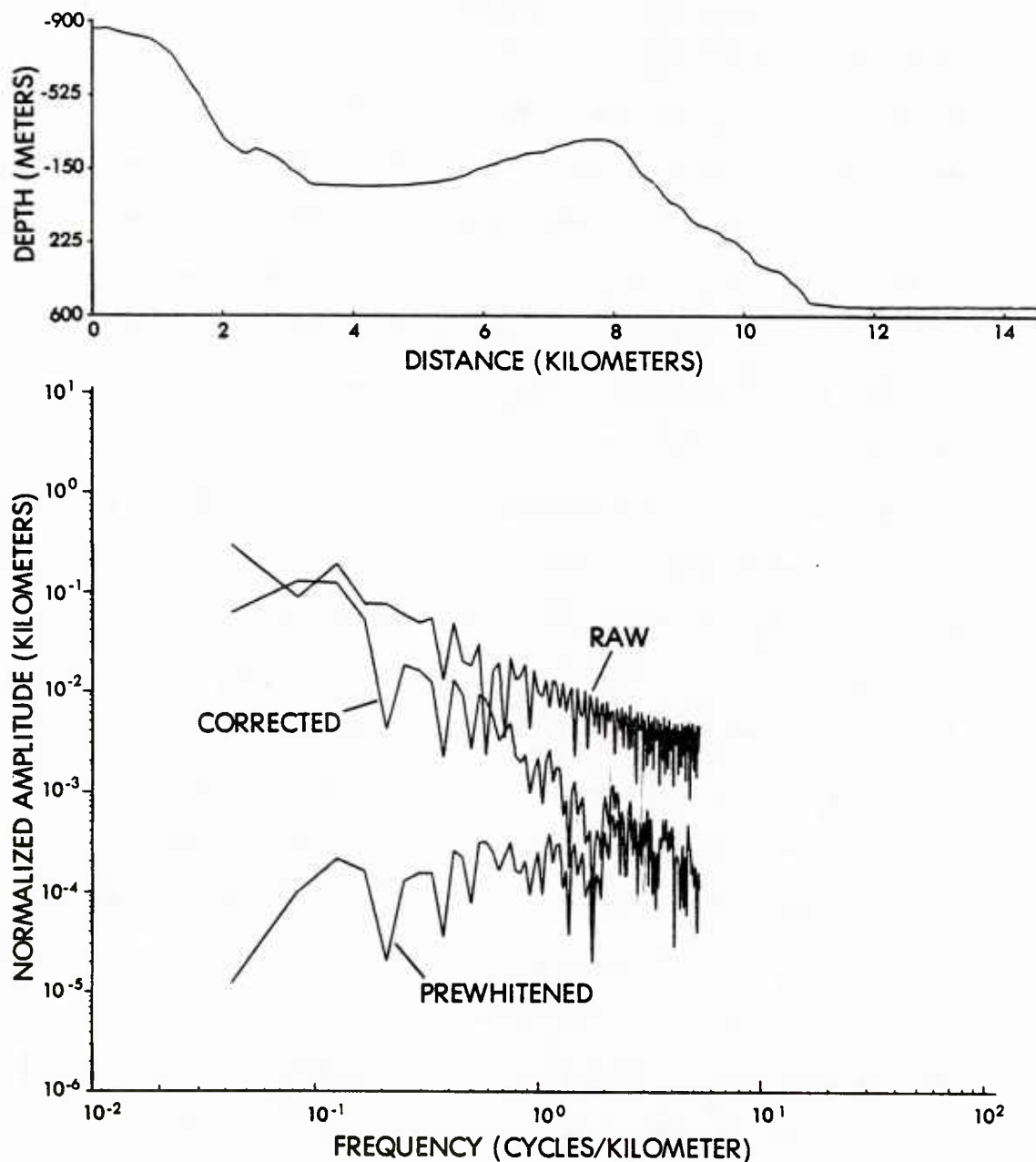


Figure 5-1 Illustration of the importance of prewhitening of amplitude spectra. The raw spectrum is the result obtained by simply performing a spectral analysis on raw data. The prewhitened spectrum is the result of performing the same analysis on data which has been convolved with a special high-pass filter. The corrected spectrum results from the quotient of the prewhitened spectrum and the frequency spectrum of the high-pass filter, and represents an estimate of the spectrum of the corresponding infinite signal from which the sample data was derived.

represents a simple scaling factor for roughness. For a given frequency (s) and exponent (\hat{b}), the amplitude (A) is proportioned to \hat{a} . Due to the method of calculation of this expression, the actual value of \hat{a} corresponds to the amplitude of the component sinusoid with a wavelength of one kilometer and is usually expressed in meters or kilometers. This particular normalization was selected because the one kilometer wavelength falls within the sampling of most surface sonar data. For example, the required 0.5 km sample rate would be obtained with a 1 minute sonar ping rate on a ship traveling 30 km/hr (or 16 knots). The value of \hat{a} does not necessarily correspond to any particular features in the signal, but only to the amplitude of the component sinusoid.

The interpretation of the exponential parameter (\hat{b}) is somewhat less intuitive. For the case of $\hat{b} = 0$, the amplitude of all component frequencies is constant and equal to \hat{a} . This is the well-known "white noise" associated with random series such as instrument noise. Such a value for \hat{b} would customarily be interpreted as instrument noise in any spectra from sea-floor topography. Values of $\hat{b} > 0$ imply that amplitudes increase at shorter wavelengths, a condition that has never been observed in bathymetric data. What is consistently observed is the case where $\hat{b} < 0$, the previously mentioned "red-noise" spectrum, in which amplitudes of component sinusoids increase with decreasing spatial frequency (longer wavelength). This indicates simply that broader features have greater height.

An interesting special case occurs when $\hat{b} = -1$. The expression

$$A = \hat{a} \cdot s^{\hat{b}}$$

becomes

$$A = \hat{a} \cdot s^{-1}$$

or

$$A = \hat{a} \cdot \lambda$$

or

$$A/\lambda = \hat{a}$$

Simply stated, for $\hat{b} = -1$, the ratio of amplitude to wavelength (or height to width) is constant and equal to \hat{a} at all scales. This condition was termed "self-similarity" by Mandelbrot (1982) and corresponds to a fractal dimension of $D = 1.5$.

One might visualize the special case $\hat{b} = -1$ as a signal which appears identical at all scales of observation. In another sense, the signal appears equally "rough" at all scales, the magnitude of roughness being prescribed by the magnitude of \hat{a} . In cases where $-1 < \hat{b} < 0$, the ratio of height to width tends to decrease at longer wavelengths, although the absolute amplitude does increase. Such signals appear rougher at high frequencies. The converse case of $\hat{b} < -1$, implies that the ratio of height to width increases at longer wavelengths, and therefore the signal appears smoother at high frequencies. Figure 5-2 summarizes these relationships.

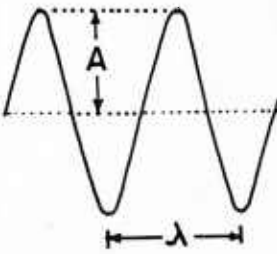

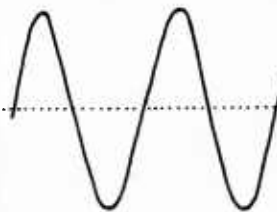
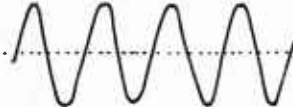
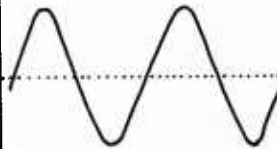
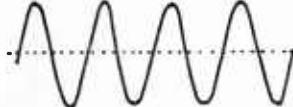
SPECTRAL SLOPE (b)	LOWER FREQUENCY COMPONENT	RELATIVE ASPECT RATIOS (A/λ)	HIGHER FREQUENCY COMPONENT
$b < -1$		$\left(\frac{A}{\lambda}\right)_{\text{Low}} > \left(\frac{A}{\lambda}\right)_{\text{High}}$	
$b = -1$		$\left(\frac{A}{\lambda}\right)_{\text{Low}} = \left(\frac{A}{\lambda}\right)_{\text{High}}$	
$b > -1$		$\left(\frac{A}{\lambda}\right)_{\text{Low}} < \left(\frac{A}{\lambda}\right)_{\text{High}}$	

Figure 5-2 Relationship of spectral slope parameter (b) to aspect ratio (A/λ) of sinusoid at different frequencies. For $b = -1$, the aspect ratio remains constant in all frequencies. For $b < -1$, the aspect ratio increases at lower frequencies. For $b > -1$, the aspect ratio increases at higher frequencies.

Although the physical interpretation of the model parameters \hat{a} and \hat{b} is clear, an important question remains as to the geological significance of these terms. Why do certain areas of the sea floor have a particular representative spectrum, and why do all spectra seem to show such a consistent power law form over large ranges of spatial frequency? An obvious hypothesis is that the spectral form reflects the unique interaction of the relief-forming processes and the materials being affected. For example, the formation of new sea-floor crust at oceanic ridge crests affects the relief of the new sea floor at all spatial frequencies. If the relief-forming process is uniform over some geographic region and interval of geologic time, there is no reason to suppose a change in the statistics of the surface being constructed, although its deterministic shape might change. Conversely, if there is a change in the relief-forming process (such as the spreading rate) or material (perhaps a change in the properties of the magma source), it is likely that the resulting relief would also be affected.

Many geological environments represent a composite of several relief-forming processes (tectonic, sedimentary, erosional) and several types of material. Such composite reliefs should result in an amplitude spectrum reflecting the composite spectra of these several processes and materials. If each style of relief is dominant over a different spatial frequency band, and each component spectrum conforms to the power law functional form observed in one-component cases, the composite spectrum should appear as a set of straight line segments on a plot of log amplitude versus log frequency. Examples of such composite spectra will be shown in a later section.

It is difficult to prove a direct relationship between statistical relief and combined process and material, but an interesting insight can be gained from a study of a highly variable environment, sedimentary microtopography. In 1981, Mark Wimbush of the University of Rhode Island deployed stereo camera on a structure on the upper continental rise northeast of Cape Hatteras. Stereo-pair bottom photographs were taken at an interval of twenty-seven days. Time-lapse photography showed that between the dates of these stereo-pair photographs, the fine scale sea-floor relief beneath the structure was altered both by biological activity and episodic bottom current events.

Two microrelief maps were generated from the stereo-pair images and these are illustrated in Figures 5-3 and 5-4. Transects of heights were taken at 0.5 cm intervals (labelled A, B, C, D) across the surface. Amplitude spectra all showed the power law form found in spectra at lower frequencies, and in addition the spectral parameters showed no significant differences in spite of the gross change in the surface (see Figure 5-5). This implies that the two surfaces merely represent two realizations of the same statistical process. In terms of frequency domain analysis, only the phase spectrum is altered by the redistribution of features, not the amplitude spectrum. This simple experiment does not unequivocally prove a causal relationship between statistical relief and process, but it does provide an encouraging result.

The Phase Spectrum

To reconstruct a profile or surface from its frequency domain representation, it is not sufficient to model only the amplitude of each com-

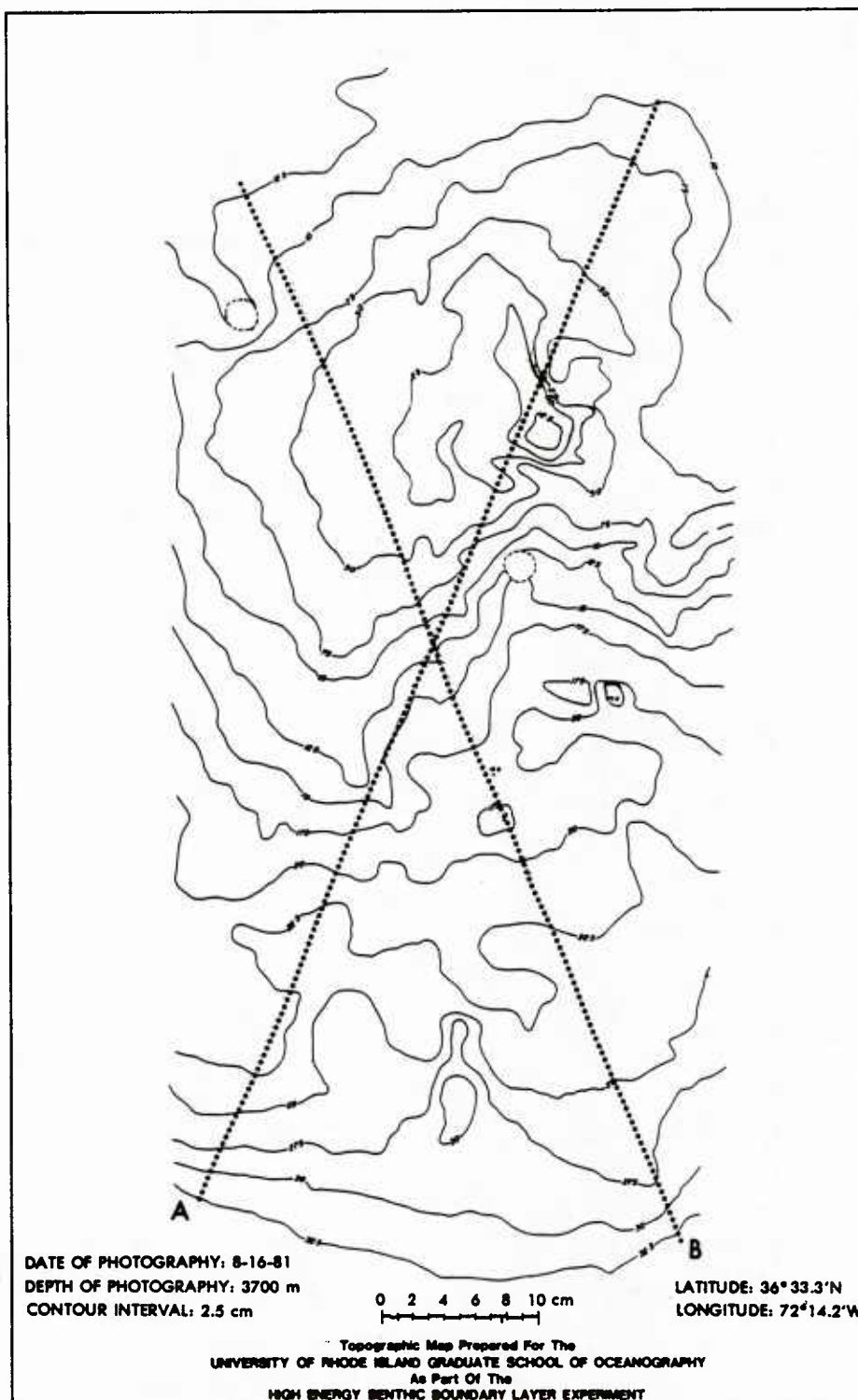


Figure 5-3 Contour representation of a bottom stereo-pair photograph collected on August 16, 1981. Dotted lines represent transects used for spectral model generation.

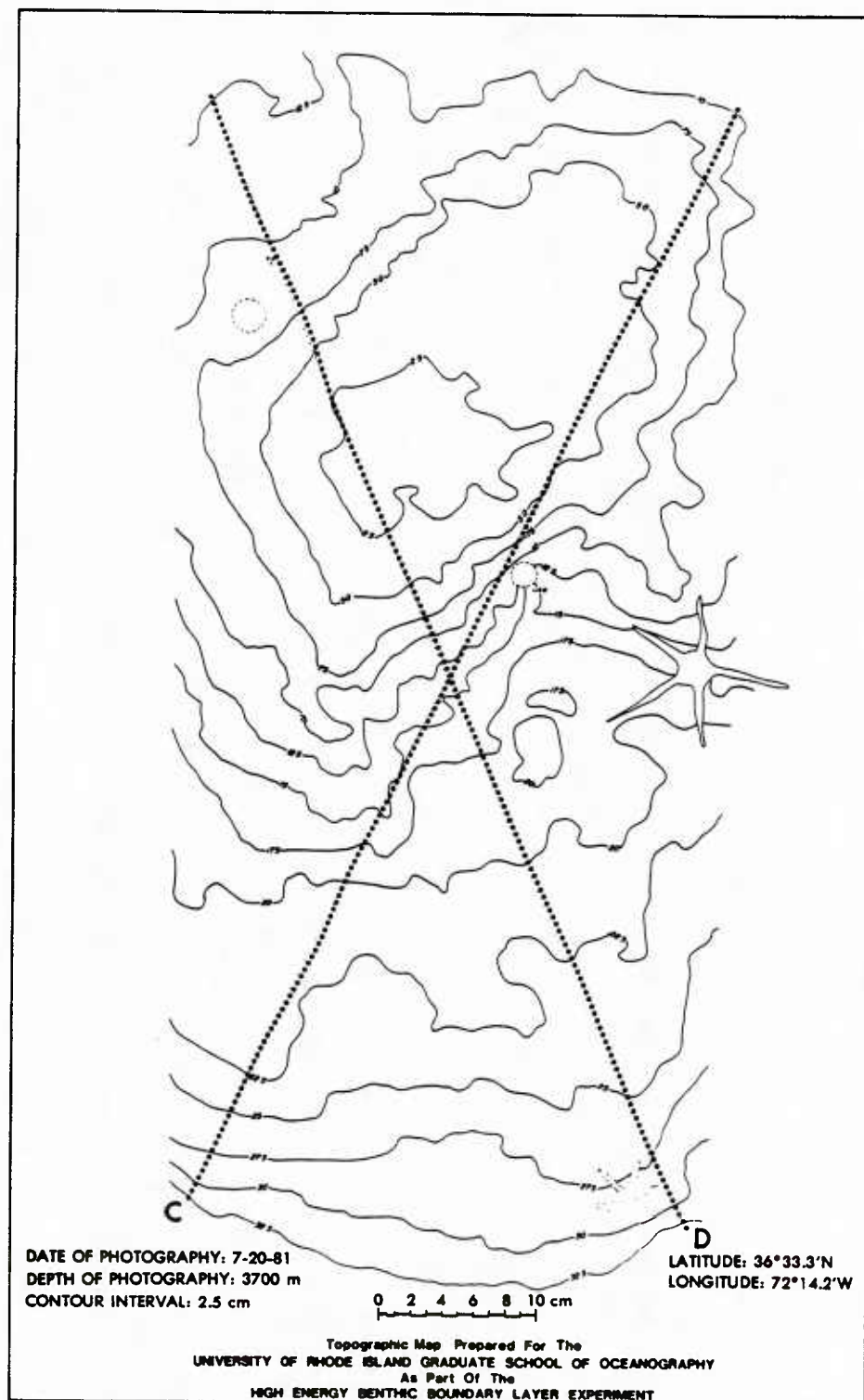


Figure 5-4 Contour representation of a bottom stereo-pair photograph collected at the same location as that shown in Figure 5-3, but 27 days earlier, on July 20, 1981. The spectral models generated along indicated transects were not significantly different from those generated from transects of Figure 5-3.

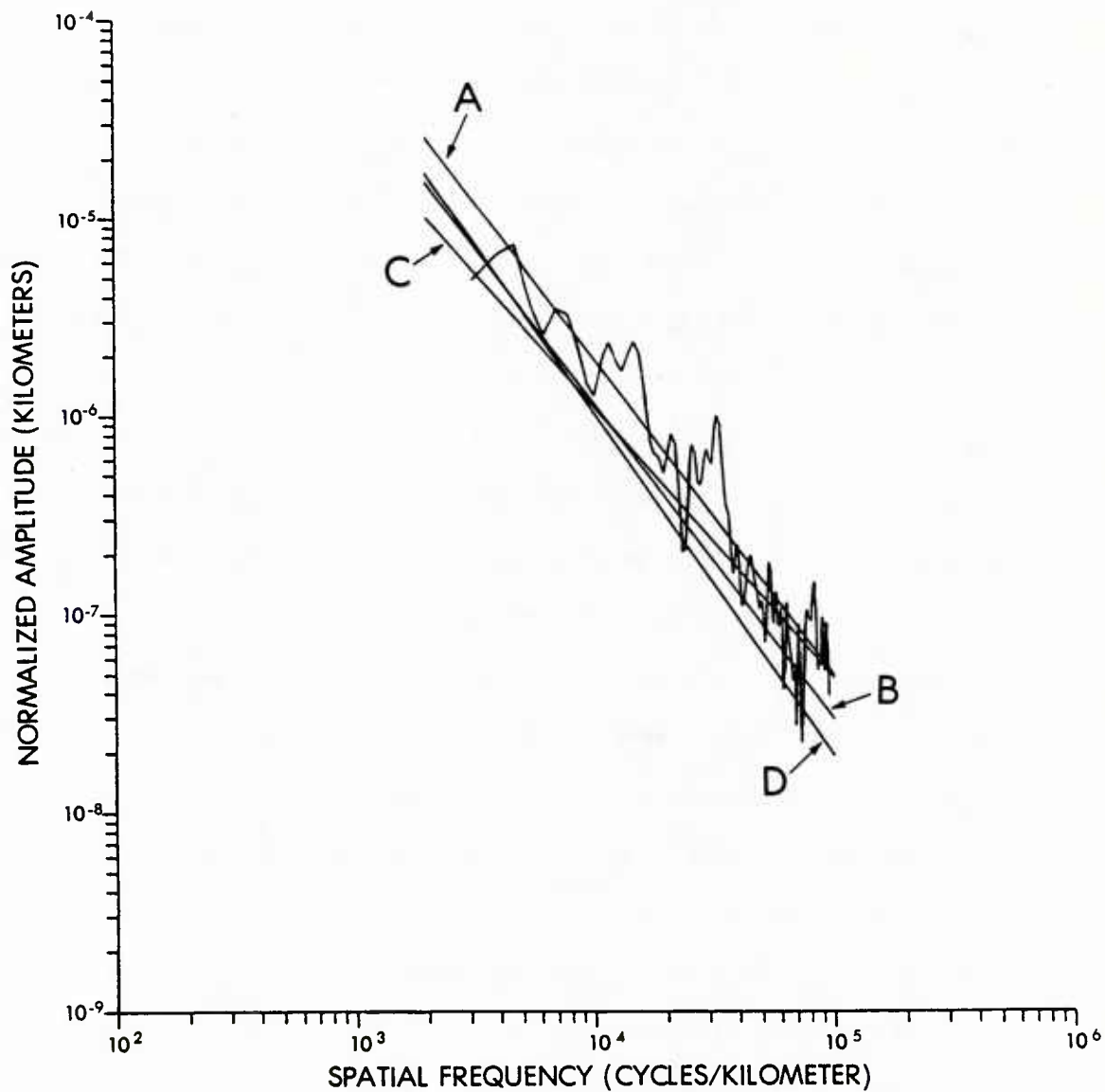


Figure 5-5 Amplitude spectrum derived from profile A illustrated in Figure 5-3. Regression lines represent model spectra from profiles A,B,C, and D. Differences between these spectra are within estimation error, indicating no significant variation in time for the microtopography at this location nor significant anisotropy within each sample.

ponent frequency. One must, in addition, define the position of each component sinusoid relative to some geographic origin. The location of each sinusoid in space is expressed by its phase relative to this geographic origin, and the composite of all component frequencies with their corresponding phases represents the phase spectrum. Since sines and cosines are trigonometric functions, phase is normally expressed as an angle between -180° and 180° .

Results from this study show that within statistically homogeneous provinces, the amplitude spectrum can be consistently modelled with a single or several power law functions. Although there is some variability of the measured amplitude around the simplified model, the calculated parameters remain consistent over often large geographic areas. However, any two sample profiles are not necessarily identical or even statistically correlated. The differences in the spatial domain manifestations of identical amplitude spectra can only be due to differences in the phase spectra.

Figure 5-6 illustrates a typical phase spectrum and the statistical distribution of its phase angles, derived from a single bathymetric profile. Several profiles were examined, which represented a variety of geographic locations and geological environments. The variability of phase angle with increasing frequency appeared to be random. A simple one-sample runs test was performed on several phase spectra, and all proved to be randomly ordered to within 95% confidence limits. The runs test is a non-parametric method (Siegle, 1956), meaning that no probability distribution of the population is assumed. Examination of the distribution of phase angles indicates a uniform statistical distribution; that is, a random distribution in which all phase angles are

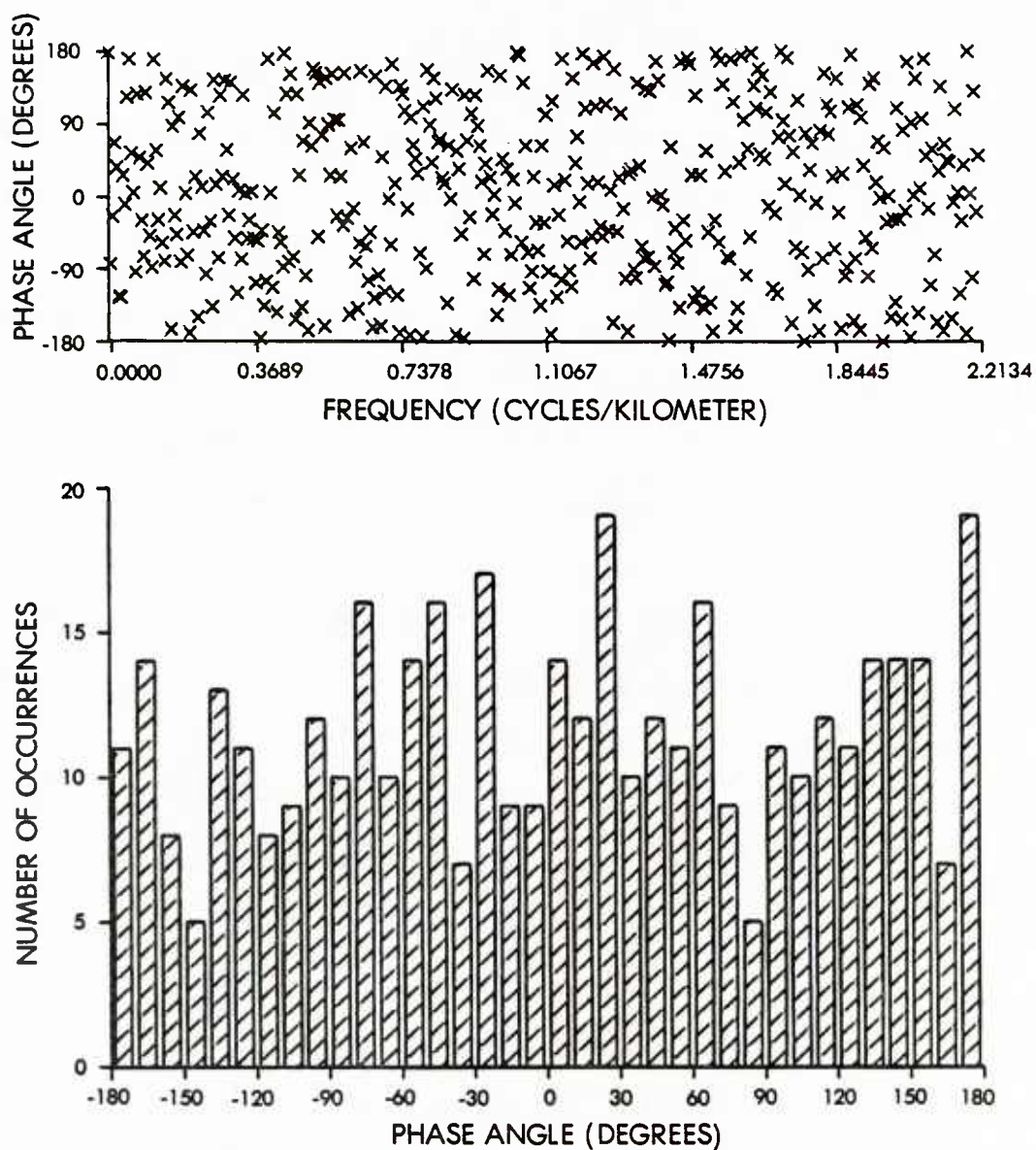


Figure 5-6 Typical phase spectrum from a bathymetric profile collected in the Cascadia Basin. The upper diagram plots phase angles versus corresponding spatial frequencies. The histogram (below) shows the distribution of phase angles by 10-degree class intervals. Statistical testing indicates the series to be uniformly distributed random noise.

equally likely to occur for any frequency component. A Kolmogorov-Smirnov goodness-of-fit test was performed on several phase spectra, and none were significantly (95%) different from the uniform distribution (Siegle, 1956).

The spatial consistency of the amplitude spectrum and the uniformly distributed random nature of the phase spectrum of topography indicate that the differences in bathymetric surfaces within statistically homogeneous provinces simply represent multiple realizations of the same statistical process. The observed changes in the microtopography recorded in Figures 5-3 and 5-4 can be modelled by combining two different random phase spectra of the same distribution with the known amplitude spectrum. With the functional representation of the amplitude spectrum for an area, a "typical" profile or surface can be produced by generating a uniformly distributed set of random numbers to represent the phase spectrum, and performing an inverse Fourier transformation to the space domain.

The concept of representing the sea floor as a deterministic surface combined with stochastic variability was introduced in an earlier section. In that discussion, the deterministic components appeared as a smoothed, long wavelength surface which was combined with a higher frequency, stochastic roughness component. By describing the higher frequency components with a spectral representation, we can now visualize the amplitude spectrum as being determined (by modelling) and the phase spectrum as being a purely random (stochastic) process.

Creation of the Model and Interpretation

Having developed the algorithms for defining quasi-stationary provinces and generating valid amplitude spectra, these methods were applied to an area off the Oregon coast. The area (42°N - 45°N , 130°W - 124°W) was selected due to data availability and the variety of geologic environments represented within this relatively small area. The area includes the continental margin (shelf and slope), Astoria deep-sea fan, Tufts Abyssal Plain, Gorda Rise spreading center, Blanco Fracture Zone, the Cascadia Channel and numerous seamounts. All spectral estimates were generated from data collected on the SASS multibeam sonar system by the U.S. Naval Oceanographic Office. Only center beam depths were used in this portion of the analysis, in order to simplify processing.

Figure 5-7 compiles the results of the combined province-picking and spectra-generating procedures. The areas delineated by the various shading patterns represent stationary provinces with similar ranges of the \hat{a} statistic; that is, the amplitude of the component sinusoid at a wavelength of one kilometer. In cases of coincident values at crossing lines, a simple average was taken, ignoring for this analysis the effects of anisotropy. In many cases, provinces separated in the province-picking procedure became recombined in the final spectral model, indicating that the provincing algorithm used is more stringent than the levels selected for presentation.

Within each of the larger provinces, the spectral slope parameter (\hat{b}) estimates were averaged and these values shown within the provinces. The standard deviation of all estimates within any province was less than 0.1 in all but one case shown. There is one province in which the

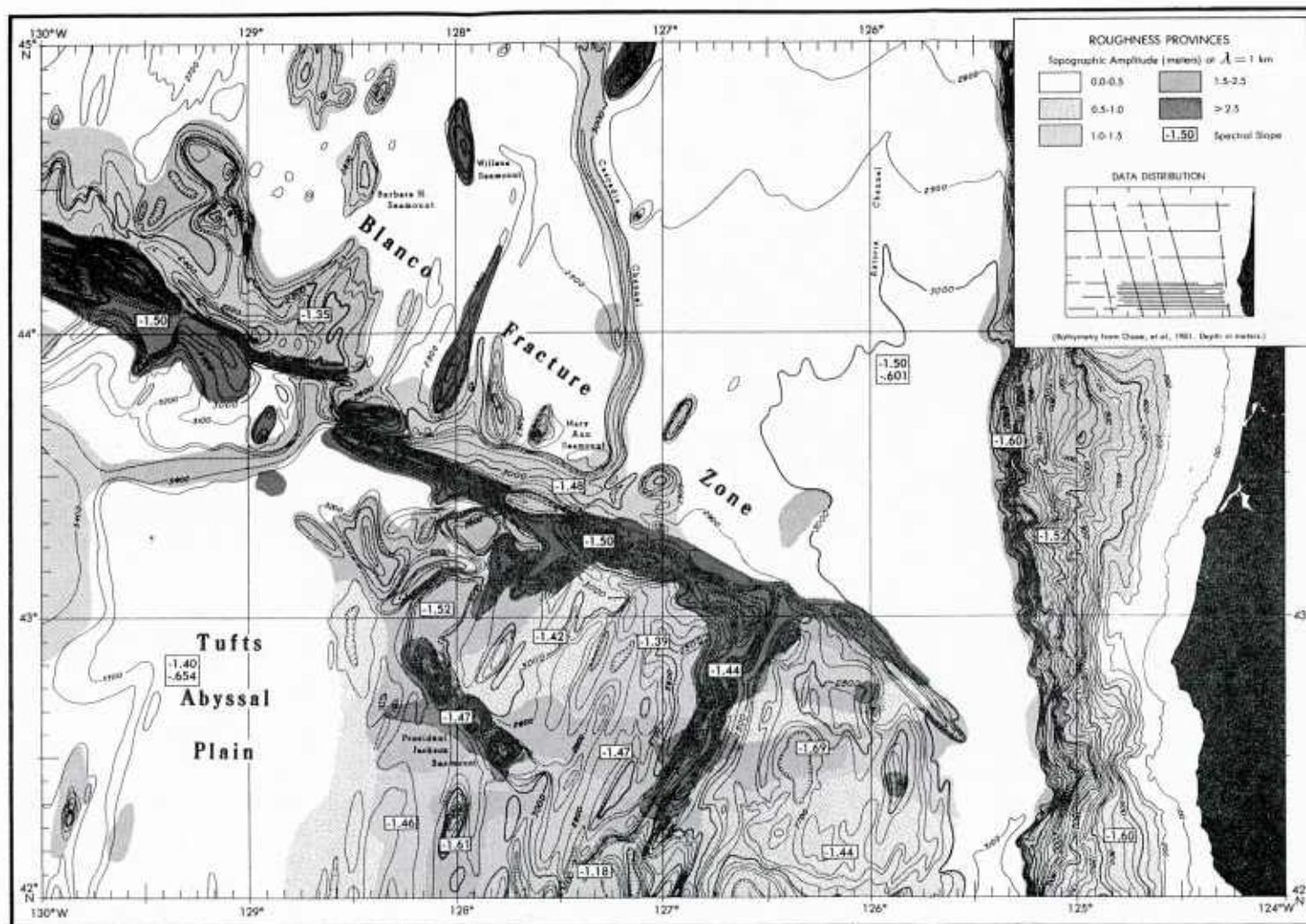


Figure 5-7 Distribution of roughness in the vicinity of the Gorda Rise, Northwest Pacific Ocean.

slope parameter is different in two areas within a single shading pattern (bottom center of chart). Many roughness province boundaries coincide with obvious physiographic province boundaries. In these cases, the bathymetry was used to trace the province boundaries between sample spectra. In many other cases, no boundary was obvious in the bathymetry and such tracing was not possible; that is, what appears as an abrupt boundary may represent simply an arbitrary contour of a continuous gradient. Notice also that the illustrated bathymetry from Chase et al. (1981) was based on a totally different data set than that used for spectral model generation, and therefore some provinces appear in the model which are apparently unsupported independently in the bathymetry.

The gross distribution of the roughness statistic \hat{a} corresponds fairly well with what one would expect intuitively. The roughest areas ($\hat{a} > 2.5$ m) are located at the Gorda Rise crest, Blanco Fracture Zone and over most seamounts, in particular the President Jackson Seamounts. The least rough areas correspond to the sedimentary provinces of the Tufts Abyssal Plain, Cascadia Basin, the Astoria deep-sea fan, and the continental shelf. The Cascadia Channel appears as an intermediate roughness province which can be traced very easily through the Blanco Fracture Zone and onto the Tufts Abyssal Plain. The Astoria Channel, located to the east of the Cascadia Channel, is too narrow (< 8 km) for this analysis and thus does not appear as a separate province.

Within this gross distribution of roughness, some more subtle patterns can be identified. The continental margin between the shelf and abyssal plain appears to be banded with the topography becoming generally rougher down slope. This particular continental slope represents a slowly converging margin between the North American Plate and the Juan

de Fuca-Gorda Plate. Carson (1977) and Barnard (1978) have both examined this convergent margin in areas to the north off the coast of Washington, and both present seismic cross-sections of this area. Presumably, similar processes are at work along the Oregon margin. Barnard (1978) infers a change of compression rate from 2.3 cm/year before 0.5 mybp to a present rate of 0.7 cm/year. Deformation of Cascadia Basin sediments is progressing westward, making the deepest areas of the margin also the most recently deformed. This westward progression of deformation process is expressed in the bathymetry as a downslope increase in surface roughness. Barnard (1978) classifies the slope terrain into an upper slope extending to a depth of about 1500 m, and an accretionary "borderlands" complex of en-echelon, anticlinal ridges. Between these ridges are sediment-filled basins. These physiographic divisions, derived by qualitative observation of the geological structure of the region, correspond closely to the roughness model generated by quantitative methods.

The Gorda Rise is one of the more active areas of the world sea floor, and a corresponding complexity is evident in the derived pattern of bottom roughness provinces. Atwater and Mudie (1973) reviewed the tectonic history of the area. Additional history of spreading rate and spreading direction changes can be found in Elvers et al. (1973). Much of this tectonic history may be peripheral to this study because the sea floor affected is now buried beneath the Tufts Abyssal Plain and Gorda Deep-Sea Fan sediments.

One interesting feature of the bottom roughness chart presented in Figure 5-7 is the very rough ridge crest which terminates abruptly on either flank. The full width of the feature is about 25 km. Were

ridge- forming processes constant through time and ridge crest relief "frozen" into the topography, the same roughness would be expected to persist, at least in long wavelengths, on older sea floor. The other major process affecting the ridge flanks, sedimentation, would be expected to affect the short wavelengths initially (due to their lower amplitude), and form a smooth transition zone, not the abrupt boundary observed in the roughness pattern. Magnetic data from the area indicate that this zone falls within the Bruhnes-Matuyama boundary and must therefore represent crust younger than 0.7 my. Recalling that Barnard (1978) found evidence of a slowing of compression rate on the continental margin at a time younger than 0.5 mybp in areas to the north, it is possible that this roughness feature reflects the same change in process, most likely a slowing of spreading rate. Future examination of other ridge axes should reveal whether this pattern is unique to the Gorda Rise or present under other tectonic conditions.

Perhaps equally interesting is the abrupt termination of this ridge crest at latitude 42°20'N. The roughness values drop (as supported by three tracklines) two and three roughness levels at the feature's terminus. This disruption of the ridge crest falls along a trend which encompasses President Jackson Seamounts and other seamounts to the northwest, and a major (900 m) bathymetric deep to the southeast. The break in the ridge crest trend also appears in the bathymetric chart.

Hey (1977) developed a "propagating rift" model to describe the plate geometrics and magnetic anomaly pattern found on the Juan de Fuca Ridge by the Pioneer survey. According to this model, the growing spreading center propagates along strike as the dying spreading center becomes inactive and is added to one of the rigid plates. As this proc-

ess continues through geologic time, a V-pattern of fossil spreading centers forms a "propagator wake", as is illustrated in Figure 5-8. This same pattern is found in the isosynchronous magnetic anomaly pattern. Since this model was proposed, similar processes have been observed on other spreading centers, in particular the Cocos-Nazca spreading center (Searle and Hey, 1983).

A propagating ridge crest model offers one explanation for the abrupt termination of the Gorda Rise crest shown in Figure 5-7. In order to test this hypothesis, a magnetic anomaly map of the Gorda Rise was constructed and is illustrated in Figure 5-9. The chart is based on original magnetic anomaly data collected by the U.S. Naval Oceanographic Office. The V-pattern associated with the "propagator wake" is evident, extending to the east and northwest from the ridge crest at 42°N. The direction of the V-pattern indicates that the ridge crest to the north is propagating toward the south at the expense of the southern portion of the Gorda Rise crest. The geometry of the schematic model by Hey (1977) for the Juan de Fuca Ridge (Figure 5-8), represents a nearly perfect analog to the magnetic anomaly pattern of Gorda Rise (Figure 5-9). It would appear that the abrupt termination of the high roughness zone shown in Figure 5-7, is due to its association with the tip of a propagating rift system.

Another feature of interest in the distribution of the \hat{a} parameters in Figure 5-7 is the existence of east-west trends of selected roughness provinces on the ridge flank. One might have expected roughness provinces to align themselves sub-parallel to the ridge strike, perhaps reflecting changes in processes through time being felt along the length of the ridge axis. This is the case with the very rough central valley

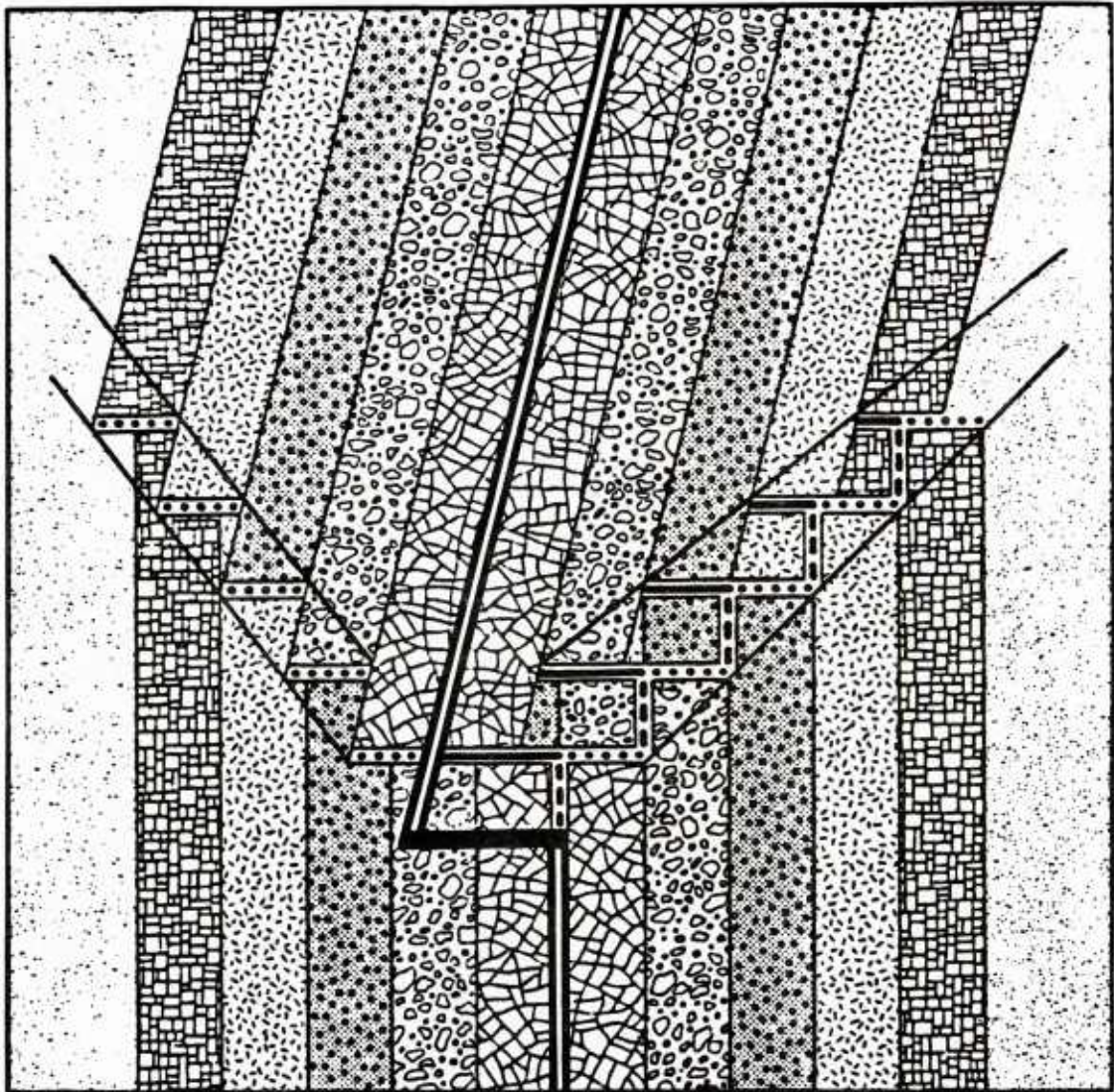


Figure 5-8 Schematic illustration (from Hey, 1977) of the pattern of isochronous seafloor resulting from a southward propagating rift. Double lines represent active spreading centers, dashed lines are fossil spreading centers, heavy line is active transform fault, and dotted lines are associated fracture zones. Diagonal trend lines indicate the so-called "propagator wake".

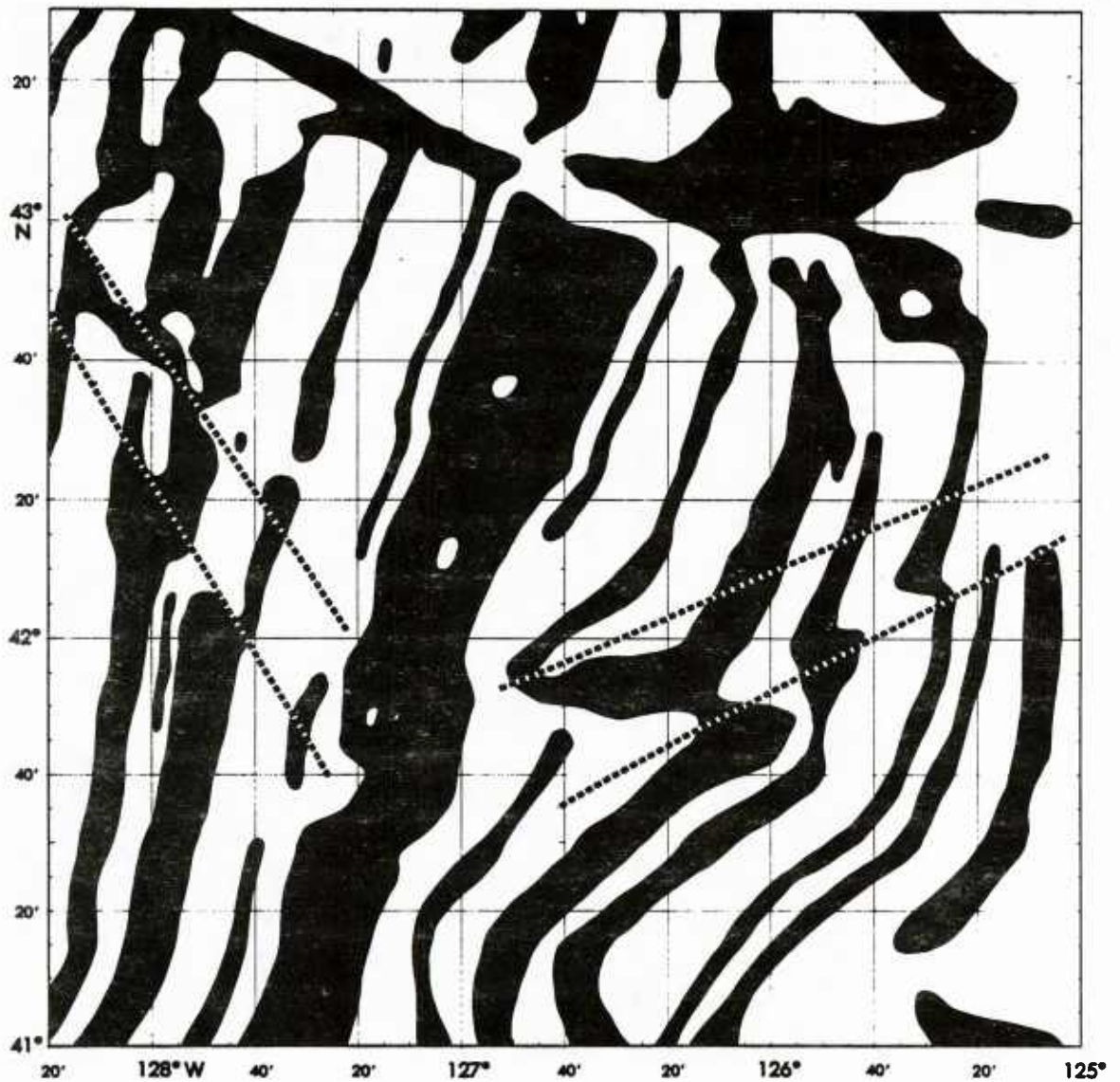


Figure 5-9 Magnetic anomaly chart of the Gorda Rise area. Positive anomalies are shown in black; negative anomalies are shown in white. The northeast-southwest trending Gorda Rise is obvious as is the northwest-southeast trend of the Blanco Fracture Zone near the northern limit of the chart. Compare the inferred "propagator wake" (indicated by dashed lines) to the theoretical model of a propagating rift illustrated in Figure 5-8.

portion. The east-west trend of roughness indicates instead relief-forming processes which act relatively constantly through time, but quite variably along the ridge strike. Francheteau and Ballard (1982) describe the along-strike variability of processes along the East Pacific Rise, and relate the changes to distance from the ridge crest/fracture zone intersection. The change in process is expressed by the relative importance of fluid lava flows and pillow lava flows. These petrologic changes are in turn associated with the elevation of the rift valley along the ridge crest; topographic highs are associated with high ratios of fluid lavas and topographic lows associated with pillow lavas. Indeed the shallowest portion of the Gorda Ridge segment is located near latitude $42^{\circ}45'N$, which shows relatively low roughness values as one would expect from the sheet-like flow of fluid lavas. Ridge flank areas become rougher adjacent to deeper axial valley segments, which might reflect the rougher surface of pillow lavas. Although other explanations for the trend of roughness on the ridge flanks could be put forth, the distributions found in this study are consistent, although not necessarily typical. Extension of the model to more thoroughly investigated ridge crests should shed light on this particular hypothesis.

The patterns apparent in the distribution of \hat{a} are not as evident when one examines the distribution of the spectral slope (\hat{b}). It is clear that the "universal" value of -1 for the spectral slope inferred by Bell (1975b) and others is not supported by this modelling effort. The reason for this discrepancy is not readily apparent, however the attention given to defining stationary sample space in this study does represent one major difference in method. In order to test this hypoth-

esis, amplitude spectra were generated for several profiles in the Gorda Rise area which spanned multiple stationary provinces. The effect of these extensions was to reduce the degree of statistical homogeneity of each profile. The computed spectral slope (\hat{b}) parameters for the resulting amplitude spectra converge consistently to the value $\hat{b} = -1.0$ as longer profiles are tested. Figure 5-10 illustrates one such long profile extending nearly 500 km from the Oregon coast. The profiles analyzed by Bell (1975b) were often much longer. No formal statistical argument for this convergence to $\hat{b} = -1.0$ will be attempted here, however, it would appear that the concatenation of multiple profiles of differing spectral characteristics results in a profile which resembles a random walk. The need to define statistically homogeneous sample spaces before generating statistics is clearly demonstrated.

Most slope values shown in Figure 5-7 cluster about -1.5 with the exception of the smooth ridge axis segment south of 42°20'N. The two large sedimentary provinces are represented by two values for spectral slope. Figure 5-11 illustrates a typical amplitude spectrum from these sedimentary provinces. The spectrum clearly separates into two distinct straight-line segments of different slope. The average values of these distinct slopes for all profiles is given in the corresponding boxes (see Figure 5-7). If the hypothesis is accepted that the characteristic spectral slope of amplitude spectra of sea-floor topography represents a dominant relief-forming process, these spectra should represent areas where two processes are at work, affecting the relief in different spatial frequency bands. It is likely that the higher frequency band ranging from $\lambda = 2.5$ km and with $\hat{b} = -.6$, represents the sedimentary regime in these areas. The lower frequency process with $\hat{b} < -1.4$, is less

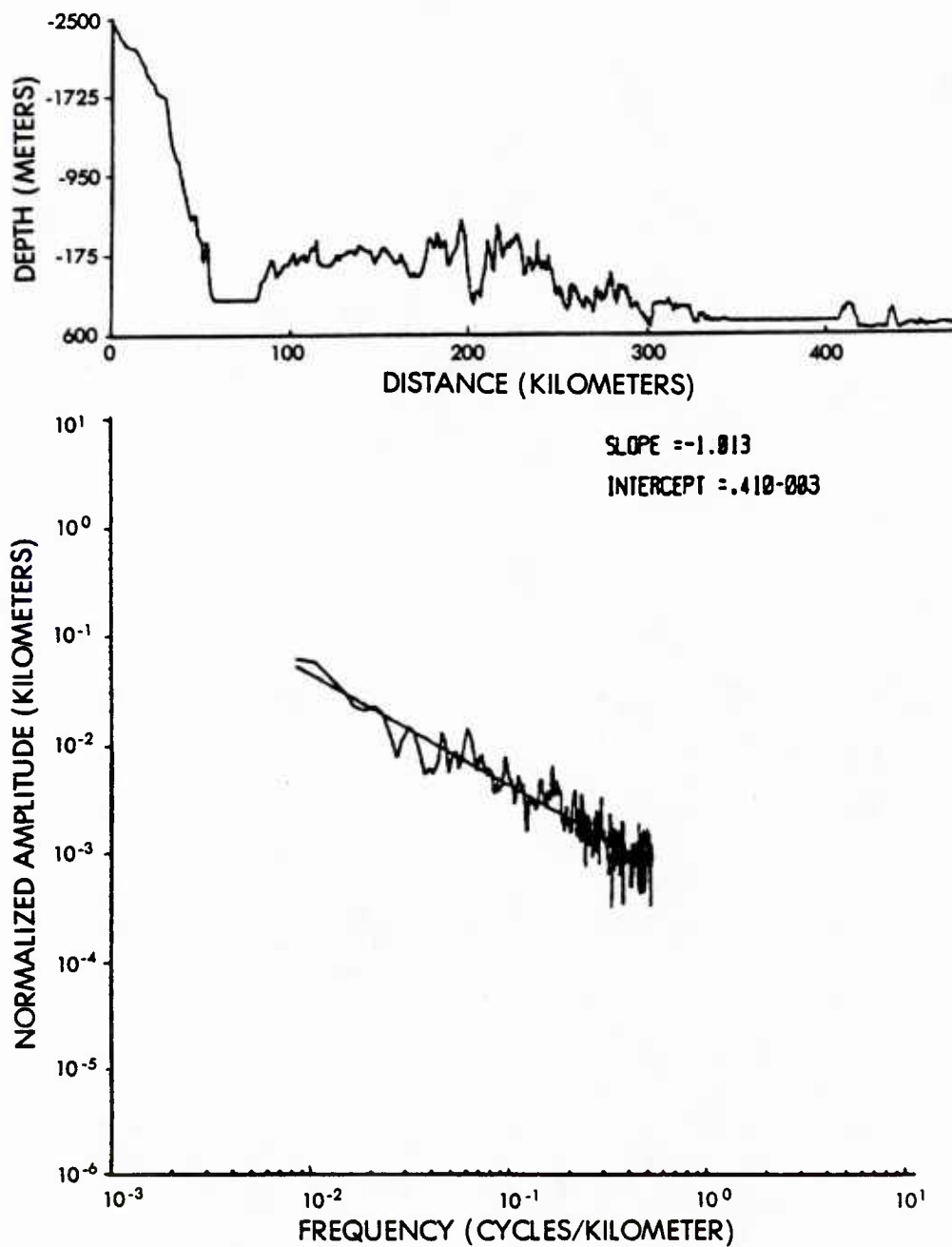


Figure 5-10 Amplitude spectrum of a long bathymetric profile, which encompasses several statistically homogeneous provinces. The inclusion of non-stationary segments into the analyses results in a spectral slope parameter which approaches $b = -1.0$.

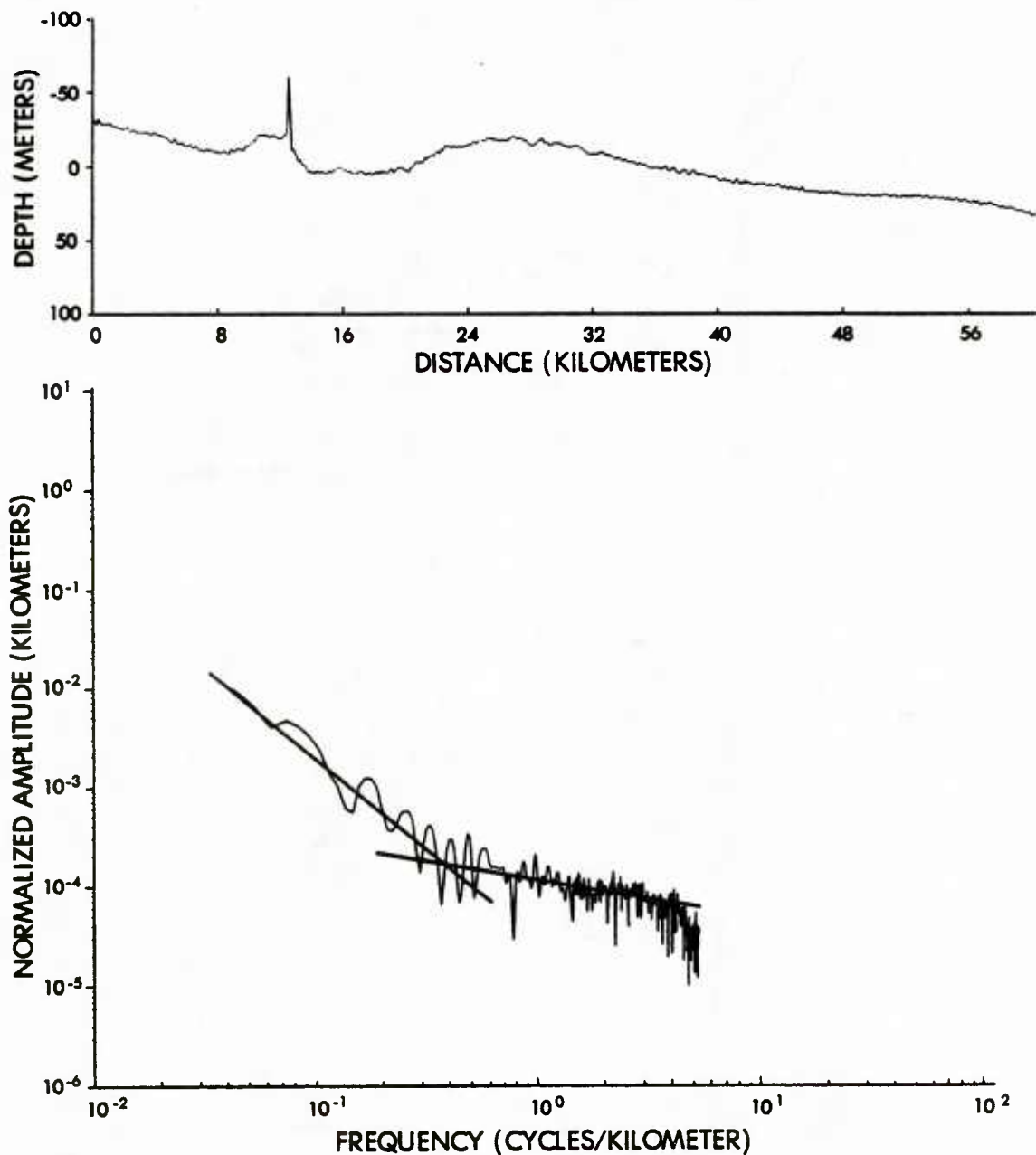


Figure 5-11 Typical amplitude spectrum of profiles collected on the Tufts Abyssal Plain. Spectrum shows two distinct straight-line segments which intersect at a spatial frequency of ~ 0.4 cycles/km. The longer wavelength portion is described by $\hat{b} = -1.847$, $\hat{a} = 0.0294$ m. The shorter wavelength segment is described by $\hat{b} = -0.541$, $\hat{a} = 0.113$ m. Profiles from the Cascadia Basin province have similar spectra, however the model parameters are slightly different.

obvious, but may well represent an underlying tectonic effect due perhaps to the compressional nature of the area overprinting a long wavelength relief on the smooth sediment.

This general correspondence of $\hat{b} < -1$ in tectonic provinces, and $-1 < \hat{b} < 0$ for sedimentary provinces is found in many areas outside this study area. The reason for this general relationship can only be speculated upon. Recall from the previous section that $\hat{b} < -1$ requires that the ratio of height to width of component features, increase at longer wavelengths. If one envisions tectonic relief forming processes, the entire morphology is constructed and then erosional and sedimentary processes begin smoothing small features first, progressing to constantly larger scales. In sedimentary processes, one can envision a smooth layer of sediment being affected by bottom current interaction for example. This constructive process begins at the highest spatial frequencies and progresses to larger scales. This is in agreement with the relationship of $-1 < \hat{b} < 0$, in which the ratio of height to width of component features increases at shorter wavelengths.

The study area illustrated in Figure 5-7 was selected because of its rich geological diversity. As such, the distribution of roughness provinces is correspondingly complex. To allow a comparison with a more tectonically stable area of the world ocean floor, a large number of tracklines off the United States east coast were analyzed to compare a passive continental margin. Although the trackline density was not adequate for a complete chart to be drawn, one interesting relationship was discovered. An extremely large area of the continental margin, comprising most of the continental rise, was found to have in common a very distinct amplitude spectrum. Figure 5-12 illustrates a typical ampli-

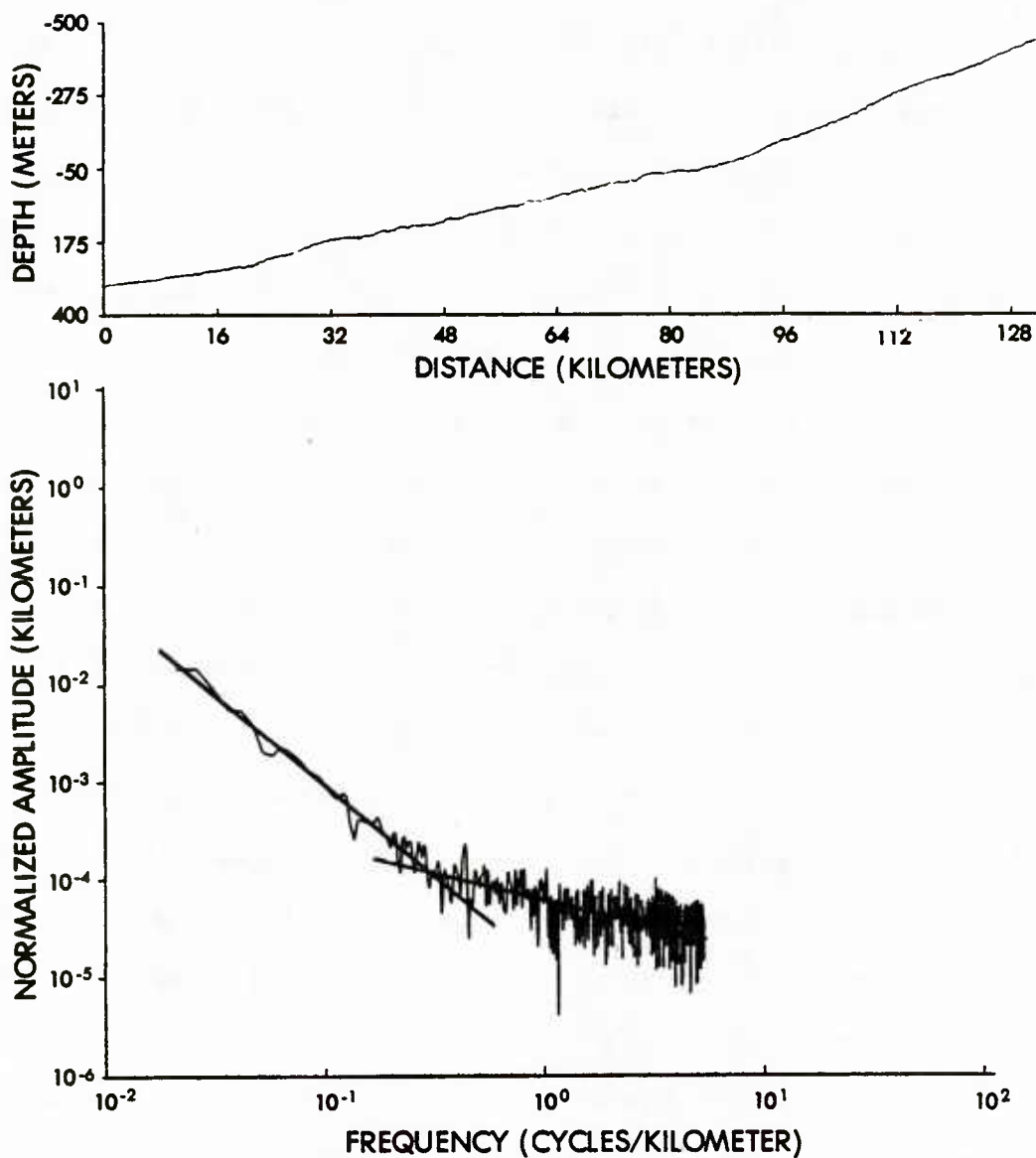


Figure 5-12 Typical amplitude spectrum of profiles collected on the Continental Rise, east coast U.S. All fourteen profiles examined in this province (shown in Figure 5-13) show nearly identical patterns. The two linear segments in this example intersect at ~ 0.3 cycles/km., with $\hat{b} = -1.813$, $\hat{a} = 0.0142$ m. for the longer wavelength model, and $\hat{b} = -.524$, $\hat{a} = 0.0645$ m. for the shorter wavelength model.

tude spectrum from this large province, and shows the same two-process nature of the spectrum in Figure 5-11. In fact, this spectrum is almost identical to the measured spectra from the Tufts Abyssal Plain and the Cascadia Basin.

Figure 5-13 shows the location of profiles with this characteristic spectrum. Some of these profiles are over 200 nm long, and the profiles are distributed over an area more than 1000 nm in extent. The total standard deviation for the spectral parameters in all fourteen profiles was only 0.15 for the slope (\hat{b}) parameters and 0.02 meters for the intercept (\hat{a}) parameters. These values apply to both the lower frequency and higher frequency line segments. The area may well extend even further northeast or southwest. Profiles are only broken by seamounts or deep-sea channels associated with submarine canyons. As such, one can see that the areal extent of a roughness province with a given level of allowed non-stationarity, can vary from hundreds of thousands of square miles to the slopes of a single seamount.

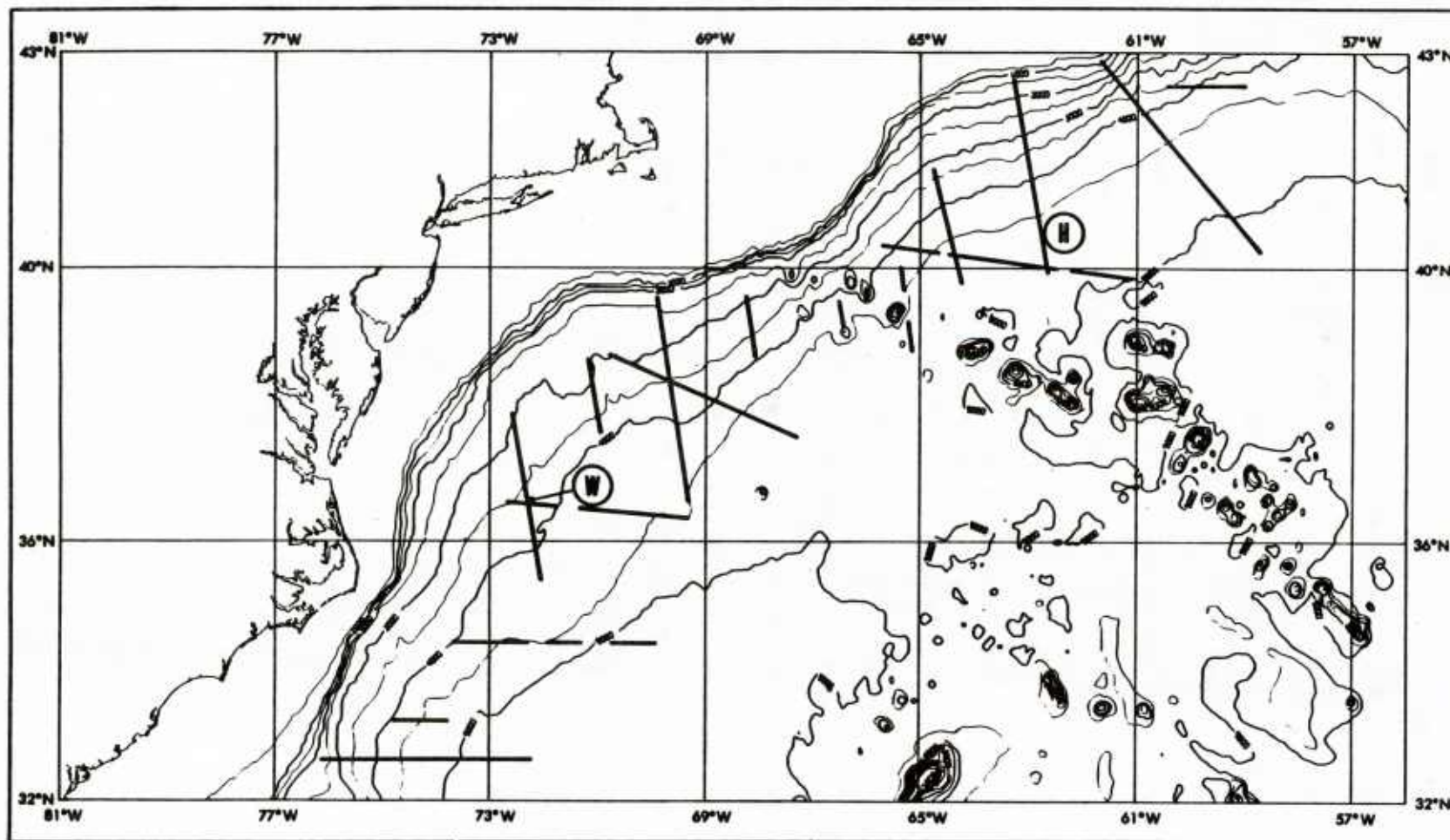


Figure 5-13 Location of bathymetric profiles showing nearly identical amplitude spectra. Bathymetry is automatically contoured (in meters) from the five-minute gridded Digital Bathymetric Data Base (DBDB) produced by the Naval Oceanographic Office. H marks the location of the HEBBLE area. W marks the location of the bottom photographs illustrated in Figures 5-3 and 5-4.

6. Anisotropy of Surfaces

The necessity of directionally treating anisotropic surfaces was introduced in Chapter 4. Any statistic generated from a one-dimensional profile of a two-dimensional surface is only valid in all directions if that surface is isotropic. This chapter examines the importance of anisotropy in detail. A simplified theoretical model of the effect of anisotropy on the frequency spectra of directionally sampled profiles is formulated and tested. Such spectra are generated for two areas of the sea floor where complete, two-dimensional bathymetric data are available from multibeam sonar. An identical study is performed on data from side-scan sonar. These results are then compared to the theoretical model. Next, the possibility of estimating such two-dimensional functions from randomly oriented bathymetric profile data is discussed.

Theoretical Model

Before examining the effect of anisotropy on measured frequency spectra derived from actual bathymetric profiles, it is instructive to examine a very simple theoretical model of this effect. Several of the concepts introduced in Chapter 4 will be utilized. There it was shown that the effect of one-dimensionally sampling a sinusoid which has been extended to two dimensions (see Figure 4-6), is to stretch the true wavelength as,

$$\lambda' = |\cos^{-1}\theta| \cdot \lambda$$

where

λ' = apparent wavelength

λ = true wavelength

θ = angle of sampling (0° = perpendicular
to linear trend)

This relationship can then be combined with the similarity theorem of Fourier Transforms to yield the transform pair

$$f(|\cos \theta| \cdot x) \supset |\cos \theta|^{-1} \cdot F(s/\cos \theta)$$

Recall that these relationships were formulated for a single component wave form extended to two dimensions. Actual sea-floor topography has a spectrum which is continuous and conforms to a power law functional form

$$A = a \cdot s^b$$

To extend the model to the continuous case, one can envision generating a topographic profile (or other signal with continuous power law form, such as a random walk model), and extending all points on the profile to the second dimension. This surface is then sampled in various directions and the spectrum of each profile evaluated for a and b above.

Combining the above relationships yields

$$f(|\cos \theta| \cdot x) \supset |\cos \theta|^{-1} \cdot a \cdot (s/\cos \theta)^b$$

or equivalently

$$f(|\cos \theta|^{-1} \cdot x) \supset |\cos \theta| \cdot a \cdot (s \cdot \cos \theta)^b$$

or

$$F(s, \theta) = |\cos \theta| \cdot a \cdot (s \cdot \cos \theta)^b$$

where $F(s, \theta)$ is the Fourier transform of $f(|\cos \theta|^{-1} \cdot x)$ expressed in terms of θ and s . The coefficient a can now be expressed as a function of θ as

$$a(\theta) = |\cos \theta| \cdot a$$

which can be generalized to

$$a(\theta) = |\cos(\theta - \theta_0)| \cdot a$$

where θ_0 is the azimuth perpendicular to the linear trend. Notice that for $\theta = \theta_0$, that is a profile generated perpendicular to trend, $|\cos(\theta - \theta_0)| = 1$ and $F(s, \theta) = a \cdot s^b$, the original function. For $\theta - \theta_0 = \pm 90^\circ$, $|\cos(\theta - \theta_0)| = 0^\circ$ and $F(s, \theta) = 0$, that is, for profiles sampled parallel to strike, the series is a constant (normalized to zero) and therefore contains no energy. The parameter b is independent of θ .

Figure 6-1 illustrates the hypothetical "plane wave" surface that is used in this simple model. As a test of the above theory, radial transects of the surface were generated and the resulting profiles input to the standard Fourier transform routines used throughout this study. Figure 6-2 depicts the sampling patterns used to generate the profiles.

Randomly Generated Plane Wave

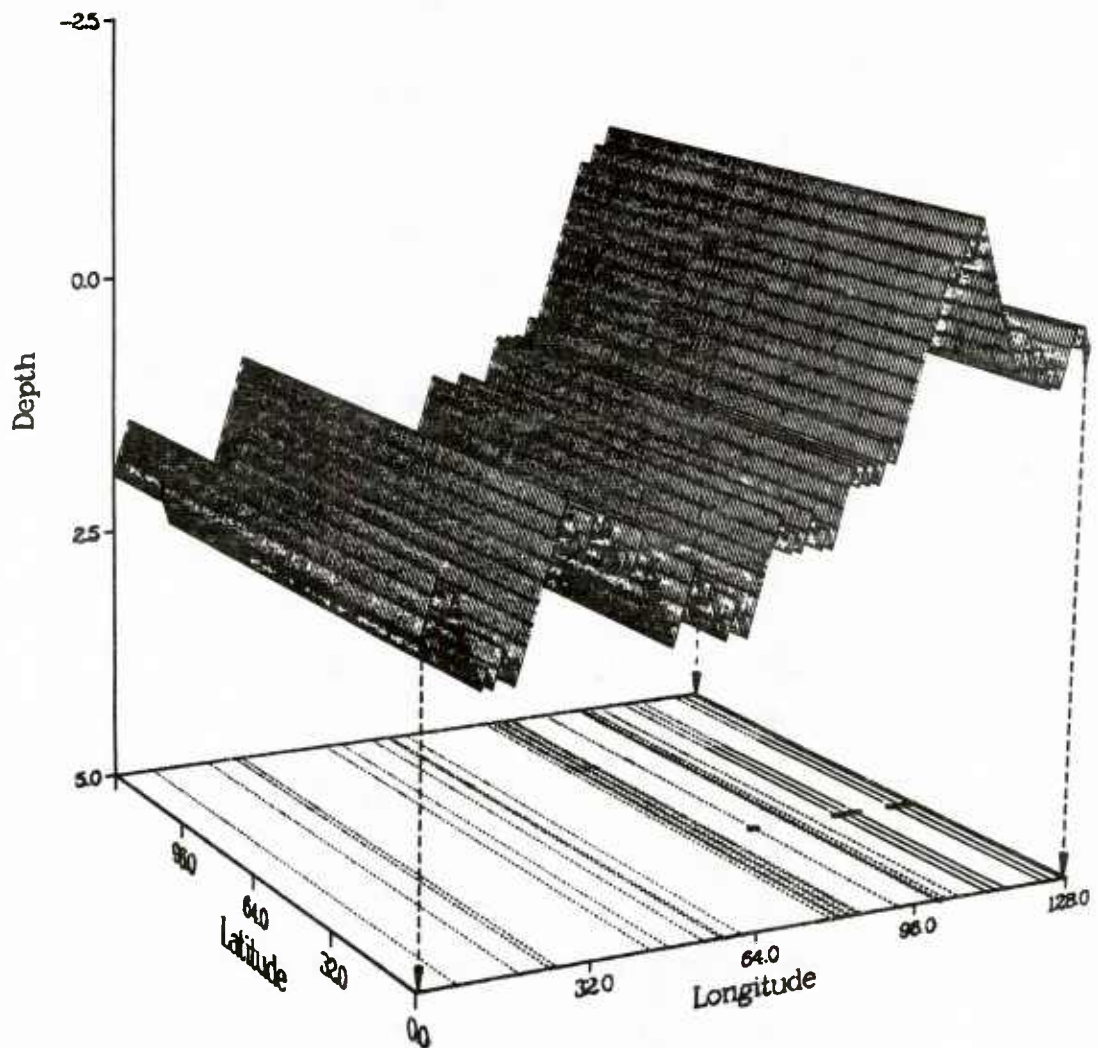


Figure 6-1 Graphic representation of an elementary theoretical model for anisotropic surfaces. The surface is created by generating a random walk (with theoretical amplitude spectrum of $A = a \cdot s^{-1}$) in the x (90° azimuth) direction. These values are simply extended to the second dimension, creating a lineated surface with strike = 0°. Viewpoint is from the southwest.

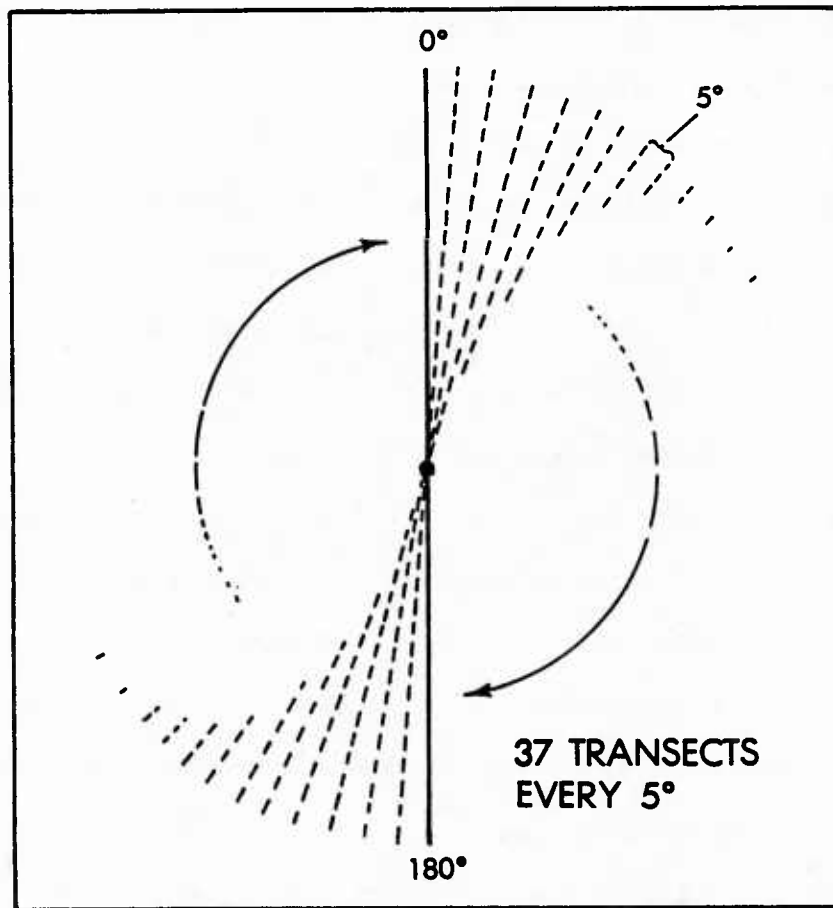


Figure 6-2 Radial sampling pattern used to generate one-dimensional amplitude spectra from various azimuths on a surface.

Figure 6-3 plots the value of \hat{a} ("intercept") and \hat{b} ("slope of spectrum") as a function of azimuth. The resulting spectral estimates are fitted with the above model. Approaching azimuths of 0° and 180° , the profiles nearly parallel the linear trend and the results are unreliable, due to the small number of depths available for analysis resulting in a very narrow frequency band width used in the model regression.

The coefficients $\hat{b}(\theta)$ do not show any relationship to the trend, as predicted by theory. This does not imply that directional dependence in $\hat{b}(\theta)$ is never found in spectra from sea-floor profiles. If a surface had two or more distinct signals (perhaps due to differing relief-forming processes) superimposed, cyclical behavior in $\hat{b}(\theta)$ would be possible. For example, envision a hypothetical surface composed of an isotropic two-dimensional signal with spectra slope $b_A(\theta)$, overlain by a simple linear trend (like the one described above) with spectral slope $b_B(\theta)$. Perpendicular to trend, $\hat{b}(\theta)$ would be some combination of $b_A(\theta)$ and $b_B(\theta)$ depending on their relative amplitudes. Parallel to trend, $\hat{b}(\theta)$ would equal just $b_A(\theta)$, in this example, since the linear trend with slope $b_B(\theta)$ is constant in the direction parallel to strike. The example spectra from the Mendocino Fracture Zone presented in Chapter 4 illustrate this effect. Appendix E examines a series of artificially generated surfaces and their spectral characteristics.

In the results shown in Figure 6-3, the parameter $\hat{a}(\theta)$ shows the expected relationship to $\cos(\theta - \theta_0)$, $\theta_0 = 90^\circ$, as predicted by theory. This model cosine function can be used to parameterize the surface anisotropy. The model sinusoid is generated by an iterative regression technique (see Appendix C.2) which determines the following equation

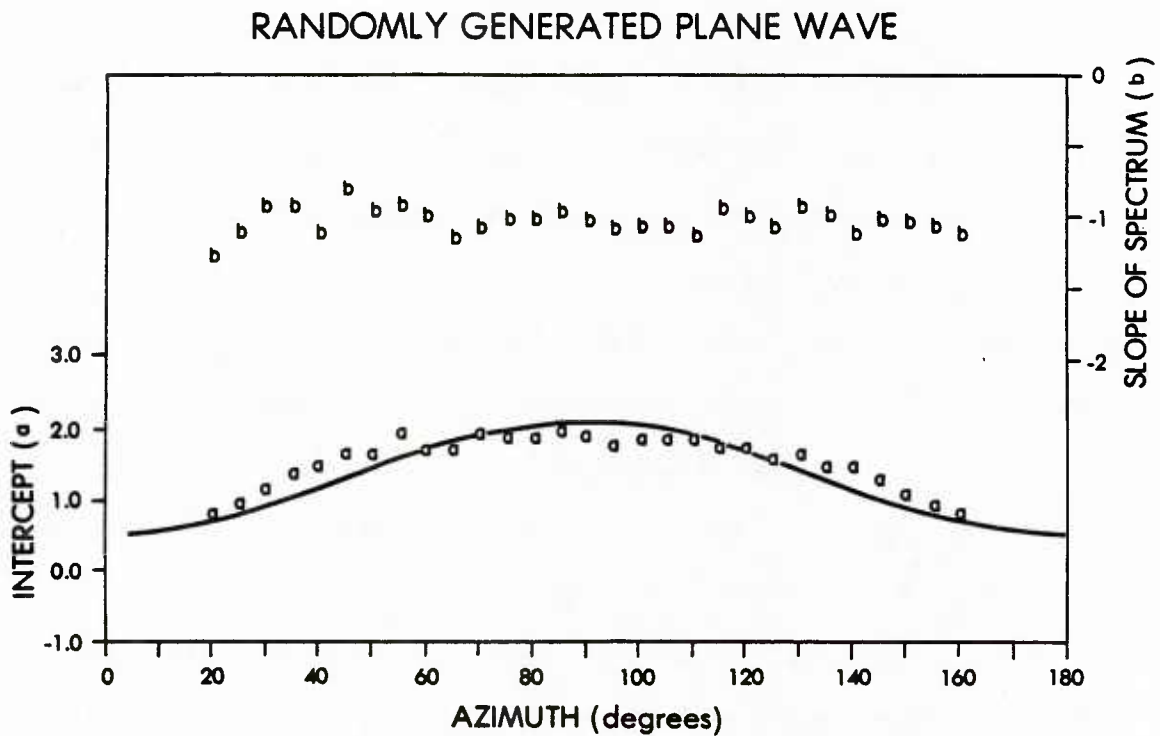


Figure 6-3 Distribution of spectral parameters versus azimuth of sampling for theoretical surface shown in Figure 6-1. The upper series represents the slope of the spectrum in log-log space and varies randomly around the theoretical value of -1 as predicted by theory. Near 0° and 180° , the estimates become unstable due to poor sampling. The lower series represents the intercept of the spectrum in log-log space (or the coefficient of frequency) and agrees well with the sinusoid model predicted by theory. Notice the maximum intercept, and therefore total spectral energy, corresponds to a sample taken perpendicular to strike (azimuth = 90°).

$$\hat{a}(\theta) = \hat{u} + \hat{v} \cdot \cos(2 \cdot (\theta - \hat{\theta}_0))$$

the three term regression technique yields estimates for \hat{u} , \hat{v} , and $\hat{\theta}_0$. These terms have definite physical meaning. \hat{u} represents the simple mean roughness level of the surface, that is the mean $\hat{a}(\theta)$ of the signal sampled in all directions. This could be visualized as the "isotropic" component of the surface. \hat{v} determines the amplitude of the sinusoidal component of the regression model and represents a measure of the degree of anisotropy of the surface. $\hat{\theta}_0$ estimates the normal to the true azimuth of the linear trend. Frequency is not estimated since the periodicity of 1 cycle/180° is known.

Unfortunately, it is not possible to decompose more than one linear trend in a surface using this method. Envision a surface consisting of two linear trends of differing orientation (θ_A and θ_B), "anisotropy" levels (v_A and v_B), and "isotropy" levels (u_A and u_B). The surface, being a simple linear combination of the two component trends can be expressed as

$$a(\theta) = (u_A + u_B) + v_A \cdot \cos(2 \cdot (\theta - \theta_A)) + v_B \cdot \cos(2 \cdot \theta - \theta_B)$$

In this example, u_A and u_B are both presumably equal to zero for "perfect" linear trends. However, even in non-perfect cases in which some energies are available parallel to strike, the \hat{u} components are linearly combined and can not be differentiated. The "anisotropy" components also combine linearly to yield another sinusoid whose amplitude and phase are dependent on the relative amplitudes and phases of the orig-

inal sinusoidal components. Appendix C presents a geometric proof of this relationship.

In the case where two or more linear trends are present in a surface, the form of $\hat{a}(\theta)$ will show a simple sinusoid with phase and amplitude which can not be uniquely decomposed into component sinusoids. If an estimate of the azimuth and amplitude of one of the trends could be produced independently, this component could be removed and the remaining component sinusoids analyzed. It should be emphasized that the inability to decompose component trends in no way invalidates the model, it simply complicates the interpretation of the model statistics in terms of formation processes.

Multiple linear trends can only be decomposed in cases where the trends are sufficiently band-limited to appear as distinct peaks in the frequency spectrum. This approach allows decomposed trends to be uniquely identified by spectra generated in two orthogonal directions, as was shown by Hayes and Conolly (1972). Their work clearly shows such trends in the large scale topography of the Antarctic-Australian Discordance. In examining a great many spectra of small-scale ($\lambda < 8$ km) topography during the present study, no significant spectral peaks have been observed, even in topography which is highly lineated at the larger scales. This result may be due in part to the presentation of these spectra in log-log form.

Comparison of Theoretical Functional Forms with Multibeam Sonar Data

The previous section developed a simple theoretical model of the effect of linear trends on frequency spectra from profiles sampled at

varying azimuths on an anisotropic surface. Figures 4-7-10 illustrated the effect of linear features on two bathymetric profiles collected at near right angles. To test the validity of the theoretical model to actual bathymetry, it is necessary to sample regularly around the compass at a single location on the sea floor. This is only possible for areas which have complete areal bathymetric coverage of high spatial resolution.

The most practical instruments available for obtaining such data are the multibeam sonar systems. These systems, which provide a "swath" of discrete soundings on a line perpendicular to the ship's track, allow complete coverage of an area. By conducting surveys in which the parallel survey tracks are spaced so that the outer beams of adjacent tracks overlap or are nearly juxtaposed, a complete two-dimensional survey can be performed. Very few of such data sets are currently available. However, two data sets from contrasting geologic environments were made available for this study (see Chapter 5, Section B). Both surveys were conducted by the U.S. Naval Oceanographic Office using the SASS multibeam sonar system (Glenn, 1970). The recent acquisition of the academic SEABEAM systems should provide more full-coverage surveys in the future. New techniques for processing side-scan sonar data from the SEAMARC-1 system allow similar two-dimensional analyses to be performed at smaller scales.

Figure 6-4 presents the contoured bathymetry from the Gorda Rise area of the northeast Pacific Ocean. Contours were created automatically and only appear where supported by multibeam soundings. The coverage is generally complete with the exception of a small area on the western margin of the chart and small gaps between swaths. This chart

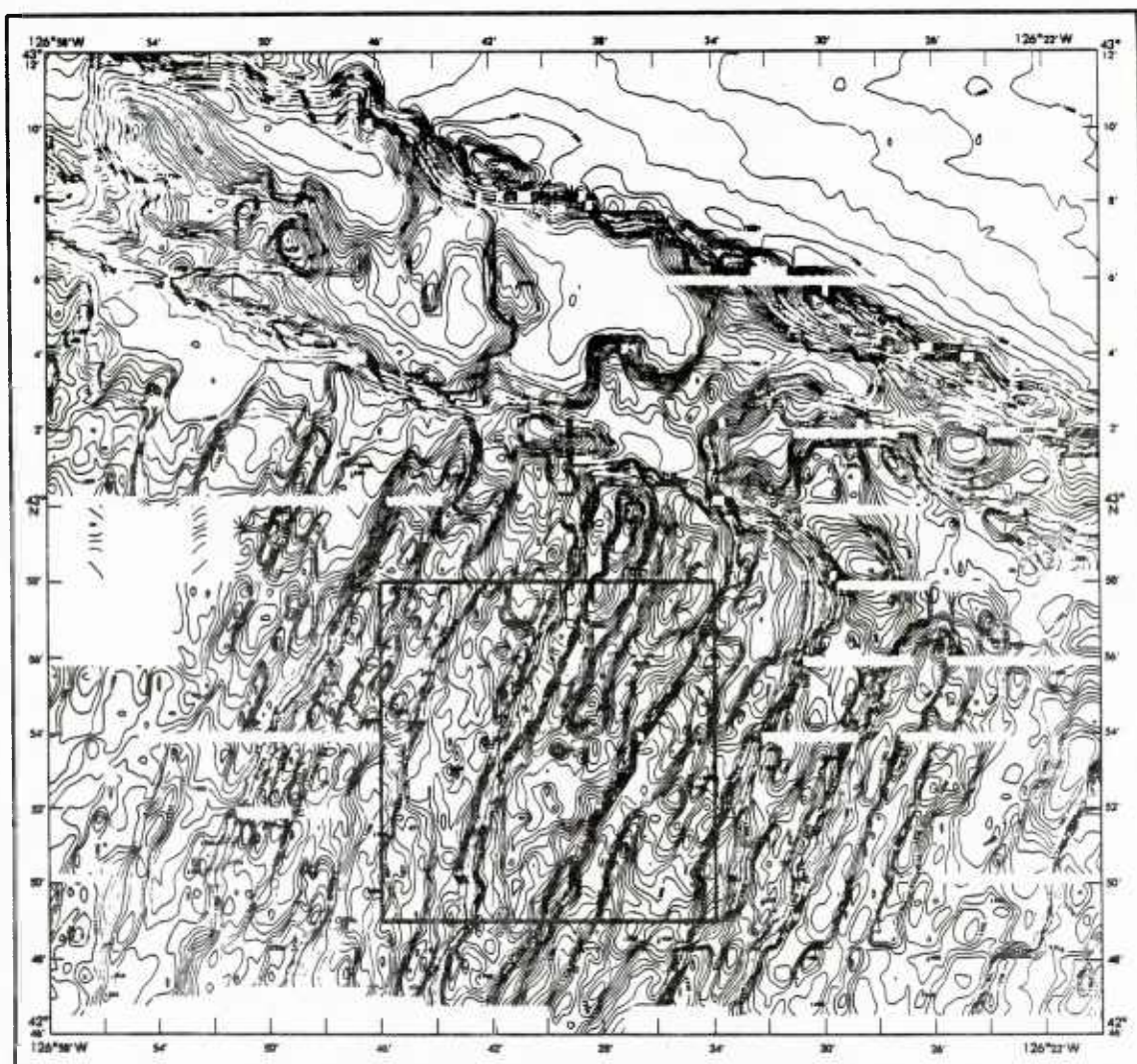


Figure 6-4 Index maps showing the location of two-dimensional SASS bathymetry data used in study of azimuthal dependence of topographic spectra. The data are in the vicinity of the crest of the Gorda Rise in highly lineated topography. Central coordinates are 42°53.5'N, 126°40'W. Contour interval is 10 fathoms.

was created using a grid spacing of 0.25 minutes of longitude and latitude ($\sim 460\text{m} \times \sim 300\text{m}$), well above the resolving capability of the SASS system.

The area shown in Figure 6-4 was selected to test the effect of anisotropy on one-dimensional amplitude spectra. The data set is located in the vicinity of the ridge crest, which was identified as a quasi-stationary province by the methods described in Chapter 5. The lineation of the topography is obvious on the index chart and trends approximately $\text{N}25^\circ\text{E}$.

Figure 6-5 represents graphically the test area. Although the grid spacing used for the illustration is 0.1 minutes of latitude and longitude, the profiles were generated from a grid with spacing of 0.05 minutes ($\sim 100\text{m}$), which approaches the resolving limit of the SASS system for these water depths and noise level conditions. Again the sampling pattern shown in Figure 6-2 was used to generate radial profiles of 256 points. No ensemble averaging was used.

The spectral parameters $\hat{a}(\theta)$ and $\hat{b}(\theta)$ are plotted versus azimuth in Figure 6-6. The results agree closely with the theoretical model developed in the previous section. Notice first that the parameter $\hat{b}(\theta)$, plotted above in these diagrams and labelled "Slope of Spectrum", shows no systematic fluctuation with azimuth, as predicted by theory. Note also that the mean slope is -1.24 , well below the -1.0 slope of the random walk (Markov process) model. The large variability of this parameter could be reduced by ensemble averaging of several spectral estimates, created by offsetting the center of the sampling pattern. The RMS variability would be reduced by $1/\sqrt{N}$, where N is the number of estimates (see Chapter 7).

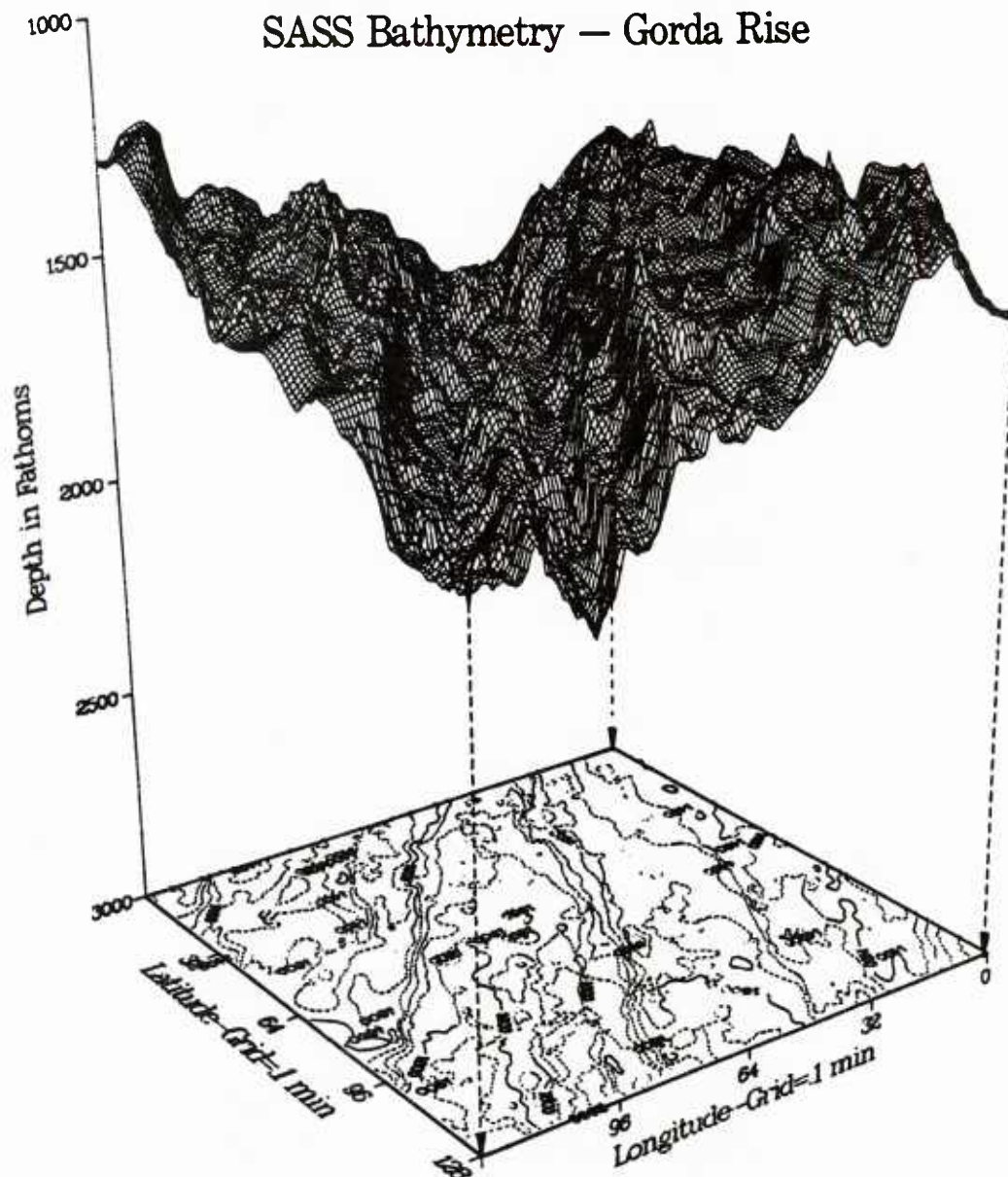


Figure 6-5 Graphic representation of SASS bathymetry data projected onto an evenly-spaced grid. Illustration uses 128 x 128 points spaced at 0.1 minutes of latitude and longitude without cartographic projection. Fourier analysis was performed on 256 points from a 0.05 minute grid. Measured strike of the lineations is approximately 25° azimuth. Viewpoint is from the northeast.

SASS BATHYMETRY—GORDA RISE

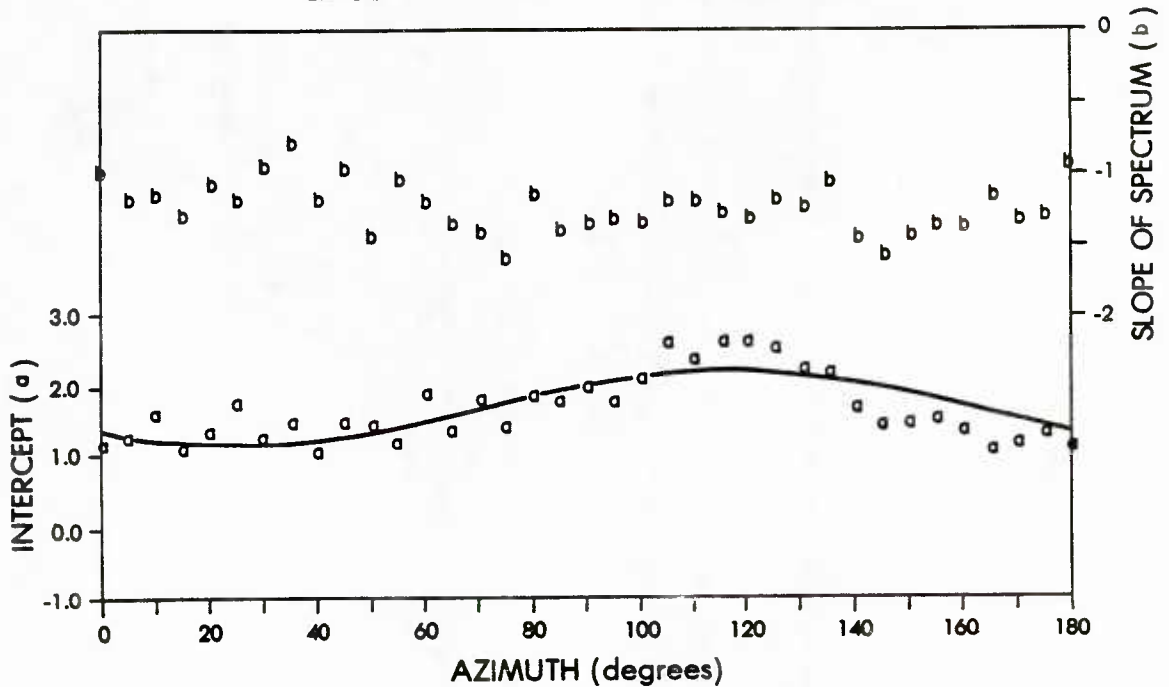


Figure 6-6 Distribution of spectral parameters versus azimuth for Gorda Rise spreading center bathymetry shown in Figure 6-4 and 6-5. Spectral slope parameter (above) shows no apparent functional relationship to azimuth as predicted by theory (notice that the mean slope is -1.24, well below -1.0, which would correspond to a Markov process). The intercept parameter (below) clearly shows the effect of seafloor anisotropy and generally conforms to the sinusoidal model. Model parameters are as follows: mean amplitude = 1.68 m, amplitude of sinusoid = 0.51 m, azimuth of maximum energy = 115° (perpendicular to observed strike).

The results for $\hat{a}(\theta)$ also conform reasonably well to the model prediction. The values, plotted below and labelled "Intercept", represent the amplitude (in meters) of the Fourier component at a wavelength of 1 kilometer. The mean intercept is 1.68 meters, indicating a relatively rough topography, and corresponding to the "isotropic" term \hat{u} in the model. The anisotropy of the surface is obvious from the large amplitude (0.51 meters) of the model sinusoid (the \hat{v} term). The maximum value of the model occurs at an azimuth of $\hat{\theta}_0 = 115^\circ$. This corresponds to the normal to the linear trend (which was measured as 25° in the full-coverage chart) as expected. These values fully parameterize the effect of surface anisotropy on the frequency domain description.

Although the functional models for $b(\theta)$ and $a(\theta)$ appear to be of the proper form, there are some obvious variations in the measured parameters from the model. In order to give an intuitive impression for the degree that the generalized model departs from the actual measured spectrum, Figure 6-7 illustrates a "worst case" example in which the modelled $a(\theta)$ differs from the observed $\hat{a}(\theta)$ by ~ 0.5 m. The selected profile is from $\theta = 115^\circ$ (see Figure 6-6). Plotted with the measured spectrum is the regression line derived from the functional model, rather than the least-square fit usually shown. The model-derived spectrum provides an excellent representation of the spectrum and appears to fall well within the estimation noise of the spectrum, even in this "worst case" example.

The second study area is shown in Figure 6-8. This data set represents a totally different style of sea-floor topography due to the geologic environment, which is controlled by sedimentological processes rather than the tectonic setting of the Gorda Rise. The broad trend of

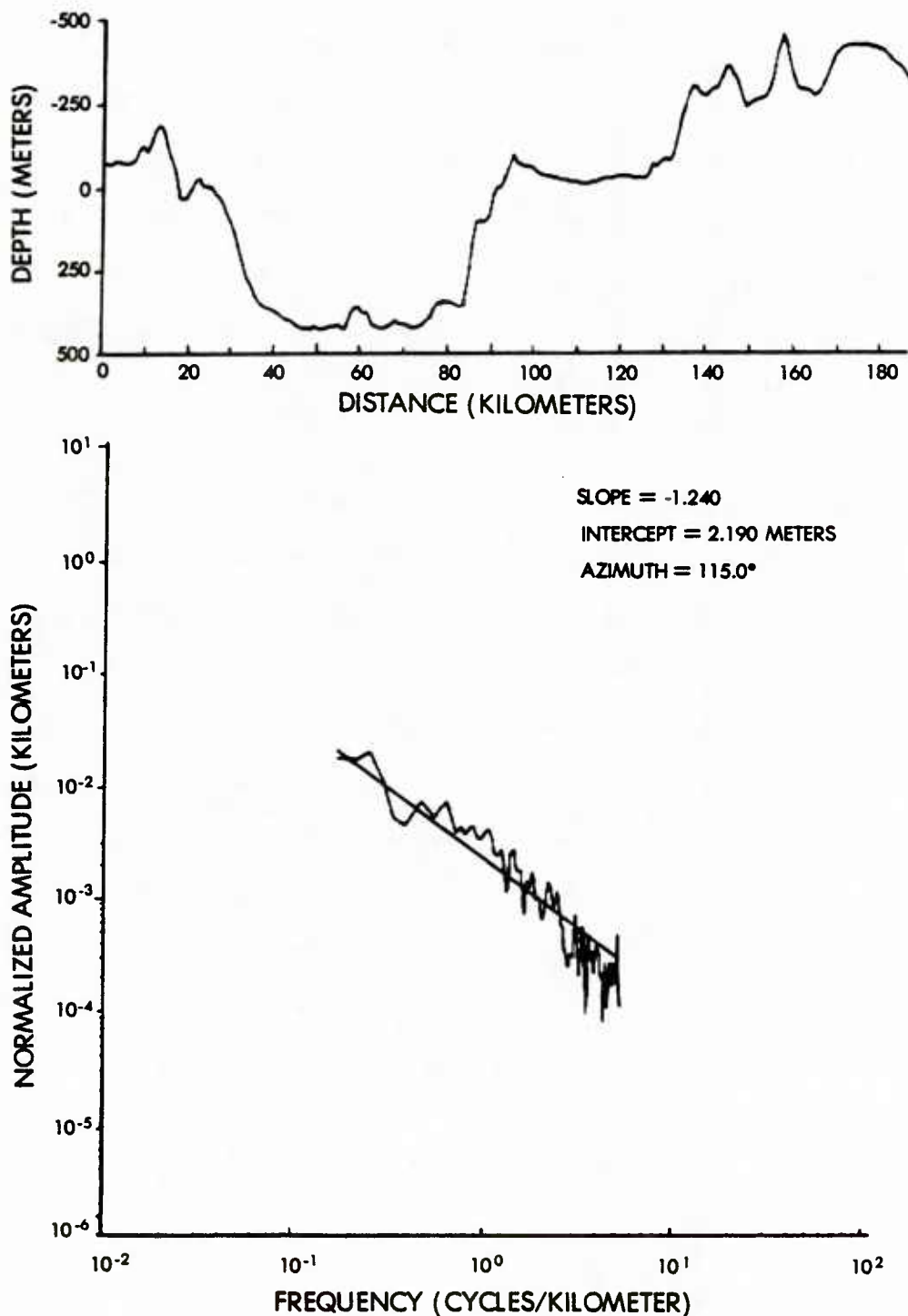


Figure 6-7 Example amplitude spectrum from the Gorda Rise crest sampled at azimuth 115 degrees. The straight line segment through the spectrum represents the model prediction, rather than a least squares fitted line. As seen in Figure 6-6, this particular azimuth represents a large deviation of the fitted parameters from the model sinusoid. The model line still appears to fall well within estimation noise, even for this "worst case" example.

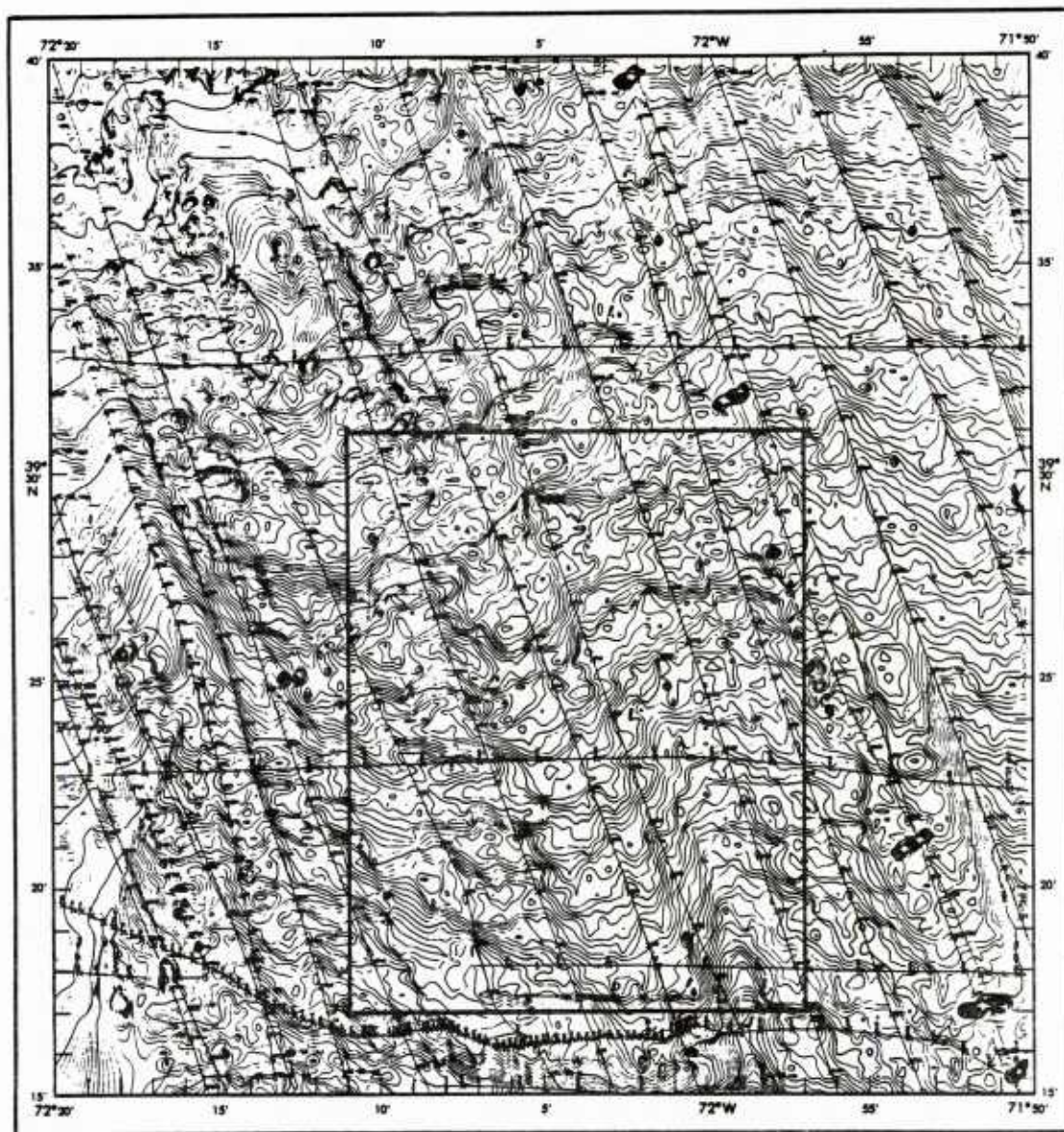


Figure 6-8 Index map showing the location of two-dimensional SASS bathymetric data used in study of azimuthal dependence of spectra of topography. The data are on the upper continental rise off the coast of Delaware, USA, and represent a relatively flat, non-lineated surface. Central coordinates are 38°24'N, 72°04'W. Contour interval is 1 fathom.

slope toward the south-southeast is very long wavelength and not included in the analysis. The small channels traversing the slope are due presumably to downslope transport of sediment and represent an apparent linear trend with wavelength of approximately 10-15 kilometers. This is at the low frequency limit of the present analysis, but might indicate such a trend in shorter wavelengths. Figure 6-9 graphically illustrates the data set (in this case gridded at 0.1 minutes of latitude and longitude), and shows this linear trend due to down-slope processes. Coincidentally, the survey track was run quasi-parallel to this trend which could further complicate interpretation.

The distribution of spectral parameters with azimuth are plotted in Figure 6-10, in the same format as the previous plots. Notice again that the parameter $\hat{b}(\theta)$ plotted above shows no functional relationship to azimuth θ , as predicted by theory. In this case, the mean value of the $\hat{b}(\theta)$'s is -1.05. The intercept parameter $\hat{a}(\theta)$ reflects the relatively smooth, isotropic nature of this sample of the sea floor. In this case, the mean amplitude of 0.097 meters is less than 6% of the same parameter in the Gorda Rise area. The "anisotropy" term, \hat{v} in this case is estimated at 0.0063 meters, only 1% of the value for the Gorda Rise. With these almost isotropic conditions, the estimate of the azimuth of maximum energy cannot be made with any fidelity.

The final test area represents an intermediate level of both general roughness and degree of anisotropy. The data were collected by the SEAMARC-1 side-scan sonar system, which is a deep-towed instrument developed by W.B.F. Ryan of Lamont-Doherty Geological Observatory. The vehicle is towed at approximately 500 m above the sea floor and collects data from side-scan sonar and from down-looking sonar. The depth of the

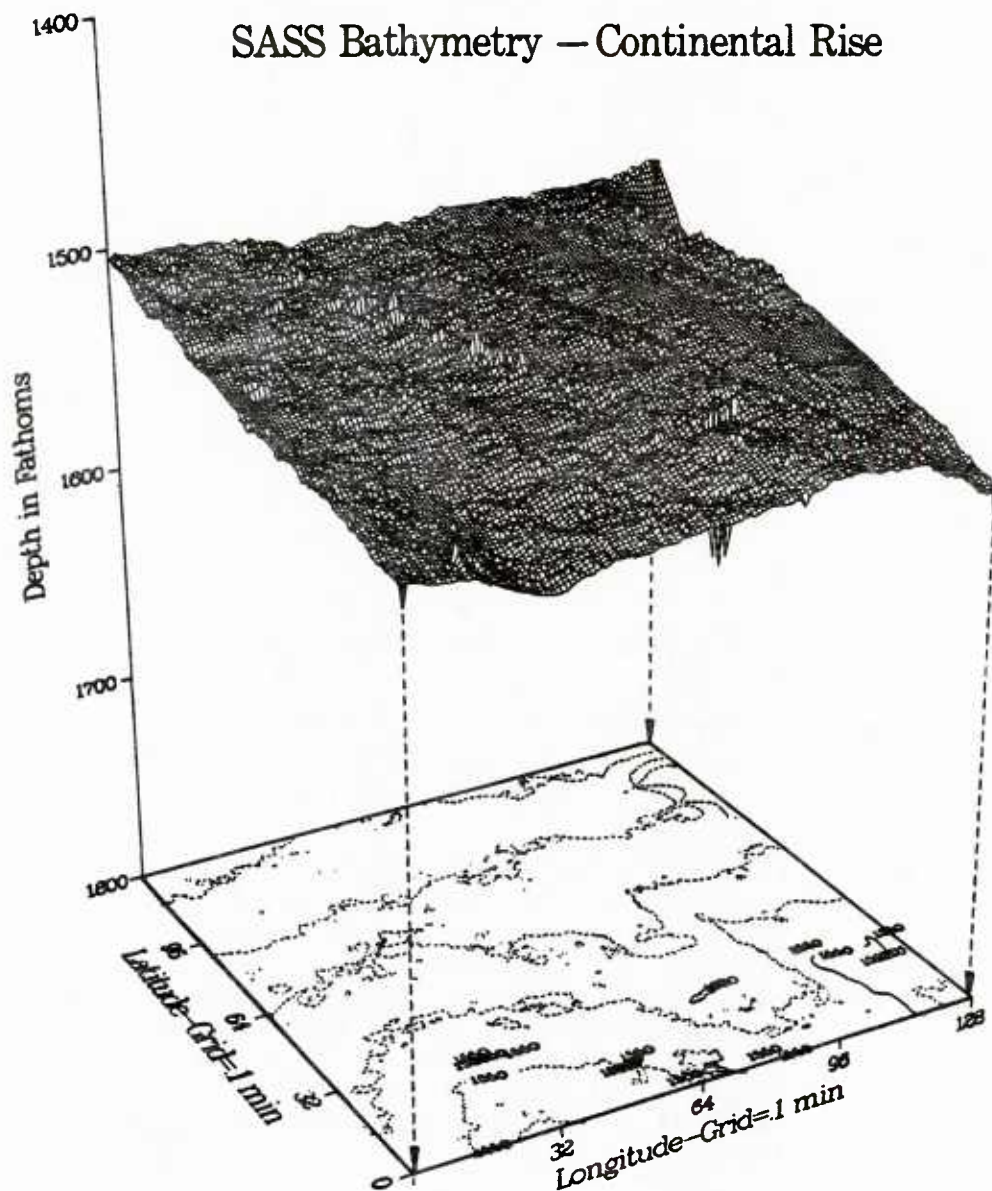


Figure 6-9 Graphic representation of SASS bathymetry data projected onto a 128 x 128 point grid. Grid spacing is 0.1 minutes of latitude and longitude and is presented without cartographic projection. Visible in the surface are spikes associated with sonar processing noise and smooth areas where surface was interpolated between tracks. Viewpoint is from the southwest.

SASS BATHYMETRY—CONTINENTAL RISE

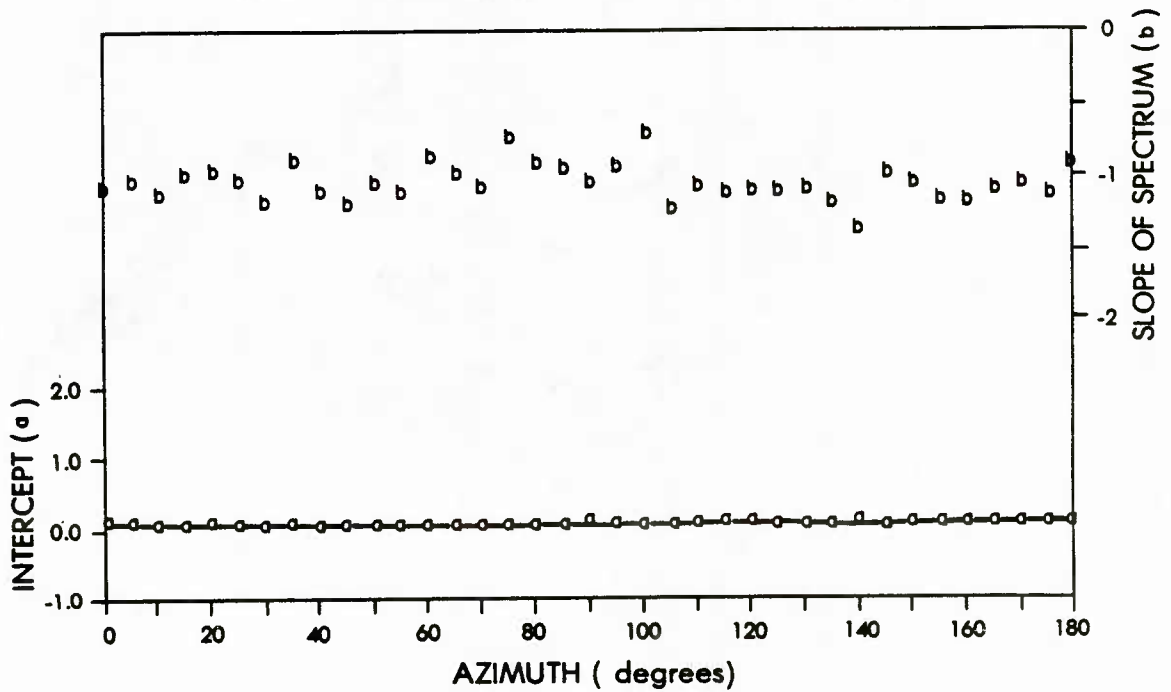


Figure 6-10 Distribution of spectral parameters versus azimuth for continental rise bathymetry shown in Figures 6-8 and 6-9. Spectral slope (above) shows no apparent functional relationship to azimuth and has a mean slope of -1.05. The intercept parameter (below) reflects the relatively smooth, isotropic nature of the surface. Model parameters are as follows: mean amplitude = 0.097 m, amplitude of sinusoid = 0.0063 m, azimuth of maximum energy = 120°. Due to the low level of anisotropy, the azimuth direction is not significant.

vehicle is continuously measured. Farre and Ryan (1984) have developed a method of combining these sources of information into a detailed contour chart of bathymetry. These contours, when evaluated for depth on an evenly spaced grid, comprise the data set used in this study.

Figure 6-11 illustrates a contour chart of the study area, which encompasses the Carteret Canyon, continental slope, and upper continental rise. The smaller area outlined was used to produce the spectral parameters illustrated in Figure 6-12. The data grid uses a spacing of only 5 meters and represents much higher resolution than the surface-derived sonar data in the other two examples. Unfortunately, due to round-off errors producing a white-noise level of 0.3 meters in the data (only whole meter depths were retained), most spectra were only above noise to the 100 m wavelength band, similar to the resolution of SASS.

Figure 6-12 illustrates the results of the azimuthal dependence of spectra study. The slope parameter (\hat{b}) shows a mean of -1.88, lower than the other two study areas. The data also indicate what might be an example of azimuthal dependence of \hat{b} , such as that observed on the Mendocino Fracture Zone and discussed in Chapter 4 and Appendix E. The intercept (\hat{a}) parameters are $\hat{u} = .87$ m, $\hat{v} = .23$ m and relative azimuth ($\hat{\theta}_0$) = 85° , which represent a level of roughness and anisotropy intermediate to the previous two examples. Because the original survey was collected at an azimuth of 140° , the true azimuth of anisotropy is 45° .

In conclusion, the simple theoretical model of the effect of linear trends on frequency domain statistics, can adequately describe anisotropy in three test areas. The parameter $\hat{b}(\theta)$ appears to be independent of azimuth in at least two areas, although quite noisy. The sinusoidal construction of the intercept parameter as

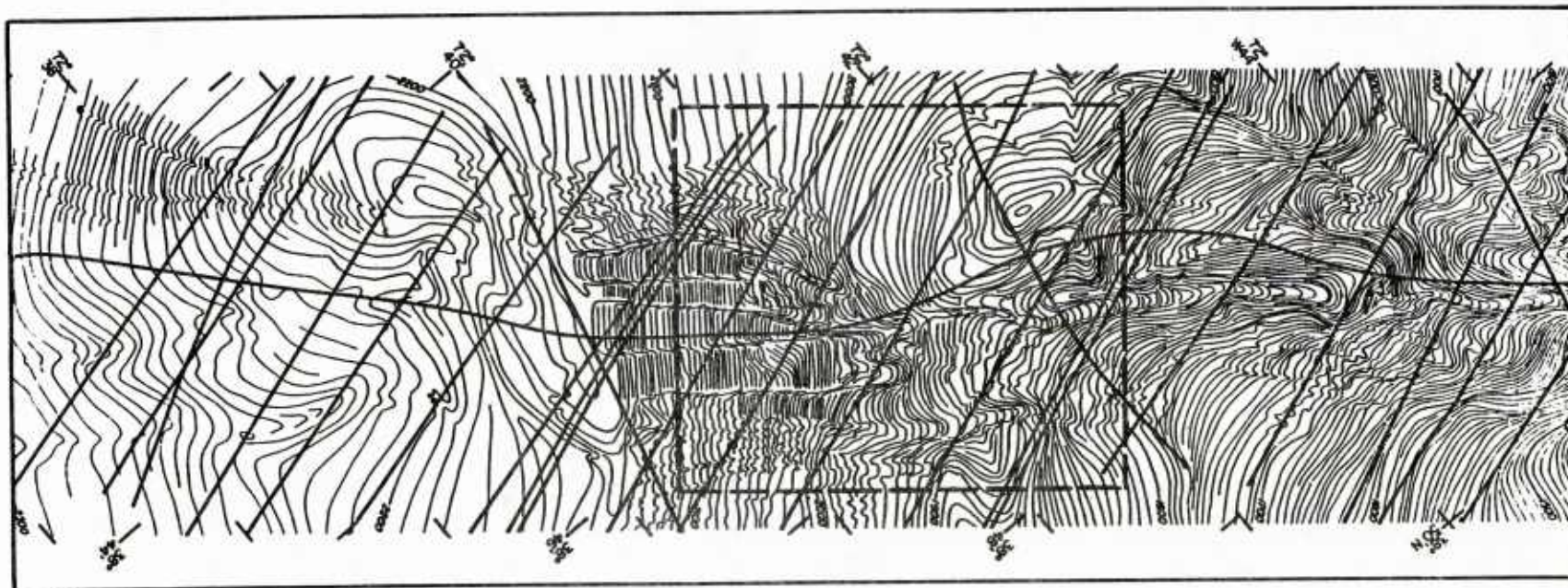


Figure 6-11 Bathymetry of the continental slope/Carteret Canyon area derived from SEAMARC-1 side-scan sonar processing. Section used for azimuth study is outlined. Data is from Farre and Ryan (1984). Heavy lines indicate the path of the sonar vehicle.

SEAMARC-1—CONTINENTAL SLOPE

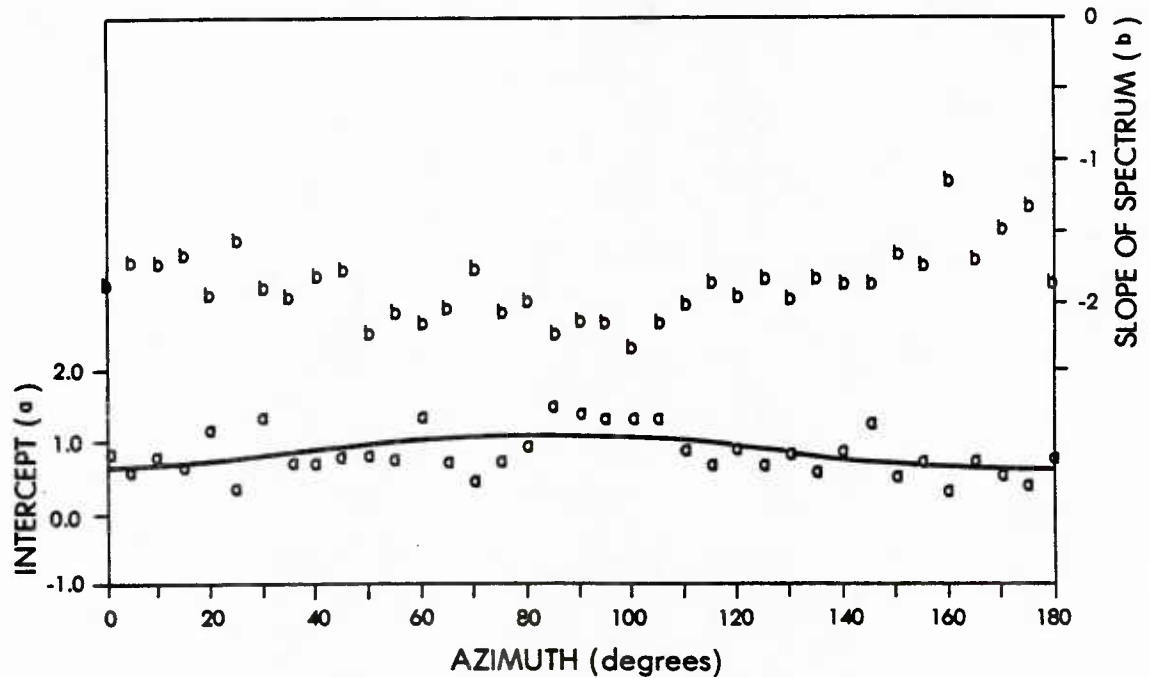


Figure 6-12 Distribution of spectral parameters versus azimuth for continental slope/submarine canyon bathymetry shown in Figure 6-11. Spectral slope (above) has a mean value of -1.88, although it may also contain a cyclical component not noted in other examples. The intercept parameters (below) represent an intermediate level of both mean roughness and anisotropy between those of the Gorda Rise and Continental Rise examples. Model parameters are as follows: mean amplitude = 0.87 m, amplitude of sinusoid = 0.23 m, azimuth of maximum energy = 85°. Due to the direction of sampling, true azimuth on the earth corresponds to 45°.

$$\hat{a}(\theta) = \hat{u} + \hat{v} \cdot \cos(2 \cdot (\theta - \hat{\theta}_0))$$

allows the background, or isotropic, roughness, as well as the degree of anisotropy and its trend to be quantified, and therefore compared in different areas.

If one assumes this simple model of anisotropy to be true, at least in some cases, an interesting insight into the effect of scale on anisotropy can be seen in the mathematics. The assumption of a constant value of $\hat{b}(\theta)$ at all azimuths can be envisioned as a family of lines in log-log space of constant slope whose levels vary with azimuth. The orthogonal azimuths which represent the extremes of anisotropy, would maintain a constant spacing in amplitude at all frequencies in log-log space. That is, if at a given frequency the amplitude in one direction were twice that of the normal azimuth, that relationship would remain constant at all frequencies.

In examining bathymetry and other geological data, it often appears that anisotropy decreases at shorter wavelengths. Bell (1975) reached that conclusion in studying the aspect ratio of shapes of seamounts of different sizes. Much of the validity of this statement depends upon how anisotropy is defined. As stated above, if a relative doubling of amplitude in the orthogonal direction occurs at one scale, this same doubling should occur at all scales. However, if one considers the absolute difference in amplitudes in orthogonal directions, at long wavelengths the difference between perhaps one and two meters of amplitude represents one meter of difference, while at very short wavelengths this same relationship might appear as the difference between one and two centimeters. Although the proportional relationship of amplitude

(doubling) is constant, the absolute difference decreases exponentially, depending upon the value of \hat{b} . Since the ability to resolve amplitude is limited, the ability to resolve anisotropy at small scales is also limited and could lead to an erroneous conclusion concerning anisotropy at high frequencies. These relationships do not apply in cases where \hat{b} varies regularly with azimuth, such as those discussed in Appendix E.

Estimation of Two-Dimensional Spectra from Randomly Oriented Ship Track

An alternative method for describing the topographic roughness of a surface over all azimuths is with the two-dimensional amplitude spectrum. The method involved is quite similar to that used in the one-dimensional case, but prewhitening requires a circularly symmetric high-pass filter, and a two-dimensional Fast Fourier Transform algorithm is used. Perhaps most important to the practical use of this method is the requirement for a complete two-dimensional array of data (depths) as input.

As mentioned previously, complete areal bathymetric surveys are available in very few areas of the world ocean. To be practical, such surveys must use a multibeam sonar array such as SASS or SEABEAM, and tracks must be spaced so that adjacent swaths are juxtaposed. Of the areas presented in the previous section, the Gorda Rise survey shown in Figure 6-4 indicated the highest degree of anisotropy and was therefore selected for two-dimensional FFT analysis.

Figure 6-13 illustrates the results of generating a two-dimensional amplitude spectrum from the gridded bathymetric data shown in Figure

TWO-DIMENSIONAL AMPLITUDE SPECTRUM

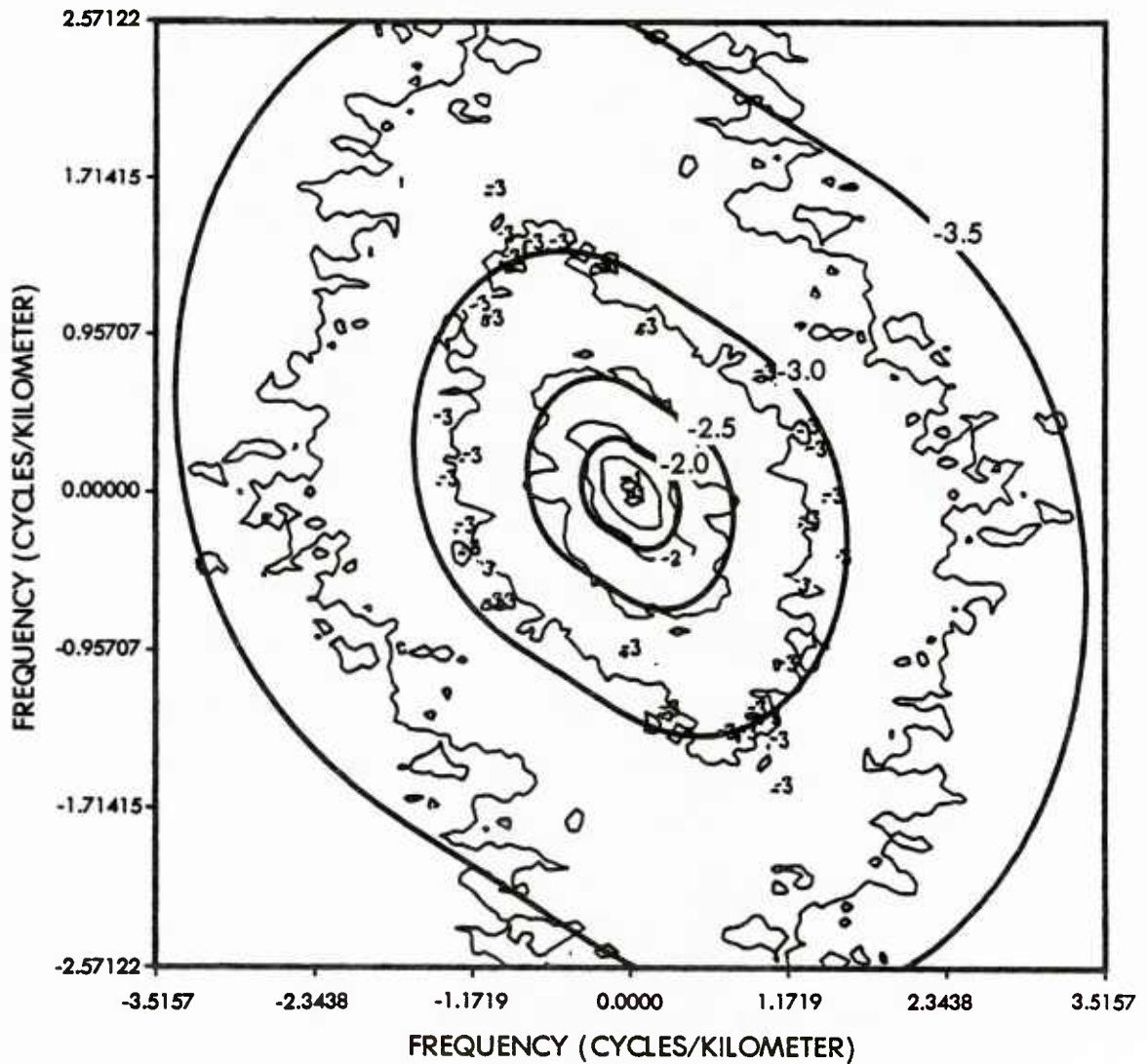


Figure 6-13 Two-dimensional amplitude spectrum from the Gorda Rise area illustrated in Figure 6-5. Log-transformed amplitude estimates, computed via a two-dimensional Fourier transform, are represented by light contours drawn every 0.5 order of magnitude. The heavy lines represent amplitude estimates predicted by the four-parameter, azimuthally dependent model derived for the area.

6-5. Amplitude estimates appear as irregular contours. The amplitude values were log transformed before plotting, and these values are plotted at integer increments. Contours are drawn each .5 order of magnitude of amplitude. The data set, and therefore its amplitude spectrum, is oriented with the columns parallel to longitude and rows parallel to latitude.

Plotted with the spectrum in heavy lines is the two-dimensional spectrum as modelled from one-dimensional profiles by the method described in the previous section. Because the gridded data base used in the analysis was spaced evenly in latitude and longitude, the spectrum as a function of spatial frequency is necessarily distorted. High frequency noise associated with the east-west oriented track lines appears as a smearing of the contours in the vertical and horizontal.

The simple model spectrum explains most of the variance in amplitude. The lineation of the topography with a strike of $\theta = 25^\circ$ can be easily seen as an elongation of the contours in the cross-strike ($\theta = 115^\circ$) direction. The degree of anisotropy (\hat{v}) term in the model determines the elongation of the contours. The model appears to overestimate the amplitudes in the high frequencies slightly, which would indicate a slightly lower slope (\hat{b}) value than that derived by the described method. An improved fit results if the value $\hat{b} = -1.5$, the value derived for the ridge crest in Chapter 5, is used. Overall, however, the match of the true two-dimensional spectrum with the model is quite good. It is questionable whether the additional detail present in the true spectrum represents a valuable signal or simply additional noise.

There are several advantages to the model proposed in this study (derived with respect to azimuth) over the two-dimensional FFT method

(constructed in cartesian coordinates). The proposed model requires only four parameters (\hat{b} , \hat{u} , \hat{v} and $\hat{\theta}_0$) to describe the surface roughness. The two-dimensional spectrum in this case requires a 128 x 128 array, or 16,384 parameters. In addition, the four parameters used in the model have physical meaning attached to them which may prove useful in comparisons of different areas. Also, the computer algorithms used to generate the model require far fewer calculations than the direct transform method.

Perhaps the most relevant advantage in the azimuthal model construction is that the two dimensional nature of the surface can be estimated from randomly oriented ship tracks. Each profile yields a one-dimensional estimate of the amplitude spectrum at the azimuth of the ship's heading. Such estimates can be thought of as cross sections through the surface contoured in Figure 6-13. For example, the profile and amplitude spectrum shown in Figure 6-7 represent a cross section of the two-dimensional surface collected at azimuth N115°E. Given a sufficient number of such randomly oriented tracks over an adequate range of headings, the model can be constructed as described in this chapter. Until a great many more multibeam surveys have been collected, this method of estimating the anisotropy of bottom roughness will remain the only available method over most of the world oceans.

7. Prediction of High Frequency Roughness

Having developed a spectral model of sea-floor topography based on measurements from surface ship sonar systems, the question remains whether this model can be extrapolated into spatial scales smaller than those resolved by the sounding system. This question is particularly important to underwater acoustic applications, where the acoustic frequencies of interest in a scattering problem do not necessarily correspond to the spatial frequencies sampled to generate the model. The concepts of measurement noise levels were introduced in Chapter 4. In this chapter, the effect of estimation errors on prediction will be examined, sources of measured high frequency bathymetry introduced, and a simple prediction test presented.

Source of Error in Spectral Estimates

The model parameters used to describe the amplitude spectrum of sea-floor topography are derived from regression estimates of spectra from profiles of noisy data collected in a generally non-stationary environment. As such, there is estimation error in the model parameters from several sources, which will necessarily result in prediction errors as the model is extrapolated to high frequencies. Although many techniques are used to reduce these errors, some level of error will always remain. Unfortunately, due to the variability of data quality, variable track-line spacing, and the presence of some level of non-stationarity in a data province, it is not possible to quantify completely the estimation

error associated with the model. Only by comparing estimated values with values measured in high frequencies over many data sets and geologic environments, can a reasonable statistical base be assembled to assess the prediction capabilities of the model quantitatively.

The effect of instrument noise (illustrated in Figure 4-5) when encountered by the signal spectrum, has the effect of reducing the spatial frequency range of amplitude estimates available to the regression analysis. Certain spectra examined in the course of this study varied from complete white-noise spectra to spectra showing only two or three amplitude estimates above the noise. Such spectra are of no use in model generation. The length of the spectrum available for regression analysis depends as well on the length of data available to the FFT. Long profiles from large quasi-stationary provinces produce correspondingly long amplitude spectra and therefore more reliable model estimates. As mentioned in Appendix B, a minimum of one hundred points is allowed in a profile for analysis. The use of a higher minimum profile length, while improving regression estimates, would allow more non-stationarity in the profile and reduce the ability to resolve small provinces.

No attempt has been made to quantify the level of non-stationarity (as defined for this study) by examining the mean variability of the spatial domain estimates used in province picking (see Appendix B). Due to the nature of the sea floor, certain provinces appear over thousands of square miles, while others fall smaller than the hundred point minimum required for analysis and must be combined. Such variability probably precludes estimating the degree of non-stationarity with any accuracy; we can only attempt to constrain the effect with the province

picking procedure. In general, however, one can treat estimates from large provinces of persistent geological processes as more reliable than those generated in a relatively small area.

One source of error in the model can be quantified, and that is the residual error from the regression. Using standard statistical techniques (see, for example, Draper and Smith, 1981), the difference in individual amplitude estimates from the regression model estimates can be expressed as a root mean square. Errors in this study averaged $\epsilon_b = \pm .03$ and $\epsilon_{\log a} = \pm .015m$ for a single spectrum. These errors reflect many of the errors associated with the model, although they cannot be decomposed into component sources.

Another important factor determining the level of error in the model is the number of estimates used in generating a composite spectrum. In the case of an anisotropic area, a variety of azimuths distributed about the compass allows a better estimate to be made. In general, the ensembling of N time series composed of signal with noise, results in a decrease of noise (as RMS) of $1/\sqrt{N}$. In the case of our spectral model, the signals are the derived amplitude spectra along an azimuth. A simple method of improving the prediction capability and accuracy of this model is to ensemble-average the amplitude versus frequency estimates from several proximal and near-parallel tracks. The multibeam sonar provides exactly this capability and future developments should take advantage of it.

Figure 7-1 illustrates this reduction of estimation error through ensemble-averaging of multibeam sonar derived spectra. For this example, sixteen parallel beams (profiles) from the SASS multibeam system were analyzed for the statistically homogeneous province of the Gorda

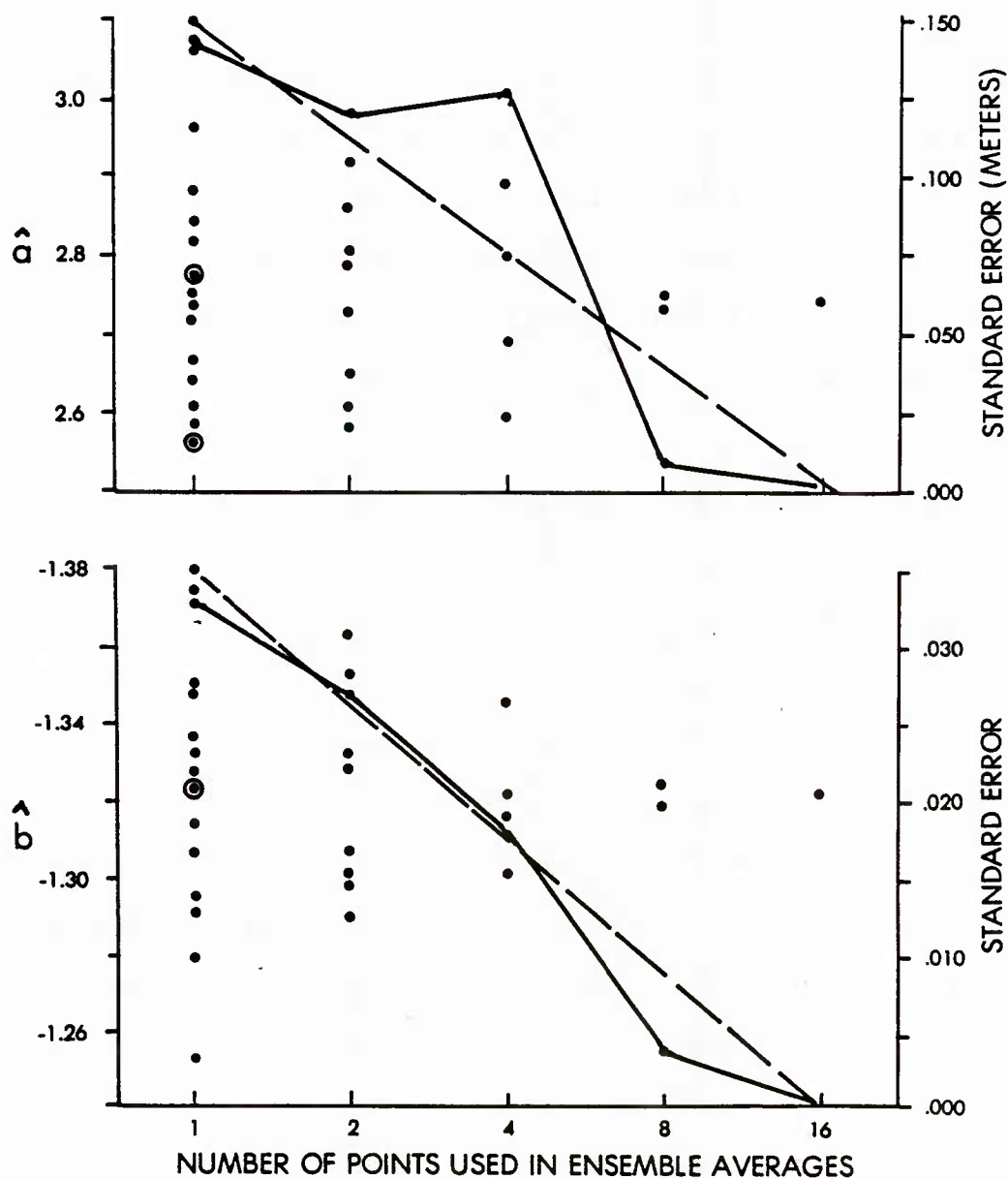


Figure 7-1 Results of ensembling the spectral estimates (a and b) from sixteen parallel profiles collected by a multibeam sonar system. Plotted points indicate the estimated parameters for each of the sixteen profiles and various ensembles of adjacent profile parameters. The calculated standard error (solid line) decreases as \sqrt{N} (dashed line), as predicted by standard statistical theory.

Rise crest. Each derived E-W profile was 17 km in length and spaced approximately 100 m apart. Amplitude spectra were generated for each profile, and rather than averaging each amplitude estimate, the derived regression parameters \hat{a} and \hat{b} were assembled for adjacent beams in groups of 2, 4, 8, and 16. Figure 7-1 plots for both \hat{a} and \hat{b} , the estimated parameters for each of the sixteen profiles and the various results of ensembling. The standard error of each set is plotted as a solid line, with the theoretical $1/\sqrt{N}$ relationship shown as a dashed line. The derived standard error for the final average of sixteen points is necessarily zero. Similar techniques could be applied in the province picking algorithm to improve reliability.

Propagation of Error to High Frequency Estimates

Although the errors associated with the model can not be determined with any accuracy, it is still instructive to examine how the errors affect the ability to predict amplitude in frequencies beyond the range of analysis. Due to the power law form of the model,

$$A = \hat{a} \cdot s^{\hat{b}}$$

where A = amplitude

s = spatial frequency

\hat{a} , \hat{b} = regression parameters

the errors of estimate (error bars) are not linear. It is therefore somewhat easier to visualize the function in $\log A$ - $\log s$ space where the error bars are linear.

As previously stated, the parameter \hat{a} represents the intercept (in meters) of the function with frequency $\log s = 0$, or wavelength $\lambda = 1$ km. The error associated with \hat{a} (ϵ_a) appears as a constant vertical shift of the regression line in log-log space. It is in fact a multiplicative factor in linear space and has the effect of multiplying or dividing the A value by $[\text{antilog } \epsilon_a]$ at any frequency. Since ϵ_a is independent of frequency, it is stable over large extrapolations. Since all spectra of topography are red noise, the absolute level of estimation error effectively decreases at higher frequencies (lower amplitudes).

The spectral slope parameter \hat{b} is not independent of frequency. In log-log space, the dimensionless \hat{b} appears as the slope of the linear regression line. Error associated with \hat{b} (ϵ_b) at $s = 0$, causes an increasing prediction error at higher or lower frequencies. The relationship in linear space is also multiplicative and depends on frequency as multiplying or dividing the A value by $[\text{antilog } (|\log s| \cdot \epsilon_b)]$. The total error of estimate requires linearly combining the two sources ϵ_a and ϵ_b , which translates into multiplying or dividing the value $A(s)$ by $[\text{antilog } (\epsilon_a + |\log s| \cdot \epsilon_b)]$. An example of these calculations is included in the following section.

Comparison of Surface Ship Sonar Results to Deep-Towed

Sonar Results and Results from Bottom Photography

To quantify accurately the ability of the spectral model derived from surface ship sonar systems to predict amplitudes at high spatial frequencies requires a large data base of small-scale bathymetry pro-

files. At present, such a large data base does not exist, at least for the meter-millimeter scales of bottom photography. One area of the world ocean (near 40°27'N and 62°20'W) has been extensively surveyed at small scales and this is the location of the High Energy Benthic Boundary Layer Experiment (HEBBLE).

The HEBBLE area falls into the large roughness province of the East Coast Continental Rise which was described in Chapter 5 and illustrated in Figures 5-12 and 5-13. A spectral model was generated for this large area based on averaging spectral estimates from all profiles illustrated on Figure 5-13. As mentioned previously, the amplitude spectrum for this area consists of two segments, the lower frequency model (with $\hat{a} = 0.0142$ m, $\hat{b} = -1.813$) extending to wavelengths of approximately $\lambda = 3$ km, and the higher frequency model (with $\hat{a} = 0.0602$ m, $\hat{b} = -0.603$) extending from $\lambda = 3$ km to $\lambda = 200$ m.

Data collected by the Deep-Tow sonar system in the HEBBLE area were provided by Scripps Institute of Oceanography. The Deep-Tow, which collects profiles from a height of only 25-50 meters above the sea floor, is able to sample bathymetry at a horizontal sample spacing of 5 meters. The vehicle is positioned via a transponder navigation system which provides relative location to the beacons every five minutes (or approximately 270 meters) of track. All depths recorded by the system in this area appear to be above the instrument noise level.

Digital height data from one stereo-pair bottom photograph collected in the HEBBLE area were provided by the University of Washington. The data set consists of six horizontal and six vertical transects sampled at 1 mm spacing. All derived spectra were virtually identical in their model characteristics.

Figure 7-2 presents a composite amplitude spectrum showing data from all three sources in the HEBBLE area. The SASS derived spectrum (from the nearest available trackline) spans wavelengths of 100 km to 200 m. The model regression lines, derived from spectra generated throughout this large province, are shown as straight line segments. The Deep-Tow derived spectrum, spanning wavelengths of 1 km to 10 m, is very well predicted by the model regression line. The lower frequency estimates begin to diverge at $\lambda \approx 300$ m., which may be due to positioning distortions from the transponder navigation system, which is interrogated at 5 minute (or ~ 300 meter) intervals. Finally, the bottom photograph derived spectrum, spanning wavelengths of 25.6 cm to 2 mm, falls approximately .5 orders of magnitude below the regression line.

The prediction residual of .5 orders of magnitude over 5 decades of frequency indicates some combination of errors in parameter estimates \hat{a} and \hat{b} . If all errors were in \hat{a} , it would be in error by .5 orders of magnitude. Similarly, the error in \hat{b} would be ± 1 , using the relationships described in the last section. The evaluation of several more bottom photograph-derived profiles from the same region would allow a more quantitative treatment of the model prediction error. It is possible that other high frequency spectra may scatter around the prediction line, due perhaps to actual variability of the microrelief in the area rather than error in the prediction model. Visual inspection of the several photograph pairs taken in HEBBLE indicate that other areas are in fact rougher than the relatively featureless photo analyzed here (Arthur Nowell, personal communication, 1983).

In any case, the prediction of millimeter scale topographic amplitude from a surface hull-mounted sonar system to within half an order of

SPECTRAL ESTIMATES FROM SEVERAL SOURCES

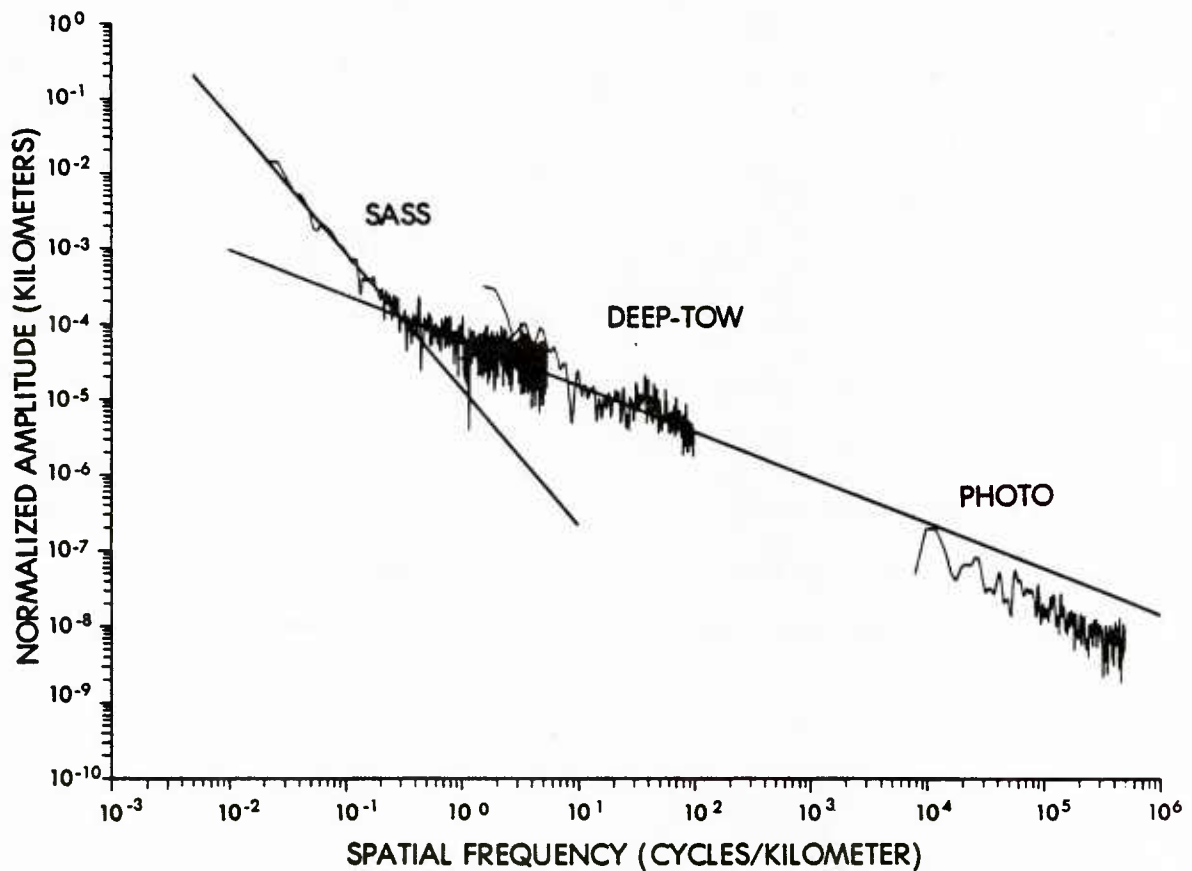


Figure 7-2 Composite amplitude spectrum of bathymetric profiles derived at various scales by different survey instruments. All data were collected on the East Coast continental rise near 40°27'N, 62°20'W, proximal to the HEBBLE area. Regression lines represent the mean bottom roughness model derived from fourteen SASS profiles illustrated in Figure 5-13. Model predicts the deep-tow derived spectrum almost exactly over ~1.5 decades of spatial frequency. The spectrum derived from a stereo-pair bottom photograph is predicted to within 0.5 orders of magnitude over ~5 decades of spatial frequency (200 meters to 2 millimeters wavelength).

magnitude is a surprisingly good result. The ability to predict high frequency roughness from a low frequency model appears to be quite possible, at least for some areas of the world ocean. One serious caution must be taken into account. The successful prediction from the SASS-derived spectrum was only possible by identifying the break in slope at 3 km. Were data only available to that 3 km wavelength, the lower frequency estimates would have been used, and prediction error of nearly six orders of magnitude incurred in estimating the millimeter scale amplitudes. If it is assumed that such slope breaks are due to changes in relief-forming processes at various frequencies, then any estimates of high frequency roughness exclusively from a lower frequency model presume a continuity of process over all intervening frequencies, and the absence of a significant break in the power law form of the spectrum.

8. Summary and Conclusions

A method has been developed to allow a valid stochastic description of sea-floor relief to be generated in a relatively simple statistical model. The fundamental statistic used is the amplitude spectrum of spatial frequency, which is both elementary enough to be generated operationally from existing digital bathymetric data bases, and general enough to be applied to a variety of engineering applications and scientific problems. The model allows relatively large areas of the world sea floor to be described by as few as two model parameters for simple isotropic surfaces. The difficulties of producing a stationary statistic in a non-stationary environment are minimized with the use of a spatial domain provincing technique. The model also accounts for the directional dependence of anisotropic surfaces. The results of one simple experiment indicate that the model may be extrapolated with high fidelity to frequencies beyond the resolving capability of surface ship sonar systems. This stochastic model when combined with lower frequency deterministic models, such as the gridded bathymetric models developed by NAVOCEANO, allows a complete description of the sea-floor relief.

There are numerous avenues available to improve the model. The use of ensembles of either data or derived statistics allows the estimation errors of the model to be reduced substantially. The availability of multibeam sonar systems makes this improvement possible immediately. The ensembling of the statistics from the sixteen beams of the SEABEAM system would reduce the estimation error to one quarter the results from a single beam. Data derived from very narrow beam sonars allow a higher rate of sampling, and therefore a wider frequency band, to be available

for model generation. The collection of more complete areal bathymetric surveys would allow further refinement of the models of sea-floor anisotropy. Future improvements in deep-towed side-scan sonars and the collection of additional bottom photographs would allow a quantitative estimate to be made of the predictive ability of the model.

The utility of the model falls into two broad categories; engineering application and scientific investigation. The application of the model to underwater acoustics is obvious. The model spectrum of the surface relief is an important environmental factor in the scattering of sound from the sea floor. Efforts are currently underway to develop scattering models which utilize such stochastic environmental information. More traditional models require the description of the bottom as a faceted surface, which can easily be derived from the derivative spectrum and a knowledge of the probability distribution of depths. Even models requiring a fully determined surface can obtain a valid realization by combining the model amplitude spectrum with a randomly generated phase spectrum.

In terms of scientific investigation, the method provides a new tool for studying the earth's geological and tectonic processes. The resulting patterns of roughness discovered on the Gorda Rise and Oregon continental margin illustrate the ability of the method to detect interesting relationships not obvious by simply studying bathymetric charts. Comparing the distribution of roughness on a variety of spreading centers, continental margins and other submarine environments, should yield valuable insight into the distribution of geologic processes on the sea floor. In the case of the patterns on the Gorda Rise, the distribution of roughness may well relate to the lava formation processes, which in

turn may be related to the distribution of polymetallic sulphide minerals formed in association with hydrothermal vents.

The ability to quantify the anisotropy of the sea floor also introduces interesting possibilities for geological investigation. The distribution and trend of these measurements provides a new tool for the quantitative investigation of deep-sea processes in various environments. Also the relationship between sea-floor spreading rate and roughness, long assumed qualitatively, could be quantified and analyzed in terms of the operative geological processes.

Finally, the author hopes that this study represents more than simply a study of sea-floor roughness. Much effort has been made to present an approach to modelling natural phenomena which could be applied to a wide variety of problems in the natural sciences. As most disciplines within the earth sciences represent a marriage of one of the "pure" sciences to the study of the earth, this study represents a crossing of natural science with engineering statistical methods. Very little such work has been done by earth scientists in the past, perhaps because the earth is rarely as well ordered as the controlled laboratories of the chemist or physicist. Due to the natural variability of the phenomena under study, the geologist's attempt to describe the earth quantitatively is particularly difficult. It is hoped that the approach and philosophy presented in this attempt will be of use to future investigators.

9. References

- Agapova, G.P., 1965, Quantitative characteristics of bottom slope angles in seas and oceans: Oceanology, vol. 5, no. 4, p. 135-138.
- Akal, T., and J. Hovem, 1978, Two-dimensional space series analysis for sea-floor roughness: Marine Geotechnology, vol. 3, no. 2, p. 171-182.
- Atwater, T., and J.D. Mudie, 1973, Detailed near-bottom geophysical study of the Gorda Rise, J. Geophys. Res., v. 78, no. 35, p. 8665-8686.
- Barker, F.S., D.R. Barraclough, and S.R.C. Malin, 1981, World Magnetic Charts for 1980 - spherical harmonic models of the geomagnetic field and its secular variation: Geophysical Journal of the Royal Astronomical Society, vol. 65, p. 525-533.
- Barnard, W.D., 1978, The Washington continental slope: quaternary tectonics and sedimentation: Marine Geology, v. 27, p. 79-114.
- Bell, T.H., 1975a, Topographically generated internal waves in the open ocean: Jour. Geophys. Res., vol. 80, p. 320-327.
- Bell, T.H., 1975b, Statistical features of sea-floor topography: Deep-Sea Research, vol. 22, p. 883-892.
- Bell, T.H., 1978, Mesoscale sea-floor roughness: Deep-Sea Research, vol. 26A, p. 65-76.
- Berkson, J.M., 1975, Statistical properties of ocean bottom roughness (abs.), power spectra of ocean bottom roughness: Jour. Acous. Soc. Amer., vol. 58, no. S1, p. 587.
- Berkson, J.M., and J.E. Matthews, 1983, Statistical properties of sea-floor roughness. In: Acoustics in the Sea-Bed, N.G. Pace (ed.), Bath University Press, p. 215-223.
- Berry, M.V., and Z.V. Lewis, 1980, On the Weierstrass-Mandelbrot fractal function: Proceeding of the Royal Society of London, vol. A370, p. 459-484.
- Blackman, R.B., and J.W. Tukey, 1958, The Measurement of Power Spectra, Dover Publications, Inc., New York, 190 pp.
- Bloomfield, P., 1976, Fourier Analysis of Time Series: An Introduction: John Wiley & Sons, Inc., New York, 258 pp.
- Bracewell, R., 1978, The Fourier Transform and its Applications: McGraw-Hill Book Co., New York, NY, 381 pp.

- Brown, Gary S., 1982, A stochastic Fourier transform approach to scattering from perfectly conducting randomly rough surfaces: IEEE Transactions on Antennas and Propagation, Vol. AP-30, No. 6, p. 1135-44.
- Brown, Gary S., 1983, New results on coherent scattering from randomly rough conducting surfaces: IEEE Transactions on Antennas and Propagation, Vol. AP-31, No. 1, p. 5-11.
- Carson, B., 1977, Tectonically induced deformation of deep-sea sediments off Washington and northern Oregon: mechanical consolidation, Marine Geology, v. 24, p. 289-307.
- Chase, T.E., P. Wilde, W.R. Normark, C.P. Miller, D.A. Seckins, and J.D. Young, 1981, Offshore Topography of the Western United States between 32° and 49° North Latitudes, Plate 2, U.S. Geological Survey Open File Map 81-443.
- Chatfield, C., 1980, The Analysis of Time Series: An Introduction: Chapman and Hill, New York, 268 pp.
- Clay, C.S., and W.K. Leong, 1974, Acoustic estimates of the topography and roughness spectrum of the sea floor southeast of the Iberian Peninsula. In: Physics of Sound in Marine Sediments, L. Hampton (ed.), Plenum Press, p. 373-446.
- Clay, C.S., and H. Medwin, 1977, Acoustical Oceanography: Principles and Applications: John Wiley & Sons, Inc., 544 pp., New York.
- Davis, J.C., 1973, Statistics and Data Analysis in Geology: John Wiley & Sons, Inc., New York, 550 pp.
- Davis, T.M., 1974, Theory and practice of geophysical survey design: NAVOCEANO TR-13, Bay St. Louis, MS, 137 pp.
- Draper, Norman and Harry Smith, Jr., 1981, Applied Regression Analysis, Second Edition: John Wiley & Sons, New York, 709pp.
- Elvers, D., S.P. Srivastava, K. Potter, J. Morley, and D. Sdidel, 1973, Asymmetric spreading across the Juan de Fuca and Gorda Rises as obtained from a detailed magnetic survey: Earth and Planet. Sci. Lett., v. 20, p. 211-219.
- Engel, A.E.J., C.G. Engel, and R.C. Havens, 1965, Chemical characteristics of oceanic basalts and the upper mantle: Bull. Geol. Soc. Am., v. 76, p. 719-734.
- Farre, J.A., and W.B.F. Ryan, 1984, A 3-D view of erosional scars on the U.S. Mid-Atlantic continental margin: AAPG submitted.
- Glenn, M.F., 1970, Introducing an operational multibeam array sonar: Int. Hydrographic Review, 47, p. 35-39.

- Godfrey, Michael D., 1967, Prediction for non-stationary stochastic processes, In: Bernard Harris (Ed.) Advanced Seminars on Spectral Analysis of Time Series: John Wiley & Sons, Inc., New York, N.Y.
- Hayes, D.E., and J.R. Conolly, 1972, Morphology of the southeast Indian Ocean. In: D. E. Hayes (ed.) Antarctic Oceanology II: The Australian-New Zealand Sector: American Geophysical Union, Washington, D.C.
- Heezen, B.C., and T.L. Holcombe, 1965, Geographic distribution of bottom roughness in the North Atlantic: Bell Telephone Labs, Inc., and Lamont-Doherty Geol. Obs. (Columbia Univ., Palisades, NY), 41 pp and 6 charts.
- Hey, Richard, 1977, A new class of "pseudofaults" and their bearing on plate tectonics: a propagating rift model: Earth and Planetary Science Letters, vol. 37, p. 321-325.
- Kanasewich, E.R., 1981, Time Sequence Analysis in Geophysics, University of Alberta Press, Edmonton, 480 pp.
- Krause, D.C., and H.W. Menard, 1965, Depth distribution and bathymetric classification of some sea floor profiles: Marine Geology, vol. 3, p. 169-193.
- Krause, D.C., P.J. Grim, and H.W. Menard, 1973, Quantitative marine geomorphology of the East Pacific Rise: NOAA Tech. Rept. ERL 275-AOML 10, p. 1-73.
- Larson, R.L., and F.N. Spiess, 1970, Slope distributions of the East Pacific Rise crest: SIO Ref. 70-8 (Scripps Inst. Ocean., Univ. California, San Diego, CA), 4 pp.
- Mandelbrot, Benoit, 1982, The Fractal Geometry of Nature, W.H. Freeman & Co., San Francisco, 460 pp.
- Martin, Marcel A., 1957, Frequency domain applications in data processing: General Electric Co., Missile and Ordinance Systems Dept. (Philadelphia) Document No. 57SD340, 128 pp.
- Matthews, J.E., 1980, An approach to the quantitative study of sea-floor topography: NORDA TN-47, Bay St. Louis, MS, 55 pp.
- McClain, C.R., and H. Walden, 1979, On the performance of the Martin digital filter for high- and low-pass applications: National Aeronautics and Space Administration Technical Memorandum 80593, Goddard Space Flight Center, Greenbelt, Md., 20771.
- McDonald, M.F., and E.J. Katz, 1969, Quantitative method for describing the regional topography of the ocean floor: Jour. Geophys. Res., vol. 74, no. 10, p. 2597-2607.

- McDonald, M.F., E.J. Katz, and R.W. Faas, 1966, Depth study report on the detectibility of submarines on the ocean bottom: Vol. III, Electric Boat Div. (Gen. Dynamics Corp., Groton, CT), Rept. U413-66-116.
- Menard, H.W., 1964, Marine Geology of the Pacific: McGraw-Hill Book Co., New York, NY.
- Naudin, J.J., et R. Prud'homme, 1980, L'Analyse cartographique: Étude numérique des caractéristiques morphologiques des surfaces: Sciences de la Terre, Paris, Série Informatique Géologique, no. 4, p. 47-71.
- Neidell, N.S., 1966, Spectral studies of marine geophysical profiles: Geophysics, vol. 31, p. 122-134.
- Papoulis, A., 1962, The Fourier Integral and Its Applications: McGraw-Hill Book Co., New York, NY, 318 pp.
- Rhines, P.B., 1977, The dynamics of unsteady currents. In: The Sea, vol. 6, E. D. Goldberg, I. N. McCave, J. J. O'Brien and J. H. Steele, editors, John Wiley, p. 189-318.
- Rhines, P., and F. Bretherton, 1973, Topographic Rossby waves in a rough-bottomed ocean: Journal of Fluid Mechanics, vol. 61, p. 583-607.
- Ross, Sheldon M., 1980, Introduction to Probability Models: Academic Press, New York, 376 pp.
- Scarborough, J.B., 1930, Numerical Mathematical Analysis: The Johns Hopkins Press, Baltimore, Md., 416 pp.
- Searle, R.C., and R.N. Hey, 1983, GLORIA observations of the propagating rift at 95.5°W on the Cocos-Nazca spreading center: Journal of Geophysical Research, vol. 88, no. B8, p. 6433-6447.
- Shapiro, R., and F. Ward, 1960, The time-space spectrum of the geostrophic meridional kinetic energy: J. Meteor., no. 17, p. 621-626.
- Siegle, Sidney, 1956, Nonparametric Statistics for the Behavioral Sciences: McGraw-Hill Book Company, New York, NY, 312 pp.
- Smith, S.M., T.E. Chase, W.E. Farrell, I.L. Taylor, and M.E. Weed, 1965, Distribution and statistical analysis of sea-floor relief in the northeast Pacific: Bell Telephone Labs and Univ. of California, San Diego, CA, Tech. Rept. 6-601347, 59 pp. and 8 charts.
- Van Wyckhouse, R.J., 1973, Synthetic bathymetric profiling system (SYNBAPS): NAVOCEANO TR-233, Washington, DC, 138 pp.

Appendix A.1

Having concluded that the frequency spectrum of submarine topography conforms to a power law functional form, it becomes critical in constructing a model based on this statistic to ensure a valid regression fit to the data. Such a regression analysis is necessary both in fitting the amplitude spectrum itself (amplitude as a function of frequency) and in fitting the energy envelopes for various spatial frequency bands for use in spatial-domain provincing. We represent our power law function as follows:

$$y = f(a,x,b) = ax^b \quad \text{where} \quad \begin{array}{l} y = \text{dependent variable (amplitude)} \\ x = \text{independent variable (frequency)} \\ a,b = \text{regression coefficients} \end{array}$$

We can use the property of power law functions that they plot linearly on log-log axes and recast the function in log-log space as follows:

$$\log(y) = \log(a) + b \log(x)$$

which can be easily solved by a simple linear regression. Upon deriving the coefficients \hat{b} and $\log(\hat{a})$, these terms can be reconverted to linear-linear space as,

$$\begin{array}{l} b = \hat{b} \\ a = \text{antilog}(\log(\hat{a})) \end{array}$$

to reconstruct our power law form,

$$y = ax^b$$

Recalling that the method of least-squares minimizes the total sum of squares of residual distance from the observed data to the resultant regression curve, the method just described minimizes these distances in log-log space. The solution derived in this manner does not minimize the total residual distance in linear-linear space, although the estimates might be quite close. Methods exist for performing the least-square fit in either log-log or linear-linear spaces, and these are discussed here. The choice of method and the use of weighting schemes depend on the distribution of the data being fit as well as the distribution of the estimation error. In all cases, the error is assumed to reside in the amplitude estimates, rather than in the independent variable.

In fitting the energy envelope estimates produced in the delineation of stationary provinces (see Chapter 5), the regression must be performed in linear-linear space without weighting. The errors associated with the envelope estimates (dependent variable), do not depend on frequency band (independent variable) and should not be log-transformed. In the case of amplitude spectra however, it was shown by Blackman and Tukey (1958) that estimation error is related to the chi-squared distribution and that error bars remain constant in log-log space. Under these conditions, the regression analysis is optimally performed on log-transformed data.

As explained in Scarborough (1930), Article 114., the log-transformation of the dependent variable (y) causes the residuals in the least-squares residual equations to be of unequal weight. In the case of a power law function (which is given as an example in Scarborough (1930) and will not be reproduced here), the weighting function is the squared dependent variable (y^2). Appendix A.2 presents an ASCII FORTRAN 77 program for doing such a weighted regression analysis in log-log space. Because of the chi-square distribution of errors associated with the amplitude spectrum, however, the residuals in this case are equally weighted and no weighting function is required.

In fitting the envelope estimates of discrete band passes for use in "province picking," there is no requirement for log transformation of the data or weighting of residuals. This is the case because the error associated with all envelope estimates is theoretically constant. In order to derive properly the regression coefficients \hat{a} and \hat{b} in linear-linear space, it is necessary to use an iterative method. The following development is modified from Scarborough (1930), Article 115., to apply to the power law functional form.

We can express the regression coefficients as the sum of initial estimates and differences as follows:

$$\hat{a} = a_0 + \Delta a$$

$$\hat{b} = b_0 + \Delta b$$

where a_0, b_0 = initial estimates

$\Delta a, \Delta b$ = correction factors

It is convenient to use the coefficients derived from performing the linear regression on log-transformed data as the initial estimates (a_0 , b_0) for the iteration process. If we define a new function in terms of estimated coefficients as,

$$y' = f(x, a_0, b_0) = a_0 x^{b_0}$$

the discrete values of this approximating function will be,

$$y'_1 = f(x_1, a_0, b_0)$$

$$y'_2 = f(x_2, a_0, b_0)$$

:

$$y'_n = f(x_n, a_0, b_0)$$

where n is the total number of data pairs used in the regression equations.

Realizing that the coefficients \hat{a} and \hat{b} produce the "best fit" solutions, the minimized residuals are represented as,

$$v_1 = f(x_1, \hat{a}, \hat{b}) - y_1$$

$$v_2 = f(x_2, \hat{a}, \hat{b}) - y_2$$

:

$$v_n = f(x_n, \hat{a}, \hat{b}) - y_n$$

where y_1, y_2, \dots, y_n are the observed dependent variables. Substituting our approximation yields

$$v_i = f(x_i, a_0 + \Delta a, b_0 + \Delta b) - y_i, i = 1, 2, \dots, n$$

or

$$v_i + y_i = f(x_i, a_0 + \Delta a, b_0 + \Delta b), i = 1, 2, \dots, n$$

Expanding the right side by Taylor's Theorem for the two variables, a and b, yields

$$v_i + y_i = f(x_i, a_0, b_0) + \Delta a \left(\frac{\partial f_i}{\partial a_0} \right) + \Delta b \left(\frac{\partial f_i}{\partial b_0} \right) + \dots; i = 1, 2, \dots, n$$

substituting $y'_i = f(x_i, a_0, b_0)$ we have

$$v_i + y_i = y'_i + \Delta a \left(\frac{\partial f_i}{\partial a_0} \right) + \Delta b \left(\frac{\partial f_i}{\partial b_0} \right) + \dots; i = 1, 2, \dots, n$$

Rearranging terms and dropping higher order derivatives yields

$$v_i \approx \Delta a \left(\frac{\partial f_i}{\partial a_0} \right) + \Delta b \left(\frac{\partial f_i}{\partial b_0} \right) + y'_i - y_i; i = 1, 2, \dots, n.$$

We define

$$r_i = y'_i - y_i \quad i = 1, 2, \dots, n$$

where the r 's are the residuals for the approximation curve $y' = f(x, a_0, b_0)$. Substituting, we can write our residual equations as

$$v_i \approx \Delta a \left(\frac{\partial f_i}{\partial a_0} \right) + \Delta b \left(\frac{\partial f_i}{\partial b_0} \right) + r_i ; \quad i = 1, 2, \dots, n$$

Since this system of equations is linear in the correction terms Δa and Δb , these terms can be derived by the method of least-squares.

At this point, one variation from the description given by Scarborough (1930) is introduced. Because the linearization of the system of equation is only valid for small Δa and Δb , it is possible to derive correction terms which yield solutions that extend beyond the local neighborhood of linearization. Under these circumstances, it is possible that the method will not converge to a valid solution. During any particular iteration, this non-convergence would appear as an increase in the total sum of squares of the residuals over the previous iterations.

To ensure a decrease in the total residuals (and therefore a converging solution) during each iteration, the correction terms are scaled by a term α to yield,

$$\begin{aligned} \hat{a} &= a_0 + \alpha \Delta a \\ \hat{b} &= b_0 + \alpha \Delta b \end{aligned}$$

The scaling term α is first set equal to one, and the calculated total residuals compared to those calculated in the previous iteration. If the residuals do not decrease, the scale factor α is halved until a decrease in the total residuals is observed. These new \hat{a} and \hat{b} become the new "initial estimates" a_0 and b_0 , which are then used in the next iteration. The process continues until the values of both Δa and Δb reach some suitable minimum, and a final \hat{a} and \hat{b} are derived. It is

theoretically possible for the solution to converge to a subsidiary minimum and therefore yield a poor model. However, the selection of the initial a_0 and b_0 by a regression in log-log space makes convergence on subsidiary maxima unlikely. An ASCII FORTRAN 77 subroutine for performing this algorithm is presented in Appendix A.3.

In practice, the regression models for the amplitude spectra (and final roughness model) are formulated interactively with a graphic display terminal. The operator can interactively edit the bathymetric profile under examination as well as control the frequency limits included in the regression analysis. This allows the software to delete white-noise levels, interpolation effects, and other contaminating factors from the analysis. The interactive control also allows the operator to detect visually spectra composed of two power law segments, and to fit each segment individually. This interactive software is included in the amplitude spectrum generating software listed in Appendix D.

Appendix A.2

```

SUBROUTINE POWWGT(A,B,FIRSTX,DELX,Y,N,ILIST,CTOFF1,CTOFF2)
C
C   THIS ROUTINE PERFORMS A BEST FIT TO DATA WITH A POWER LAW
C   FUNCTION OF THE FORM  $Y=A*X**B$  USING A WEIGHTING METHOD
C   AS DESCRIBED IN SCARBOROUGH(1930), ART. 114.
C   INPUTS ARE
C       A=COEFFICIENT OF X
C       B= EXPONENT OF X
C       X= ARRAY OF INDEPENDENT VARIABLE VALUES
C       Y= ARRAY OF DEPENDENT VARIABLE VALUES
C       N= NUMBER OF DATA PAIRS OF X AND Y
C       AMIN= MINIMUM VALUE FOR A CORRECTION TO STOP ITERATION
C       BMIN= MINIMUM VALUE FOR B CORRECTION TO STOP ITERATION
C       ILIST= 1 FOR SUMMARY OF ITERATION PROCESS, = 0 , NO LISTING
C   PROGRAMMED BY C.G.FOX-ADVANCED TECHNOLOGY STAFF,NAVOCEANO,4/15/83
C
C   DIMENSION X(1024),Y(1024)
C
C   COMPUTE INITIAL ESTIMATE OF A AND B BY PERFORMING A SIMPLE
C   LINEAR FIT ON LOG TRANSFORMED DATA
C
C   YSQR=1.
C   YQSUM=0.0
C   XPROD=0.0
C   XSUM=0.0
C   YSUM=0.0
C   XSQR=0.0
C   X(1)=FIRSTX
C   DO 10 I=2,N
10  X(I)=X(I-1)+DELX
C   WRITE(6,'(80X,2F10.4)') (X(I),Y(I),I=1,20)
C   DO 50 J=1,N
C   IF(Y(J).LE.0.0) GO TO 50
C   YTEMP=ALOG10(Y(J))
C   XTEMP=ALOG10(X(J))
C   IF(XTEMP.GT.CTOFF2.OR.XTEMP.LT.CTOFF1) GO TO 50
C   YSQR=YTEMP*YTEMP
C   XPROD=XPROD+(YTEMP*XTEMP*YSQR)
C   XSUM=XSUM+XTEMP*YSQR
C   YSUM=YSUM+YTEMP*YSQR
C   YQSUM=YQSUM+YSQR
C   XSQR=XSQR+(XTEMP*XTEMP*YSQR)
50  CONTINUE
C   B=((YQSUM*XPROD)-(XSUM*YSUM))/((YQSUM*XSQR)-(XSUM*XSUM))
C   A=(YSUM/YQSUM)-(B*(XSUM/YQSUM))
C   A=10.**A
C   RETURN
C   END

```

Appendix A.3

```

SUBROUTINE POWFIT(A,B,X,Y,N,AMIN,BMIN,ILIST)
C
C   THIS ROUTINE PERFORMS A BEST FIT TO DATA WITH A POWER LAW
C   FUNCTION OF THE FORM  $Y=A*X**B$  USING AN ITERATIVE METHOD
C   AS DESCRIBED IN SCARBOROUGH(1930), ART. 115.
C   INPUTS ARE
C       A=COEFFICIENT OF X
C       B= EXPONENT OF X
C       X= ARRAY OF INDEPENDENT VARIABLE VALUES
C       Y= ARRAY OF DEPENDENT VARIABLE VALUES
C       N= NUMBER OF DATA PAIRS OF X AND Y
C       AMIN= MINIMUM VALUE FOR A CORRECTION TO STOP ITERATION
C       BMIN= MINIMUM VALUE FOR B CORRECTION TO STOP ITERATION
C       ILIST= 1 FOR SUMMARY OF ITERATION PROCESS, = 0 , NO LISTING
C   PROGRAMMED BY C.G.FOX-ADVANCED TECHNOLOGY STAFF,NAVOCEANO,4/15/83
C
C   DIMENSION X(10),Y(10)
C
C   COMPUTE INITIAL ESTIMATE OF A AND B BY PERFORMING A SIMPLE
C   LINEAR FIT ON LOG TRANSFORMED DATA
C
C   XN=FLOAT(N)
C   XPROD=0.0
C   XSUM=0.0
C   YSUM=0.0
C   XSQR=0.0
C   WRITE(6,'(2F10.4)') (X(I),Y(I),I=1,N)
C   DO 50 J=1,N
C       IF(Y(J).EQ.0.0) GO TO 50
C       YTEMP=ALOG10(Y(J))
C       XTEMP=ALOG10(X(J))
C       XPROD=XPROD+(YTEMP*XTEMP)
C       XSUM=XSUM+XTEMP
C       YSUM=YSUM+YTEMP
50  XSQR=XSQR+(XTEMP*XTEMP)
C       BO=((XN*XPROD)-(XSUM*YSUM))/((XN*XSQR)-(XSUM*XSUM))
C       AO=(YSUM/XN)-(BO*(XSUM/XN))
C       AO=10.**AO
C
C   COMPUTE SUM OF SQUARES OF THE RESIDUALS
C
C   POLD=0.0
C   DO 100 I=1,N
100  POLD=POLD+((Y(I)-F3(X(I),AO,BO))**2)
C       ITERAT=0
C       NBIS=0
C       IF(ILIST.EQ.1)WRITE(6,110)
110  FORMAT(' ITERATION      # OF BISECTIONS          A          B
C       *RESIDUALS**2')
C       IF(ILIST.EQ.1)WRITE(6,120)ITERAT,NBIS,AO,BO,POLD

```

```

120 FORMAT(' ',I6,10X,I4,6X,3(4X,F10.4))
C
C   ZERO OUT MATRIX TERMS
C
150 A1=0.0
    B1=0.0
    D1=0.0
    E1=0.0
    G1=0.0
C
C   COMPUTE TERMS FOR LEAST SQUARES MATRIX CONSTRUCTION
C
    DO 200 I=1,N
      PARTA=F1(X(I),A0,B0)
      PARTB=F2(X(I),A0,B0)
      POWF=F3(X(I),A0,B0)
      A1=A1+(PARTA**2)
      B1=B1+(PARTA*PARTB)
      D1=D1+(PARTB**2)
      E1=E1+(PARTA*(Y(I)-POWF))
200  G1=G1+(PARTB*(Y(I)-POWF))
      C1=B1
C
C   COMPUTE CORRECTION TERMS FOR A AND B
C
      DIVSOR=(A1*D1-B1*C1)
      ACORR=(D1*E1-B1*G1)/DIVSOR
      BCORR=(A1*G1-C1*E1)/DIVSOR
C
C   CREATE NEW A AND B
C
230 A=A0+ACORR
    B=B0+BCORR/A0
C
C   COMPUTE NEW SUM OF SQUARES OF RESIDUALS WITH NEW ESTIMATES
C
    PNEW=0.0
    DO 250 I=1,N
250  PNEW=PNEW+((Y(I)-F3(X(I),A,B))**2)
C
C   TEST FOR CONVERGENT SOLUTION(PNEW < POLD)
C   IF NOT, BISECT CORRECTIONS AND RECOMPUTE
C
      IF(PNEW.LT.POLD) GO TO 300
      ACORR=.5*ACORR
      BCORR=.5*BCORR
      NBIS=NBIS+1
      IF(NBIS.GT.10) GO TO 300
      GO TO 230
C
C   TEST FOR MINIMUM CHANGE OF A AND B
C
300 IF(ABS(A-A0).GT.AMIN) GO TO 500

```

```

        IF (ABS(B-B0).GT.BMIN) GO TO 500
        GO TO 900
C
C      CORRECTION TERM NOT FINE ENOUGH, START NEW ITERATION
C
500  ITERAT=ITERAT+1
      AO=A
      BO=B
      POLD=PNEW
      IF (ILIST.EQ.1) WRITE (6,520) ITERAT,NBIS,AO,BO,POLD
520  FORMAT(' ',I6,10X,I4,6X,3(4X,F10.4))
      NBIS=0
      GO TO 150
900  ITERAT=ITERAT+1
      IF (ILIST.EQ.1) WRITE (6,920) ITERAT,NBIS,AO,BO,POLD
920  FORMAT(' ',I6,10X,I4,6X,3(4X,F10.4))
      RETURN
      END
C
C
C      FUNCTIONS TO CALCULATE POWER LAW FUNCTION AND PARTIAL
C      DERIVATIVES WITH RESPECT TO A AND B
C
      FUNCTION F1(X3,A3,B3)
C      CALCULATE PARTIAL OF  $A \cdot X^{**}B$  WITH RESPECT TO A
      F1=X3**B3
      A3=A3
      RETURN
      END
C
      FUNCTION F2(X4,A4,B4)
C      CALCULATE PARTIAL OF  $A \cdot X^{**}B$  WITH RESPECT TO B
      F2=(X4**B4)*ALOG(X4)
      A4=A4
      RETURN
      END
C
      FUNCTION F3(X5,A5,B5)
C      CALCULATE POWER LAW  $A \cdot X^{**}B$ 
      F3=A5*X5**B5
      RETURN
      END

```

Appendix B.1

Before generating amplitude spectra from a statistically non-stationary sample space, such as the sea floor, one must initially define provinces which are relatively homogeneous with respect to the frequency spectrum. Since generating an amplitude spectrum directly by Fourier transform assumes stationarity over the length of the input series, this "province picking" procedure must be performed by estimating the spectrum discretely in the spatial domain. Although the present application is new, the concept of estimating spectra in the time/space domain is not. Blackman and Tukey (1958) referred to such estimates as "pilot spectra" and describe two methods for their calculation. Godfrey (1967) also describes a method, very similar to that detailed here, which is used for predicting non-stationary time series. This section gives details of the procedure used in this study, presents performance tests of the algorithm, and include full FORTRAN-77 software for performing the analysis.

The initial step in processing is identical to that required for running an FFT. The data must be projected onto a straight-line segment and interpolated to even increments in distance. The straight line is generated by a simple least-squares fit of the navigation track; the best results are obtained when relatively straight line navigation is input. Large deviations in the track greatly degrade results. Next, points are mapped onto the nearest location on the least-squares line, without alteration if they are within a designated "pivot distance," or modified according to the local gradient if beyond this distance. Finally, the data are interpolated at a specified interval using a one-

dimensional cubic spline, which tends to preserve frequency content. The full algorithm is included in SUBROUTINE MAPCTN.

The subsequent stage of processing requires band-pass filtering of the interpolated data at ten nearly equi-spaced frequency bands. Filtering is done by sequential application of low-pass and high-pass filters, using a non-recursive, symmetric, least-squares filter developed by Martin (1957). The frequency response of this bank of filters is illustrated in Figure B-1. A review of the performance of the Martin filter can be found in McClain and Walden (1979). The filter cutoffs are designed to juxtapose at the 100% energy pass level. The total frequency bank was selected to span .02 - .25 cycles/data interval, or wavelengths of approximately 2 - .16 nautical miles for data recorded at 12 second intervals, or 10 - .8 nautical miles for one minute data. The filtering is performed by SUBROUTINE FILTER.

The next step of the algorithm requires estimating the instantaneous amplitude of all ten band-passed signals. Davis (1974) used a simple full-wave rectification, followed by a low-pass smoother to estimate the energy envelope. For this study, a true Hilbert transform is performed and manipulated to generate the energy envelope. The reader is referred to Kanasewich (1981) for a full development. Notice that the calculation of the envelope via Hilbert transform does require operating in the frequency domain. However, because the complete Fourier Transform is retained throughout, the requirement of stationarity is not applicable. The enveloping algorithm is contained in SUBROUTINE ENVEL.

The envelope generated in the previous step represents a continuous estimate of amplitude through space, for each selected frequency band. To estimate the full amplitude spectrum at each point on the profile,

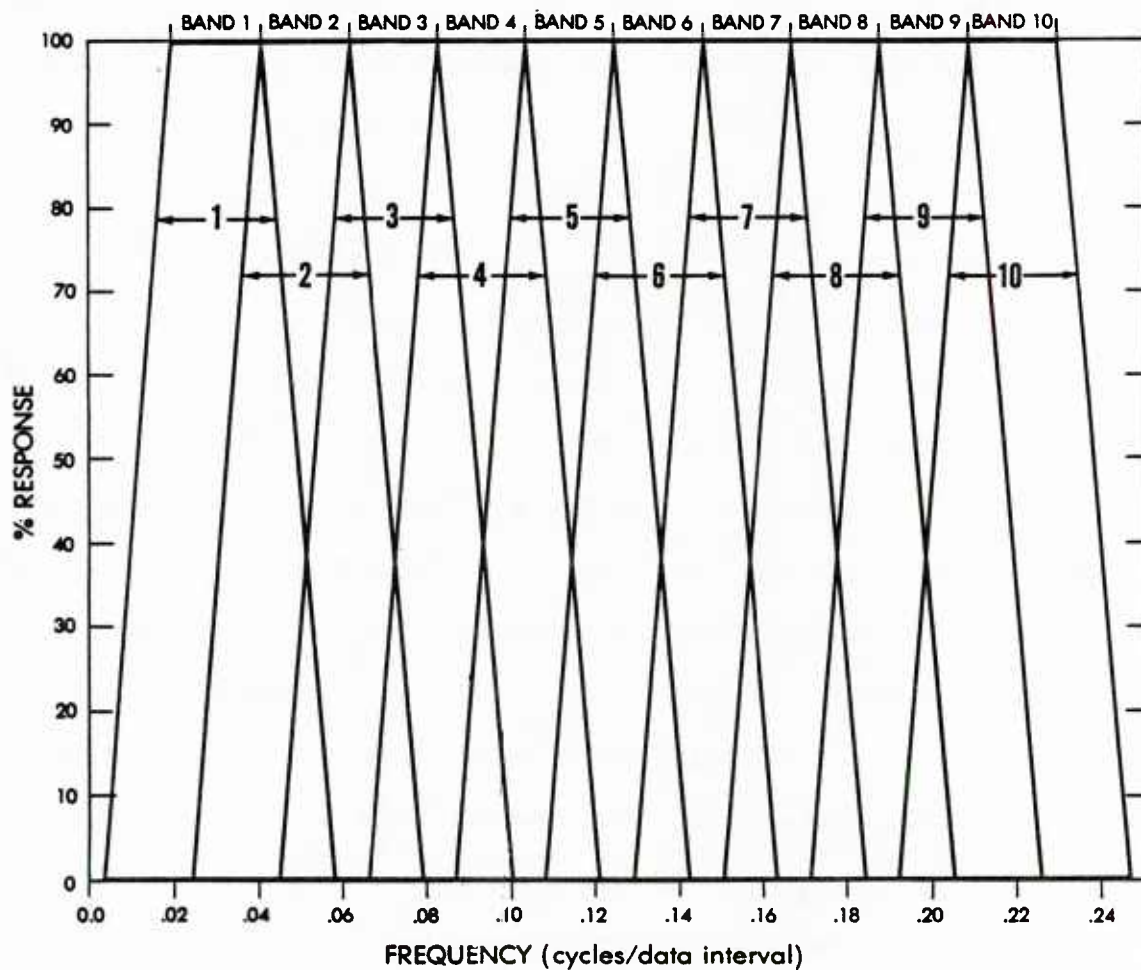


Figure B-1 Simplified frequency response of the bank of band-pass filters used to estimate amplitude spectra discretely in the spatial domain. Actual responses include side lobe leakages of less than 5%.

all ten amplitude versus frequency estimates are considered. Since the power law form of the spectrum is known, this functional form is used in an iterative regression procedure described in Appendix A and performed in SUBROUTINE POWFIT. The regression coefficients vary widely along the profile, and therefore it is desirable, in order to aid in the detection procedure, to smooth these estimates. To save calculation time, this is done by averaging 91 envelope estimates at each frequency before entering the regression routine. This process tends to smear the boundaries somewhat, but makes detection of provinces more reliable.

With smoothed estimates of the amplitude spectrum available continuously along a profile, the final stage of processing is to detect significant changes in the estimated spectra and on this basis impose province boundaries. The regression coefficients \hat{a} and \hat{b} represent the antilog of the y intercept, and the slope, respectively, of the spectrum projected in log-log space. The spectral slope, \hat{b} (which is related to the so-called Fractal dimension) is a worthwhile parameter for province detection. A simple algorithm is run across the slope estimates to detect significant, rapid changes (boundaries).

The regression coefficient \hat{a} is correlated to \hat{b} and therefore does not represent an independent parameter for detection. An alternative is to look at the total, band-limited RMS energy of the estimated spectra for significant shifts in total energy. These RMS parameters are easily calculated using Parseval's Formula (integrating the power spectrum) applied to the estimated spectra. In addition to detecting rapid changes as with the slope, the RMS is contoured to form segments of some minimum size. Although these detectors have proven fairly reliable, it is often necessary to interpret certain boundaries where the various

detectors disagree. All of the pertinent software is listed in Appendix B.2. The program runs with a core size of approximately 540 K bytes, and was written in ANSI Standard FORTRAN (1977) for a UNIVAC 1180/2 computer. The maximum profile length is 4100 interpolated data points and 145 points are lost from the end of the signal due to filtering.

Just as an electrical engineer investigates the performance of an instrument by operating on signals of known properties, the same technique can be used here to test the performance of the province picker algorithm. While an engineer might use a step, ramp, or impulse function as input, random signals with known spectral forms are used in this analysis. Many of the seemingly arbitrary choices of filters, averaging procedures, and other design decisions incorporated into the present province picker, were selected through feedback from performance tests with known signals.

An obvious choice of a signal with a known amplitude spectrum is random "white noise," with a continuous spectrum of zero slope. There are several means of producing such a signal. The simplest is to generate pseudo-random noise series of either a normal or uniform distribution. Figures B-2 and B-3 illustrate such signals with their spectra, which are indeed relatively flat. Notice the large amount of scatter in the amplitude estimates. An alternative method of generating "white noise" is actually to use a constant amplitude spectrum and uniformly distributed random phase spectrum, separate their real and imaginary parts, and inverse-transform the signals using the FFT. In this manner a perfectly flat, non-varying spectrum is assured, as is illustrated in Figure B-4. This is the signal source used in testing for this study, and the algorithm is presented in SUBROUTINE WHINOI.

UNIFORMLY DISTRIBUTED NOISE

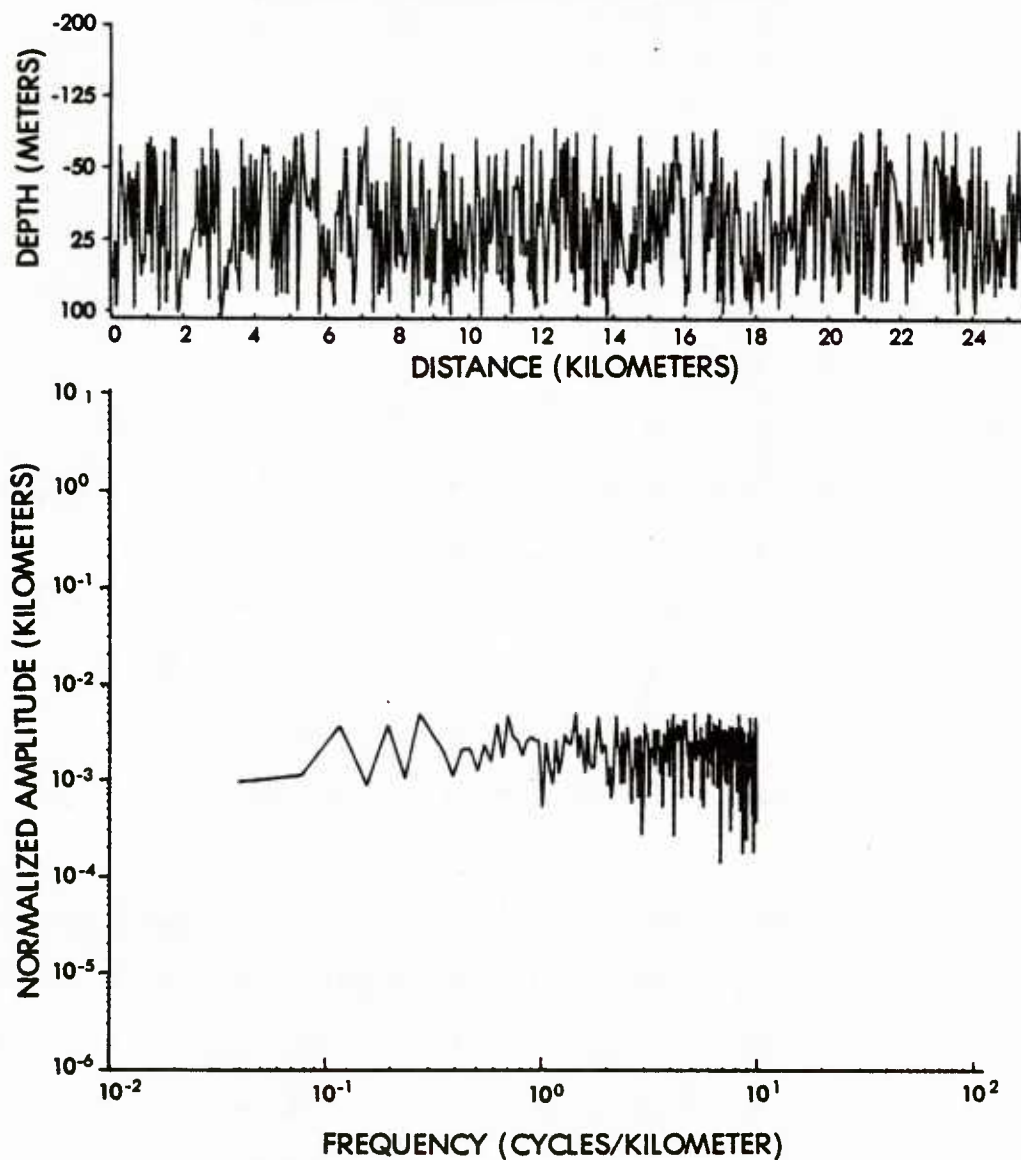


Figure B-2 An example of uniformly distributed random noise is shown in upper profile. Its corresponding amplitude spectrum (in lower profile) shows the flat (zero slope) form indicative of white noise. Notice the high degree of scatter in amplitude estimates. The same computer software was used as that used for bathymetric data.

NORMALLY DISTRIBUTED NOISE

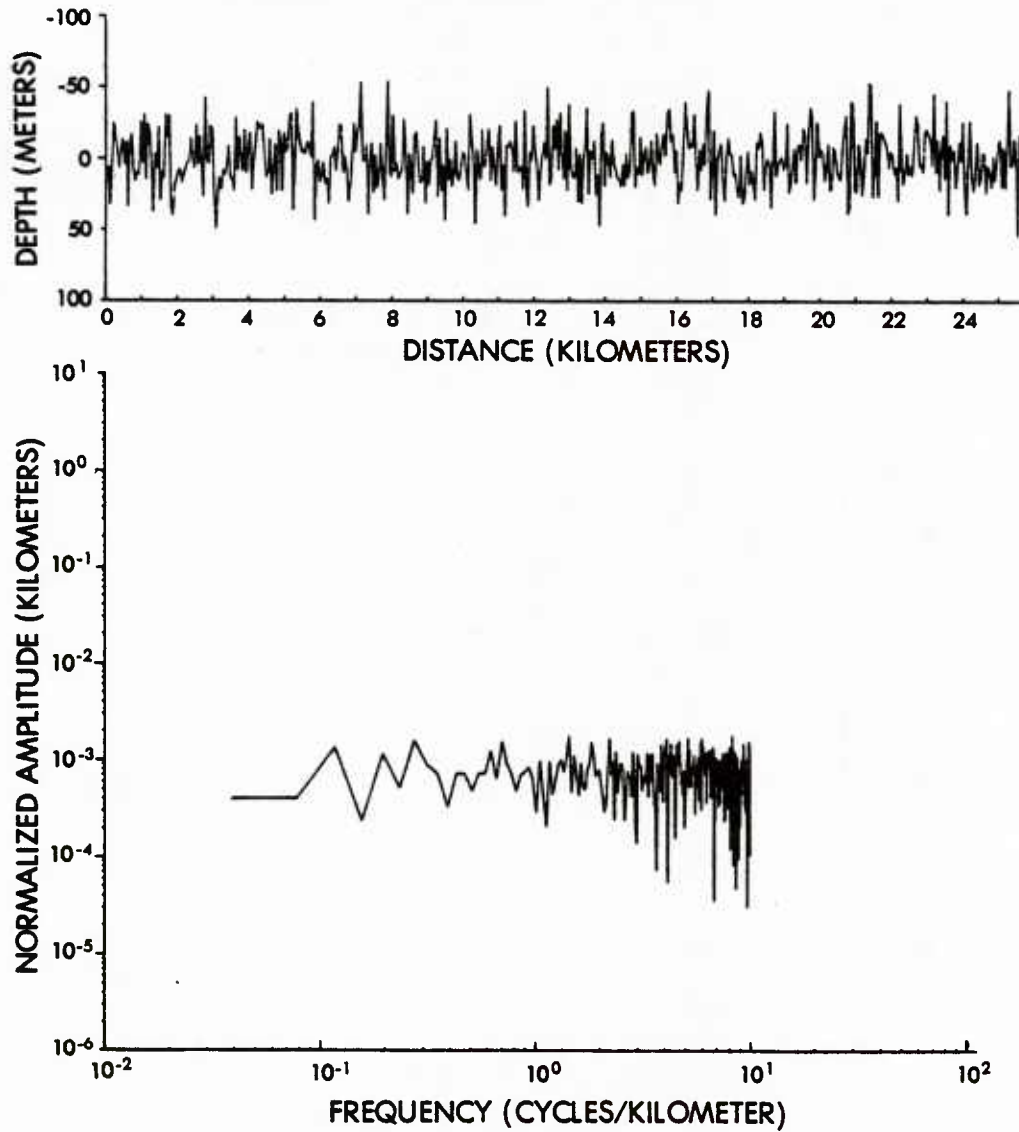


Figure B-3 An example of normally distributed random noise in the same format as Figure B-2. Notice the tendency of values to cluster about the mean (normal distribution) and the large scatter of amplitude estimates in the amplitude spectrum.

INVERSE TRANSFORM NOISE

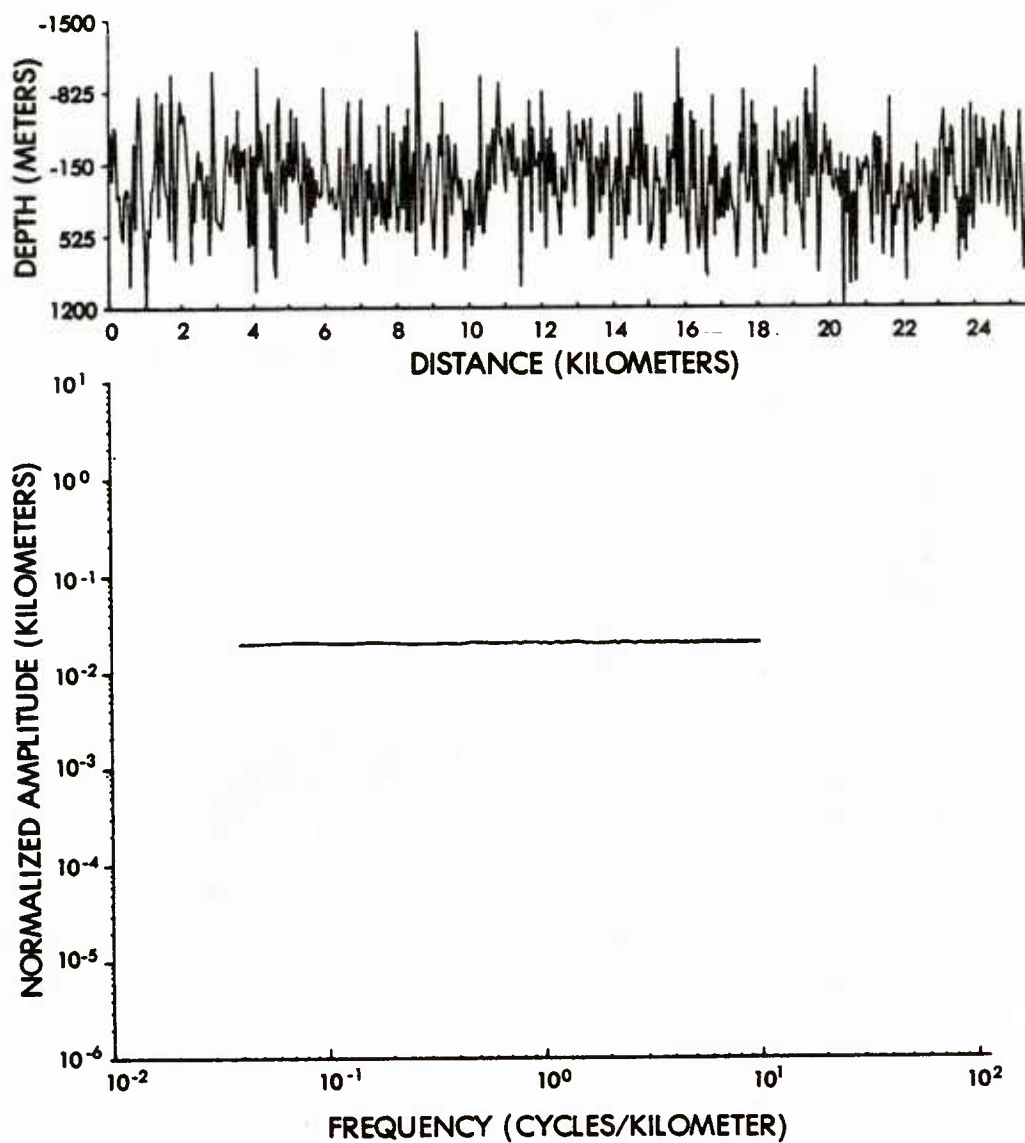


Figure B-4 An example of random "white noise" generated using an inverse Fast Fourier Transform. The method of calculation forces a perfectly constant amplitude spectrum. This "white noise" generator was used for performance testing of the province picker algorithm.

Figure B-5 illustrates the performance of the province picker when white noise is input. Examination of this output results in some interesting insights into the nature of stochastic processes. Despite the known property that the input signal has a perfectly flat, non-variable amplitude spectrum, all ten band-pass filtered signals show large fluctuations in amplitude. The amplitude recorded in the frequency spectrum represents simply an average amplitude computed over the length of the input time series. At any discrete point, the amplitude at a frequency could be widely removed from the average value. It was discovered through experimentation that these fluctuations were damped when wider band-pass filters were used; thus, the overlapping filter bank illustrated in Figure B-1 was designed. The slope values (plotted above the ten band-passed signals) do fluctuate about zero as expected. The standard deviation about zero averages about 0.2 over several runs which implies (assuming a normal distribution) that a change of slope of ± 0.4 can be detected with 95% confidence. Many of the decisions made in generating the regression analysis and smoothing, were designed to minimize this fluctuation.

In order to design a province detector properly, it is necessary to combine known signals of differing spectral slopes and RMS energies. For the purpose of this study, the resulting signal must also have an amplitude spectrum with power law form. One method of generating such a signal is through a Markov chain with a probability transition matrix which allows subsequent events either to raise or lower a constant increment with probability of 0.5 (see Ross, 1980). This signal, which is a special case of a random walk, fluctuates about its initial value and has a spectral form of

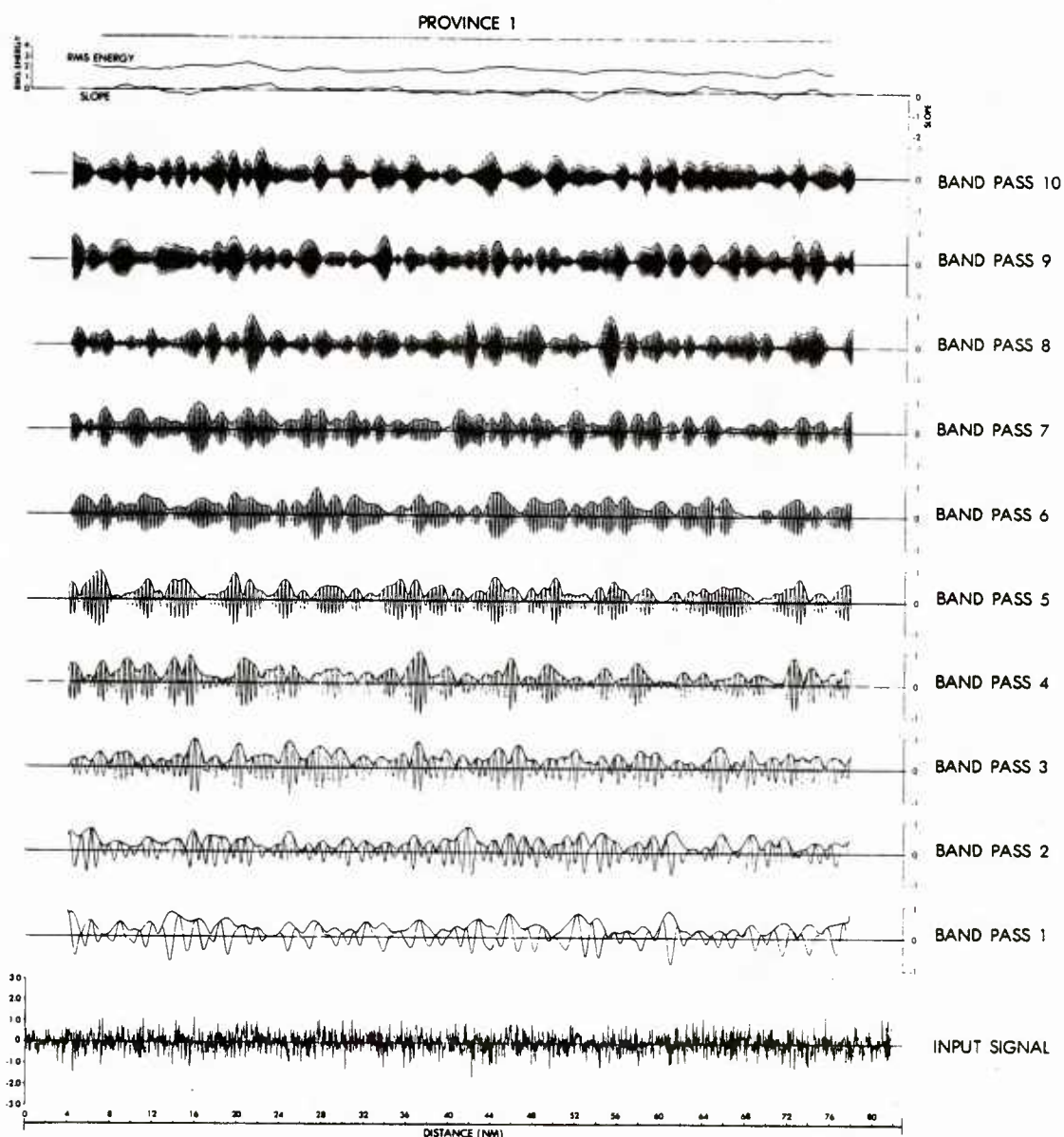


Figure B-5 Example of province picker output with "white noise" input illustrated in Figure B-4. The input signal is shown at the bottom, above which are the output of ten band-pass filters convolved with the data. The lowest signal (Band Pass 1) is the lowest frequency pass, while the highest (Band Pass 10) is the highest frequency pass. Above each band-passed signal is the energy envelope calculated by the Hilbert Transform method. Notice the large variability in energy for each band despite the constant amplitude input. At the top, the estimated spectral exponent (slope of log-transformed spectra) and the band-limited RMS energy calculated along the profile are plotted. Standard deviation of the slope parameter is .2. The algorithm was designed to minimize this "natural" variability.

$$A = \hat{a}s^{-1}$$

It is now possible with two known signals of different spectral characteristics to study the response of the province picker as it crosses the boundary between two such signals (provinces). Since it is also necessary to detect changes in total RMS energy without a change of slope, each signal can be multiplied by a constant using a corollary of the addition theorem of Fourier transforms (see Bracewell, 1965).

Figure B-6 illustrates an artificially generated random signal which consists of four distinct provinces. The first half of the signal is composed of "white noise" and the second half of 1/s noise generated via the random walk technique. Notice the rapid change in the slope parameter from 0 to -1 at the boundary, which was easily detected.

Within each half of the signal, the provinces are again divided with the second halves (second and fourth quarters) representing a doubling of the first halves (first and third quarters). Notice the obvious change of RMS energy, although the slope parameter is unaffected, illustrating the importance of detecting on two uncorrelated parameters. Several false alarms are observed on the derivative detector, but the province boundaries derived from contouring (represented by straight lines above the RMS energy profile) correspond to the known boundaries in the signal. Notice that provinces one and four show the same RMS energy level, but are delineated by their differences in spectral slope.

As stated earlier, the automatic detection is an aid to province boundary recognition, but in some cases, human intervention is needed to resolve inconsistencies. Also, the setting of contour interval or slope

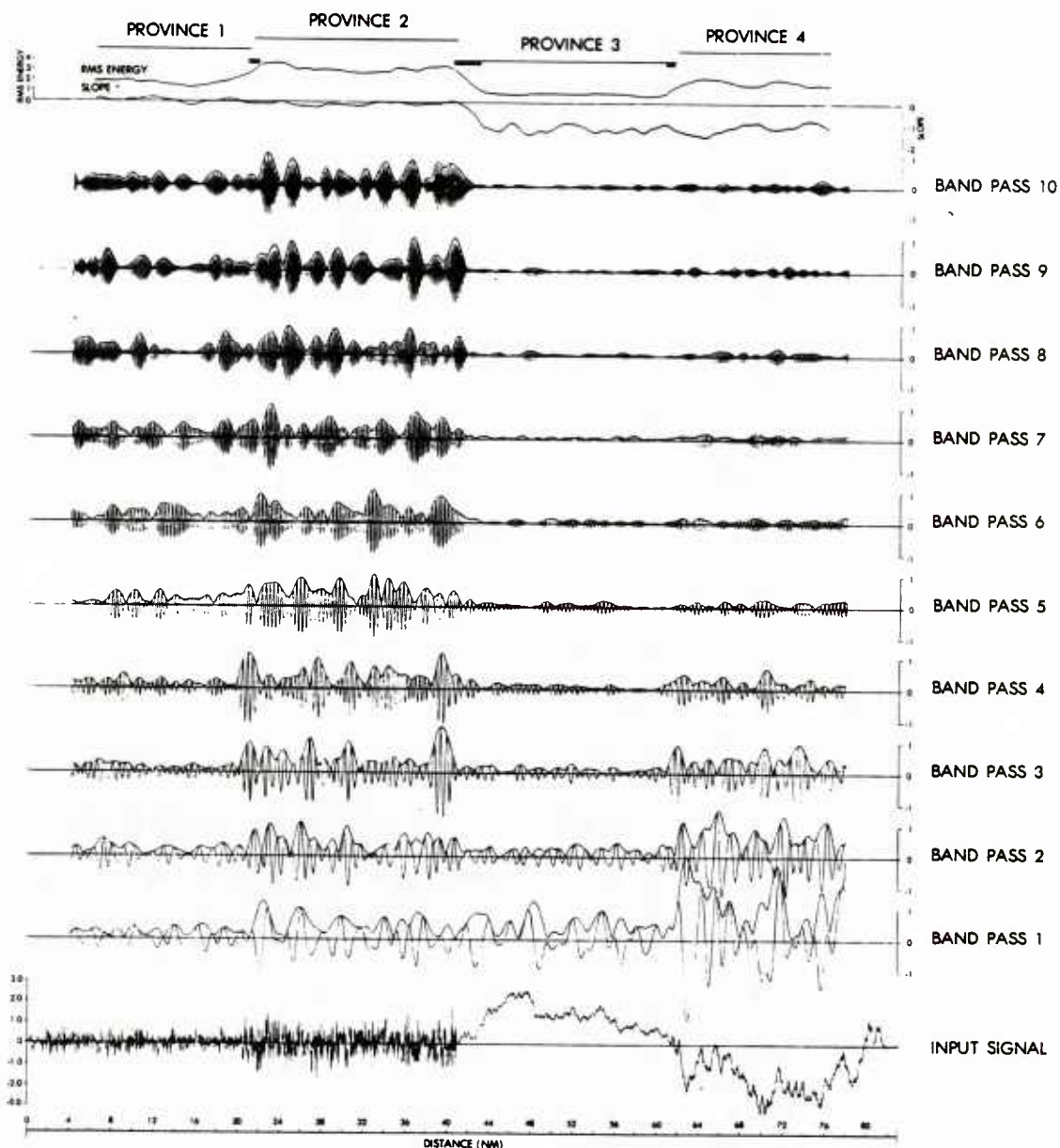


Figure B-6 Example of province picker output with mixed input of known signals. The first half of the signal is white noise ($A = as^0$), joined to the second half of random walk generated noise ($A = as^{-1}$) the amplitude of each half is doubled at the mid-point. The break in spectral slope parameter is easily detected. The change in level of RMS energy is contoured, as shown by straight line segments above the RMS energy profile.

threshold can be modified by the investigator depending upon the amount of resolution desired. Figure B-7 is a sample profile from real bathymetric data collected by the SASS system in the vicinity of the Gorda Rise. Boundaries are less distinct than in the artificially generated signal, as one would expect, however distinct changes of RMS energy (and in two cases changes of slope) do define quasi-stationary provinces. In practice, the slope parameter has offered little independent information for province picking, and therefore, construction of a simplified province detector based on RMS energy alone may prove to be adequate.

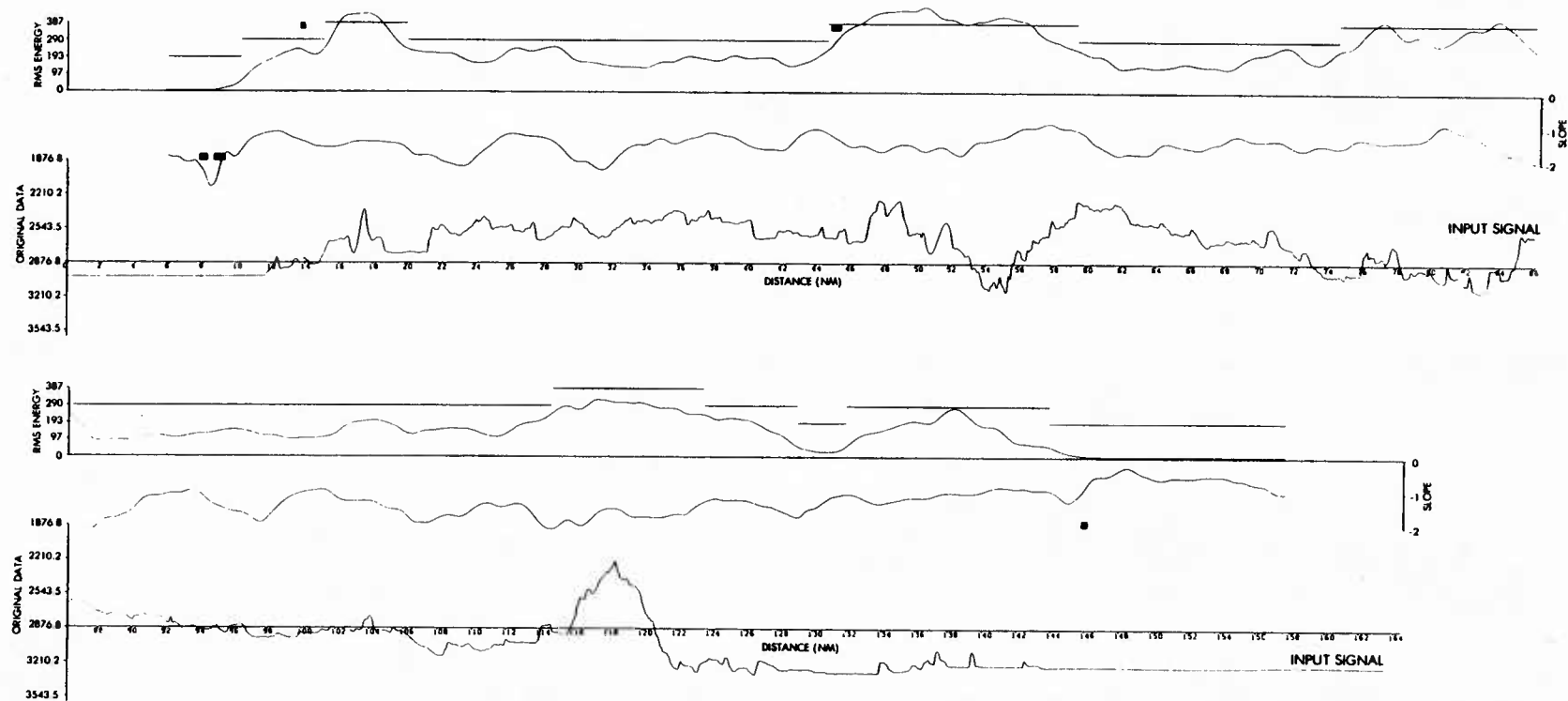


Figure B-7 Example of province picker output with SASS bathymetry input. Most province boundaries are defined by changes in RMS energy level. Data profiles corresponding to each province segment are later Fourier-analyzed to produce model parameters.

Appendix B.2

```

PROGRAM TO SELECT PROVINCES FOR SPECTRUM GENERATION

PROGRAMMED BY C.G. FOX,ADVANCED TECHNOLOGY STAFF,NAVOCEANO,5/15/84

PROVINCE SELECTION IS BASED ON A SPATIAL DOMAIN ESTIMATE OF THE
FUNCTIONAL DESCRIPTION OF THE SPECTRUM BASED ON A POWER LAW MODEL

      AMPLITUDE= A*FREQUENCY**B

THE SPECTRUM PARAMETERS A & B ARE ESTIMATED BY PERFORMING A
REGRESSION ANALYSIS ON THE ENERGY ENVELOPES GENERATED ON TEN
BAND PASSES OF THE DATA SPACED EVENLY IN FREQUENCY.  PROVINCE
BOUNDARY SELECTION IS BASED ON CHANGES IN THE BAND LIMITED
RMS LEVEL OF EACH LOCATION ALONG THE TRACKLINE AS DERIVED
BY INTEGRATING THE RESULTS OF THE REGRESSION MODEL.

PROGRAM CONTROLS ARE ENTERED IN FREE FORMAT FOLLOWING @XQT

JTOTL= NUMBER OF TRACKLINES OF DATA TO BE ANALYZED IN THIS ANALYSIS
      MAXIMUM IS CURRENTLY SET TO 50

IPLOT= 1, PRODUCE PLOT TAPE ON UNIT 10 OF INTERPOLATED DATA,
      OPTIONAL BAND PASS PLOTS, PROVINCES SPECTRAL PARAMETER
      ESTIMATES, AND PROVINCE BOUNDARIES.
      OUTPUT CAN GO TO ZETA OR CALCOMP PLOTTER
      0, NO PLOT TAPE IS PRODUCED

IBAND= 1, PLOT ALL BAND PASSED SIGNALS WITH ENVELOPES
      0, NO BAND PASSES
      IGNORED IF IPLOT=0

ISAVE1= 1, SAVE DATA WITHIN EACH PROVINCE ON UNIT 13 FOR LATER
      ANALYSIS IN FFT PROGRAM.
      0, NO DATA SAVED

ILIST= 1, PRODUCE COMPLETE LISTING OF ANALYSIS
      0, ONLY RUDIMENTARY LISTING IS PRODUCED

GRID= DESIRED SPACING OF INTERPOLATED DATA IN NAUTICAL MILES
      THIS SPACING IS NORMALLY SLIGHTLY LESS THAN THE ORIGINAL
      SPACING OF THE RAW DATA.

KPTS= NUMBER OF RAW DATA VALUES TO BE ANALYSED IN EACH PROFILE.
      READING OF THE DATA WILL CEASE WHEN THIS NUMBER IS REACHED

DATA INPUT IS CURRENTLY DESIGNED SUCH THAT FOLLOWING THIS CONTROL
CARD, THE PROGRAM EXPECTS A CARD IMAGE CONTAINING THE NAME(LESS

```

```

C      THAN 20 CHARACTERS) OF A FILE IN WHICH IS CONTAINED A LIST OF
C      ALL FILE NAMES TO BE USED IN THE ANALYSIS.  AFTER READING THIS
C      FILE NAME, JTOTL FILE NAMES ARE READ FROM THE FILE AND THE
C      PROGRAM AUTOMATICALLY OPENS THESE DATA FILES AS NEEDED.  USERS
C      MUST INSURE THAT THE FILE NAME LIST FILE AND ALL DATA FILES
C      ARE AVAILABLE TO THE RUN AT EXECUTION.  ONE CONVENIENT WAY
C      TO PROVIDE DATA TO THE RUN IS BY CREATING DATA AND LIST
C      ELEMENTS IN A PROGRAM FILE AND THEN CREATE AN @ADD ELEMENT TO
C      COPY ALL ELEMENTS INTO TEMPORARY FILES BEFORE EXECUTION
C
C      PARAMETER (ISIZ=7000)
C      DIMENSION X(ISIZ),Y(ISIZ),Z(ISIZ),AX(ISIZ),AY(ISIZ),AZ(ISIZ),
1WGT(240),K1(1000),K2(1000),K3(1000)
2,FRLOW(10),FRHIGH(10),ENVEST(10),TZ(ISIZ,12)
3,FRMEAN(10)
4,ENERGY(ISIZ),TZ11(ISIZ),TZ12(ISIZ)
EQUIVALENCE(TZ(1,11),TZ11(1)),(TZ(1,12),TZ12(1))
CHARACTER*20 FILE(50)
CHARACTER*20 INFILE
C      FRHIGH=HIGH FREQUENCY FOR DATA BANDPASS
C      FRLOW= LOW FREQUENCY FOR DATA BANDPASS
DATA FRLOW/.002,.023,.044,.065,.086,.107,.128,.149,.170,.191/
DATA FRHIGH/.041,.062,.083,.104,.125,.146,.167,.188,.209,.230/
C      SET FILTER PARAMETERS FOR BANDPASSES
FILSLP=.008
NUMFIL=50
C      NFIT IS LENGTH OF AVERAGE OVER ENERGY ENVELOPES
NFIT=91
C2MAX=0.0
C      SET PARAMETERS TO CONTROL DERIVATIVE PICKS ON SPECTRAL PARAMETERS
SLWIN=.4
SLWID1=1.
SLWID2=14.
ENWIN=400.
ENWID1=20.
ENWID2=100.
C      PDEL DETERMINES THE INTERVAL OF RMS ENERGY USED FOR PROVINCE
C      DETECTION
PDEL=.03
C      MIN=MINIMUM NUMBER OF POINTS ALLOWED WITHIN A PROVINCE
MIN=91
C      OSCALE=SCALING FACTOR(INCHES/UNIT) OF ORIGINAL DATA FOR PLOTTING
OSCALE=-1.
C      ESCALE= SCALING FACTOR FOR ENVELOPE UNITS
ESCALE=.0001
READ(5,*) JTOTL,IPLOT,IBAND,ISAVE1,ILIST,GRID,KPTS
3 IKONT=0
LTPS=1000
GRIDKM=GRID*1.852
IF(IPLOT.NE.1) GO TO 24
C      INITIALIZE PLOTTER

```

```

C      USE FOLLOWING CALL FOR CALCOMP PLOTTER OUTPUT
C      CALL PLOTS(0,0,10)
C      USE FOLLOWING CALL FOR ZETA PLOTTER OUTPUT
      CALL PLOTS(53,0,-10)
      CALL FACTOR(.5)
      CALL PLOT(1.0,1.0,-3)
C      READ NAME OF FILE CONTAINING LIST OF DATA FILE NAMES
24 READ(5,'(A20)') INFILE
25 OPEN(UNIT=18,FILE=INFILE,STATUS='OLD')
C      READ LIST OF DATA FILE NAMES FROM FILE INFILE
      DO 5 IK=1,JTOTL
      READ(18,'(A20)') FILE(IK)
5 CONTINUE
      CLOSE(UNIT=18)
C      READ X,Y,Z, VALUES FOR THIS TRACK.FIRST POINT IS
C      ASSUMED TO BE ORIGIN,PUT END OF FILE AT THE END OF EACH TRACK.
440 IKONT=IKONT+1
C      ZERO OUT TEMPORARY ARRAYS
      DO 441 J=1,10
      DO 441 I=1,ISIZ
441 TZ(I,J)= 0.0
      DO 442 I=1,ISIZ
      AX(I)=0.0
      AY(I)=0.0
      AZ(I)=0.0
      Z(I)=0.0
      Y(I)=0.0
442 X(I)=0.0
      IAVPLT=0
C      INPUT X(I)=LONGITUDE(DEC. DEG.),Y(I)=LAT,Z(I)=DEPTH
C      N=# OF POINTS - 1
      IKNT=IKONT
      JPTS=KPTS
      IF(ILIST.EQ.1) WRITE(6,45) FILE(IKONT)
45 FORMAT(' OPENING FILE ',A20)
C      ROUTINE TO READ LAT,LON,DEPTH FROM FILE # IKNT
      CALL PROVDR(JPTS,Y,X,Z,IKNT,FILE)
4 N=JPTS-1
      IF(ILIST.EQ.1) WRITE(6,'(24H NUMBER OF INPUT POINTS ,I5)')N
C      INTERPOLATE DATA ON STRAIGHT LINE
      CALL MAPCTN(GRID,X,Y,Z,N,AX,AY,AZ,JCT)
      IF(ILIST.EQ.1)WRITE(6,'(31H NUMBER OF INTERPOLATED POINTS ,I6)')
1JCT
839 C=JCT
      AZAVE=0.0
C      PLOT INTERPOLATED DATA
      DO 261 I=1,JCT
261 AZAVE=AZAVE+(AZ(I)/C)
      IF(IPLT.NE.1) GO TO 26
      XL=(C*.02)+0.5
      DV=50.*GRID
      CALL NEWPEN(1)

```

```

CALL AXES(0.,0.,12HDISTANCE(NM),-12,XL,0.,1.,0.,DV,-1)
EV=AZAVE-(3.0/OSCALE)
DV=1.0/OSCALE
CALL AXES(0.,-3.,13HORIGIAL DATA,!#,¢.,(),!.,EV,DV,1)
CALL SYMBOL(XL+.75,-.25,.5,12HINPUT SIGNAL,0.0,12)
IF(C2MAX.LT.XL) C2MAX=XL
CALL PLOT(0.0,(AZ(1)-AZAVE)*OSCALE,3)
DO 26 I=1,JCT
AJ=I-1
C=AJ*.02
D=(AZ(I)-AZAVE)*OSCALE
CALL PLOT(C,D,2)
26 CONTINUE
DO 27 I=1,JCT
27 Z(I)=AZ(I)
IF(IPLT.EQ.1)CALL PLOT(0.0,1.0,-3)
DO 237 IRUN=1,10
XRUN=IRUN
ENVMAX=0.0
IF(IPLT.EQ.1.AND.IBAND.EQ.1)CALL PLOT(0.0,4.0,-3)
C   BAND PASS FILTER DATA AT SPECIFIED INTERVAL
CALL FILTER(AZ,JCT,FRLOW(IRUN),FILSLP,NUMFIL,1,WGT)
CALL FILTER(AZ,JCT,FRHIGH(IRUN),FILSLP,NUMFIL,0,WGT)
IF(IPLT.EQ.1) CALL PLOT(0.0,0.0,3)
WGTMN=0.0
XNORM=((FRHIGH(IRUN)+.2)-FRLOW(IRUN))*(1./GRIDKM)
C   XNORM=1.
NTWICE=2*NUMFIL
DO 31 I=NTWICE,JCT-NTWICE
C---1
IF(IPLT.NE.1.OR.IBAND.NE.1) GO TO 31
C---1
AJ=I-1
C=AJ*.02
B=(AZ(I)/XNORM)*ESCALE
IF(I.EQ.NTWICE) CALL PLOT(C,B,3)
CALL PLOT(C,B,2)
31 AZ(I)=(AZ(I))/XNORM
C---1
IF(IPLT.NE.1.OR.IBAND.NE.1) GO TO 32
C---1
EV=-1.5/ESCALE
DV=1./ESCALE
CALL PLOT(0.0,0.0,3)
CALL AXES(0.,0.,1H,1,XL,0.,1.,0.,0.,-2)
CALL AXES(XL,-1.5,13HFILTERED DATA,-13,3.,90.,1.5,EV,DV,0)
CALL SYMBOL(XL+.75,-.25,.5,9HBAND PASS,0.0,9)
CALL NUMBER(XL+5.75,-.25,.5,XRUN,0.0,-1)
CALL PLOT(0.0,0.0,3)
CALL NEWPEN(2)
C COMPUTE APPROXIMATION TO ENVELOPE OF BAND PASSED DATA
32 CALL ENVEL(AZ,JCT)

```

```

        IF(IPLOT.EQ.1) CALL PLOT(0.0,0.0,3)
        ENVAVG=0.0
C---1
        IF(IPLOT.NE.1.OR.IBAND.NE.1) GO TO 321
C---1
        DO 44 I=NTWICE,JCT-NTWICE
        AJ=I-1
        C=AJ*.02
        B=AZ(I)*ESCALE
        IF(I.EQ.NTWICE) CALL PLOT(C,B,3)
        CALL PLOT(C,B,2)
        GO TO 322
321 DO 44 I=NTWICE,JCT-NTWICE
322 AZ(I)=ABS(AZ(I))
        IF(AZ(I).GT.ENVMAX) ENVMAX=AZ(I)
        ENVAVG=ENVAVG+(AZ(I)/(JCT-2*NUMFIL))
C      ENVELOPE ENERGY IS STORED IN THE APPROPRIATE COLUMNS
C      OF 2-DIMENSIONAL ARRAY TZ
        44 TZ(I,IRUN)=AZ(I)
        FRDIFF=FRHIGH(IRUN)-FRLOW(IRUN)
        IF(IPLOT.EQ.1) CALL PLOT(0.0,0.0,3)
        IF(IPLOT.EQ.1) CALL NEWPEN(1)
        DO 836 I=1,JCT
836 AZ(I)=Z(I)
837 CONTINUE
C      LINEAR REGRESSION OF TEN ENVELOPE ESTIMATES FOR EACH POSITION
C      FIRST COMPUTE AVERAGE ENVELOPE
        840 DO 841 I=1,10
        FRMEAN(I)=(((FRLOW(I)+.017)+FRHIGH(I))/2.)
C      CONVERT CYCLES/DI TO CYCLES/KM
        841 FRMEAN(I)=FRMEAN(I)*(1./GRIDKM)
        FR1=(FRLOW(1)+.017)*(1./GRIDKM)
        FR2=FRHIGH(10)*(1./GRIDKM)
        DO 850 I=NTWICE,JCT-(NTWICE+NFIT)
        DO 846 J=1,10
        ENVEST(J)=0.0
        FIT=FLOAT(NFIT)
        DO 845 K=1,NFIT
        ENVEST(J)=ENVEST(J)+TZ(I+K,J)
845 CONTINUE
C      IF(FIT.EQ.0.0) GO TO 846
        ENVEST(J)=ENVEST(J)/FIT
846 CONTINUE
C      PERFORM ITERATIVE REGRESSION, STORE B & A IN
C      COLUMNS 11 & 12 OF ARRAY TZ
        850 CALL POWFIT(TZ12(I+((NFIT/2)+1)),TZ11(I+((NFIT/2)+1)),FRMEAN(1),
        *ENVEST(1),10,0.000001,.01,0)
C      PLOT SLOPE PARAMETER B
        IF(IPLOT.NE.1) GO TO 859
        CALL PLOT(0.0,4.0,-3)
        CALL AXES(0.0,0.0,1H,1,XL,0.,1.,0.,0.,-2)
        CALL NEWPEN(2)

```

```

      CALL AXES(XL,-2.0,5HSLOPE,-5,2.0,90.,1.0,-4.0,2.0,-1)
      CALL PLOT(0.0,0.0,3)
859  AVSLP=0.0
      KKNT=0
      SLWID=SLWID2-SLWID1
      ENWID=ENWID2-ENWID1
      INWID1=IFIX(ENWID1)
      LSWID1=IFIX(SLWID1)
      INWID2=IFIX(ENWID2)
      LSWID2=IFIX(SLWID2)
      DO 877 K=(NTWICE+1)+(NFIT/2),JCT-((NTWICE+1)+(NFIT/2))
      KKNT=KKNT+1
      C=(K-1)*.02
      B=(TZ(K,11))/2.
      AVSLP=AVSLP+(TZ(K,11)/(JCT-(4*NUMFIL+(NFIT+1))))
      IF(IPL0T.NE.1) GO TO 876
      IF(KKNT.EQ.1) CALL PLOT (C,B,3)
      CALL PLOT(C,B,2)
876  IF(KKNT.LE.LSWID2) GO TO 877
      IF(K.GE.(JCT-(NTWICE+NFIT/2+1+LSWID2))) GO TO 877
      PREAV=0.0
      POSTAV=0.0
C      DO 8761 KNB=LSWID1,LSWID2
C      PREAV=PREAV+(TZ(K-KNB,11)/SLWID)
C8761 POSTAV=POSTAV+(TZ(K+KNB,11)/SLWID)
C      IF(ABS(POSTAV-PREAV).LT.SLWIN) GO TO 877
C      CALL SYMBOL(C,-2.,.2,16,0.0,-1)
C      CALL PLOT(C,B,3)
877  CONTINUE
C      PLOT ARRAY OF RMS ENERGY
      IF(IPL0T.EQ.1) CALL NEWPEN(1)
      KKNT=0
      AVENER=0.0
      DO 878 L=(NTWICE+1)+(NFIT/2),JCT-((NTWICE+1)+(NFIT/2))
C      CALCULATE BAND LIMITED RMS-FIRST SQUARE FUNCTION AND INTEGRATE
C      INTEGRAL((A**B)**2)=(A**2/(2*B+1)*F**(2*B+1)
      XINTLO=(TZ(L,12)**2/(2.*TZ(L,11)+1.))*FR1**(2.*TZ(L,11)+1.)
      XINTHI=(TZ(L,12)**2/(2.*TZ(L,11)+1.))*FR2**(2.*TZ(L,11)+1.)
C      SINCE SPECTRUM IS SYMMETRIC ABOUT ZERO, CAN EVALUATE INTEGRAL
C      BY MULTIPLYING EVALUATED RESULT BY TWO
      ENERGY(L)=2.*(XINTHI-XINTLO)
C      TO CALCULATE MEAN SQUARE, DIVIDE BY WIDTH
      ENERGY(L)=ENERGY(L)/(2.*(FR2-FR1))
C      NOW TAKE SQUARE ROOT TO DETERMINE RMS
      ENERGY(L)=SQRT(ENERGY(L))
878  AVENER=AVENER+(ENERGY(L)/(JCT-(4*NUMFIL+(NFIT+1))))
      ENSCAL=4.*AVENER
      IF(IPL0T.NE.1) GO TO 8782
      CALL AXES(0.0,0.0,10HRMS ENERGY,10,2.,90.,0.5,0.0,AVENER/2.,
      *-1)
      CALL PLOT(0.0,0.0,3)
8782 DO 8781 L=(NTWICE+1)+(NFIT/2),JCT-((NTWICE+1)+(NFIT/2))

```

```

KKNT=KKNT+1
C=(L-1)*.02
B=ENERGY(L)*(1./AVENER)
IF(L.EQ.(NTWICE+1)+(NFIT/2).AND.IPLOT.EQ.1) CALL PLOT(C,B,3)
IF(IPLOT.EQ.1) CALL PLOT(C,B,2)
IF(KKNT.LE.INWID2) GO TO 8781
IF(L.GE.(JCT-((NTWICE+NFIT/2+1)+INWID2))) GO TO 8781
PREAV=0.0
POSTAV=0.0
DO 8771 KNB=INWID1,INWID2
PREAV=PREAV+(ENERGY(L-KNB)/ENWID)
8771 POSTAV=POSTAV+(ENERGY(L+KNB)/ENWID)
IF(ABS(POSTAV-PREAV).LT.ENWIN) GO TO 8781
CALL SYMBOL(C,2.,.2,16,180.0,-1)
CALL PLOT(C,B,3)
8781 CONTINUE
DO 879 I=(NTWICE+1)+(NFIT/2),JCT-((NTWICE+1)+(NFIT/2))
RMSSLP=RMSSLP+ABS((TZ(I,11)-AVSLP)**2)/(JCT-(4*NUMFIL+(NFIT-1)))
879 RMSENG=RMSENG+ABS((ENERGY(I)-AVENER)**2)/(JCT-(4*NUMFIL+(NFIT-1)))
RMSSLP=SQRT(RMSSLP)
RMSENG=SQRT(RMSENG)
C WRITE(6,'(4(F8.3,2X))') AVSLP,RMSSLP,AVENER,RMSENG
IST=(NTWICE+1)+(NFIT/2+1)
IEND=JCT-(IST-1)
333 CONTINUE
C PICK PROVINCE BOUNDARIES,STORE PROVINCE NUMBER FOR EACH POINT IN X
DO 34 I=IST,IEND
X(I)=IFIX(SQRT(ENERGY(I))/PDEL)+1
34 CONTINUE
C OUTPUT POSITIONS OF PROVINCE BOUNDARIES
C WRITE(06,60) CUT
C 60 FORMAT(' PROV.NO TYPE 1ST LAT LONG LAST LAT LONG
C 1 RMS-FILTERED CUT=',F7.5)
IPNUM=X(IST)
SUM=0.0
JST=IST
KST=1
DO 35 I=IST,IEND
JPNUM=X(I)
SUM=SUM+X(I)
IC=I-JST
IF(JPNUM.EQ.IPNUM.AND.I.LT.IEND) GO TO 35
C IF((IC+1).LT.MIN) GO TO 35
JJ=I
C COMPUTE AVERAGE PROVINCE NO.
AC=IC+1
AVE=SUM/AC
IAVE=AVE
BAVE=IAVE
AVE=AVE-BAVE
IF(AVE.GE.0.5) IAVE=IAVE+1
IPNUM=IAVE

```

```

K1(KST)=JST
K2(KST)=JJ
K3(KST)=IPNUM
JST=JJ
SUM=0.0
IPNUM=X(JST)
IF(KST.EQ.1) GO TO 116
MST=KST-1
IF(IAVE.NE.K3(MST)) GO TO 116
K2(MST)=K2(KST)
GO TO 35
116 KST=KST+1
IF(KST.GT.LTPS) GO TO 117
35 CONTINUE
GO TO 118
117 WRITE(06,119)
119 FORMAT(' YOU HAVE TOO MANY PROVINCES-INCREASE DIMENSION OR PDEL')
GO TO 500
C NOW OUTPUT FINAL PROVINCE BOUNDARIES OF AT LEAST MIN. SIZE
118 K3(KST)=99
KST=KST-1
C SMOOTH SMALL PROVINCE SEGMENTS
CALL PRVFIX(K1,K2,K3,MIN,KST)
J2=1
DO 36 I=1,KST
II=I+1
IF(K3(II).EQ.K3(I)) GO TO 36
JST=K1(J2)
JJ=K2(I)
IPNUM=K3(J2)
ISDLAT=AY(JST)
A=ISDLAT
SELAT=ABS(AY(JST)-A)*60.
ISDLNG=AX(JST)
A=ISDLNG
SELNG=ABS(AX(JST)-A)*60.
IDLAT=AY(JJ)
A=IDLAT
EELAT=ABS(AY(JJ)-A)*60.
IDLNG=AX(JJ)
A=IDLNG
EMLNG=ABS(AX(JJ)-A)*60.
IDIFF=K2(I)-K1(I)
C COMPUTE RMS LEVEL OF HIGH PASSED DATA FOR THIS PROVINCE
C ALSO AVERAGE SPECTRAL SLOPE AND Y-INTERCEPT
C3=ABS(JJ-JST+1)
RMS=0.0
SLOPEX=0.0
XINTER=0.0
DO 37 IE=JST,JJ
SLOPEX=SLOPEX+(TZ(IE,11)/C3)
XINTER=XINTER+(TZ(IE,12)/C3)

```

```

37 RMS=RMS+(ENERGY(IE)/C3)
C  ADJUST ENERGY LEVEL IN LOG-LOG SPACE AFTER NORMALIZATION
    XINTER=10**(ALOG10(XINTER)-.5)
    IPNUM=IFIX(SQRT(RMS)/PDEL)+1
    IF(ILIST.EQ.1)WRITE(6,51)I,IPNUM,ISDLAT,SELAT,ISDLNG,SELNG,IDLAT,
1  EELAT,IDLNG,EMLNG,RMS,IDIFF,SLOPEX,XINTER
C    LOOP TO INSERT DATA INTO FILE FOR LATER FFT RUNS
    IF(ISAVE1.NE.1) GO TO 49
    ENDMRK=9.999999
    NPTS=JJ-JST
    WRITE(13,46) FILE(IKONT),I,SLOPEX,XINTER,GRID,NPTS
    WRITE(13,50)I,IPNUM,ISDLAT,SELAT,ISDLNG,SELNG,IDLAT,EELAT,
1  IDLNG,EMLNG,RMS
    WRITE(13,47)(AZ(IQ),IQ=JST,JJ)
    XRMS=SRMS(AZ(JST),NPTS)
46  FORMAT(A20,I2,1X,F8.3,1X,E9.3,1X,F7.4,I5)
47  FORMAT(10F8.6)
    WRITE(13,47)ENDMRK
49  IF(IPLOT.NE.1) GO TO 248
    APNUM=.5+IPNUM*.5
    AJ=JST-1
    BJ=JJ-1
    C1=AJ*.02
    C2=BJ*.02
    CALL PLOT(C1,APNUM,3)
    CALL PLOT(C2,APNUM,2)
50  FORMAT(I5,I8,4(1X,I4,F6.2),F10.4)
51  FORMAT(I5,I8,4(1X,I4,F6.2),F10.4,I6,2F10.6)
248 J2=II
36  CONTINUE
880 IF(IKONT.EQ.JTOTL) GO TO 500
C  REPOSITION PLOTTER FOR NEXT PLOT
    IF(MOD(IKONT,4).NE.0) GO TO 882
    C2MAX=C2MAX+15.0
    IF(IPLOT.EQ.1) CALL PLOT(C2MAX,-44.0,-3)
    C2MAX=0.0
    GO TO 440
882 IF(IPLOT.EQ.1) CALL PLOT(0.0,8.0,-3)
    GO TO 440
500 IF(IPLOT.EQ.1) CALL PLOT(0.0,0.0,999)
    IF(ISAVE1.GT.0) CLOSE(UNIT=13)
    STOP
    END

```

```

C   READER SUBROUTINE FOR PROVICK
      SUBROUTINE PROVVD(NP,XLAT,XLONG,DEPTH,IKONT,FILE)
      DIMENSION XLAT(3000),XLONG(3000),DEPTH(3000)
      CHARACTER*20 FILEN
      CHARACTER*20 FILE(20)
      KNTER=0
      400 FILEN=FILE(IKONT)
C   WRITE(6,433)FILEN
      433 FORMAT(' OPENING FILE ',A20)
      OPEN(UNIT=12,FILE=FILEN,STATUS='OLD',FORM='FORMATTED')
      DO 420 I=1,NP
      438 READ(12,434,END=470) XLAT(I),XLONG(I),IDEPH
      434 FORMAT(9X,F12.8,F13.8,I7)
      KNTER=I
C   IF(IDEPH.LE.0) PRINT *,'DATA POINT SKIPPED'
      IF(IDEPH.LE.0) GO TO 438
      DEPTH(I)=IDEPH*.0018288
      420 IF(I.LT.30)WRITE(6,*)XLAT(I),XLONG(I),DEPTH(I)
      GO TO 490
      470 NP=KNTER
      490 CLOSE(UNIT=12)
      WRITE(6,492)NP
      492 FORMAT(' NUMBER OF POINTS READ =',I5)
      RETURN
      END

```

```

      SUBROUTINE MAPCTN(GRID,X,Y,Z,N,AX,AY,AZ,ICT)
C  ROUTINE TO MAP DATA VALUES(Z) WITH ASSOCIATED POSITIONS
C  (X=LONG DECIMAL DEG.,Y=LAT DECIMAL DEG.)FROM A RELATIVELY STRAIGHT
C  SEGMENT OF SURVEY TRACK ONTO A STRAIGHT LINE,ADJUST THE (Z) VALUE FOR
C  THE AMOUNT OF SHIFT REQUIRED BY THE MAPPING AND INTERPOLATE NEW (Z)
C  VALUES(AZ) AT AN EQUALLY SPACED DISTANCE(GRID IN DECIMAL NAUTICAL MI.
C  AND ASSOCIATED POSITIONS AX,AY ALONG THIS STRAIGHT LINE.
C** N=NO.OF ORIGINAL X,Y,Z INPUT PTS., ICT= NO.OF OUTPUT PTS.
C** NOTE-SINCE THIS IS A CARTESIAN MAP WHICH DOES NOT ACCOUNT FOR LONG
C  CONVERGENCE,IT SHOULD NOT BE USED FOR SEGMENTS COVERING A LARGE
C  LATITUDE RANGE.
C** NOTE-ORIGINAL XYZ DATA IS DESTROYED IN THIS ROUTINE
C*** THIS ROUTINE CALLS GINT, SPLINE,SPLICO,SortY
      DIMENSION X(7000),Y(7000),Z(7000),AX(7000),AY(7000),AZ(7000),
      *DIST(7000)
      DO 55 I=1,7000
55  DIST(I)=0.0
      JDIR=1
      IF(ABS(X(N)-X(1)).GE.ABS(Y(N)-Y(1))) JDIR=0
      ATER=9999.99
      RAD=0.00029089
      BLONG=X(1)*60.0
      BLAT=Y(1)*60.0
      DO 1 I=1,N
      IF(JDIR.EQ.1)GO TO 3
      X(I)=BLONG-X(I)*60.0
      Y(I)=Y(I)*60.0-BLAT
      GO TO 1
3  AY(I)=BLONG-X(I)*60.0
      X(I)=Y(I)*60.0-BLAT
      Y(I)=AY(I)
1  CONTINUE
      AN=N
C  MAP INPUT POSITIONS ONTO STRAIGHT LINE TO PREPARE DATA FOR
C  INTERPOLATION ON AN EQUAL DISTANCE BASIS
      A=0.0
      B=0.0
      C=0.0
      D=0.0
      DO 5 I=1,N
      A=A+X(I)
      B=B+X(I)**2
      C=C+Y(I)
5  D=D+Y(I)*X(I)
      A1=(C*B-D*A)/(AN*B-A**2)
      A2=(C-A1*AN)/A
      IF(ABS(A2).LT.0.000001)A2=0.000001
C  LEAST SQUARES LINE IS Y=A1+A2X
C  NOW SEARCH FOR A POINT LESS THAN PIVOT DISTANCE FROM TRACK LINE
C  TO USE FOR 1ST PIVOT AND MAP PTS.ONTO TRACK WITH CORRECT Z VALUE
C  POINTS LT PIVOT DIST FROM TRACK WILL HAVE THEIR POSITS MAPPED ONTO
C  THE TRACK BUT THEIR Z VALUE WILL NOT BE CHANGED
      SUM=0.0

```

```

DO 6 I=1,N
DIST(I)=ABS((Y(I)-A2*X(I)-A1)/ (SQRT(A2**2+1.0)))
6 SUM=SUM+DIST(I)**2
PIVOT=SQRT(SUM/AN)
C REMOVE POINTS THAT MAY HAVE A BAD POSITION
XPIVOT=3.0*PIVOT
J=0
DO 42 I=1,N
IF(DIST(I).GT.XPIVOT) GO TO 42
J=J+1
X(J)=X(I)
Y(J)=Y(I)
Z(J)=Z(I)
DIST(J)=DIST(I)
42 CONTINUE
N=J
AN=N
DO 7 I=1,N
IF (DIST(I)- PIVOT) 8,8,7
7 CONTINUE
8 A3= -1.0/A2
AX(I)=(A1+A3*X(I)-Y(I))/(A3-A2)
AY(I)= A2*AX(I) +A1
AZ(I)=Z(I)
IA=I+1
C NOW WORK BACKWARDS ON TRACK TO PICK UP POINTS THAT FAILED
C PIVOT TEST
11 J=I-1
IF(J)12,12,9
9 DELZ=(Z(J)-Z(I))/SQRT((X(I)-X(J))**2 +(Y(I)-Y(J))**2)
AX(J)=(A1+A3*X(J)-Y(J))/(A3-A2)
AY(J)=A2*AX(J)+A1
AZ(J)=(DELZ*SQRT((AX(I)-AX(J))**2+(AY(I)-AY(J))**2))+AZ(I)
I=J
GO TO 11
C NOW WORK FORWARD ON TRACK TO PICK UP REMAINING PTS.
12 DO 13 I=IA,N
IF (DIST(I)- PIVOT) 14,14,15
14 AX(I)=(A1+A3*X(I)-Y(I))/(A3-A2)
AY(I)= A2*AX(I) +A1
AZ(I)=Z(I)
GO TO 13
15 J= I-1
DELZ=(Z(I)-Z(J))/SQRT((X(I)-X(J))**2 +(Y(I)-Y(J))**2)
AX(I)=(A1+A3*X(I)-Y(I))/(A3-A2)
AY(I)=A2*AX(I) +A1
AZ(I)=(DELZ*SQRT((AX(I)-AX(J))**2+(AY(I)-AY(J))**2))+AZ(J)
13 CONTINUE
C SORT INPUT SO THAT THE INDEPENDENT VARIABLE IS MONOTONIC AND REMOVE
C CLOSELY SPACED POINTS TO CONTROL SPLINE INTERPOLATION
DAVE=0.0
DO 44 I=2,N
J=I-1

```

```

44 DAVE=DAVE+X(I)-X(J)
   DAVE=0.3*(ABS(DAVE/AN))
   CALL SORTY(AY,AX,AZ,Y,X,Z,N,1,1,DAVE)
   IF(JDIR.LT.1) GO TO 92
   DO 93 I=1,N
     Z(I)=AZ(I)
     X(I)=AX(I)
93  Y(I)=AY(I)
   GO TO 94
92  DO 95 I=1,N
     Z(I)=AZ(I)
     X(I)=AX(I)
95  Y(I)=AY(I)
94  CONTINUE
C RESET ORIGIN TO FIRST MAPPED POINT
   BLAT=BLAT+Y(1)
   BLONG=BLONG-X(1)
   DX=X(1)
   DY=Y(1)
   DO 71 I=1,N
     X(I)=X(I)-DX
71  Y(I)=Y(I)-DY
C NOW INTERPOLATE ALONG TRACK AT DESIRED GRID SPACING
C COMPUTE APPROX.LENGTH OF LONGITUDE FOR THIS TRACK
C USE APPROX. MIDLATITUDE AS BASIS AND TABLE 6(BOWDITCH)
   NN=N/2
   AL=(Y(NN)+BLAT)*RAD
   A=(111415.13*COS(AL)-94.55*COS(3.*AL)+.012*COS(5.*AL))/60.0
C UNITS OF A ARE METERS/MINUTE OF LONGITUDE
C COMPUTE APPROX.NAUTICAL MILES/MINUTE OF LONGITUDE
   19 B=A*(1.0/1852.0)
C CONVERT X COORDINATE OF MAPPED POSITION TO MILES AND COMPUTE DISTANCE
C DOWN TRACK.
   DO 25 I=1,N
25  DIST(I)=SQRT((X(I)*B)**2+Y(I)**2)
     IF(ABS(X(N)).LT.0.00001) X(N)=0.00001
     THETA=ATAN2(Y(N),(X(N)*B))
     CALL GINT(GRID,N,0.0,DIST(N),ICT,DIST,Z,AX,AZ)
C STORE NEW POSIT OF INTERPOLATED PT.IN AX(LONG,AY(LAT) DECIMAL DEG.
C NEW INTERPOLATED VALUE OF Z IS STORED IN AZ
   DO 26 I=1,ICT
     AY(I)=(AX(I)*SIN(THETA)+BLAT)/60.0
26  AX(I)=(BLONG-(AX(I)*COS(THETA)/B))/60.0
   RETURN
   END

```

```

C      FUNCTION TO CONVERT LATITUDE INTO MERIDIONAL PARTS
      FUNCTION YMP(Z)
      DATA AP/0.7853981634/
      Y=ABS(Z)*0.290888209E-03
      T=TAN(AP+Y*0.5)
      YM=7915.7045*ALOG10(T)-23.268932*SIN(Y)
      YMP=YM*SIGN(1.0,Z)
      RETURN
      END

```

```

SUBROUTINE SORTY(X,Y,Z,AX,AY,AZ,K,KODE,JCODE,GRID)
C   Y=INPUT VARIABLE TO BE SORTED, X,Z=VALUES ASSOCIATED WITH Y
C   K=LENGTH OF Y,IF KODE=1,VALUES OF Y WHICH ARE WITHIN 1 GRID INT OF
C   PREVIOUS VALUE ARE REMOVED,IF KODE=0 ALL VALUES OF Y ARE
C   RETAINED,IF JCODE=+1,Y IS SORTED IN INCREASING ORDER,IF JCODE=-1,
C   Y IS SORTED IN DECREASING ORDER,OUTPUT IS SORTED VALUES OF
C   Y WITH ASSOCIATED X AND Z
  DIMENSION Y(20),X(20),Z(20),AX(20),AY(20),AZ(20)
  KB = K
  CODE=JCODE
  J = 1
129  I = 1
     JCT=0
     AY(J) = Y(I)
132  TEMP= CODE*(AY(J)-Y(I+1))
     IF((ABS(TEMP))-GRID+0.0001) 122,120,120
120  IF(TEMP) 121,136,123
121  I = I + 1
     IF((I + 1) - KB) 132,132,125
123  JCT = 1
     AY(J) = Y(I + 1)
     AX(J) = X(I + 1)
     AZ(J) = Z(I + 1)
     KT = I + 2
     GO TO 121
122  IF(KODE) 120,120,136
136  KD=I+2
     IF (KD-KB) 124,124,139
139  K=K-1
     KB=KB-1
     GO TO 125
124  DO 126 JD=KD,KB
     JF = JD - 1
     Y(JF) = Y(JD)
     X(JF) = X(JD)
126  Z(JF) = Z(JD)
     KB = KB - 1
     K = K - 1
     GO TO 132
125  IF(JCT) 127,127,128
127  AY(J) = Y(1)
     AX(J) = X(1)
     AZ(J) = Z(1)
     KT = 2
128  J = J + 1
     IF(J - K) 131,133,133
131  DO 134 KA = KT,KB
     JT = KA - 1
     Y(JT) = Y(KA)
     X(JT) = X(KA)
134  Z(JT) = Z(KA)
     KB = KB - 1
     GO TO 129

```

```

133 IF(JCT) 137,137,138
137 KB=KB+1
138 AY(K) = Y(KB- 1)
    AX(K) = X(KB- 1)
    AZ(K) = Z(KB- 1)
    DO 135 I = 1,K
        Y(I) = AY(I)
        X(I) = AX(I)
135 Z(I) = AZ(I)
    RETURN
    END

```

```

      SUBROUTINE GINT(DELX,M,XBGN,XEND,ICT,X,Y,AX,AY)
C MODIFICATION OF ORIGINAL GINT SO THAT INPUT DATA IS NOT DESTROYED
C GENERAL 1-D SPLINE INTERPOLATION FOR MIN.STORAGE
C INTERPOLATES OVER 50 INPUT PTS WITH OVERLAP
C DELX=DESIRED INTERPOLATION INTERVAL,X AND Y ARE INPUT WITH X=INDEP.
C VARIABLE,AX AND AY ARE OUTPUT,M=LENGTH OF X, XBGN AND XEND=DESIRED
C BEGINNING AND ENDING VALUES OF AX,ICT=LENGTH OF AX
C***NOTE IF M MOD 50 IS LESS THAN 2 INTERPOLATED OUTPUT MAY STOP SHORT
C OF XEND
C THIS ROUTINE REQUIRES SPLINE AND SPLICO SUBROUTINES
      DIMENSION X(1),Y(1),AX(1),AY(1)
      ICT=(ABS(XEND-XBGN)/DELX)+1.0
      ISECT=M/50
      IA=ISECT*50
      IC=0
      JJ=0
      MM=49
      IF(IA.EQ.0) MM=M
      IF((M-IA).GE.2) JJ=1
C OVERLAP INTERPOLATION INTERVALS BY 2 INPUT PTS SO SPLINE ROUTINE
C IS DIMENSIONED TO MAX OF 53 PTS
      JCONT=1
      KA=1
      KC=MM+1
      IF(IA.EQ.0) KC=KC-1
      K=1
53  IKT= (ABS(X(MM)-XBGN)/DELX)+1.0
      IF(MM.EQ.M) IKT=ICT
      ATER=9999.999
      DO 26 I=KA,IKT
      AJ=I-1
      XINT=AJ*DELX+XBGN
      IF(XINT.GT.XEND) GO TO 58
      CALL SPLINE(X(K),Y(K),KC,XINT,YINT,ATER)
      AX(I)=XINT
26  AY(I)=YINT
      JCONT=JCONT+1
      IF(IA.EQ.0) GO TO 56
      IF(JCONT.GT.ISECT) GO TO 55
      JC=JCONT*50
57  IMM=MM-1
      K=IMM
      MM=MM+50
      IF(IC.EQ.1) MM=M
      KA=IKT+1
      KC=JC-IMM+1
      GO TO 53
55  IF(JJ.LT.1) GO TO 56
      IC=1
      JJ=0
      JC=M
      GO TO 57
58  ICT=I-1

```

```
RETURN  
56 ICT=IKT  
RETURN  
END
```

```

SUBROUTINE SPLINE (X,Y,M,XINT,YINT,ATER)
C   SEE PENNINGTON REF. FOR DESCRIPTION OF THIS SUBROUTINE
    DIMENSION X(1),Y(1),C(4,53)
    K=0
    IF(X(1)+Y(M)+Y(M-1)+X(M-1)+Y(M-2)-ATER) 10,3,10
10  CALL SPLICO (X,Y,M,C)
    ATER= X(1)+Y(M)+Y(M-1)+X(M-1)+Y(M-2)
    K=1
    3 IF(ABS(XINT-X(1)).LT.0.00001) GO TO 1
    IF(XINT-X(1)) 70,1,2
70  K=1
    GO TO 7
    1 YINT=Y(1)
    RETURN
    2 IF(ABS(XINT-X(K+1)).LT.0.00001) GO TO 4
    IF(XINT-X(K+1))6,4,5
    4 YINT=Y(K+1)
    RETURN
    5 K=K+1
    IF(M-K) 71,71,3
71  K=M-1
    GO TO 7
    6 IF(ABS(XINT-X(K)).LT.0.00001) GO TO 12
    IF(XINT-X(K))13,12,11
    12 YINT=Y(K)
    RETURN
    13 K=K-1
    GO TO 6
    11 YINT=(X(K+1)-XINT)*(C(1,K)*(X(K+1)-XINT)**2+C(3,K))
    YINT=YINT+(XINT-X(K))*(C(2,K)*(XINT-X(K))**2+C(4,K))
    RETURN
C   7 PRINT 101,XINT
    7 CONTINUE
101  FORMAT(' CAUTION VALUE AT POSITION',F10.2,'WAS EXTRAPOLATED')
    GO TO 11
    RETURN
    END

```

```

SUBROUTINE SPLICO (X,Y,M,C)
DIMENSION X(1),Y(1),C(4,53),D(53),P(53),E(53),A(53,3),B(53),Z(53)
MM=M-1
DO 2 K=1,MM
D(K)=X(K+1)-X(K)
P(K)=D(K)/6.
2 E(K)=(Y(K+1)-Y(K))/D(K)
DO 3 K=2,MM
3 B(K)=E(K)-E(K-1)
A(1,2)=-1.-D(1)/D(2)
A(1,3)=D(1)/D(2)
A(2,3)=P(2)-P(1)*A(1,3)
A(2,2)=2.*(P(1)+P(2))-P(1)*A(1,2)
A(2,3)=A(2,3)/A(2,2)
B(2)=B(2)/A(2,2)
DO 4 K=3,MM
A(K,2)=2.*(P(K-1)+P(K))-P(K-1)*A(K-1,3)
B(K)=B(K)-P(K-1)*B(K-1)
A(K,3)=P(K)/A(K,2)
4 B(K)=B(K)/A(K,2)
Q=D(M-2)/D(M-1)
A(M,1)=1.+Q+A(M-2,3)
A(M,2)=-Q-A(M,1)*A(M-1,3)
B(M)=B(M-2)-A(M,1)*B(M-1)
Z(M)=B(M)/A(M,2)
MN=M-2
DO 6 I=1,MN
K=M-I
6 Z(K)=B(K)-A(K,3)*Z(K+1)
Z(1)=-A(1,2)*Z(2)-A(1,3)*Z(3)
DO 7 K=1,MM
Q=1./(6.*D(K))
C(1,K)=Z(K)*Q
C(2,K)=Z(K+1)*Q
C(3,K)=Y(K)/D(K)-Z(K)*P(K)
7 C(4,K)=Y(K+1)/D(K)-Z(K+1)*P(K)
RETURN
END

```

```

SUBROUTINE AXES(X,Y,IBCD,NC,AXLEN,ANG,DELTIC,FIRSTV,DELVAL,NDEC)
C   MODIFIED CALCOMP AXIS SUBROUTINE---RANKIN,NOV.1971
C   X,Y      COORDINATES OF STARTING POINT OF AXIS IN INCHES
C   IBCD     AXIS TITLE
C   NC       NUMBER OF CHARACTERS IN TITLE
C   IF NC IS(-),HEADING AND TICKS ARE BELOW THE AXIS
C   AXLEN    FLOATING POINT AXIS LENGTH IN INCHES
C   ANG      ANGLE OF AXIS FROM HORIZONTAL IN DEGREES
C   DELTIC   DISTANCE BETWEEN TIC MARKS IN INCHES
C   FIRSTV   SCALE VALUE AT FIRST TIC MARK
C   DELVAL   SCALE INCREMENT
C   NDEC     NUMBER OF DECIMAL PLACES OF TIC ANNOTATION PLOTTED(PUNCH
C   -1 IF ONLY INTEGER(NO DECIMAL POINT)IS DESIRED)
C   -2 IF NO ANNOTATION DESIRED IE. ONLY TICKS
C   DIMENSION IBCD(10)
C   A=1.0
C   KN=NC
C   IF(NC)1,2,2
1  A=-A
C   KN=-NC
2  XVAL=FIRSTV
C   STH=ANG*0.0174533
C   CTH=COS(STH)
C   STH=SIN(STH)
C   DXB=-0.1
C   DYB=0.15*A-0.05
C   XN=X+DXB*CTH-DYB*STH
C   YN=Y+DYB*CTH+DXB*STH
C   NTIC=AXLEN/DELTIC+1.0
C   NT=NTIC/2
C   DO 10 I=1,NTIC
C   IF(NDEC.EQ.-2) GO TO 12
C   CHANGED NUMBER HEIGHT FROM .105 TO .15
C   CALL NUMBER(XN,YN,0.15,XVAL,ANG,NDEC)
12  XVAL=XVAL+DELVAL
C   XN=XN+CTH*DELTIC
C   YN=YN+STH*DELTIC
C   IF(NT)10,11,10
11  Z=KN
C   DXB=-0.07*Z+AXLEN*0.5
C   DYB=0.325*A-0.075
C   XT=X+DXB*CTH-DYB*STH
C   YT=Y+DYB*CTH+DXB*STH
C   CHANGED HEIGHT FROM .14 TO .18
C   CALL SYMBOL(XT,YT,0.18,IBCD(1),ANG,KN)
10  NT=NT-1
C   CALL PLOT(X+AXLEN*CTH,Y+AXLEN*STH,3)
C   IF(NDEC.EQ.-2) GO TO 14
C   DXB=-0.07*A*STH
C   DYB=0.07*A*CTH
C   GO TO 13
14  DXB=-0.05*A*STH
C   DYB=0.05*A*CTH

```

```

13 A=NTIC-1
   XN=X+A*CTH*DELTIC
   YN=Y+A*STH*DELTIC
   DO 20 I=1,NTIC
     CALL PLOT(XN,YN,2)
     CALL PLOT(XN+DXB,YN+DYB,2)
     CALL PLOT(XN,YN,2)
     XN=XN-CTH*DELTIC
     YN=YN-STH*DELTIC
20  CONTINUE
   RETURN
   END
   FUNCTION SRMS(X,N)
   DIMENSION X(1)
   AVE=0.0
   SRMS=0.0
   DO 10 I=1,N
10  AVE=AVE+(X(I)/FLOAT(N))
   DO 20 I=1,N
20  SRMS=SRMS+((X(I)-AVE)**2)
   SRMS=SRMS/FLOAT(N)
   SRMS=SQRT(SRMS)
   RETURN
   END

```

```

      SUBROUTINE FILTER(X,NP,CUT,H,N,K,WGT)
C GENERAL ROUTINE TO HIGH OR LOW PASS A SET OF EQUALLY
C SPACED DATA USING MARTIN FILTERS.
C X=INPUT DATA AND OUTPUT DATA,NP=NO.OF POINTS IN X,CUT=NORMALIZED
C CUTOFF OF FILTER IN CYCLES/DATA INTERVAL,H=SLOPE PARAMETER,
CN=HALF LENGTH OF FILTER,TOTAL LENGTH=2N+1,
C K=1=HIGH PASS,=0 FOR LOW PASS.
C WEIGHTS STORED IN WGT
      DIMENSION X(1),WGT(1)
      NA=N+1
      WGT(1)=2.0*(CUT+H)
C CENTER WEIGHT STORED IN LOCATION 1
      SUM=0.0
      PI=3.1415926
      DO 61 I=2,NA
      P=I-1
      Q=1.0-16.0*H**2*P**2
      IF(ABS(Q).GT.0.0001) GO TO 62
      WGT(I)=SIN(2.*PI*P*(CUT+H))/(4.0*P)
      GO TO 61
62 WGT(I)=((COS(2.*PI*P*H))/Q)*((SIN(2.*PI*P*(CUT+H)))/(PI*P))
61 SUM=SUM+WGT(I)
      DELTA=1.-(WGT(1)+2.*SUM)
      AX=2*N+1
      IF(K.LT.1) GO TO 78
      DO 65 I=2,NA
65 WGT(I)=(WGT(I)+DELTA/AX)*(-1.0)
      WGT(1)=1.0-(WGT(1)+DELTA/AX)
      GO TO 79
78 DO 80 I=1,NA
80 WGT(I)=WGT(I)+DELTA/AX
79 NB=NP-N
C CONVOLVE WEIGHTS WITH DATA.
      DO 63 I=NA,NB
      II=I+1-NA
      SUM=0.0
      DO 64 J=1,NA
      J1=I+J-1
      J2=I-J+1
64 SUM=SUM+WGT(J)*(X(J1)+X(J2))
63 X(II)=SUM-WGT(1)*X(I)
C SHIFT FILTERED DATA TO CORRECT LOCATION AND ZERO ENDS.
      II=NB+1-NA
      DO 67 I=1,II
      J=II+1-I
      L=J+N
67 X(L)=X(J)
      DO 68 I=1,N
68 X(I)=0.0
      NC=NB+1
      DO 69 I=NC,NP
69 X(I)=0.0
      RETURN
      END

```

```

SUBROUTINE ENVEL(DATA,NP)
C   THIS ROUTINE RECEIVES A TIME SERIES OF LENGTH NP
C   IN ARRAY DATA, AND RETURNS ENVELOPE ESTIMATES BASED
C   ON A HILBERT TRANSFORM METHOD AS DESCRIBED IN KANASEWICH
C   (1981),P. 362-368.
C   C.G.FOX,ADVANCED TECHNOLOGY STAFF,NAVOCEANO-5/12/83
DIMENSION DATA(1)
COMPLEX XDATA(2048)
NSTART=1
NPSEG=NP
10 IF(NPSEG.LE.0) RETURN
C   PERFORM ENVELOPE CALCULATIONS IN SEGMENTS OF 2048 POINTS
IF(NPSEG.GT.2048) THEN
    NPSEG=NPSEG-2048
    LENGTH=2048
    GO TO 100
ELSE
    LENGTH=NPSEG
    NPSEG=0
END IF
C   TRANSFER INPUT DATA TO REAL PORTION OF COMPLEX ARRAY XDATA
100 DO 110 I=1,LENGTH
110 XDATA(I)=(1.0,0.0)*DATA(NSTART+(I-1))
C   ZERO FILL ARRAY IF LESS THAN 2048 POINTS
IF(LENGTH.EQ.2048) GO TO 200
DO 120 I=LENGTH+1,2048
120 XDATA(I)=(0.0,0.0)
C   FOURIER TRANSFORM TO FREQUENCY DOMAIN USING FFT
200 CALL NLOGN(11,XDATA,-1.0)
C   COMPUTE HILBERT TRANSFORM IN THE FREQUENCY DOMAIN. THE
C   TRANSFORM IS COMPUTED AS  $I \cdot \text{SGN}(\Omega) \cdot F(\Omega)$ , WHERE
C    $\Omega$ =FREQUENCY  $F(\Omega)$ =FOURIER TRANSFORM
C    $\text{SGN}(X)=1, (X>0), =0, (X=0), =-1 (X<0)$ 
C   THIS OPERATION INDUCES A NINETY DEGREE PHASE SHIFT ON
C   COMPLEX PLANE. THE CALCULATION IS DONE BY ZEROING X(1),
C   ( $\Omega=0$ ),TRANSFERRING REAL TO IMAGINARY,MINUS IMAG TO REAL
C   FOR  $X(2)-X(N/2)$ , ( $\Omega>0$ ), AND TRANSFERRING MINUS REAL TO
C   IMAGINARY,AND IMAGINARY TO REAL FOR  $X(N/2+1)$  TO  $X(N)$ ,
C   ( $\Omega<0$ )
XDATA(1)=(0.0,0.0)
DO 250 I=2,1024
    TEMPR=REAL(XDATA(I))
    TEMPI=AIMAG(XDATA(I))
250 XDATA(I)=CMPLX(-TEMPI,TEMPR)
DO 260 I=1025,2048
    TEMPR=REAL(XDATA(I))
    TEMPI=AIMAG(XDATA(I))
260 XDATA(I)=CMPLX(TEMPI,-TEMPR)
C   INVERSE TRANSFORM SHIFTED DATA
CALL NLOGN(11,XDATA,+1.0)
C   CALCULATE ENVELOPE AFTER EQUATION 21.3-1 OF KANASEWICH
C   DUE TO SYMMETRIES IN THE TRANSFORM, IMAGINARY PORTION
C   OF XDATA IS NEAR ZERO AND CAN BE IGNORED

```

```
DO 300 I=1,2048
    N=NSTART+(I-1)
300 DATA(N)=SQRT((DATA(N)*DATA(N))+(REAL(XDATA(I))**2))
    NSTART=NSTART+2048
GO TO 10
END
```

```

      SUBROUTINE NLOGN(N,X,SIGN)
C*****NLOGN COMPUTES THE DISCRETE FOURIER TRANSFORM BY THE FAST FOURIER
C*****TRANSFORM METHOD.REFERENCE ROBINSON,PAGE 63.
C*****THIS SUBROUTINE CONTAINS 51 STATEMENTS.
C*****N=POSITIVE INTEGER FOR THE POWER OF 2 DESIRED.
C*****X=INPUT AND OUTPUT DATA ARRAY(COMPLEX).
C*****SIGN=-1.0 FOR FOURIER TRANSFORM,+1.0 FOR INVERSE FOURIER TRANSFORM.
      DIMENSION M(15),X(2)
      COMPLEX X,WK,HOLD,Q
      LX = 2**N
      DO 1 I = 1,N
1  M(I) = 2**(N - I)
      DO 4 L = 1,N
      NBLOCK = 2**(L - 1)
      LBLOCK = LX / NBLOCK
      LBHALF = LBLOCK / 2
      K = 0
      DO 4 IBLOCK = 1,NBLOCK
      FK = K
      FLX = LX
      V = SIGN * 6.2831853071796 * FK / FLX
      WK = CMPLX(COS(V),SIN(V))
      ISTART = LBLOCK * (IBLOCK - 1)
      DO 2 I = 1,LBHALF
      J = ISTART + I
      JH = J + LBHALF
      Q = X(JH) * WK
      X(JH) = X(J) - Q
      X(J) = X(J) + Q
2  CONTINUE
      DO 3 I = 2,N
      II = I
      IF(K.LT.M(I)) GO TO 4
3  K = K - M(I)
4  K = K + M(II)
      K = 0
      DO 7 J = 1, LX
      IF (K.LT.J) GO TO 5
      HOLD = X(J)
      X(J) = X(K + 1)
      X(K + 1) = HOLD
5  DO 6 I = 1,N
      II = I
      IF(K.LT.M(I)) GO TO 7
6  K = K - M(I)
7  K = K + M(II)
      IF(SIGN.LT.0.0) RETURN
      DO 8 I = 1,LX
8  X(I) = X(I) / FLX
      RETURN
      END

```

```

SUBROUTINE PRVFIX(K1,K2,K3,MIN,KST)
DIMENSION K1(1000),K2(1000),K3(1000),T1(200),T2(200),T3(200)
C SUBROUTINE FOR USE WITH THE PROVINCE PICKER PROGRAM
C SEARCHES PROVINCE BOUNDARIES FOR SEGMENTS LESS THAN MIN
C SEGMENTS ARE INCORPORATED INTO ADJACENT PROVINCES IF THEY
C ARE EQUAL-SETS BOUNDARY TO INCLUDE SEGMENT IN ROUGHEST
C PROVINCE IF ADJACENT PROVINCES ARE UNEQUAL-DELETES
C SEGMENTS AT ENDS OF TRACKLINE
C C.G.FOX-LDGO-JULY 6,1982
C
MINSAV=MIN
MIN=0
10 ISKIP=0
ICYCLE=0
MIN=MIN+5
IF(MIN.GT.MINSAV)MIN=MINSAV
DO 100 I=1,KST
IF(ICYCLE.GE.1) GO TO 95
IX=I-ISKIP
II=I+1
C TEST FOR ADJACENT PROVINCES OF SAME NUMBER
IF(K3(I).NE.K3(II)) GO TO 30
T1(IX)=K1(I)
T2(IX)=K2(II)
T3(IX)=K3(I)
ICYCLE=1
ISKIP=ISKIP+1
GO TO 100
C TEST FOR MINIMUM PROVINCE SIZE
30 IDIFF=K2(I)-K1(I)
IF(IDIFF.LT.MIN)GO TO 40
C NORMAL PROVINCE - STORE IN T ARRAY AND CONTINUE
T1(IX)=K1(I)
T2(IX)=K2(I)
T3(IX)=K3(I)
GO TO 100
C LESS THAN MINIMUM SIZE-TEST NUMBER OF ADJACENT PROVINCES
C IF FIRST OR LAST PROVINCE OF LINE, DELETE
40 IF(I.NE.KST.OR.IX.NE.1) GO TO 50
ISKIP=ISKIP+1
GO TO 100
C TEST IF SURROUNDING PROVINCES ARE EQUAL
50 IF(T3(IX-1).NE.K3(II)) GO TO 70
C IF EQUAL, EXTEND SECOND BOUNDARY OF PREVIOUS PROVINCE
C TO END OF FOLLOWING PROVINCE
T2(IX-1)=K2(II)
ICYCLE=1
ISKIP=ISKIP+2
GO TO 100
C ADJACENT PROVINCES ARE DIFFERENT-SET BOUNDARY CLOSER TO
C LOWER VALUED PROVINCE
C 70 IF(T3(IX-1).LT.K3(II)) GO TO 75
C T1(IX)=K1(I)

```

```

C      T2(IX)=K2(II)
C      T3(IX)=K3(I)
C      IF((K2(II)-K1(II)).GT.IDIFF)T3(IX)=K3(II)
C      GO TO 80
C 75   T2(IX-1)=K2(I)
C      T1(IX)=K1(II)
C      T2(IX)=K2(II)
C      T3(IX)=K3(I)
C      IF((K2(II)-K1(II)).GT.IDIFF)T3(IX)=K3(II)
C      BISECT SEGMENT AND PUT HALVES INTO ADJACENT PROVINCES
70   K=(K2(I)+K1(I))/2
      T2(IX-1)=K
      T1(IX)=K
      T2(IX)=K2(II)
      T3(IX)=K3(II)
80   ISKIP=ISKIP+1
      ICYCLE=1
      GO TO 100
95   ICYCLE=ICYCLE-1
100  CONTINUE
      IF(ISKIP.EQ.0.AND.MIN.EQ.MINSAV) GO TO 500
      KST=KST-ISKIP
      DO 150 I=1,KST
      K1(I)=T1(I)
      K2(I)=T2(I)
150  K3(I)=T3(I)
      K3(KST+1)=99
      GO TO 10
500  RETURN
      END

```

```

      FUNCTION DECDEG(I,X)
C    CONVERT DEGREES+MINUTES TO DECIMAL DEGREES
      DECDEG=ABS(I)+X/60.
      DECDEG=SIGN(DECDEG,I)
      RETURN
      END
      SUBROUTINE DEGMIN(A,J,B)
C    CONVERT DECIMAL DEGREES(A) TO DEGREES(J)+MINUTES(B)
      J=INT(A)
      B=ABS((A-FLOAT(J))*60.)
      RETURN
      END

```

Appendix C.1

The addition of two sinusoids of different amplitude and phase, but identical wavelength results in another sinusoid of the same wavelength, but amplitude and phase which is a function of the amplitudes and phases of the component sinusoids. Assuming two sinusoids of differing amplitudes (v_A and v_B) and phases (θ_A and θ_B), their sum can be expressed in terms of a new sinusoid of amplitude v_C and phase θ_C as

$$v_A \cdot \cos(\theta - \theta_A) + v_B \cdot \cos(\theta - \theta_B) = v_C \cdot \cos(\theta - \theta_C) \quad (C-1)$$

Using the addition formula of sinusoids,

$$\begin{aligned} v_A \cdot \cos\theta \cdot \cos\theta_A + v_A \cdot \sin\theta \cdot \sin\theta_A + v_B \cdot \cos\theta \cdot \cos\theta_B + \\ v_B \cdot \sin\theta \cdot \sin\theta_B = v_C \cdot \cos\theta \cdot \cos\theta_C + v_C \cdot \sin\theta \cdot \sin\theta_C \end{aligned} \quad (C-2)$$

Combining terms, and equating sine and cosine terms

$$(v_A \cdot \cos\theta_A + v_B \cdot \cos\theta_B) \cdot \cos\theta = (v_C \cdot \cos\theta_C) \cdot \cos\theta \quad (C-3)$$

and

$$(v_A \cdot \sin\theta_A + v_B \cdot \sin\theta_B) \cdot \sin\theta = (v_C \cdot \sin\theta_C) \cdot \sin\theta \quad (C-4)$$

Since C-3 and C-4 are true for any value of θ , the unknown v_C and θ_C are determined from:

$$v_A \cdot \cos\theta_A + v_B \cdot \cos\theta_B = v_C \cdot \cos\theta_C \quad (C-5)$$

$$v_A \cdot \sin\theta_A + v_B \cdot \sin\theta_B = v_C \cdot \sin\theta_C \quad (C-6)$$

Squaring both sides and summing equations C-5 and C-6 removes the θ_C terms ($\cos^2\theta + \sin^2\theta = 1$),

$$v_C^2 = v_A^2 \cdot \cos^2\theta_A + v_B^2 \cdot \cos^2\theta_B + 2 \cdot v_A \cdot v_B \cdot \cos\theta_A \cdot \cos\theta_B + v_A^2 \cdot \sin^2\theta_A + v_B^2 \cdot \sin^2\theta_B + 2 \cdot v_A \cdot v_B \cdot \sin\theta_A \cdot \sin\theta_B \quad (C-7)$$

Again using the relationship $\cos^2\theta + \sin^2\theta = 1$, the addition formula for cosines, and taking the root of the result gives the formula for the v_C term as,

$$v_C = (v_A^2 + v_B^2 + 2 \cdot v_A \cdot v_B \cdot (\cos(\theta_A - \theta_B)))^{1/2} \quad (C-8)$$

The unknown resulting phase angle θ_C can be derived by dividing (C-6) by (C-5),

$$\tan\theta_C = \frac{v_A \cdot \sin\theta_A + v_B \cdot \sin\theta_B}{v_A \cdot \cos\theta_A + v_B \cdot \cos\theta_B} \quad (C-9)$$

or

$$\theta_C = \tan^{-1} \left(\frac{v_A \cdot \sin\theta_A + v_B \cdot \sin\theta_B}{v_A \cdot \cos\theta_A + v_B \cdot \cos\theta_B} \right) \quad (C-10)$$

These general results show the dependence of a sinusoid of given wavelength on a linear combination of two other sinusoids of the same wavelength. The same combination process could be extended to any number of component sinusoids.

Appendix C.2 contains FORTRAN -77 software to perform an iterative fit of a sinusoid to data.

Appendix C.2

```

SUBROUTINE COSFIT(A,B,PHI,X,Y,N,AMIN,BMIN,PHIMIN,ILIST)
C
C   THIS ROUTINE PERFORMS A BEST FIT TO DATA WITH A TRIGONOMETRIC
C   FUNCTION OF THE FORM  $Y=A+B*(\cos(4*PI*(X-PHI)))$  USING AN ITERATIVE
C   METHOD AS DESCRIBED IN SCARBOROUGH(1930), ART. 115.
C   INPUTS ARE
C       A=CONSTANT
C       B=AMPLITUDE OF SINUSOIDAL COMPONENT
C       PHI= ANGLE OF MAXIMUM AMPLITUDE
C       X= ARRAY OF DEPENDENT VARIABLE VALUES
C       Y= ARRAY OF DEPENDENT VARIABLE VALUES
C       N= NUMBER OF DATA PAIRS OF X AND Y
C       AMIN= MINIMUM VALUE FOR A CORRECTION TO STOP ITERATION
C       BMIN= MINIMUM VALUE FOR B CORRECTION TO STOP ITERATION
C       PHIMIN= MINIMUM VALUE FOR PHI CORRECTION TO STOP ITERATION
C       ILIST= 1 FOR SUMMARY OF ITERATION PROCESS, = 0 , NO LISTING
C   PROGRAMMED BY C.G.FOX-ADVANCED TECHNOLOGY STAFF,NAVOCEANO,8/30/83
C
C   DIMENSION X(1024),Y(1024)
C   REAL I9,J9,K9,L9
C
C   COMPUTE INITIAL ESTIMATE OF A AND B BY PERFORMING A SIMPLE
C   LINEAR FIT ON LOG TRANSFORMED DATA
C
C   XN=FLOAT(N)
C   XPRCJ=0.0
C   XSUM=0.0
C   YSUM=0.0
C   XSQR=0.0
C   WRITE(6,'(2F10.4)') (X(I),Y(I),I=1,N)
C   FIND MEAN LEVEL AND CONVERT X TO RADIANS
C   DO 50 I=1,N
C       X(I)=X(I)/57.2957795
C   50 AO=AO+(Y(I)/XN)
C   LOCATE LARGEST POSITIVE DIFFERENCE FROM THE MEAN AND ITS PHI
C   DO 60 I=1,N
C       IF((Y(I)-AO).LT.B0) GO TO 60
C       B0=Y(I)-AO
C       PHI0=X(I)
C   60 CONTINUE
C
C   COMPUTE SUM OF SQUARES OF THE RESIDUALS
C
C   POLD=0.0
C   DO 100 I=1,N
C   100 POLD=POLD+((Y(I)-F3(X(I),AO,B0,PHI0))**2)
C   ITERAT=0
C   NBIS=0
C   IF(ILIST.EQ.1)WRITE(6,110)
C   110 FORMAT(' ITERATION      # OF BISECTIONS          A          B

```

```

      *PHIO      RESIDUALS**2)
      IF(ILIST.EQ.1)WRITE(6,120)ITERAT,NBIS,A0,B0,PHIO,POLD
120  FORMAT(' ',I6,10X,I4,6X,4(4X,F10.4))
C
C      ZERO OUT MATRIX TERMS
C
150  A9=0.0
      B9=0.0
      C9=0.0
      E9=0.0
      F9=0.0
      I9=0.0
      J9=0.0
      K9=0.0
      L9=0.0
C
C      COMPUTE TERMS FOR LEAST SQUARES MATRIX CONSTRUCTION
C
      DO 200 I=1,N
      PARTA=F1(X(I),A0,B0)
      PARTB=F2(X(I),A0,PHIO)
      PARTP=F4(X(I),A0,B0,PHIO)
      POWF=F3(X(I),A0,B0,PHIO)
      A9=A9+(PARTA**2)
      B9=B9+(PARTA*PARTB)
      C9=C9+(PARTA*PARTP)
      E9=E9+(PARTB**2)
      F9=F9+(PARTB*PARTP)
      I9=I9+(PARTP**2)
      J9=J9+(PARTA*(Y(I)-POWF))
      K9=K9+(PARTB*(Y(I)-POWF))
200  L9=L9+(PARTP*(Y(I)-POWF))
      D9=B9
      G9=C9
      H9=F9
C
C      COMPUTE CORRECTION TERMS FOR A AND B
C
      D=A9*E9*I9+B9*F9*G9+C9*D9*H9-C9*E9*G9-B9*D9*I9-A9*F9*H9
      ACORR=((E9*I9-F9*H9)*J9)+((C9*H9-B9*I9)*K9)+((B9*F9-E9*C9)*L9))/D
      BCORR=((G9*F9-D9*I9)*J9)+((A9*I9-G9*C9)*K9)+((D9*C9-A9*F9)*L9))/D
      PCORR=((D9*H9-G9*E9)*J9)+((G9*B9-A9*H9)*K9)+((A9*E9-B9*D9)*L9))/D
C
C      CREATE NEW A AND B
C
230  A=A0+ACORR
      B=B0+BCORR
      PHI=PHIO+PCORR
C
C      COMPUTE NEW SUM OF SQUARES OF RESIDUALS WITH NEW ESTIMATES
C
      PNEW=0.0
      DO 250 I=1,N

```

```

250 PNEW=PNEW+((Y(I)-F3(X(I),A,B,PHI))**2)
C
C TEST FOR CONVERGENT SOLUTION(PNEW < POLD)
C IF NOT, BISECT CORRECTIONS AND RECOMPUTE
C
    IF(PNEW.LT.POLD) GO TO 300
    ACORR=.5*ACORR
    BCORR=.5*BCORR
    PCORR=.5*PCORR
    NBIS=NBIS+1
    IF(NBIS.GT.10) GO TO 300
    GO TO 230
C
C TEST FOR MINIMUM CHANGE OF A AND B
C
300 IF(ABS(A-A0).GT.AMIN) GO TO 500
    IF(ABS(B-B0).GT.BMIN) GO TO 500
    IF(ABS(PHI-PHI0).GT.PHIMIN) GO TO 500
    GO TO 900
C
C CORRECTION TERM NOT FINE ENOUGH, START NEW ITERATION
C
500 ITERAT=ITERAT+1
    AO=A
    BO=B
    POLD=PNEW
    IF(ILIST.EQ.1)WRITE(6,520)ITERAT,NBIS,AO,BO,PHI0,POLD
520 FORMAT(' ',I6,10X,I4,6X,4(4X,F10.4));
    NBIS=0
    GO TO 150
900 ITERAT=ITERAT+1
    IF(ILIST.EQ.1)WRITE(6,920)ITERAT,NBIS,AO,BO,PHI0,POLD
920 FORMAT(' ',I6,10X,I4,6X,4(4X,F10.4))
C RECONVERT RADIANS TO DEGREES
    DO 930 I=1,N
930 X(I)=X(I)*57.2957795
    PHI=PHI*57.2957795
    PRINT *,A,B,PHI
    RETURN
    END
C
C
C FUNCTIONS TO CALCULATE POWER LAW FUNCTION AND PARTIAL
C DERIVATIVES WITH RESPECT TO A AND B
C
    FUNCTION F1(X3,A3,B3)
C CALCULATE PARTIAL OF FUNCTION WITH RESPECT TO A
    F1=1.
    A3=A3
    X3=X3
    B3=B3
    RETURN

```

```

      END
C
      FUNCTION F2(X4,A4,PHI4)
C      CALCULATE PARTIAL OF FUNCTION WITH RESPECT TO B
      F2=COS(2.*(X4-PHI4))
      A4=A4
      RETURN
      END
C
      FUNCTION F3(X5,A5,B5,PHI5)
C      CALCULATE FUNCTION
      F3=A5+B5*COS(2.*(X5-PHI5))
      RETURN
      END
C
      FUNCTION F4(X6,A6,B6,PHI6)
C      CALCULATE PARTIAL WITH RESPECT TO PHI
      F4=2.*SIN(2.*(X6-PHI6))
      A6=A6
      B6=B6
      RETURN
      END

```

Appendix D

NOTE: Many of the subroutines required by the following routines are common to the province selection software listed in Appendix B.2.

C GENERATE AMPLITUDE SPECTRUM OF DEPTHS OUTPUT FROM PROVINCE PICKER.
C PROGRAM IS A SLIGHT MODIFICATION OF THE ORIGINAL CREATED BY
C T.M.DAVIS, IN WHICH THE INPUTS HAVE BEEN SET WITHIN THE CODE
C AND ONLY THOSE PARAMETERS NECESSARY FOR DAILY USE HAVE BEEN LEFT
C FOR INPUT BY THE USER. INPUT IS EXPECTED FROM UNIT 13, WHICH IS
C THE UNIT NUMBER USED BY PROVPICK. THE PROGRAM ADDS AN INTERACTIVE
C GRAPHICS SECTION WHICH ALLOWS MODIFICATION OF THE INPUT SERIES,
C DELETION OF SECTIONS, AND CONTROL OF THE INDEPENDENT VARIABLE FOR
C REGRESSION ANALYSIS. ROUGHNESS MODEL PARAMETERS A & B ALONG WITH
C LATITUDE AND LONGITUDE INFORMATION FOR EACH PROFILE ARE OUTPUT
C TO UNIT 14 FOR LATER USE IN PROVCHART PROGRAM.

C PROGRAMMED BY C.G.FOX,ADVANCED TECHNOLOGY STAFF,NAVOCEANO,5/17/84

C THE FOLLOWING COMMENTS ARE FROM THE ORIGINAL PROGRAM BY T.M.DAVIS

C PROGRAM TO COMPUTE PREWHITENED,CORRECTED AND SMOOTHED AMPLITUDE
C SPECTRUM CUT,H,N=PARAMETERS TO CONTROL PREWHITENING AND SMOOTHING
C FILTERS,ANORM=SPECTRUM NORMALIZATION IN TERMS OF DATA INTERVALS
C XORG,YORG=LOG-LOG PLOT ORIGIN IN POWERS OF 10,ITG=HEADING
C IUNIT=5 IF CONTROL DATA ON CARDS = TAPE UNIT IF ON TAPE
C SAME FOR JUNIT FOR INPUT DATA
C TAPE UNIT 2=OUTPUT
C CODE IFEOF=1 IF EOF FOLLOWS EACH SET
C FIRST SET OF FILTER PARAMETERS ARE FOR HIGH PASS PREWHITENING
C SECOND SET ARE FOR LOW PASS SMOOTHING
C IF N(1)=-1 COSINE TAPER IS APPLIED,=0 NO TAPER OR PREWHITENING
C LEAVE HIGH OR LOW PASS PARAMETERS BLANK IF NO FILTER DESIRED
C INPUT DATA LIMIT IS 2048 PTS,NP=NO.OF INPUT PTS
C IF ANORM IS BLANK SET TO 1 IN PROGRAM
C USES SUBROUTINE NLOGN FROM ROBINSON
C IN FIRST CONTROL CARD NSETS=NO.OF SETS OF DATA THIS RUN
C SET KPHA=1 IF PHASE SPECTRUM IS DESIRED
C IORGN=NO.OF INPUT DATA PT.TO USE AS ORIGIN FOR PHASE SPECTRUM
C IF PHASE IS DESIRED CODE IPHA=0 IF PHASE IN DEGREES OR CODE IPHA
C =NO.OF DATA INTERVALS/INCH FOR PLOT IF YOU WANT PHASE IN DATA INT.
C SET JCODE=1 IF ONLY PLOT OF FINAL SMOOTHED SPECTRUM DESIRED
C SET JCODE=-1 FOR NO PLOT AT ALL
C CODE ILIST=1 IF YOU DESIRE ONLY LISTING OF SMOOTHED SPECTRUM
C **IMPORTANT-IF YOU HAVE ALREADY ADDED ZEROES TO THE BEGINNING OR END
C OF YOUR INPUT DATA AND YOU REQUEST PREWHITENING OR COSINE TAPER
C YOU MUST CODE IADJ=1 FOR PROPER EXECUTION
C IMEAN=1 IF YOU WANT THIS MEAN REMOVED
C DIMENSION DATA(4500),STO(2500),CUT(2),H(2),N(2),ADATA(4100)

```

1,SDATA(4500),BDATA(2050),CDATA(2050),PHASE(2050),SMPH(2050)
COMMON/BOUND/I,IPNUM,ISDLAT,SELAT,ISDLNG,SELNG,IDLAT,EELAT,
1IDLNG,EMLNG
CHARACTER*4 ITH(8),ITG(8)
CHARACTER*1 RESPON
C READ(5,*)NSETS,JCODE,IUNIT,JUNIT,IFEOF,GRIDNM
NSETS=1000
JCODE=1
IUNIT=5
JUNIT=2
IFEOF=1
C GRID SPACING IS READ FROM DATA FILE
IF(JCODE.GE.0) CALL PLOTS(STO,2500,2)
CALL FACTOR(.65)
JSET=1
IF(JCODE.GE.0) CALL PLOT(1.0,0.0,-3)
C READ(IUNIT,*)NP,KXORG,KYORG,ANORM1,(CUT(I),H(I),N(I),I=1,2),IMEAN,
C 1 KPHA,IPHA,IORGN,ILIST,IADJ
C NUMBER OF POINTS IS READ FROM DATA FILE, MAXIMUM IS HELD TO 2000
NPTS=2000
KXORG=-2
KYORG=-7
ANORM1=2.0
CUT(1)=-1.0
H(1)=.2
N(1)=3
CUT(2)=.08
H(2)=.2
N(2)=3
IMEAN=1
KPHA=0
IPHA=0
IORGN=1
ILIST=0
IADJ=1
245 CONTINUE
APHA=IPHA
XORG=10.0**KXORG
YORG=10.0**KYORG
IOUT=7
IF(ABS(ANORM1).LT.1.0E-20)ANORM=1.0
CALL PRVOUT(NP,DATA,ITG,XINTER,SLOPEX,GRIDNM)
GRIDKM=GRIDNM*1.852
C XINTER=10**(ALOG10(XINTER)-(ALOG10(1./GRIDKM)+.5))
2451 CTOFF2=.5*(1./GRIDKM)
CTOFF1=.01*(1./GRIDKM)
CTOFF1=ALOG10(CTOFF1)
CTOFF2=ALOG10(CTOFF2)
CT1SV=CTOFF1
CT2SV=CTOFF2
C SAVE DATA ARRAY IN SDATA ARRAY
DO 2452 I=1,NP
2452 SDATA(I)=DATA(I)

```

```

25 IF (ANORM1.GT.1.) ANORM=1./FLOAT(NP)
38 IF (CUT(1).NE.-1.0) GO TO 29
C   FUNDAMENTAL FREQUENCY, H(1)=.2, N(1)=3
   CUT(1)=.8/(FLOAT(NP))
   H(1)=.2
   N(1)=3
   IF (ANORM1.GT.1.) ANORM=1./(FLOAT(NP)-(2*(N(1)-1)))
29 IF (IADJ.NE.1) GO TO 383
C   COMPUTE INDEX OF FIRST NON-ZERO POINT
28 DO 385 J=1,NP
   K1=J
   IF (DATA(J).NE.0.0) GO TO 386
385 CONTINUE
   WRITE(IOUT,82) XORG,YORG,ANORM,ITG
82  FORMAT(15H PLOT ORIGIN X=,E11.4,4H Y= ,E11.4,15HNORMALIZATION =,
1E11.4,30A1)
C   COMPUTE INDEX OF LAST NON-ZERO POINT
386 DO 391 J=NP,K1,-1
   K2=J
   IF (DATA(J).NE.0.0) GO TO 392
391 CONTINUE
C   SHIFT DATA TO LEFT AND RECOMPUTE NO.OF INPUT POINTS
392 NP=K2-K1+1
   DO 393 J=1,NP
   K=K1+J-1
393 DATA(J)=DATA(K)
C   DEMEAN DATA AND APPLY COSINE TAPER
383 SUM=0.0
   XNP=NP
   DO 388 J=1,NP
388 SUM=SUM+DATA(J)
   AVE=SUM/XNP
   IF (N(1).GE.0.AND.IMEAN.EQ.0) GO TO 381
   DO 389 J=1,NP
389 DATA(J)=DATA(J)-AVE
   CALL BATHXS(DATA,NP,GRIDKM)
   IF (N(1).GE.0) GO TO 381
   DO 382 J=1,NP
   AM=J-1
   TNP=NP-1
   TNP=TNP/2.0
   AM=3.14159*(AM-TNP)/TNP
382 DATA(J)=DATA(J)*0.5*(1.0+COS(AM))
C   RAISE NO.OF PTS TO A POWER OF 2(M) AND STORE IN INP
381 KOUNT=1
   DO 5 M=1,12
   I=2**M
   IF (I-NP) 5,6,7
5  CONTINUE
6  INP=I
   GO TO 9
7  INP=I
   NPP=NP+1

```

```

      DO 8 J=NPP,INP
      DATA(J)=0.0
      AINP=INP
      DELR=1.0/AINP
      DELK=(1.0/AINP)/GRIDKM
C     INP= TOTAL NO.OF DATA PTS.TO A POWER OF 2
C     DELR=NORMALIZED FREQUENCY INTERVAL IN CYCLES PER DATA INTERVAL
      WRITE(IOUT,50)DELR,INP,NP
50  FORMAT(' FREQ.INT=',E8.3,' POWER OF 2 DATA PTS=',I6,' NO.OF INPUT
      1 DATA PTS=',I6)
      WRITE(IOUT,560)IORGN
560  FORMAT(' ORIGIN FOR PHASE SPECTRUM IS INPUT PT.NO.',I4)
C     NOW STORE DATA IN COMPLEX FORM IN ADATA
      DO 2 J=1,INP
      I=(J*2)-1
      ADATA(I)=DATA(J)
      IA=I+1
      2  ADATA(IA)=0.0
C     COMPUTE AND PLOT NORMALIZED AMPLITUDE SPECTRUM
      CALL NLOGN(M,ADATA,-1.0)
      INX=INP+1
      IF(KOUNT-2) 301,301,302
C     CORRECT FFT OF PREWHITENING FILTER FOR PHASE SHIFT
302  ANN=N(1)
      CALL TSHIFT(M,ADATA,ANN,DELR)
      DO 303 I=1,INX,2
      JX=(I+1)/2
      J=I+1
      BDATA(JX)=(SQRT(ADATA(I)**2+ADATA(J)**2))*ANORM
      IF(ADATA(I).LT.0.0) BDATA(JX)=-BDATA(JX)
303  CONTINUE
      GO TO 204
301  DO 201 I=1,INX,2
      JX=(I+1)/2
      J=I+1
      201  BDATA(JX)=( SQRT(ADATA(I)**2 +ADATA(J)**2))*ANORM
C     COMPUTE ROUGH PHASE SPECTRUM FROM PREWHITENED DATA
C     OR COSINE TAPERED DATA
      IF(KPHA.EQ.1.AND.N(1).LE.0) GO TO 567
      IF(KPHA.EQ.1.AND.KOUNT.EQ.2) GO TO 567
      GO TO 568
567  ANN=IORGN-1
C     CORRECT PHASE SPECTRUM FOR DESIRED ORIGIN
      CALL TSHIFT(M,ADATA,ANN,DELR)
      DO 569 I=1,INX,2
      JX=(I+1)/2
      B=JX-1
      B=B*DELR*360.0
      J=I+1
      IF(ABS(ADATA(I)).LT.1.E-20) ADATA(I)=ADATA(I)+1.E-20
      PHASE(JX)=(ATAN2(ADATA(J),ADATA(I)))*57.295779
569  IF(IPHA.GT.0.AND.B.GT.0)PHASE(JX)=PHASE(JX)/B
      IF(IPHA.GT.0) GO TO 541

```

```

        WRITE(IOUT,570)
570 FORMAT(' ROUGH PHASE SPECTRUM(DEG)')
        GO TO 542
541 WRITE(IOUT,543)
543 FORMAT(' ROUGH PHASE SPECTRUM(DATA INTERVALS)')
542 IF(ILIST.NE.1) WRITE(IOUT,81)(PHASE(J),J=1,JX)
568 IF(KOUNT-2)202,203,204
202 WRITE(IOUT,75)
    75 FORMAT(28H AMP.SPECT.OF ORIGINAL DATA )
    77 IF(ILIST.NE.1) WRITE(IOUT,81)(BDATA(J),J=1,JX)
    81 FORMAT(10E11.4)
        GO TO 206
203 WRITE(IOUT,76)
    76 FORMAT(30H AMP.SPECT.OF PREWHITENED DATA)
        GO TO 77
204 WRITE(IOUT,91) CUT(1),H(1),N(1)
    91 FORMAT(' SPECT.OF PREWHITENING FILTER WITH PHASE REVERSALS CUTOF
    1F=',F5.4,' H=',F5.4,' N=',I3)
        DO 92 J=1,JX
    92 BDATA(J)=BDATA(J)/ANORM
        IF(ILIST.NE.1) WRITE(IOUT,81)(BDATA(J),J=1,JX)
C    CORRECT SPECTRUM OF FILTERED DATA FOR PREWHITENING FILTER
        DO 93 J=1,JX
        IF(ABS(BDATA(J)).LT.1.E-20)BDATA(J)=BDATA(J)+1.E-20
    93 BDATA(J)=ABS(CDATA(J)/BDATA(J))
        WRITE(IOUT,94)
    94 FORMAT(' FINAL ROUGH CORRECTED SPECTRUM WITHOUT PHASE REVERSALS')
        IF(ILIST.NE.1) WRITE(IOUT,81)(BDATA(J),J=1,JX)
        GO TO 206
    95 CONTINUE
C    SMOOTH FINAL ROUGH CORRECTED SPECTRUM
C    COMPUTE LOW PASS WEIGHTS
        K=2
        IF(N(2).EQ.0) GO TO 330
C    STORE ROUGH SPECTRUM IN DATA
        DO 97 J=1,JX
    97 DATA(J)=BDATA(J)
        GO TO 98
    83 DO 99 I=1,NA
    99 BDATA(I)=BDATA(I)+DELTA/X
C    CONVOLVE LOW PASS SMOOTHING WEIGHTS WITH ROUGH SPECTRUM
        NB=JX-N(K)
        GO TO 235
206 IF(JCODE.EQ.1.AND.N(2).GT.0) GO TO 311
        IF(JCODE.LT.0) GO TO 311
        X=ALOG10 ( DELK/XORG)*3.0125
        TPP=BDATA(2)/YORG
        IF(TPP.LT.1.E-20) TPP=YORG
        Y=-0.5+ALOG10(TPP)*1.35714
        CALL PLOT(X,Y,3)
        DO 42 J=3,JX-1
        XJ=J-1
        X=ALOG10((XJ*DELK)/XORG)*3.0125

```

```

      TPP=BDATA(J)/YORG
      IF(TPP.LT.1.E-20) TPP=YORG
      Y=-0.5+ALOG10(TPP)*1.35714
42  CALL PLOT(X,Y,2)
311 IF(KOUNT-2)78,79,95
      78 KOUNT=2
C    COMPUTE WEIGHTS FOR PREWHITENING FILTER AND STORE IN BDATA
      IF(N(1).LE.0) GO TO 95
      K=1
98  NA=N(K)+1
      BDATA(1)=2.0*(CUT(K)+H(K))
C    CENTER WEIGHT STORED IN LOCATION 1
      SUM=0.0
      PI=3.1415926535898
C    COMPUTE REMAINING WEIGHTS
      DO 40 I=2,NA
      P=I-1
      Q=1.0-16.*H(K)**2*P**2
      IF( ABS(Q).GT.0.0001) GO TO 11
      BDATA(I)= SIN(2.*PI*P*(CUT(K)+H(K)))/(4.0*P)
      GO TO 40
11  BDATA(I)=(( COS(2.*PI*P*H(K)))/Q)*(( SIN(2.*PI*P*(CUT(K)+H(K))))
1  /(PI*P))
40  SUM=SUM+BDATA(I)
C    CORRECT WEIGHTS FOR UNITY GAIN
      DELTA=1.-(BDATA(1)+2.*SUM)
      X=2*N(K)+1
C    COMPUTE FINAL CORRECTED WEIGHTS,HIGH PASS OR LOW PASS
      IF(K.EQ.2) GO TO 83
      DO 41 I=2,NA
41  BDATA(I)= (BDATA(I)+ DELTA/X)*(-1.0)
      BDATA(1)=1.0-(BDATA(1)+DELTA/X)
      NB=NP-N(K)
C    CONVOLVE HIGH PASS WEIGHTS WITH ORIGINAL DATA,STORE IN ADATA
235 DO 44 I=NA,NB
      IA=I-NA+1
      SUM=0.0
      DO 43 J=1,NA
      J1=I+J-1
      J2=I-J+1
43  SUM=SUM+BDATA(J)*(DATA(J1) + DATA(J2))
44  ADATA(IA)=SUM-BDATA(1)*DATA(I)
      IF(K.EQ.2) GO TO 236
C    STORE PREWHITENED DATA IN DATA AND FILL IN ZEROES
      NJ=NB-N(K)
      DO 51 J=1,NJ
51  DATA(J)=ADATA(J)
      NJ=NJ+1
      DO 54 J=NJ,INP
54  DATA(J)=0.0
C    PUT WEIGHTS IN PROPER ORDER -N.O.N AND STORE IN CDATA
      JJ=N(K)+1
      DO 52 J=1,JJ

```

```

      J1=J+N(K)
      J2=JJ-(J-1)
      CDATA(J1)=BDATA(J)
52  CDATA(J2)=CDATA(J1)
C    COMPUTE AMPLITUDE SPECTRUM OF PREWHITENED DATA AND PLOT
      GO TO 53
79  CONTINUE
C    STORE HIGH PASS WEIGHTS IN DATA AND AMP.SPECT.OF PREWHITENED
C    DATA IN CDATA
      JJ=2*N(K)+1
      DO 102 J=1,JJ
102  DATA(J)=CDATA(J)
      JJ=JJ+1
      DO 104 J=JJ,INP
104  DATA(J)=0.0
      DO 103 J=1,JX
103  CDATA(J)=BDATA(J)
C    COMPUTE AMPLITUDE SPECTRUM OF PREWHITENING FILTER
      KOUNT=3
      GO TO 53
236 CONTINUE
C    OUTPUT SMOOTHED SPECTRUM AND PLOT
      FIRST=(N(2)+1)*DELR
      FIRSTK=(N(2)+1)*DELK
      WRITE(IOUT,237) FIRSTK
237 FORMAT(38H FINAL SMOOTHED AND CORRECTED SPECT. ,16HFIRST FREQUENC
1Y=,E8.3)
      CALL PARSVL(ADATA,NP,INP,AVE,ANOIS,N(2),ANORM)
      WRITE(IOUT,491)AVE,ANOIS
491 FORMAT(' VALUE OF AMP SPECT OF NOISE=',E10.4,' RMS WHITE NOISE LE
1VEL=',E10.4)
      WRITE(IOUT,81)(ADATA(J), J=2,IA)
4911 CALL POWWGT(B0,B1,FIRSTK,DELK,ADATA(2),IA-1,0,CTOFF1,CTOFF2)
      BOSAVE=B0
      B1SAVE=B1
C    CALCULATE RMS FOR WHITE NOISE WITH INTERCEPT(B0)
      AVE=B0
      AVE=AVE/ANORM
      AVE=AVE**2
      ANOISE=(AVE*INP)/(NP*INP)
      ANOISE=SQRT(ANOISE)
      WRITE (IOUT,492)AVE,ANOISE
492 FORMAT(' AVE= ',F8.3,' RMS WHITE NOISE = ',F8.3)
      IF(JCODE.LT.0) GO TO 486
      ENCODE(13,601,ITH) B1
601  FORMAT('SLOPE =',F6.3)
      CALL SYMBOL(7.5,8.5,.20,ITH,0.,13)
      ENCODE(19,602,ITH)B0
602  FORMAT('INTERCEPT =',E8.3)
      CALL SYMBOL(7.5,8.0,.20,ITH,0.,19)
C    PLOT REGRESSION LINE FROM POWWGT
C    CALL NEWPEN(3)
      IPLPSS=0

```

```

603 FIRST1=FIRSTK
C   WRITE(IOUT,'(8HFIRST1= ,E11.4)')FIRST1
    X=ALOG10(FIRST1/XORG)*3.0125
    AMP1=BO*FIRST1**B1
C   WRITE(IOUT,'(6HAMP1= ,E11.4)')AMP1
    TPP=AMP1/YORG
    IF(TPP.LT.1.E-20) TPP=ABS(TPP)
    Y=-0.5+ALOG10(TPP)*1.35714
    CALL PLOT(X,Y,+3)
C   CALL SYMBOL ( X,Y,.1,32,0.0,-1)
    FIRST1=((IA)*DELK)
C   WRITE(IOUT,'(8HFIRST1= ,E11.4)')FIRST1
    X=ALOG10(FIRST1/XORG)*3.0125
    AMP1=BO*FIRST1**B1
C   WRITE(IOUT,'(6HAMP1= ,E11.4)')AMP1
    TPP=AMP1/YORG
    IF(TPP.LT.1.E-20) TPP=ABS(TPP)
    Y=-0.5+ALOG10(TPP)*1.35714
    CALL PLOT(X,Y,+2)
C   CALL SYMBOL ( X,Y,.1,32,0.0,-2)
C   CALL NEWPEN(1)
C   PLOT SPECTRAL ESTIMATES
    X=ALOG10 (FIRSTK/XORG)*3.0125
    TPP=ADATA(2)/YORG
    IF(TPP.EQ.0.0)TPP=1.E-15
    IF(TPP.LT.1.E-20) TPP=ABS(TPP)
    Y=-0.5+ALOG10(TPP)*1.35714
    CALL PLOT(X,Y,+3)
C   CALL SYMBOL ( X,Y,.05,32,0.0,-1)
    DO 238 J=3,IA-1
    XJ=J-1+N(2)
    X=ALOG10((XJ*DELK)/XORG)*3.0125
    TPP=ADATA(J)/YORG
    IF(TPP.EQ.0.0)TPP=1.E-15
    IF(TPP.LT.1.E-20) TPP=ABS(TPP)
    Y=-0.5+ALOG10(TPP)*1.35714
238 CALL PLOT(X,Y,+2)
C 238 CALL SYMBOL ( X,Y,.05,32,0.0,-2)
    CALL PLOT(0.0,0.0,+3)
    IF(IPLSS.EQ.1) GO TO 330
    IF(LPASS.EQ.1) GO TO 330
    IPLSS=1
    BO=XINTER
    B1=SLOPEX
C   INCLUDE NEXT LINE IF A PLOT OF SPATIAL DOMAIN ESTIMATE IS DESIRED
C   GO TO 603
C   PLOT AXIS
330 IF(ANORM.EQ.1.0) GO TO 333
    CALL AXES(0.,-.5,'NORMALIZED AMPLITUDE (IN KM)',27,9.5,90.0
    *,1.3514,10.0,0.0,-1)
    GO TO 332
333 CALL AXES(0.,-.5,'AMPLITUDE (IN KILOMETERS)',25,9.5,90.0
    *,1.3514,10.0,0.0,-1)

```

```

332 CALL AXES(0.,-0.5,'FREQUENCY(CYCLES/KILOMETER)',27,12.2,0.0
*,3.0125,10.0,0.0,-1)
CALL SYMBOL(4.0,-1.4,.32,ITG,0.0,30)
AYORG=KYORG
AXORG=KXORG
DO 362 J=1,8
AA=J-1
Y=(1.35714*AA)-0.37
FPN=AYORG+AA
362 CALL NUMBER(-.25,Y,.16,FPN,90.0,-1)
DO 363 J=1,5
AA=J-1
X=(3.0125*AA)+0.20
FPN=AXORG+AA
363 CALL NUMBER(X,-.25,.16,FPN,0.0,-1)
DO 364 J=1,4
IB=KXORG+J-1
DO 364 JC=2,9
AC=JC
AA=AC*10.0**IB
X=ALOG10(AA/XORG)*3.0125
CALL PLOT(X,-.5,3)
364 CALL PLOT(X,-.46,2)
DO 365 J=1,7
IB=KYORG+J-1
DO 365 JC=2,9
AC=JC
AA=AC*10.0**IB
Y=-0.5+ALOG10(AA/YORG)*1.35714
CALL PLOT(0.0,Y,3)
365 CALL PLOT(-.04,Y,2)
CALL PLOT(0.0,-1.0,3)
CALL PLOT(0.0,-1.0,3)
C
C INTERACTIVE ROUTINE TO MODIFY INPUT STRING
C
WRITE(6,3641)
3641 FORMAT(T70,' ARE YOU SATISFIED WITH THE DATA SET BOUNDARIES?'/
*T70,' ENTER E TO END RUN')
READ(5,3652) RESPON
IF(RESPON.EQ.'E') GO TO 487
IF(RESPON.EQ.'Y') GO TO 3650.
WRITE(6,3642)
3642 FORMAT(T70,' WOULD YOU LIKE TO ELIMINATE THE ENTIRE SEGMENT?')
READ(5,3652) RESPON
IF(RESPON.EQ.'N') GO TO 3644
CALL ERASE
GO TO 3658
3644 WRITE(6,3643)
3643 FORMAT(T70,' ENTER FIRST,SECOND LOCATIONS(IN KM) FOR TRUNCATION')
READ(5,*)FIR,SEC
NFIR=FIR/GRIDKM
IF(NFIR.LT.0) NFIR=0

```

```

      NSEC=SEC/GRIDKM
      IF(NSEC.GT.NP) NSEC=NP
C     RECREATE DATA ARRAY
      DO 3645 ICHG=1,NP
      LOCCHG=ICHG+NFIR
      DATA(ICHG)=SDATA(LOCCHG)
      IF(LOCCHG.EQ.NSEC) GO TO 3646
3645 CONTINUE
C     INTERPOLATE NEW LAT & LON
3646 SDIFF=FLOAT(NSEC)/FLOAT(NP)
      FDIFF=FLOAT(NFIR)/FLOAT(NP)
      FLAT=DECDEG(ISDLAT,SELAT)
      FLON=DECDEG(ISDLNG,SELNG)
      SLAT=DECDEG(IDLAT,EELAT)
      SLON=DECDEG(IDLNG,EMLNG)
      FNLAT=((SLAT-FLAT)*FDIFF)+FLAT
      SNLAT=((SLAT-FLAT)*SDIFF)+FLAT
      FNLON=((SLON-FLON)*FDIFF)+FLON
      SNLON=((SLON-FLON)*SDIFF)+FLON
C     RECONSTRUCT INTO DEGREES AND MINUTES
      CALL DEGMIN(FNLAT,ISDLAT,SELAT)
      CALL DEGMIN(FNLON,ISDLNG,SELNG)
      CALL DEGMIN(SNLAT,IDLAT,EELAT)
      CALL DEGMIN(SNLON,IDLNG,EMLNG)
      NP=NSEC-NFIR
      CALL ERASE
      GO TO 2451

C
C     INTERACTIVE ROUTINE TO MODIFY REGRESSION FIT TO SPECTRUM
C
3650 WRITE(6,3651)
3651 FORMAT(T70,' ARE YOU SATISFIED WITH THE REGRESSION FIT?')
      READ(5,3652)RESPON
3652 FORMAT(A1)
      IF(RESPON.EQ.'Y') GO TO 3656
      WRITE(6,3653)
3653 FORMAT(T70,' ENTER LOG(LOWER FREQUENCY),LOG(UPPER FREQUENCY)')
      READ(5,*) CTOFF1,CTOFF2
      CALL ERASE
      LPASS=1
      GO TO 4911
3656 CTOFF1=CT1SV
      CTOFF2=CT2SV
      CALL ERASE
      LPASS=0
      WRITE(14,399)NP,IPNUM,ISDLAT,SELAT,ISDLNG,SELNG,IDLAT,EELAT,
1 IDLNG,EMLNG,B1SAVE,BOSAVE
399 FORMAT(I5,I8,4(1X,I4,F6.2),F6.3,E9.3)
C     PLOT PHASE SPECTRUM
3658 IF(KPHA.NE.1) GO TO 581
      CALL PLOT(15.0,0.0,-3)
      X=ALOG10(DELK/XORG)*3.0125
      Y=ABS(PHASE(2)/30.0)

```

```

        IF(IPHA.GT.0) Y=Y*30.0/APHA
        IBB=4
        IF(Y.LT.8.0.AND.PHASE(2).GE.0.0) GO TO 552
        IF(Y.LT.8.0.AND.PHASE(2).LT.0.0) IBB=2
        IF(Y.GE.8.0) Y=8.5
        CALL SYMBOL(X,Y,.05,IBB,0.,-1)
        GO TO 553
552 CALL PLOT(X,Y,3)
553 DO 571 J=3,JX
        XJ=J-1
        X=ALOG10((XJ*DELK)/XORG)*3.0125
        Y=ABS(PHASE(J)/30.0)
        IF(IPHA.GT.0) Y=Y*30.0/APHA
        IBB=4
        IF(Y.LT.8.0.AND.PHASE(J).GE.0.0) GO TO 554
        IF(Y.LT.8.0.AND.PHASE(J).LT.0.0) IBB=2
        IF(Y.GE.8.0) Y=8.5
        CALL SYMBOL(X,Y,.05,IBB,0.,-2)
        GO TO 571
554 CALL PLOT(X,Y,2)
571 CONTINUE
486 CONTINUE
C   COMPUTE AND PLOT SMOOTHED PHASE SPECTRUM
        IF(N(2).EQ.0) GO TO 579
        DO 572 I=NA,NB
            IA=I-NA+1
            SUM=0.0
            DO 573 J=1,NA
                J1=I+J-1
                J2=I-J+1
573 SUM=SUM+BDATA(J)*(PHASE(J1)+PHASE(J2))
572 SMPH(IA)=SUM-BDATA(1)*PHASE(I)
            IF(IPHA.GT.0) GO TO 544
            WRITE(IOUT,582) FIRSTK
582 FORMAT(' SMOOTHED PHASE SPECTRUM(DEG)-FIRST FREQ.=' ,E8.3)
            GO TO 545
544 WRITE(IOUT,546) FIRSTK
546 FORMAT(' SMOOTHED PHASE SPECTRUM(DATA INT.)-FIRST FREQ.=' ,F8.5)
545 WRITE(IOUT,81)(SMPH(J),J=2,IA)
            IF(JCODE.LT.0) GO TO 581
C   CALL NEWPEN(1)
            X=ALOG10(FIRSTK/XORG)*3.0125
            Y=ABS(SMPH(2)/30.0)
            IF(IPHA.GT.0) Y=Y*30.0/APHA
            IBB=4
            IF(Y.LT.8.0.AND.SMPH(2).GE.0.0) GO TO 548
            IF(Y.LT.8.0.AND.SMPH(2).LT.0.0) IBB=2
            IF(Y.GE.8.0) Y=8.5
            CALL SYMBOL(X,Y,.05,IBB,0.,-1)
            GO TO 549
548 CALL PLOT(X,Y,3)
549 DO 574 J=3,IA
            XJ=J-1+N(2)

```

```

X=ALOG10((XJ*DELK)/XORG)*3.0125
Y=ABS(SMPH(J)/30.0)
IF(IPHA.GT.0)Y=Y*30.0/APHA
IBB=4
IF(Y.LT.8.0.AND.SMPH(J).GE.0.0) GO TO 550
IF(Y.LT.8.0.AND.SMPH(J).LT.0.0) IBB=2
IF(Y.GE.8.0) Y=8.5
CALL SYMBOL(X,Y,.05,IBB,0.,-2)
GO TO 574
550 CALL PLOT(X,Y,2)
574 CONTINUE
C   PLOT PHASE AXIS
579 IF(JCODE.LT.0) GO TO 581
C   CALL NEWPEN(1)
IF(IPHA.GT.0) GO TO 547
CALL AXES(0.,0.,14HABS PHASE(DEG),14,6.,90.,1.,0.,30.,-1)
GO TO 558
547 CALL AXES(0.,0.,20HABS PHASE(DATA INT.),20,8.,90.,1.,0.,APHA,-1)
558 CALL AXES(0.,0.,ITG,+30,12.2,0.,3.0125,10.,0.,-1)
CALL SYMBOL(2.0,-.2,.14,33HTRIANGLE INDICATES NEGATIVE PHASE,0.0,
1 33)
581 CONTINUE
IF(N(2).EQ.0) GO TO 331
C   COMPUTE AMPLITUDE SPECTRUM OF SMOOTHING FILTER
DELX= 0.01
DO 239 J=1,51
AJ=J-1
XJ=AJ*DELX
SUM=0.0
DO 240 I=2,NA
AI=I-1
240 SUM=SUM+2*BDATA(I)* COS(2.*PI*AI*XJ)
DATA(J)= SUM+BDATA(1)
239 CDATA(J)=XJ
WRITE(IOUT,241) CUT(2),H(2),N(2)
241 FORMAT(' AMP.SPECT.OF SMOOTHING FILTER CUTOFF=',F5.4,
1' H=',F5.4,' N=',I3)
IF(ILIST.NE.1) WRITE(IOUT,242)(CDATA(I),DATA(I),I=1,51)
242 FORMAT(8(F5.2,F8.3))
331 WRITE(IOUT,243) JSET
243 FORMAT(' END OF DATA SET NO.',I3)
C   END FILE 12
C   END FILE 12
IF(JSET.EQ.NSETS) GO TO 244
JSET=JSET+1
IF(JCODE.LT.0) GO TO 245
C   CALL PLOT(15.0,0.0,-3)
GO TO 245
244 IF(JCODE.LT.0) GO TO 487
CALL PLOT(0.0,0.0,999)
487 END FILE 14
END FILE 14
STOP
END

```

```

C   THIS SUBROUTINE IS A SUPPLEMENT TO FFT1D PROGRAM
C   AND DRAWS A PROFILE OF BATHYMETRIC DATA
C   COMPILER(DIAG=3)
      SUBROUTINE BATHXS(DATA,NPTS,GRIDKM)
      DIMENSION DATA(1)
C   CONVERT DEPTHS IN KILOMETERS TO METERS
C   WRITE(IOUT,3)(DATA(I),I=1,10)
C   3  FORMAT(' ',10(F10.5,1X))
      DO 5 I=1,NPTS
        5 DATA(I)=DATA(I)*1000.
      CALL PLOT(0.,10.,-3)
C   FIND MAXIMUM AND MINIMUM DEPTH
      DEPMIN=0.0
      DEPMAX=0.0
      DO 10 I=1,NPTS
        IF(DATA(I).LT.DEPMIN) DEPMIN=DATA(I)
        10 IF(DATA(I).GT.DEPMAX) DEPMAX=DATA(I)
CC  ROUND TO NEAREST 100
      DEPMAX=(AINT(DEPMAX/100.)*100.)+100.
      DEPMIN=(AINT(DEPMIN/100.)*100.)-100.
      IF(GRIDKM.GT.0.0001) GO TO 11
      DEPMAX=-1.0
      DEPMIN=1.0
      GO TO 12
      11 IF(GRIDKM.GE.0.01) GO TO 12
      DEPMAX=-20.0
      DEPMIN=20.0
      12 YSCALE=-(DEPMAX-DEPMIN)/4.
C   SETUP AXES
      CALL AXES(0.,0., ' DEPTH (IN METERS)',18,4.0,90.,1.00,DEPMAX,YSCALE
        *, -1)
      XDIST=FLOAT(NPTS)*GRIDKM
      XSCALE=12.805/XDIST
      XINC=1.0
      55 XTICK=XSCALE
      56 IF(XTICK.GT.1.) GO TO 60
      XINC=2.*XINC
      XTICK=2.*XTICK
      GO TO 56
      60 IF(GRIDKM.GT.0.0001) GO TO 70
      CALL AXES(0.0,0.0, 'DISTANCE (IN 0.1 METERS)',24,12.805,0.0,XTICK
        *,0.0,1.0,1)
      GO TO 90
      70 IF(GRIDKM.GT.0.01) GO TO 80
      CALL AXES(0.0,0.0, 'DISTANCE (IN 100 METERS)',24,12.805,0.0,XTICK
        *,0.0,1.0,3)
      GO TO 90
      80 CALL AXES(0.0,0.0, 'DISTANCE (IN KILOMETERS)',24,12.805,0.0,XTICK
        *,0.0,XINC,-1)
      90 DO 100 I=1,NPTS
        YVAL=-((DEPMAX-DATA(I))/YSCALE)
        XVAL=(FLOAT(I)*GRIDKM)*XSCALE
        IF(I.EQ.1) CALL PLOT(0.0,YVAL,3)

```

```
100 CALL PLOT(XVAL,YVAL,2)
    CALL PLOT(0.,-10.,-3)
C    CONVERT BACK TO KILOMETERS
    DO 105 I=1,NPTS
105 DATA(I)=DATA(I)/1000.
    RETURN
    END
```

```

SUBROUTINE PRVOUT(NP,DEPTH,ITG,XINTER,SLOPE,GRID)
  DIMENSION DEPTH(5000)
  COMMON/BOUND/I,IPNUM,ISDLAT,SELAT,ISDLNG,SELNG,IDLAT,EELAT,
1IDLNG,EMLNG
  CHARACTER*4 ITG(8)
C   READER ROUTINE FOR DEPTH OUTPUT FROM PROVINCE PICKER
  READ(13,5,END=500) (ITG(I),I=1,6),SLOPE,XINTER,GRID,NP
5  FORMAT(6A4,F7.3,1X,E9.3,1X,F7.4,I5)
  NP=NP+1
  ITG(7)='    '
  ITG(8)='    '
  WRITE(6,55,END=500) (ITG(I),I=1,6),SLOPE,XINTER,GRID,NP
55 FORMAT(T70,6A4,F7.3,1X,E10.5,F7.4,I5)
  READ(13,50)I,IPNUM,ISDLAT,SELAT,ISDLNG,SELNG,IDLAT,EELAT,
1IDLNG,EMLNG,RMS
50 FORMAT(I5,I8,4(1X,I4,F6.2),F10.4)
  READ(13,6) (DEPTH(I),I=1,NP)
  6  FORMAT(10F8.6)
  IF(NP.GT.2048) NP=2048
  READ(13,7) CHECK
  7  FORMAT(F8.2)
  IF(CHECK.NE.9.999999) PRINT 8
  8  FORMAT(' NINES RECORD DOES NOT CHECK')
  GO TO 900
500 DEPTH(1)=9.999999
900 RETURN
END

```

```

      SUBROUTINE PARSVL(DATA,NP,INP,AVE,ANOIS,NWGT,ANORM)
C  ROUTINE TO COMPUTE THE AVE VALUE OF THE LAST 10 PERCENT OF THE
C  HARMONICS(AVE) OF AN AMPLITUDE SPECTRUM(DATA) AND USE THIS VALUE WITH
C  PARSEVALS FORMULA TO COMPUTE THE RMS WHITE NOISE LEVEL(ANOIS).
C** NP=THE NO.OF ORIGINAL PTS INPUT TO THE FFT USED TO COMPUTE DATA ARRAY
C** INP=THE NO.OF POINTS TO A POWER OF 2 USED FOR THE FFT
C** DATA= UNNORMALIZED FFT AMPLITUDE SPECTRUM WITH UNITS OF
C** INPUT UNITS/CYCLE/DATA INTERVAL AND IS OF LENGTH(INP/2)+1-2*NWGT
C** NWGT=LENGTH OF SMOOTHING FILTER YOU USED ON YOUR FFT -NWGT..0..+NWGT
      DIMENSION DATA(1)
      IF(ANORM.EQ.1.) GO TO 11
      DO 10 I=1,NP
10 DATA(I)=DATA(I)/ANORM
11 JX=INP/2+1-2*NWGT
      JT=JX-(JX/10)
      X=0.2*INP
      JX=X-2.0
      T=0.13*INP
      JT=T-2.0
      DIF=JX-JT+1
      ANP=NP
      AVE=0.0
      AVEPS=0.0
      DO 1 I=JT,JX
      AVE=AVE+DATA(I)
1 AVEPS=AVEPS+DATA(I)**2
      AVE=AVE/DIF
      AVEPS=AVEPS/DIF
C  PARSEVALS FORMULA IS MEAN SQ NOISE=(INP*AVEPS)/(NP*INP)
      ANOIS=SQRT(AVEPS/ANP)
      IF(ANORM.EQ.1.) RETURN
      DO 12 I=1,NP
12 DATA(I)=DATA(I)*ANORM
      RETURN
      END

```

```

      SUBROUTINE TSHIFT(M,DATA,A,DELF)
C*****THIS SUBROUTINE CONTAINS 26 STATEMENTS.
C*****TSHTF APPLIES EFFECTS OF TIME SHIFT ON REAL AND IMAGINARY PARTS OF THE
C*****FOURIER TRANSFORM.
C*****M == POWER OF 2 WHICH IS EQUAL TO THE NUMBER OF REAL OR IMAGINARY PARTS
C*****      OF THE FOURIER TRANSFORM.
C*****DATA == SERIES ... REAL PARTS ARE ODD INDEX, IMAGINARY PARTS ARE EVEN.
C*****A == YAXIS SHIFT, IE. TO CORRECT THE FOURIER TRANSFORM OF A FUNCTION
WHICH
C*****      HAS BEEN SHIFTED A DATA INTERVALS IN THE +X DIRECTION,SIGN OF A IS
+.
C*****DELF == NORMALIZED FREQUENCY INCREMENT.
      DIMENSION DATA(1)
      M2=2*2**M
      PI=3.1415926536
      SFT=2.0*PI*A*DELF
      DO 1 I=1,M2,2
      J=I+1
      TRE=DATA(I)
      TIM=DATA(J)
      K=I/2
      ARG=SFT*K
      CN=COS(ARG)
      SN=SIN(ARG)
      DATA(I)=TRE*CN-TIM*SN
1 DATA(J)=TIM*CN+TRE*SN
      RETURN
      END

```

Appendix E

In Chapter 6, a simple model of an anisotropic surface was created, and the variation of its spectral characteristics as a function of azimuth was derived analytically and confirmed by empirical results. The surface was constructed by generating a random signal of known spectral properties and extending each value of the series into the second dimension. In the resulting relationship,

$$A = a(\theta) \cdot b(\theta)$$

The proportionality factor $a(\theta)$ was shown to vary as a sinusoid and $b(\theta)$ remained constant over all θ . Results from multibeam-sonar-derived bathymetry indicated that this simple model is adequate to describe some actual surfaces on the earth, such as the Gorda Rise spreading center.

Beyond this very simple model, a more elaborate surface can be generated by summing several signals of differing characteristics at a variety of orientations. If one assumes that the simple corrugated surface presented in the elementary model of Chapter 6 is the result of a dominant, unidirectional process, then these composite surfaces would represent areas of the sea floor where several geological processes have been active, perhaps acting in different directions. The Gorda Rise, particularly at the ridge crest, is dominated by the processes associated with crustal formation, and its relief does appear to conform to the one-process surface model.

The relief of the Mendocino Fracture Zone shown in Figures 4-7-10, although only represented by spectra from two azimuths, indicates a

clear difference in spectral slope ($b(\theta)$), which would not be expected in a simple surface dominated by one process. In fact, the main east-west trend of the fracture zone is produced by tectonic processes which are reflected in profiles collected in a north-south orientation. The various mass-wasting processes acting down this slope produce a different style of relief which is evident in profiles collected east-west. The bathymetry shown in Figure 6-10 from the continental slope might also be the results of two processes at work. This is reflected in the possible variation of $b(\theta)$ as shown in Figure 6-11.

No attempt will be made to derive a general mathematical (geometrical) form for the azimuthally-dependent spectra of these multiple component surfaces. Such a treatment would be beyond the scope of this study. However, an insight into the nature of these surfaces can be gained by examining a few examples. All of the examples following are generated using the same algorithms. First, two random signals of specified spectral characteristics (a and b) are generated using an inverse FFT method. One signal becomes the initial row, and the other the initial column, of a 128×128 element matrix. Each element of the matrix is then computed by summing the appropriate row and column element. This method results in a surface which when sampled at 0° azimuth, produces one of the input signals displaced by a random constant. For the 90° azimuth, the other input signal is sampled, similarly displaced. To study the spectra of the combined signals in other azimuths, the matrices were sampled and analyzed in an identical fashion to the bathymetry grids of Chapter 6.

Four examples of two spectral component surfaces are shown in Figures E-1 through E-4. A variety of combinations were used. Figure E-1

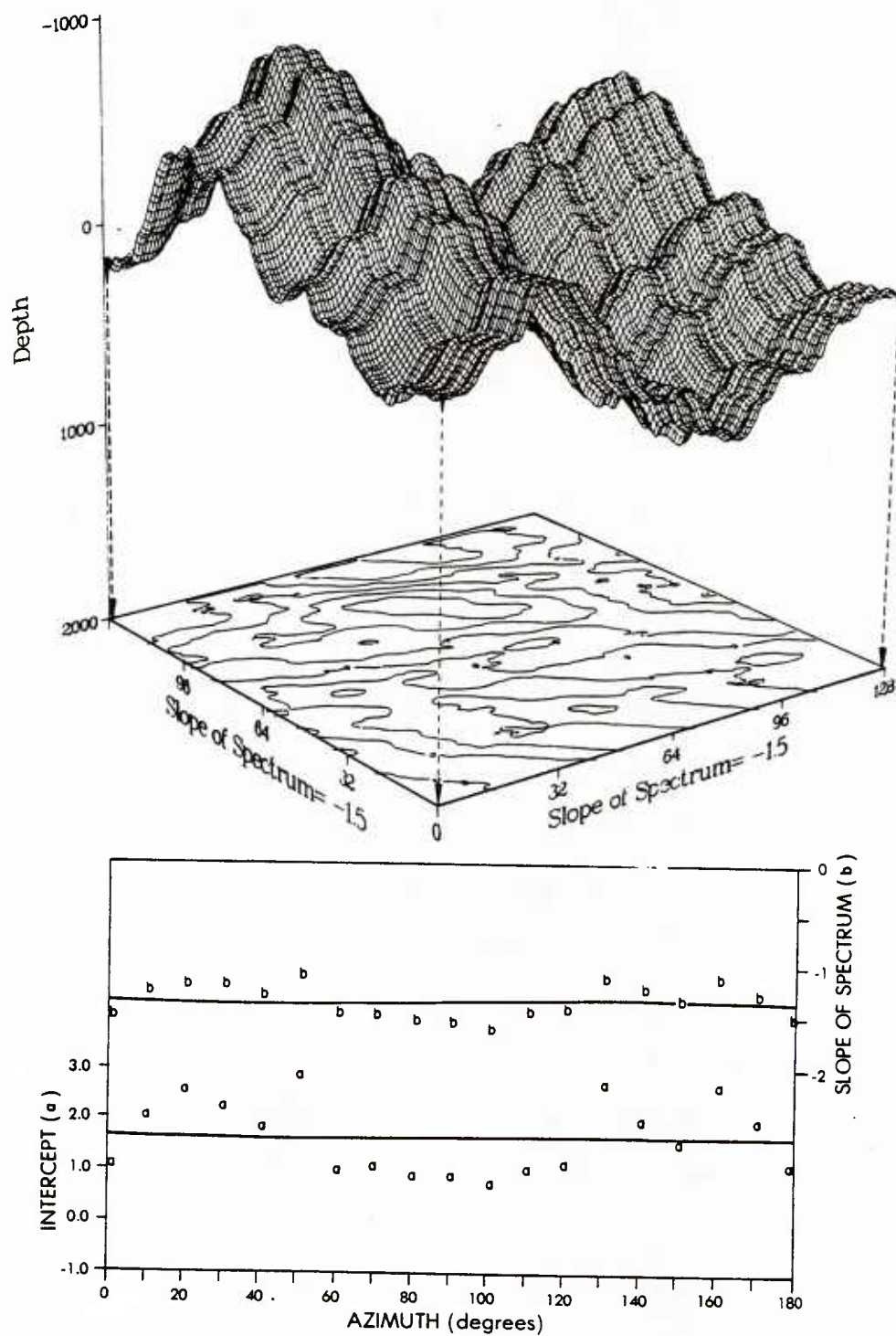


Figure E-1

Artificially generated surface composed of two identical orthogonal trends, both with spectral slope $b = -1.5$, and spectral intercept $a = 1.0$. Viewpoint is from the southwest. Below, the variation of parameters \hat{a} and \hat{b} are shown versus azimuth.

illustrates the characteristics of a surface in which two signals of identical spectral slope ($b = -1.5$) and intercept ($a = 1.0$) were combined in orthogonal directions. Arbitrarily assuming a viewpoint from the southwest for all examples, the input signals represent pure signals in the east-west and north-south orientations. The resulting surface shows a clear northwest-southeast trend. Another realization might yield a northeast-southwest trend. With only a knowledge of the resulting surface, an investigator might infer a single process acting at 45° or 135° azimuth. The trend actually results from the vector sum of two orthogonal processes.

The distribution of spectral parameters with azimuth clearly reflects the departure of this surface from a one process model. The spectral slope parameter (\hat{b}) does show the designated value of -1.5 at azimuths of 0° , 90° and 180° , as it must. The corresponding intercept (\hat{a}) parameters also correspond to the input value of 1.0 , indicating that these profiles represent uncontaminated samples of the input signals. At intermediate azimuths, however, both parameters are consistently higher than those of the input signal. Whereas in the simple model of Chapter 6 the slope (\hat{b}) parameter remains constant with azimuth, the same parameter shows two clear maxima in the range 0° to 180° . The intercept (\hat{a}) parameter also shows two maxima, rather than the single maximum of the corrugated surface model. Figure E-2 presents a similar surface in which the intercept (a) parameter in the east-west direction has been increased to 1.2 . The variation of spectral parameters with azimuth is also very similar to that shown in Figure E-1, however the variation of both \hat{a} and \hat{b} is amplified.

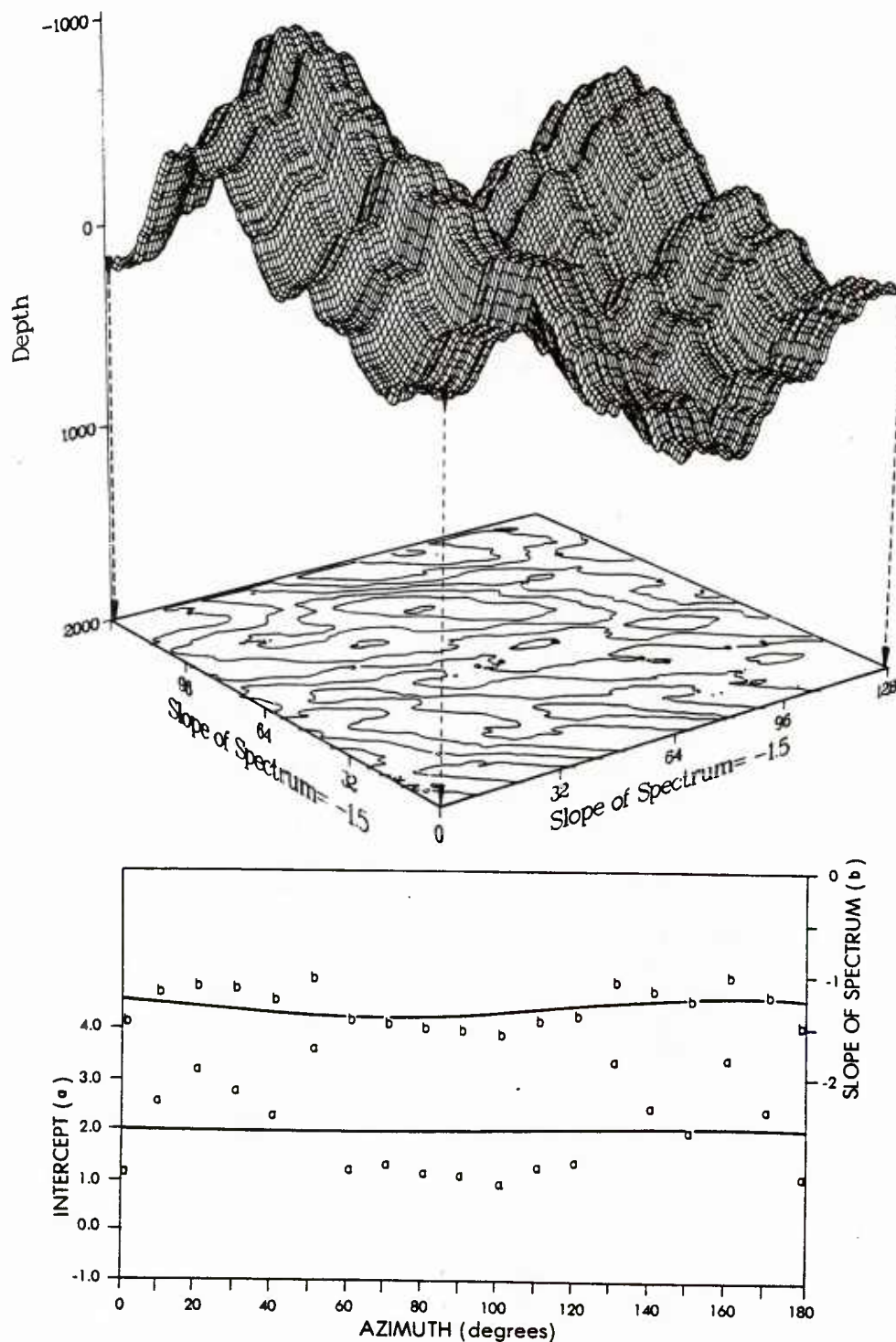


Figure E-2 : Artificially generated surface composed of two orthogonal trends, both with spectral slopes of $b = -1.5$, and $a = 1.0$ in the N-S direction, $a = 1.2$ in the E-W direction. Viewpoint is from the southwest. The variation of \hat{a} and \hat{b} parameters with azimuth are plotted below.

In Figure E-3, the intercept terms (a) are again set equal, but the spectral slopes (b) of the component signals differ. The north-south component has spectral slope $b = -1.5$, while the east-west component has a spectral slope $b = -1.0$. The artificial surface was designed to mimic the bathymetry of the Mendocino Fracture Zone. The north-south signal dominates the surface, as reflected in an east-west trending contour chart. The wavelength associated with the intercept term a, was arbitrarily selected to correspond to a wavelength of two data points. Because of the higher angle of negative slope in the spectrum of the north-south profile, this trend contains higher amplitudes in all frequencies lower than one-cycle-per-two-data intervals. Only at the very southern limit of the surface, where the north-south signal is relatively constant, can the orthogonal trend be detected.

At higher frequencies, the spectra of the two component signals cross over, and the east-west signal contains higher amplitudes and dominates the surface topography. This somewhat complicated set of circumstances is not outside geological experience. For a terrestrial example, envision a long ridge of several kilometers width and perhaps one thousand meters height, oriented east-west. On the side of this ridge are a series of north-south trending streams and gullies with relief of tens-of-meters which shed the runoff from the ridge. If one were to travel in the north-south direction, the effect of the streams would be minimal, and the long wavelength shape of the ridge would present the only obstacle. If one were to travel in the east-west direction on the face of the ridge, the obstacles in the terrain would be dominated by the lower amplitude, but higher frequency streambeds. This difficulty of travel represents in a very direct sense the concept of surface

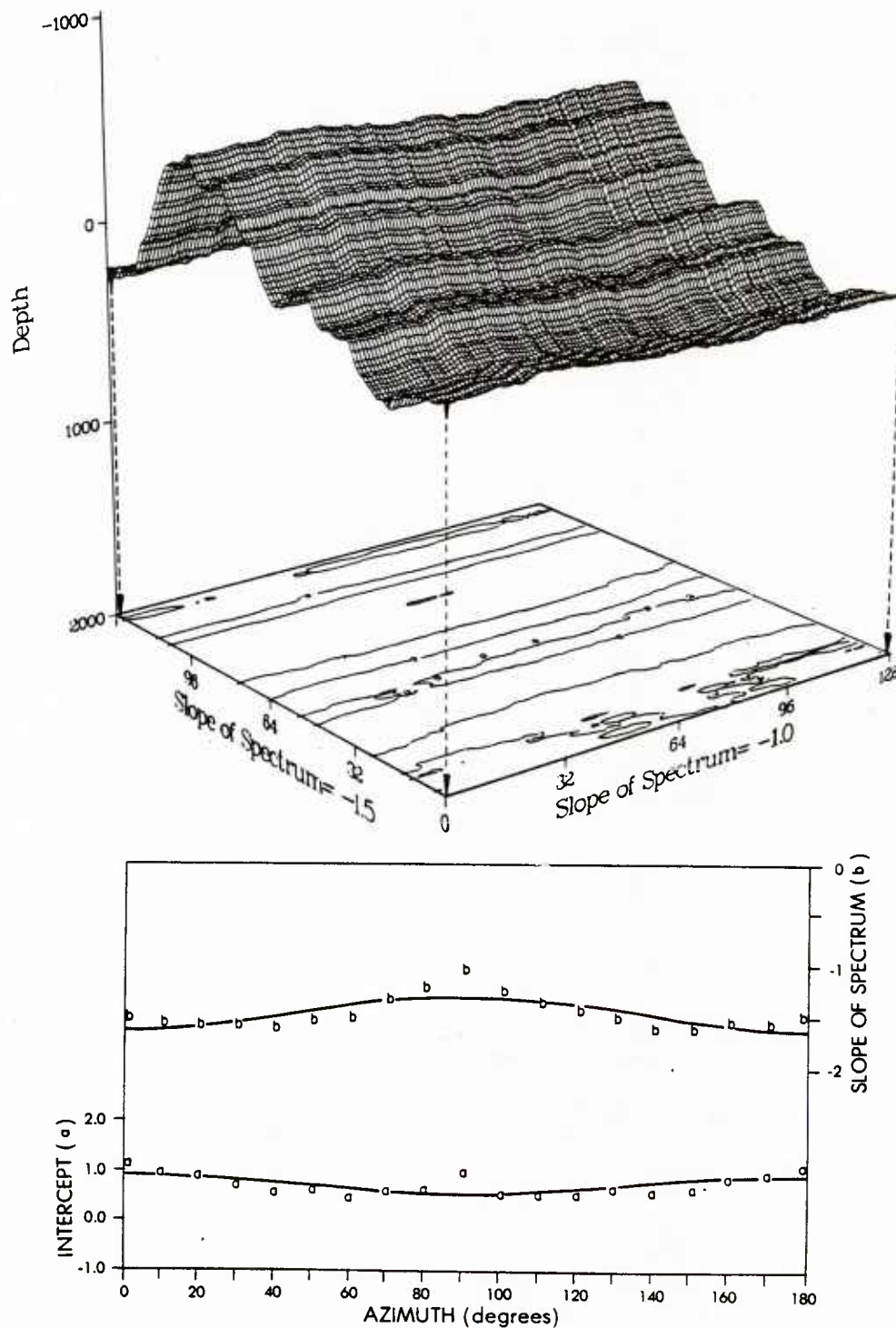


Figure E-3

Artificially generated surface composed of two orthogonal trends with identical intercepts of $a = 1.0$, but spectral slopes of $b = -1.5$ in the N-S direction and $b = -1.0$ in the E-W direction. Azimuthally dependent spectral parameters are plotted below.

roughness. The artificial surface shown in Figure E-3, as well as the Mendocino Fracture Zone shown in Chapter 4, are analogous to this hypothetical example.

The computed spectral parameters shown below in Figure E-3 also reflect the complexities of this surface. The $\hat{a}(\theta)$ parameters appear to vary regularly with azimuth, although not following the cosine curve derived by simple regression, the variation occurs in spite of the fact that the input signals have identical a's. Only at exactly 90° azimuth, does the \hat{a} parameter jump to the input value. The $\hat{b}(\theta)$ values also follow a complex pattern which is not described by the illustrated cosine curve. Extensive analytical geometry would be necessary to reach an understanding of these variations.

A final artificial surface is presented as Figure E-4. In this case, both the spectral slopes (b) and intercepts (a) of the input signals are different. The construction is identical to that shown in Figure E-3, with the exception that the intercept (a) parameter in the east-west direction has been increased to 2.0. Between the input values at 0°, 90°, and 180°, the variation of the spectral parameters appears even more complicated than the results from Figure E-3. The combination of signals at oblique azimuths, or the combination of more than two signals, would result in an even more complex pattern.

With the insight gained by examining these artificially generated surfaces, a more complete analysis of the anisotropy of the Mendocino Fracture Zone can now be conducted. Figure E-5 presents a contour chart of the surface used in this analysis, which represents a subarea of the base chart shown in Figure 4-7. The digital data, collected by the SASS multibeam sonar system, is gridded at a spacing of 0.05 minutes of lati-

tude and longitude. Figure E-6 shows a graphic representation of this surface and its spectral parameters as a function of azimuth, in the same format as the artificially generated surfaces shown in Figures E-1 through E-4.

Compare the bathymetric surface shown in Figure E-6 to the artificially generated surface shown in Figures E-3 and E-4. The overall morphologies are quite similar, with a longer wavelength, higher amplitude component in the north-south direction relative to the orthogonal trend. This similarity in morphologies is also expressed as a similarity in the azimuthally dependent roughness models, although the parameters generated from the bathymetric surface are somewhat noisier than the artificially generated examples. In all cases, the slope parameter \hat{b} is not constant with azimuth, as was the case for the surfaces studied in Chapter 6. Like the artificial surfaces of Figures E-3 and E-4, the spectral slope is approximately $\hat{b} = -1.5$ in the 0° or 180° azimuth and approaches $\hat{b} = -1.0$ for the 90° azimuth. The intercept parameter in Figure E-6 reaches its maximum at $\theta \approx 90^\circ$, similar to the example in Figure E-4. In the case of the Mendocino Fracture Zone, this parameter is approximately doubled in the east-west direction over the north-south direction. This indicates that for wavelengths near 1 km, the Fracture Zone surface is twice as rough for $\theta = 90^\circ$ as for $\theta = 0^\circ$. In longer wavelengths, this relationship is reversed as evidenced by the much higher total relief in the north-south direction. Such a reversal is only possible for near orthogonal trends with different spectral slopes. Sinusoidal regression lines, which comprise the basic model of Chapter 6, are included in Figure E-6 to emphasize how poorly this simple model describes the two-trend case.

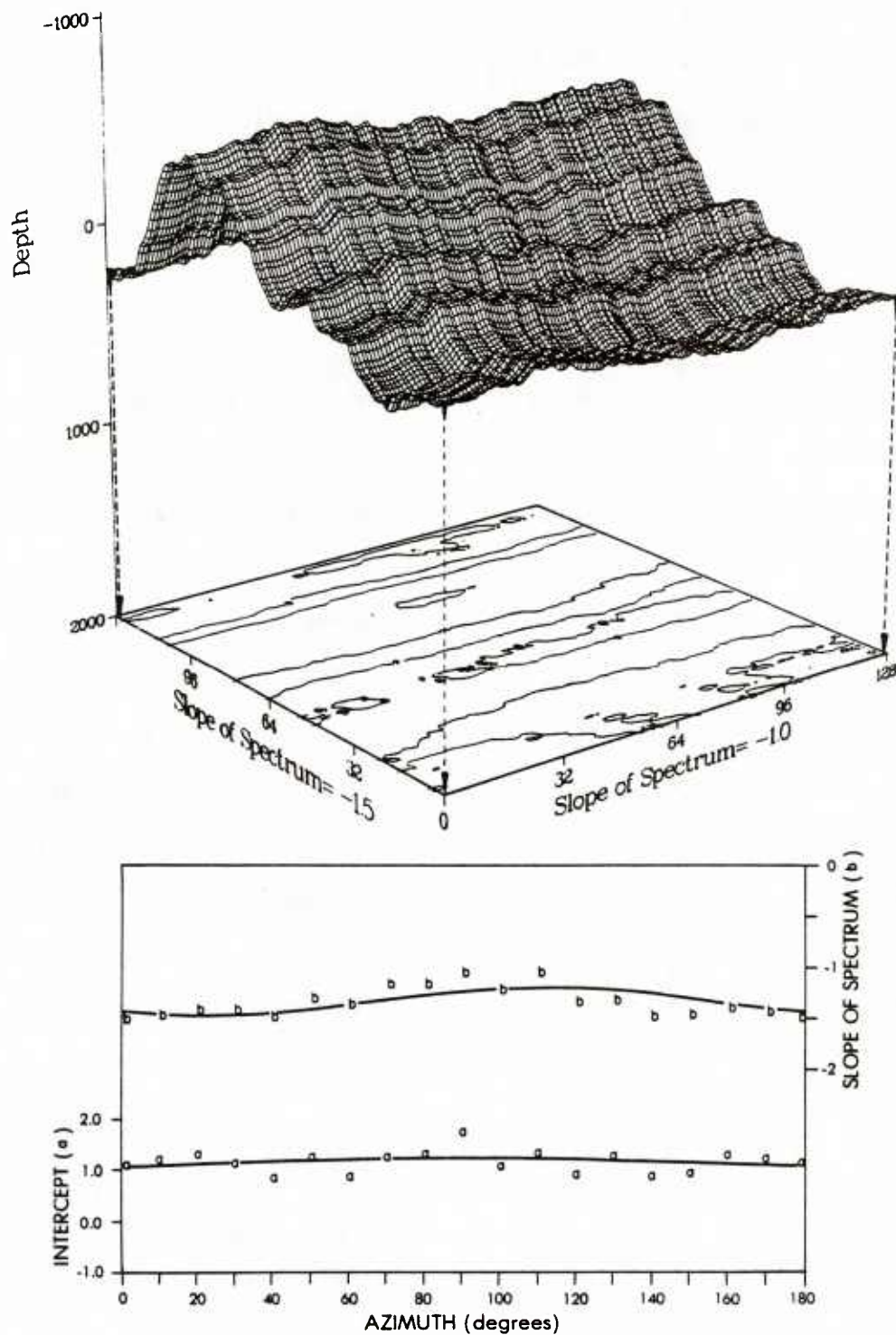


Figure E-4 Artificially generated surface composed of orthogonal trends with spectral parameters $b = -1.5$, $a = 1.0$ in the N-S direction, and $b = -1.0$, $a = 2.0$ in the E-W direction. Azimuthally dependent spectral parameters are plotted below.

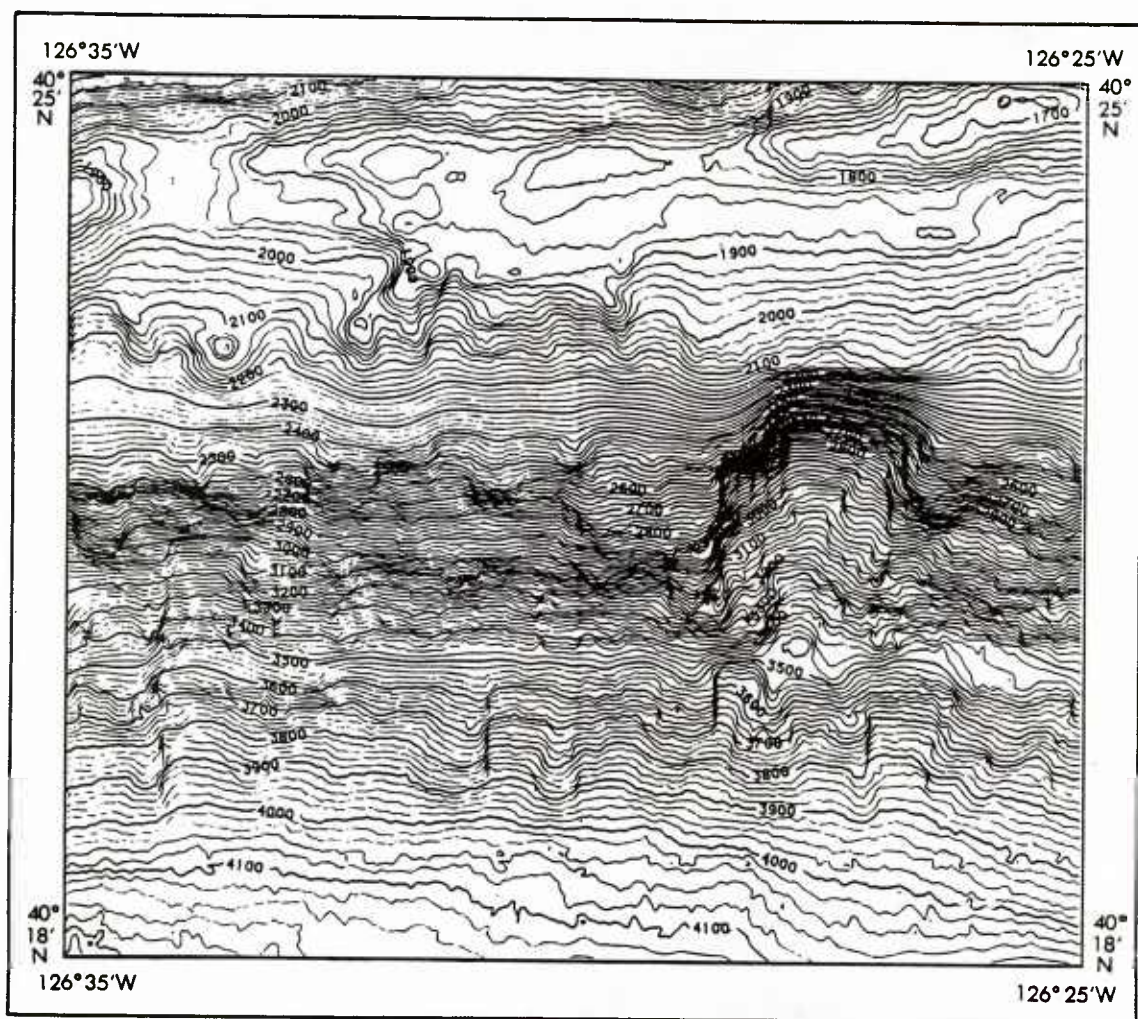


Figure E-5 Contour chart of a segment of the Mendocino Fracture Zone. Automatically generated contours are based on SASS multibeam sonar data gridded at 0.05 minutes of latitude and longitude.

tude and longitude. Figure E-6 shows a graphic representation of this surface and its spectral parameters as a function of azimuth, in the same format as the artificially generated surfaces shown in Figures E-1 through E-4.

Compare the bathymetric surface shown in Figure E-6 to the artificially generated surface shown in Figures E-3 and E-4. The overall morphologies are quite similar, with a longer wavelength, higher amplitude component in the north-south direction relative to the orthogonal trend. This similarity in morphologies is also expressed as a similarity in the azimuthally dependent roughness models, although the parameters generated from the bathymetric surface are somewhat noisier than the artificially generated examples. In all cases, the slope parameter \hat{b} is not constant with azimuth, as was the case for the surfaces studied in Chapter 6. Like the artificial surfaces of Figures E-3 and E-4, the spectral slope is approximately $\hat{b} = -1.5$ in the 0° or 180° azimuth and approaches $\hat{b} = -1.0$ for the 90° azimuth. The intercept parameter in Figure E-6 reaches its maximum at $\theta \approx 90^\circ$, similar to the example in Figure E-4. In the case of the Mendocino Fracture Zone, this parameter is approximately doubled in the east-west direction over the north-south direction. This indicates that for wavelengths near 1 km, the Fracture Zone surface is twice as rough for $\theta = 90^\circ$ as for $\theta = 0^\circ$. In longer wavelengths, this relationship is reversed as evidenced by the much higher total relief in the north-south direction. Such a reversal is only possible for near orthogonal trends with different spectral slopes. Sinusoidal regression lines, which comprise the basic model of Chapter 6, are included in Figure E-6 to emphasize how poorly this simple model describes the two trend case.

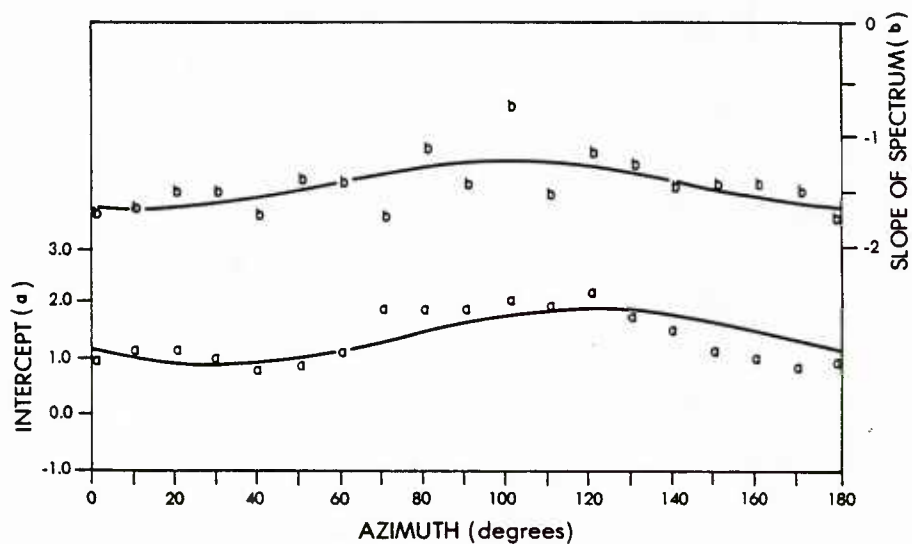
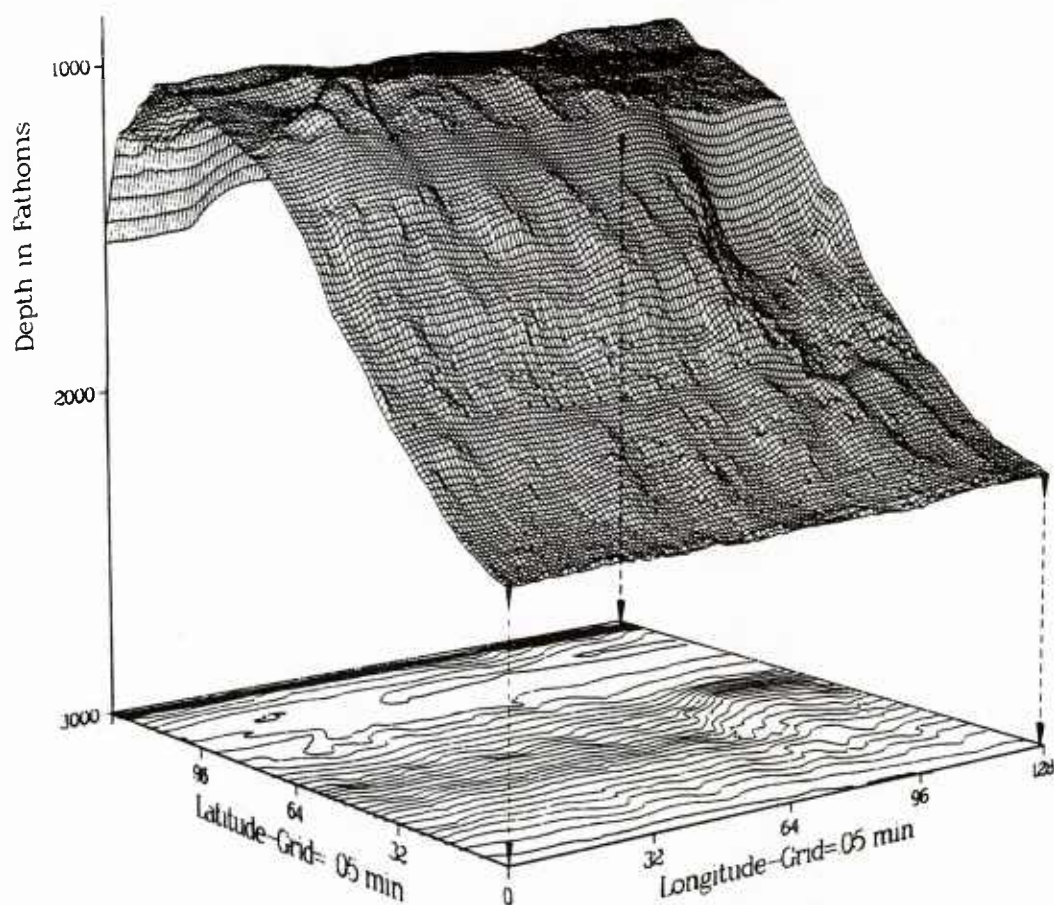


Figure E-6 Graphic representation of the Mendocino Fracture Zone bathymetry shown in Figure E-5 is shown above (viewpoint from the southwest). Shown below are the spectral estimates versus azimuth for this surface. Compare this example to the artificially generated surfaces shown in Figures E-3 and E-4.

DESCRIPTION OF TERMS

This informal glossary is included to aid readers who represent diverse backgrounds in geology, geophysics, acoustics, statistics, and other fields. The descriptions of terms, phrases, and acronyms included are intended to reflect their use within this report, rather than a general or rigorous definition.

Amplitude

The departure of a periodic function from its mean.

Anisotropy

Condition of having different properties in different directions.

Band-limited

Condition in which a signal contains a finite range of frequency. With reference to Fourier analysis, this band ranges from the fundamental frequency to the Nyquist frequency.

Boxcar function

A function which equals unity over some finite length and zero everywhere else. The multiplication of this function with an infinite series represents mathematically the sampling of a finite series from an infinite process. Sometimes called a rectangle function.

Chi-square distribution

The probability distribution for the estimation error of the power spectrum. Due to the form of the distribution, the errors associated with the amplitude spectrum appear constant when plotted on log-transformed axes.

Coherent signal

A signal in which the phase relationship of the various frequency components is retained.

Convolution

A mathematical operation which is equivalent to multiplication in the opposite transform domain.

Deterministic model

A numerical model in which the mathematical parameters represent specific measurable quantities of the process under study.

Ensemble average

The mean value of a group of repetitive samplings for a given statistical measure.

FFT

Fast Fourier Transform. A numerical algorithm for estimating the Fourier transform with a greatly reduced number of operations.

Fractal dimension

A topological term which refers to a dimension which may be either integer or fractional. The fractal dimension (D) is related to the spectral slope (b) by $b = -(5/2 - D)$. Refer to Mandelbrot (1982) for a complete discussion.

Functional form

Refers to the type of function or functions used as a model for the distribution of data in a regression analysis. The term does not apply to the calculated parameters used to describe a specific data set.

Fundamental frequency

The lowest frequency treated in a Fourier analysis, corresponding to the inverse of the length of data.

HEBBLE

High Energy Benthic Boundary Layer Experiment

Isotropy

Condition of having the same properties in all directions.

Leakage

In spectral analysis, the transfer of energy from one frequency into other frequency bands.

Linear-linear space

A two-dimensional coordinate system in which both orthogonal axes represent simple evenly-spaced scales. Usually called a rectangular Cartesian coordinate system.

Log-log space

A two-dimensional coordinate system in which both orthogonal axes are scaled by evenly spacing the logarithm of the linear scale. In this study, all such transformations use base-ten logarithms.

Magnetic anomaly

The departure of the measured magnetic field from some low frequency model.

Markov process

A stochastic process in which the conditional probability state is unaffected by the historical state of the system.

Multibeam sonar

A bathymetric sounding system in which several discrete soundings of the sea floor can be derived by a single discharge of acoustic energy.

NAVOCEANO

United States Naval Oceanographic Office

Non-parametric statistics

Statistical theory in which the probability distribution of the underlying data is not assumed.

Nyquist frequency

The highest frequency treated in a Fourier analysis, corresponding to the inverse of twice the data spacing.

Orthogonal

An orientation in which all axes intersect perpendicularly.

Phase

The location of a periodic function along an axis relative to some arbitrary origin.

Planetary Rossby waves

A large-scale, stable wave motion in the global ocean.

Power

The squared amplitude of a periodic function.

Power law

A mathematical relationship of the form $y=ax^b$. This function plots linearly in log-log space.

Prewhitening

A technique which reduces the effect of spectral leakage in analyzing non-white-noise signals.

Process (geological)

A natural continuing activity or function.

Process (statistical)

Any quantity which is defined in terms of its relationship to some independent variable, usually time or space.

Provincing

Techniques which divide a sample space into discrete regions based on some predefined statistical property.

Random walk

A stochastic process of independent increments.

Regression model

A functional description of a relationship between a dependent variable and independent variable(s), usually derived by the method of least-squares.

Round-off error

The level of uncertainty in a data set due to the finite number of digits retained.

SASS

Sonar Array Sub-System. A multibeam sonar system operated by the U.S. Navy.

SEABEAM

A commercially available multibeam sonar system.

SEAMARC-1

A commercially available deep-towed geophysical instrument package.

Sedimentary process

Relief-forming process which involves the transportation of suspended material.

Sinc function

The function $y = \sin(x)/x$.

Sinusoid

A function having the form of a sine or cosine function, but with a variable phase value.

Spatial frequency

The inverse of wavelength.

Spectral intercept

The intersection of an amplitude spectrum with the amplitude axis. This term is specific to this report.

Spectral slope

The slope of an amplitude spectrum which has been plotted on log-log axes. This value becomes the exponent of spatial frequency following transformation to linear-linear space. This term is specific to this report.

Spreading center

A region of the sea floor where recent crustal material is being formed.

Stationarity

Although rigorously defined in statistical theory, used in this report to imply relative constancy of a particular statistical parameter as a function of position; statistically homogeneous.

Stereo-pair bottom photography

A photogrammetric technique which allows the measurement of micro-relief on the sea floor by analyzing photographic images of a surface from offset viewpoints.

Stochastic model

A numerical model in which the mathematical parameters describe the process under study in terms of its random variability.

Strike

The bearing of the long axis of a linear trend.

Tectonic process

Relief-forming process which involves the deformation of the earth's crust.

White noise

A random series whose amplitude spectrum is constant with frequency.

DISTRIBUTION LIST

CNO (OP-952, OP-212, PME-124)	3
ASSTSECNAV RES	2
ONR	5
COMNAVOCEANCOM	2
NRL (B. Adams, D. Berman, R. Feden)	3
USNA	2
NAVPGSCOL	2
NAVSWC	1
NORDA (110, 200, 220, 240, 250, 250B, 260, 270, 300, 340, 350, 360, 361, 362)	14
NOSC	1
NUSC (Newport, RI)	1
NUSC (New London, CN-T. Bell, J. Dobler, J. Schumacher)	3
NOAA/PMEL (E. Bernard, R. Burns, S. Hammond, R. Embley)	4
NOAA/NGDC (T. Holcombe)	1
UT/ARL (H. Boehm, P. Widmar)	2
JHU/APL	1
PSU/ARL	1
UW/APL (D. Jackson, D. Winebrenner)	2
UW/DGS (A. Nowell)	1
CU/LDGO (D. Hayes, A. Watts, J. Weissel, S. Lewis, W. Ryan, D. Martinson G. Mountain)	7
Cornell (D. Turcotte)	1
UC/SIO	1
DMA/HTC	1
WHOI	1
UH/HIG	1
UH/HIG (P. Taylor)	1

U219054

TR 279

Description, Analysis, and Prediction of
Sea-Floor Roughness Using Spectral Models

April 1985